

DEPARTMENT OF ZOOLOGY

Characterisation of DNA polymerase δ exonuclease domain mutations associated with cancer predisposition using fission yeast

Sophia Irenee Toumazou

A thesis presented for the degree of Doctor of Philosophy

Department of Zoology
Department of Oncology
University of Oxford

Trinity Term 2021

In Loving memory of Niki Tyrimou-Toumazou and Carol Walker

Characterisation of DNA polymerase δ exonuclease domain mutations associated with cancer predisposition using fission yeast

Sophia Toumazou
St Cross College
MPLS Division

Doctor of Philosophy
University of Oxford
Trinity 2021

Heterozygous germline exonuclease/proofreading domain mutations (EDMs) in DNA polymerase delta (Pol δ) are linked predominantly to colorectal and endometrial cancers with microsatellite stability (MSS), such as *POLD1* S478N. Pol δ synthesises the lagging strand during DNA replication and partakes in DNA repair.

To assess the pathogenicity of more cancer-associated EDMs that affect highly conserved residues, *POLD1* P327L, G321S, L474P and D316N variants were constructed in *Schizosaccharomyces pombe* (*S. pombe*) *pol3* and mutation rate assays were carried out. *Pol3(d)D316N* had the highest mutation rate, comparable to *Pol3* with no 3'-5' exonuclease activity (exo-null). *Pol3(d)L474P* had a moderate mutator phenotype, and *pol3(d)P327L* and *pol3(d)G321S* did not have increased mutation rates compared to wild type but showed hydroxyurea (HU) sensitivity, suggesting that DNA replication under stressful conditions is defective.

Some Pol ε EDMs are hypermutating, but this is not seen with Pol δ EDMs. Interestingly, none of the variants had hyper-mutation rates in excess of Pol δ exo-null, unlike some Pol ε variants. To investigate this further, *pol3(d)P327R*, equivalent to the hypermutating *pol2(e)P286R* variant, was constructed but this had a low mutation rate.

The HU-sensitivity phenotype of *pol3P327L* and *pol3G321S* was further investigated. A significant proportion of cells expressing *pol3P327L* displayed mitotic abnormalities during HU treatment. *Pol3G321S* cells took longer to complete S phase compared to the other mutants after HU block and release and had reduced viability in hydroxyurea. Both strains were synthetically sick with Rad3 inactivation, suggesting dependence on the DNA replication or repair checkpoint.

Thirdly, a genome-wide systematic screen was carried out to identify any novel negative synthetic interactions with *pol3L474P*. The screen yielded 565 possible hits, of which 28 were designated for further characterisation. This identified *fen1* and *msh2*, which have been previously reported as synthetically lethal with exo-null *pol3*.

Acknowledgements

Firstly I would like to thank my supervisors, Prof Stephen Kearsey, Dr Timothy Humphrey and Prof Jane Mellor for all their invaluable support, guidance and patience during the course of my studies. I would particularly like to thank my primary supervisor, Stephen Kearsey, for all his help and teaching over the years, and Tim Humphrey for providing me with a new lab home.

I would like to thank all of the members of the Kearsey and Humphrey laboratories past and present. You have all made this experience worthwhile and I have made great friends! In particular, I would like to thank Carol Walker for all her help with the Bioneer Screen and Christos Andreadis for guiding me in my first two years of the DPhil.

I would like to thank my amazing family and friends for all their love and support which has kept me sane throughout the years. I would like to dedicate this thesis to Carol Walker, who unfortunately passed away not long ago. Carol was my “lab mum” and now she is with my mum. Carol, you will never be forgotten; we miss you. Finally, I would like to pay my deepest respects to my late mother, Niki Tyrimou-Toumazou, who always told me that knowledge is infinite and wisdom is a gift. She was my moral compass and my biggest cheerleader in life. This is for you, mum!

Declaration

I declare:

The work presented in this thesis is my own. The Bioneer screen experiment and analysis for synthetic sick/lethal interactions were performed both by Carol and myself.

Some of this work has been accepted for publication (**Appendix V**) in the following paper:

Soriano, I., E. Vazquez, N. De Leon, S. Bertrand, E. Heitzer, S. Toumazou, C. Palles, C.-C. Pai, T. Humphrey, I. Tomlinson, S. Cotterill, and S.E. Kearsey. 2021. Expression of the cancer-associated DNA polymerase ε P287R in fission yeast leads to translesion synthesis polymerase dependent hypermutation and defective DNA replication. *PLoS Genetics*. 17:1-27.

No portion of this work has been previously submitted for another qualification at this, or any other university.

Signed ……..……

Sophia Toumazou

Contents

Abstract i

Acknowledgements ii

Declaration iii

Contents iv

List of Figures viii

List of Tables x

Nomenclature xi

Abbreviations xii

Chapter 1 Introduction 1

1.1 GENOME INSTABILITY AS A HALLMARK OF CANCER 1
1.2 MUTAGENESIS IN COLON CANCER 2
1.3 DNA REPLICATION AND REPLICATIVE DNA POLYMERASES 3
1.3.1 Overview of DNA replication 3
1.3.2 Polymerase alpha (Pol α) 8
1.3.3 Polymerase epsilon (Pol ε) 8
1.3.4 Polymerase delta (Pol δ) 10
1.3.5 Pol ε versus Pol δ 13
1.3.6 Polymerase fidelity, exonuclease activity and other DNA repair roles 14
1.4 EXONUCLEASE DOMAIN MUTATIONS (EDMs) AND CANCER 20
1.4.1 EDMs increase mutation rates 20
1.4.2 EDMs cause cancer predisposition 22
1.4.2.1 *Germline POLD1 S478N and POLE L424V exonuclease domain mutations* 22
1.4.2.2 *POLD1 EDMs: P327L, L474P, D316N and G321S* 25
1.4.2.3 *Somatic POLE/POLD1 EDMs* 30
1.5 AIMS OF THE PROJECT 32

Chapter 2 Materials and Methods 35

2.1 *S. pombe* METHODS 35
2.1.1 General methods 35
2.1.2 Genetic crosses 39
2.1.2.1 *Random spore analysis* 40
2.1.2.2 *Tetrad analysis* 41
2.1.3 Yeast transformation 41
2.1.4 Colony PCR 41
2.1.5 Fluctuation assays 46
2.1.6 Spot tests 47
2.1.7 Microscopy 48
2.1.7.1 *Ethanol fixation* 48
2.1.7.2 *DAPI (4'6'-diamidino-2-phenylindole) staining nuclei* 48
2.1.7.3 *Septum staining with calcofluor* 49
2.1.8 Flow Cytometry 49
2.1.9 Growth rate assays 49
2.1.10 Bioneer cross 50

2.2 DNA METHODS 51
2.2.1 Cloning 51
2.2.1.1 *Plasmids* 52
2.2.1.2 *Restriction digestion* 52
2.2.1.3 *DNA ligation* 53
2.2.1.4 *E. coli general methods* 53
2.2.2 DNA analysis by gel electrophoresis 54
2.2.3 Quantification of DNA samples 54
2.2.4 Construction of *pol3(d)* mutant plasmids by PCR 54
2.2.5 Sequencing 55
2.3 PROTEIN METHODS 56
2.3.1 TCA protein extraction 57
2.3.2 SDS-polyacrylamide gel electrophoresis (SDS-PAGE) 57
2.3.3 Western blotting 58
2.3.4 Western blot stripping 58

Chapter 3 The construction and characterisation of *pol3* exonuclease domain mutations in *S. pombe* 59

3.1 INTRODUCTION 59
3.1.1 Aims of Chapter 3 59
3.2 RESULTS 60
3.2.1 Construction of *pol3* yeast mutants 60
3.2.1.1 *Construction of equivalent POLD1 exonuclease domain mutants (EDMs) in fission yeast* 60
3.2.1.2 *Construction of fission yeast strain expressing pol3(d)D386A mutation: an exonuclease null pol3 strain* 71
3.2.1.3 *Construction of fission yeast strain expressing pol3(d)P311R mutation* 71
3.2.2 Mutation rate assays 75
3.2.2.1 *Mutation rates of pol3 EDMs* 76
3.2.2.2 *Mutation rate of strain expressing pol3P311R* 81
3.2.3 Guanine-thymine (GT) repeat stability in the *pol3* mutant strains 82
3.2.3.1 *Construction of fission yeast pol3 strains with GT repeats in the ade6 marker gene* 83
3.2.3.2 *Mutation rates of pol3 mutants with $(GT)_8$ repeat in ade6* 83
3.2.4 Growth rate of the *pol3* exonuclease domain mutants (EDMs) 84
3.2.5 *Pol3P311L* and *pol3G305S* strains exhibit growth defects under replication stress 90
3.3 DISCUSSION 100
3.3.1 Pol δ mutant orthologues in humans and in yeasts 100
3.3.2 Summary of results 100
3.3.3 Overview of the pathogenicity of *pol3* EDMs 101
3.3.4 *Pol2P287R* and *pol3P311R* are homologous mutations affecting two separate eukaryotic polymerases but have different mutator phenotypes 108

Chapter 4 Characterisation of the hydroxyurea sensitivity observed with some of the *pol3* variants 111

4.1 INTRODUCTION 111
4.1.1 The DNA damage response (DDR) 113
4.1.2 DNA integrity checkpoints 114
4.1.2.1 *Sensing the damage* 115
4.1.2.2 *Signal transduction* 117
4.1.2.3 *Arresting the cell cycle* 119

4.1.3 An overview of the role of Mus81 in eukaryotes 120
4.1.4 Aims of Chapter 4 122
4.2 RESULTS 125
4.2.1 Pol3 levels in the *pol3* EDMs 125
4.2.1.1 *Construction of FLAG-tagged pol3 variants* 125
4.2.1.2 *The pol3 variants all have physiological levels of Pol3* 126
4.2.2 *Pol3P311L* cells appear to have defective checkpoint arrest, whereas *pol3G305S* cells have overactive checkpoint arrest 131
4.2.3 The viability of *pol3P311L* and *pol3G305S* mutants is dependent on Rad3 activation 136
4.2.3.1 *Construction of pol3 mutations in a rad3ts background strain* 136
4.2.3.2 *Spot tests* 136
4.2.3.3 *The synthetic interaction between pol3L458P and rad3 genes* 140
4.2.4 The viability of the *pol3G305S* mutant is compromised in hydroxyurea-induced replicative stress 142
4.2.5 *Pol3G305S* recovers more slowly after S phase arrest compared to wild type 144
4.2.6 The effect of Mus81 on replication fork stability in the *pol3* mutants 150
4.2.6.1 *Construction of pol3, mus81Δ double mutant strains* 150
4.2.6.2 *The exonuclease active site variants, pol3D300N and pol3D386A, are synthetically sick upon the deletion of the mus81 gene* 151
4.2.6.3 *The growth of the pol3, mus81Δ double mutant strains is further attenuated by HU compared to mus81Δ* 152
4.2.7 The implications of increased dNTP pools on exonuclease *pol3* variants 158
4.2.7.1 *Construction of pol3, cdc22-D57N double mutant strains* 158
4.2.7.2 *Raised dNTP levels do not fully rescue the HU sensitivity phenotype of the low-mutator pol3 variants* 159
4.3 DISCUSSION 162
4.3.1 Summary of key findings 162
4.3.2 The *pol3D300N* and *pol3D386A* exonuclease-null mutant strains are not sensitive to hydroxyurea-induced replicative stress and are not dependent upon Rad3 activation for viability in unperturbed DNA replication 163
4.3.3 The *pol3P311L* and *pol3G305S* mutant strains are sensitive to hydroxyurea and require Rad3 for viability 165
4.3.4 The augmentation of nucleotide levels in the *pol3P311L* and *pol3G305S* cells partially rescues their hydroxyurea sensitivities 170
4.3.5 The augmentation of nucleotide levels in *pol3L458P* mutant cells causes synthetic lethality 171

Chapter 5 High-throughput genetic interaction mapping in the fission yeast *S. pombe* expressing *pol3L458P* 173

5.1 INTRODUCTION 173
5.1.1 Aims of Chapter 5 174
5.2 RESULTS 175
5.2.1 Genetic Interaction Mapping in *S. pombe* using the Pombe Epistasis Mapper-2 (PEM-2) System 175
5.2.1.1 *Construction of the PEM-2 strategy in the pol3L458P strain* 176

5.2.2 The Bioneer deletion library 177
5.2.3 High-throughput genetic interaction mapping using the colony replicating robot ROTOR HDA 181
5.2.4 Bioneer screen results and identification of SSL hits 181
5.2.5 Criteria for selection of SSL hits 182
5.2.6 SSL hits confirmed via tetrad analysis 192
5.2.7 Results overview from tetrad analyses 195
5.2.8 The *pol3L458P* mutation is not SSL in an *mre11Δ* or a *rad50Δ* genetic background 198
5.3 DISCUSSION 209
5.3.1 Summary of results 209
5.3.2 General discussion 209

Chapter 6 General discussion 215

6.1 THE POL δ EDMs HAVE INDIVIDUAL PHENOTYPES 215
6.2 THE HYDROXYUREA-SENSITIVITIES OF THE *pol3P311L* AND *G305S* STRAINS 218
6.3 GENOME-WIDE EPISTASIS ANALYSIS SCREENS IN *S. pombe* 220

References 222

Appendices 247

List of Figures

Figure 1.1	Factors that determine DNA replication fidelity	6
Figure 1.2	The different pathways involved in rectifying a replication error made by Pol ε or δ	7
Figure 1.3	The eukaryotic DNA replication fork	12
Figure 1.4	Crystal structure of *S. cerevisiae* Pol ε catalytic domain	19
Figure 1.5	The location of germline and somatic Pol δ and ε exonuclease domain mutations associated with cancer	27
Figure 1.6	Sequence alignment of *POLD1* exonuclease domain mutations in different species	28
Figure 1.7	Schematic outlining the main aims of the project	34
Figure 3.1	The first step in constructing the exonuclease domain mutations (EDMs) in *S. pombe* is via site-directed mutagenesis	63
Figure 3.2	Steps II, III and IV in the construction of the EDMs. Digestion and ligation of the vector and insert, followed by transformation of the vector-insert construct into *E. coli*	65
Figure 3.3	The final two steps (V and VI) in the construction of EDMs in *S. pombe*. Linearisation of the mutant plasmid is required prior to yeast transformation	67
Figure 3.4	Characterisation of yeast transformants' genotype via colony PCR and restriction digestion	69
Figure 3.5	Yeast strains contain the desired *pol3* mutations	70
Figure 3.6	Confirmation of introduction of the *pol3D386A* mutation in *S. pombe*	73
Figure 3.7	*Pol3P311L/R* is homologous to *pol2P287R*, which affects a conserved proline residue required for proofreading. The *pol3P311R* mutation in strains is confirmed	74
Figure 3.8	Diagrams outlining the canavanine resistance fluctuation assay method	79
Figure 3.9	Can^r mutation rates of the indicated strains relative to wild type, determined by fluctuation analysis	80
Figure 3.10	*Pol2P287R* has a mutation rate 30-40 times higher than that of *pol3P311R*	86
Figure 3.11	The *pol3* EDMs do not have increased replicative slippage when synthesising GT repeat sequences	87
Figure 3.12	The *pol3* proofreading domain mutations do not have growth defects	89
Figure 3.13	DNA damaging agents	92
Figure 3.14	The *pol3* mutants are not sensitive to UV or 4NQO DNA damage	94
Figure 3.15	*Pol3L458P* is not sensitive to UV and 4NQO DNA damage	95
Figure 3.16	*Pol3P311L* and *pol3G305S* mutants confer sensitivity to HU	97
Figure 3.17	*Pol3L458P, D300N and D386A* mutants are not sensitive to DNA damaging agents	99
Figure 4.1	Components involved in the *S. pombe* checkpoint response	118
Figure 4.2	Mus81 cleaves stalled and unresolved replication forks	124
Figure 4.3	A schematic outlining the construction of Pol3-tagged EDMs	128
Figure 4.4	Characterisation of *pol3*-tagged yeast transformants' genotype via colony PCR	129
Figure 4.5	*Pol3* EDMs have physiologically normal levels of the Pol3 protein	130
Figure 4.6	Diagram of the '*cut*' phenotype assay	133
Figure 4.7	A significant proportion of *pol3P311L* cells show a '*cut*' phenotype in HU and the length of *pol3G305S* cells is significantly greater than wild type under normal conditions	135
Figure 4.8	The *pol3P311L* and *pol3G305S* mutations are synthetically sick upon *rad3* inactivation. The *pol3L458P* strain is temperature-sensitive (ts)	139
Figure 4.9	Schematic: Step-by-step flow chart of the relative viability assay method	146

Figure 4.10	The viability of *pol3G305S* is compromised in HU	147
Figure 4.11	FACS analysis of cells released from S phase arrest, induced by the addition of HU: *pol3G305S* has a relatively slower recovery from cell cycle block and release	149
Figure 4.12	The *pol3D300N* and *pol3D386A* mutations are synthetically sick with *mus81*Δ	156
Figure 4.13	The *pol3*, *mus81*Δ double mutants grow modestly worse than *mus81*Δ in the presence of hydroxyurea	157
Figure 4.14	Increased RNR activity, followed by elevated dNTP pools, partially rescues the HU sensitivities of the *pol3P311L* and *pol3G305S* strains	161
Figure 4.15	A proposed model to explain the HU sensitivities of the *pol3P311L* and *G305S* EDMs	168
Figure 5.1	A schematic representation of a genetic cross using the PEM-2 system	178
Figure 5.2	Simplified step-by-step diagrams depicting the construction of the PEM-2 system in the query strain and subsequent systematic genetic interaction mapping	179
Figure 5.3	Examples of epistatic analysis and confirmation of two renowned synthetic interactions via tetrad analysis	190
Figure 5.4	Flow chart illustrating the selection criteria for synthetically sick/lethal (SSL) interactions and the identification of known and novel genetic interactions with *pol3*	191
Figure 5.5	Tetrad analyses to confirm a selection of hits from the high-throughput screen	205
Figure 5.6	There is no clear negative synthetic interaction between *pol3L458P* and *mre11*	207
Figure 5.7	*Pol3L458P* does not have an SSL interaction with *rad50*, part of the MRN complex	208

List of Tables

Table 1.1	The genes and subunit sizes of Pols α, ε, and δ across different species	13
Table 1.2	Fidelity rate and key functions of replicative polymerases	14
Table 2.1	Strains used in this study	37
Table 2.2	Primers used during the course of mutant construction, colony PCR and sequencing of plasmids and genomic *S. pombe* DNA	43
Table 2.3	Plasmids used and constructed in this study	52
Table 2.4	Antibodies used in this study	56
Table 3.1	Rate of spontaneous mutation in haploid *pol3* mutants	81
Table 3.2	*POLD1* EDM orthologues	100
Table 5.1	Twenty-six potential SSL interactions that were validated by tetrad analysis	192

Nomenclature

Species are denoted in italics, for example, *S. pombe*, *S. cerevisiae* and *H. sapiens*. Designated prefixes are used where necessary to avoid confusion: Sp. = *Schizosaccharomyces pombe*, Sc. = *Saccharomyces cerevisiae* and Hs. = *Homo sapiens*, e.g. Sp. Pol3.

Schizosaccharomyces pombe

Genes in the wild-type locus are given the $^{+}$ suffix, e.g. *rad3*$^{+}$. Genes are denoted by lower-case letters in italics. Deletion/null mutants are indicated by Δ, e.g. *mus81*Δ. A double colon (::) designates an insertion into the genome disrupting the gene in question, e.g. *mus81::ura4* signifies the *mus81* gene disrupted by *ura4*. Equally, "::" also means that the gene or the mutation introduced into the gene of interest is marked by a selective marker, such as G418 antibiotic resistance: e.g. *pol3(d)L458P::kanMX6*. Letters and numbers following the gene name identify mutant alleles, e.g. *ade6-M210*. Names of proteins are denoted by non-italics with a capital first letter, e.g. Mus81.

Saccharomyces cerevisiae

Genes are denoted by capital letters in italics, e.g. *MEC1*. Deletion/null mutants are signified by lower-case italics, e.g. *pol3*, with a suffix designating the allele where necessary, e.g. *pol3-01*. Names of proteins are denoted by non-italics letters with a capitalised first letter e.g. Pol3.

Mammalian/human

Genes are denoted by capital letters in italics, e.g. *POLD1*. Homozygous or heterozygous knockouts are shown as -/- or +/-, respectively. Protein names are denoted by capital letters in non-italics, e.g. POLD1.

Abbreviations

ºC	degrees Celsius
Δ	gene deletion
µg	micrograms
µl	microlitres
µM	micromolar
4NQO	4-nitroquinoline 1-oxide
A	amps
ADS	anti-diploid selection
APC	adenomatous polyposis coli
ATM	ataxia telangiectasia mutated
ATR	ATM and Rad3-related
ATRIP	ATR interacting protein
BER	base excision repair
BIR	break-induced replication
BLM	bloom syndrome helicase
bp	base pair
BrC	breast cancer
Can	canavanine
Can^r	canavanine resistant/resistance
CCD	charge-coupled-device
CDK	cyclin dependent kinase
CIA	cytosolic iron-sulfur protein assembly
CIN	chromosome instability
CMG	Cdc45-MCM-GINS
CNV	copy number variant
CPT	camptothecin
CRC	colorectal cancer
CLRC	cullin-dependent E3 ubiquitin ligase/histone H3-K9 methyltransferase
CSN	COP9 signalosome complex
cut	cell untimely torn
CYC	cycloheximide
Cyh^R	cycloheximide resistant/resistance
Cyh^S	cycloheximide sensitive/sensitivity
DAPI	4’6’-diamidino-2-phenylindole
DDC	DNA damage checkpoint
DDK	dbf4-dependent kinase
DDR	DNA damage response
DMS	double mutant selection
DMSO	dimethyl sulfoxide
DNA	deoxyribonucleic acid
dNTP	deoxyribonucleotide triphosphate
dATP	deoxyadenosine triphosphate
dCTP	deoxycytidine triphosphate
dGTP	deoxyguanosine triphosphate
dTTP	deoxythymidine triphosphate
DSB	double-strand break

DSBR	double-strand break repair
dsDNA	double-stranded DNA
EC	endometrial cancer
EDM	exonuclease domain mutant/mutation
EDTA	ethylenediamine tetra-acetic acid
E-MAP	epistatic mini-array profile
EMM	edinburgh minimal medium
FACS	fluorescence-activated cell sorting
FAP	familial adenomatous polyposis
$G418^R$	geneticin resistance
$G418^S$	geneticin sensitivity
GCR	gross chromosomal rearrangement
GI	genetic interaction
GINS	Go-Ichi-Ni-San
GO	gene ontology
GT	guanine-thymine
HCl	hydrochloric acid
HF	high fidelity
HJ	holliday junction
HR	homologous recombination
HNPCC	hereditary non-polyposis colorectal cancer
Hs	homo sapiens
HU	hydroxyurea
HYG	hygromycin
HYG^R/Hyg^R	hygromycin resistant/resistance
HYG^R/Hyg^S	hygromycin sensitive/sensitivity
indels	insertions and deletions
$Kan^R/G418^R$	kanamycin/G418 resistant/resistance
kb	kilobase
kbp	kilobase base pair
kDa	kilodalton
L	litres
LB	luria-Bertani/lysogeny broth
LiAc	lithium acetate
LOH	loss of heterozygosity
M	molar
MCM	minichromosome maintenance
mg	milligrams
ml	millilitres
mM	millimolar
MMR	mismatch repair
MMS	methyl methanesulfonate
mol	moles
MRN	Mre11, Rad50, Nbs1
MSI	microsatellite instable/microsatellite instability
MSS	microsatellite stable/microsatellite stability
MSS-MLE	Ma-Sandri-Sarkar Maximum Likelihood Estimator
MTL	mating-type locus
MTS	mating-type selection
MUTYH	MutY DNA glycosylase

MW	molecular weight
NEB	New England Biolabs
NER	nucleotide excision repair
nm	nanometres
nM	nanomolar
NPD	non-parental ditype
OD	optical density
OD_{600}	optical density (absorbance at 600 nm wavelength)
ORC	origin recognition complex
ORF	open reading frame
PI3KK	phosphatidylinositol 3-kinase-related kinases
PI3K	phosphatidylinositol 3-kinase
PBS	phosphate buffered saline
PBS-T	phosphate buffered saline, 0.1% tween
PCNA	proliferating cell nuclear antigen
PCR	polymerase chain reaction
PD	parental ditype
PEM	*pombe* epistasis mapper
PEM-2	*pombe* epistasis mapper-2
PMG	*pombe* glutamate medium
pmol	picomoles
Pol α	DNA polymerase alpha
Pol δ	DNA polymerase delta
Pol ε	DNA polymerase epsilon
PPAP	polymerase proofreading associated polyposis
pre-RC	pre-replicative complex
PRR	post-replication repair
RC	replication checkpoint
RFC	replication factor C
rNMP	ribonucleoside monophosphate
RNA	ribonucleic acid
RNR	ribonucleotide reductase
ROS	reactive oxygen species
RPA	replication protein A
Sc/*S. cerevisiae*	*Saccharomyces cerevisiae*
SD	standard deviation
SDS	sodium dodecyl sulphate
SDS-PAGE	SDS-polyacrylamide gel electrophoresis
SEM	standard error of the mean
SGA	synthetic genetic array
Sp/*S. pombe*	*Schizosaccharomyces pombe*
SPAS	sporulation agar with supplements
SSB	single-strand break
ssDNA	single-stranded DNA
SSL	synthetically sick/lethal
t	time-point
TAE	tris/acetate/EDTA
TCA	trichloroacetic acid
TCGA	The Cancer Genome Atlas
TLS	translesion synthesis

Top1	topoisomerase 1
Tris-HCl	tris-hydrochloric acid
ts	temperature-sensitive/temperature sensitivity
TT	tetratype
U	units
UV	ultraviolet
V	volts
WRN	Werner syndrome ATP-dependent helicase
WT/Wt	wild-type/wild type
YES	yeast extract with supplements
YFG	your favourite gene

Chapter 1 Introduction

1.1 GENOME INSTABILITY AS A HALLMARK OF CANCER

In the revised Hallmarks of Cancer, genome instability is defined as an 'enabling characteristic' of cancer, as well as tumour-promoting inflammation (Hanahan and Weinberg, 2011). Two emerging hallmarks were also identified: deregulating cellular energetics and escaping immune destruction (Hanahan and Weinberg, 2011). Genomic instability generates stochastic mutations that occasionally introduce genetic changes that drive cancer cells to obtain the other hallmarks, which are sustained proliferation signalling, angiogenesis, metastasis and evading apoptosis (Hanahan and Weinberg, 2000).

Genomic instability can originate from defects in DNA replication, repair, chromosome segregation and cell cycle checkpoints. This can subsequently lead to elevated mutation rates, gross chromosomal rearrangements (GCRs) and aneuploidy. Cancer cells can exhibit numerous GCRs including translocations, deletions, inversions and duplications (Lengauer et al., 1998). The genetic changes that contribute to tumourigenesis tend to affect three main types of genes – proto-oncogenes, tumour suppressor genes, and DNA repair genes (the caretaker genes). These changes are sometimes called "drivers" of cancer. Hanahan and Weinberg (2011) state that mutagenesis and, thus, genomic instability, confers a selective advantage for neoplastic progression in tumours. During the course of acquiring mutations in certain genes required to bring about tumourigenesis, cancer cells frequently increase the rates of mutation through increased sensitivity to mutagenic agents and/or through a malfunction in one or more components of the genomic maintenance and surveillance systems (Salk et al., 2010; Hanahan and Weinberg, 2011).

According to Negrini et al (2010), chromosomal instability (CIN) is the predominant form of genomic instability both in hereditary and sporadic (non-hereditary) cancers. Chromosome instability refers to abnormal chromosome number and structure, and is associated with aberrant mitoses (Negrini et al., 2010). There are other forms of genomic instability apart from CIN, such as increased frequencies of base-pair mutations and microsatellite instability (MSI), which is defined by the expansion or contraction of the number of short repeats present in microsatellite sequences (Fishel et al., 1993). MSI is commonly the product of mutations in DNA mismatch repair (MMR) genes and is prevalent in colon cancer (Fishel et al., 1993; Leach et al., 1993).

1.2 MUTAGENESIS IN COLON CANCER

Colon cancer is an important cause of mortality worldwide and is most common in developed countries where it accounts for 10% of all cancer cases (Ferlay et al., 2010). More than 20% of colon cancer cases are associated with a family history of the disease and there are mutations in certain DNA repair genes that make a person more likely to develop colorectal cancer (CRC) in his/her adult life (Valle, 2014). CRC syndromes caused by known high-penetrance CRC genes collectively account for 2%-6% of all cases of CRC (Valle, 2014), and some examples of those affected genes include: the APC gene (a tumour suppressor), mismatch repair (MMR) genes (including MSH2, MLH1, MSH6 and PMS1/2) and the base excision repair gene MUTYH (Briggs and Tomlinson, 2013; Lynch and De la Chapelle, 2003; Sieber et al., 2003). Most CRCs result from defects in the MMR genes that are present in Lynch syndrome, which is also called hereditary non-polyposis colorectal cancer (HNPCC) (Lynch and Smyrk, 1996). However, in recent whole-genome sequencing studies, a small sub-set of familial patients presenting with colorectal adenocarcinomas did not possess any germline mutations in the known cancer predisposition genes (The Cancer Genome Atlas Network, 2012). This led to the

discovery of two germline mutations located in the conserved exonuclease (proofreading) domain motifs of eukaryotic DNA Polymerases ε and δ (Palles et al., 2013). These mutations define a new type of CRC genetic predisposition and Palles et al (2013) is the first paper that represents the association between defects in core replicative processes and human cancer predisposition.

Furthermore, the fission yeast *Schizosaccharomyces pombe* (*S. pombe*) shares many genetic and biochemical characteristics with higher eukaryotic cells. Since *S. pombe* can be rapidly cultured and genetically manipulated in the laboratory, it provides a good model for studying evolutionarily highly conserved cellular processes, such as DNA replication, and it can elucidate the link between failed replicative processes and the development of cancer. In this study, I focus on the correlation between exonuclease domain mutations (EDMs) in Pol δ and potential tumourigenesis due to increased mutation rate or other replication defects.

To understand the impact that DNA polymerase defects can have on tumourigenesis, it is important to revise their main roles in the cell.

1.3 DNA REPLICATION AND REPLICATIVE DNA POLYMERASES

1.3.1 Overview of DNA replication

DNA replication begins at an origin and usually proceeds bidirectionally (Huberman and Riggs, 1968; Newlon et al., 1974). DNA replication is notoriously semiconservative (Meselson and Stahl, 1958). DNA helicases unwind double-stranded DNA (dsDNA) to reveal single-stranded DNA (ssDNA) for replication. Each DNA strand serves as a template for the synthesis of a new strand, producing two new DNA molecules, each with one new strand and one old strand. A new strand of DNA is always synthesised in the 5'-3' direction. Subsequently, DNA polymerases work by incorporating four deoxynucleotides (dTTP, dCTP, dGTP, dATP) at the

free 3'-OH in the growing nascent DNA chain, that is complementary to the parent/template ssDNA, using the base pair rules A•T and G•C (Watson and Crick, 1953). The precursor nucleotides are assembled complementarily on the growing ssDNA chain with great precision due to the phenomenon of Watson-Crick base pairing. The underlying features of DNA replication have been proven to be similar in eukaryotes and prokaryotes, allowing for some divergence in different organisms.

The main function of replicative DNA polymerases is to replicate the genome accurately, so to permit the transmission of correct genetic information during cell division. In eukaryotic cells, this occurs during S phase and the replicated chromosomes are then split to daughter cells during mitosis and cytokinesis. The faithful replication of DNA is a prerequisite for maintaining genome stability in the cell by preventing mutagenesis and tumourigenesis (Kunkel and Bebenek, 1988). Eukaryotic DNA replication has extremely high fidelity: it is estimated that one incorrect base occurs for every 10^9 to 10^{10} nucleotides replicated (**Figure 1.1**) (Loeb, 1991). This remarkably low error rate is due to a combination of highly accurate nucleotide incorporation, the intrinsic proofreading abilities of the two main replicative polymerases (Pols ε and δ), and post-replication repair, otherwise known as DNA mismatch repair (MMR) (**Figures 1.1 and 1.2**) (Kunkel, 2004; Loeb and Monnat, 2008; Umar and Kunkel, 1996).

DNA replication is an intricate process involving many proteins. The synthesis of a DNA molecule is divided into three steps: initiation, elongation and termination. Initiation is a tightly regulated process, as such that replication occurs only once in each cell cycle. Initiation of replication in all eukaryotes starts with the origin recognition complex (ORC) which marks origins. Initiation leads to assembly of the replication complex, also called the replisome, in a two-step process: the first is pre-replicative complex (pre-RC) formation, which then signals the assembly of more replication factors in a second step via CDK and DDK (two serine-

threonine kinases) activation, and this leads to initiation of DNA replication. This process is well-controlled by the loading of replication factors in series (Kearsey and Cotterill, 2003; Zegerman and Diffley, 2007; Diffley, 2011; Yeeles et al., 2015; Deegan et al., 2016), and the binding of numerous replication factors to chromatin is interdependent. The elongation step of replication includes two distinct parallel functions, which are leading-strand synthesis and lagging-strand synthesis.

Eukaryotic DNA polymerases fall into five families: A, B, RT, X and Y, based on sequence comparisons between the polymerase families (Cotterill and Kearsey, 2009). DNA polymerases have a number of different functions, such as bulk chromosomal replication, DNA repair, recombination and specialised types of replication (e.g. translesion synthesis) (Lange et al., 2011). The replicative polymerases belong to the B family of polymerases and there are four within this family: Pols α, ε, δ and ζ. Pols α, ε and δ are involved in the bulk of chromosomal DNA replication during S phase but Pols ε and δ also play a role in DNA repair which will be later discussed in more detail (Hubscher et al., 2002; Shcherbakova et al., 2003a; Lange et al., 2011). Only Pols δ and ε possess 3'-5' exonuclease (proofreading) activity (Garg and Burgers, 2005). Pol ζ is not responsible for the bulk of DNA replication but is important in bypassing DNA lesions by replicating over them to allow the smooth and efficient progression of replication forks and the completion of DNA replication (Gan et al., 2008; Lange et al., 2012). Pol ζ is classed as a translesion synthesis (TLS) polymerase and this type of synthesis is error-prone (Suzuki et al., 2018; Lee et al., 2014).

Cells with faulty DNA replication can rapidly accumulate mutations that evoke deleterious changes to cell-cycle regulation, leading to cancer. Therefore, it is paramount that replication is executed with high fidelity to preserve genomic stability.

Figure 1.1

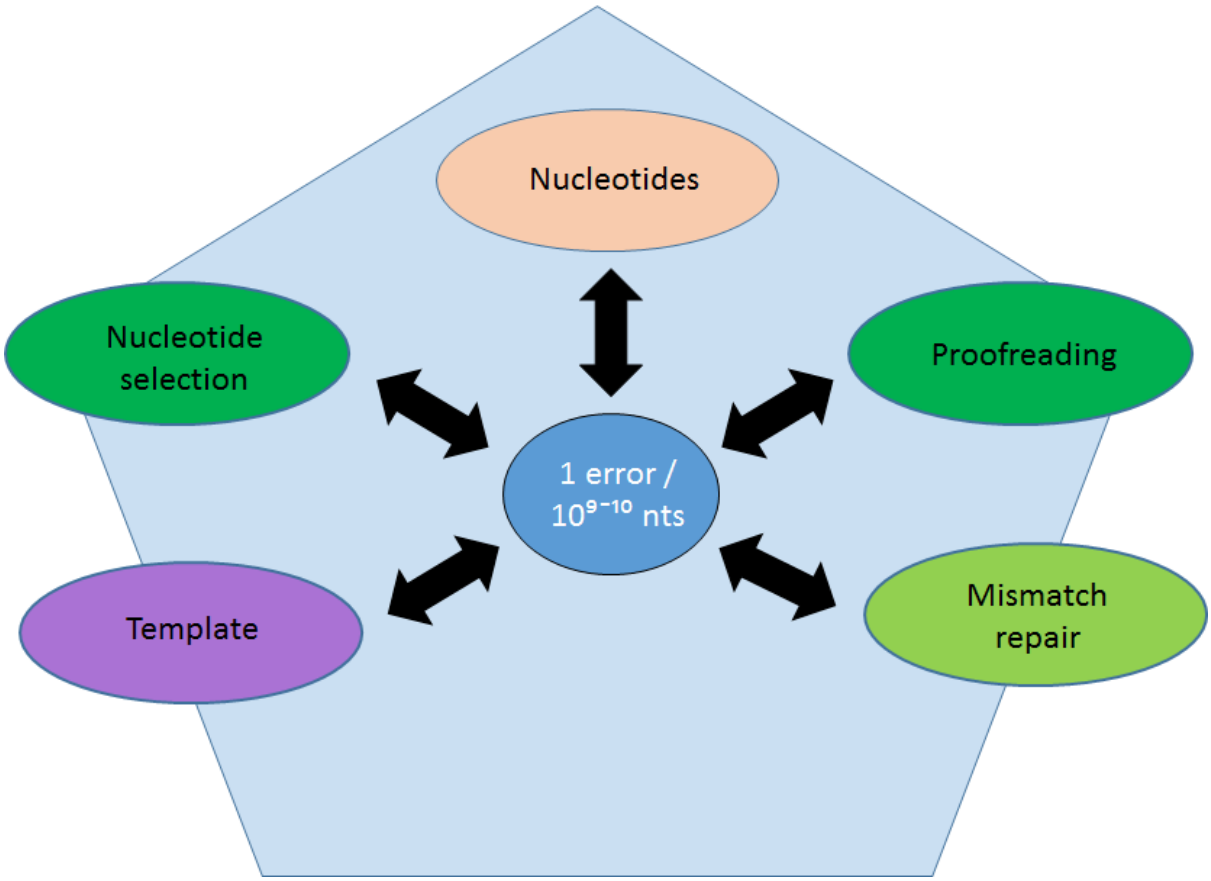


Figure 1.1: Factors that determine DNA replication fidelity. The key factors involved in managing the overall fidelity of DNA replication are: nucleotide selectivity, proofreading activity, mismatch repair, nucleotide pools and the nature of the DNA template (sequence context and the presence of DNA lesions). Missense mutations in the DNA polymerase can affect the nucleotide selectivity and proofreading efficiency and, subsequently, decrease replication fidelity. Inactivation of mismatch repair reduces fidelity. The sequence context and presence of DNA lesions in the DNA template will impact replication fidelity. Altered dNTP pools, such as an increase in ribonucleotides or an increase/decrease in dNTPs, can impact fidelity creating either a mutator or antimutator phenotype in the cell. Figure adapted from Ganai and Johansson (2016).

Figure 1.2

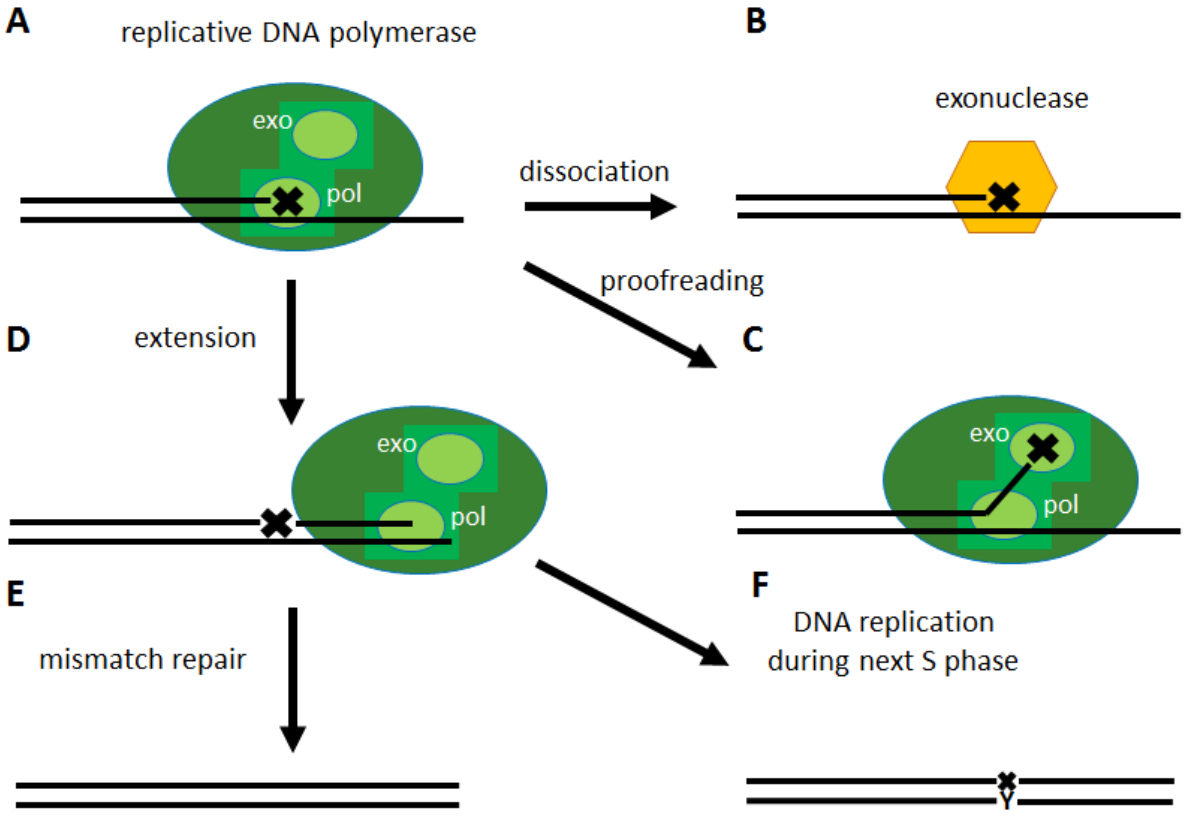


Figure 1.2: The different pathways involved in rectifying a replication error made by Pol ε or δ. (A) A substitution, insertion or deletion mutation is created by the Pol ε/δ in the growing nascent DNA strand. **(B)** The replicative DNA polymerase stalls as a result of the mutational barrier and, subsequently, dissociates from the replisome. Another protein with exonuclease activity removes the replication error and then Pol ε/δ resumes DNA synthesis: e.g., Pol δ can proofread errors made by Pol ε or Pol α. **(C)** The replication error is removed via the replicative DNA polymerase's intrinsic 3'-5' exonuclease activity. Thereafter, DNA synthesis continues. **(D)** Pol ε/δ inserts an incorrect nucleotide and continues to add more nucleotides. **(E)** Post-replication repair, called mismatch repair, corrects the mutation. **(F)** If the replication error is not rectified, a permanent alteration to the DNA sequence will be made when the genome is next duplicated. Figure adapted from Ganai and Johansson (2016).

1.3.2 Polymerase alpha (Pol α)

In order to initiate synthesis on an ssDNA molecule, DNA polymerases need a primer, consisting of RNA or DNA, and Pol α is important in primer synthesis (**Figure 1.3**) (Johansson and Macneill, 2010). Pol α is a four subunit enzyme: the largest subunit (Sp. Pol1) is responsible for polymerase activity and the two smallest subunits (Sp. Spp1 and Spp2) possess DNA primase activity, responsible for synthesising short RNA primers (approximately 10 nucleotides) (see **Table 1.1**) (Perera et al., 2013; Hübscher et al., 2000; Zhu et al., 2007). Following primer synthesis, DNA synthesis is carried out by the largest subunit of Pol α to produce a short stretch of DNA, 30-40 nucleotides long, which tends to be error-prone because Pol α does not have exonuclease proofreading ability (Hübscher et al., 2000; Zhu et al., 2007; Perera et al., 2013). Pol α synthesises the primer to initiate DNA synthesis, allowing Pol ε and Pol δ to take over leading and lagging strand synthesis, respectively (**Figure 1.3**) (Pavlov et al., 2006b). The primer that Pol α synthesises provides a 3'-hydroxyl (3'-OH) group that can be extended by the incoming polymerase; this configuration of the primer is paramount because polymerases can only polymerise in the 5' to 3' direction (Cotterill and Kearsey, 2009). The process of either Pol ε or Pol δ taking over DNA synthesis from Pol α is called polymerase switching (Maga et al., 2000; Mossi et al., 2000). Replication errors made by Pol α can be corrected via the following pathways: strand-displacement synthesis, ribonucleotide excision repair (RER) involving the RNase H enzymes, and/or MMR (reviewed in Kunkel and Erie, 2015; McElhinny et al., 2010b). The latter, except RER, will be discussed later in this chapter.

1.3.3 Polymerase epsilon (Pol ε)

Pol ε is a tetrameric (four subunit) complex which in *S. pombe* comprises a large catalytic subunit Pol2/Cdc20 and three smaller subunits Dpb2, Dpb3 and Dpb4 (see **Table 1.1**). Pol ε replicates the leading strand during DNA replication (Pursell et al., 2007; McElhinny et al.,

2008; Kunkel and Burgers, 2008): the leading strand is the strand copying the 3'-5' old/template strand, thus Pol ε can synthesise the nascent strand continuously from the 5' to 3' direction without dissociating from the replication fork. The largest, catalytic subunit consists of both 5'-3' polymerase and 3'-5' exonuclease activities (Shevelev and Hübscher, 2002). Pol ε is loaded at origins of replication via a very complex process involving interaction with replication factors, such as Sld2, Sld3, Dpb11 and the Cdc45 MCM2-7 GINS (CMG) complex, to form the pre-loading complex, which is essential for the initiation of DNA replication (Muramatsu et al., 2010; Kang et al., 2012). After a single priming event by Pol α, Pol ε can synthesise the leading strand (**Figure 1.3**) (Cotterill and Kearsey, 2009). It is speculated that Proliferating Cell Nuclear Antigen (PCNA), which is assembled onto DNA via Replication Factor C (RFC), interacts with Pol ε and maintains its association to the primer or template (**Figure 1.3**) (Burgers, 1991; Hamatake et al., 1990; Kearsey and Cotterill, 2003). A region of Pol ε may also have a role in initiation as it associates with origins and has a C-terminal domain that is essential for replication initiation (Zegerman, 2013; Pavlov et al., 2006b). Pol ε is intrinsically more processive than Pol δ because it is thought to contain a unique domain in the catalytic subunit that permits Pol ε to encircle the nascent dsDNA, which prevents the enzyme from readily dissociating from the replication fork in the absence of PCNA (Hogg et al., 2014; Jain et al., 2014). There is no evidence to suggest that Pol ε substitutes for DNA synthesis on the lagging strand, nor does it perform 3'-5' exonuclease degradation of misincorporated nucleotides on the lagging strand during replication (Pursell et al., 2007; Miyabe et al., 2011; Georgescu et al., 2015). This may be because Pol ε is highly processive and strongly associated with the replication fork.

The other smaller subunits of Pol ε are important in the overall integrity of the enzyme, loading of the polymerase on to double-stranded DNA (dsDNA), interaction with cofactors such as PCNA and CMG, and replication checkpoint signalling (Kunkel and Burgers, 2008; Aksenova

et al., 2010; Garbacz et al., 2015; Langston et al., 2014; Sengupta et al., 2013). Secondly, in addition to chromosomal DNA replication, Pol ε has an epigenetic role: the non-essential subunits, Dpb3 and Dpb4, consist of histone-fold motifs required for the stable epigenetic inheritance of a telomere gene (Iida and Araki, 2004). Moreover, Fei et al (2012) showed that the main catalytic subunit, Cdc20, is a part of a silencing complex (involved in H3K9 methylation) that regulates RNA Pol II activity in heterochromatin.

1.3.4 Polymerase delta (Pol δ)

Pol δ is a tetramer consisting of a large catalytic subunit Pol3/Cdc6 and three smaller subunits, Cdc27, Cdc1 and Cdm1, however, the smallest of these subunits, Cdm1, is not essential and does not exist in some species, such as budding yeast (Reynolds et al., 1998) (**Table 1.1**). The largest catalytic subunit, like Pol ε, comprises both the polymerase and exonuclease motifs (Shevelev and Hübscher, 2002). It has been shown that Pol δ, and not Pol ε, replicates the lagging strands of the replication fork via Okazaki fragment synthesis (Pavlov et al., 2006a; McElhinny et al., 2008; Larrea et al., 2010; Miyabe et al., 2011). Lagging-strand synthesis is the strand whose orientation does not allow it to be continuously synthesised in the 5'-3' direction; instead, it must be synthesised in a discontinuous manner. That is why Pol δ produces a series of short pieces of DNA, called Okazaki fragments, that are subsequently processed and joined together by other proteins, like Fen1 and DNA ligase (**Figure 1.3**) (Garg and Burgers, 2005). Pol α primes each Okazaki fragment on the lagging strand and then polymerase switching occurs to Pol δ involving PCNA and replication factor C (RFC) (**Figure 1.3**) (Garg and Burgers, 2005; Garg et al., 2004). Therefore, Pol δ is loaded many more times onto the replication fork than Pol ε which, once having started replicating, does not readily dissociate from the leading strand. Unlike Pol ε, PCNA remains tethered to Pol δ and topologically linked

to dsDNA throughout replication, enhancing the processivity of Pol δ (Cotterill and Kearsey, 2009; Arroyo et al., 1996).

Since Okazaki fragments are initiated with Pol α–synthesised RNA, DNA ligation cannot occur until the RNA is excised. This removal primarily requires both Pol δ and the structure specific flap endonuclease I (Fen1) (Kunkel and Erie, 2015). When Pol δ reaches the 5′ terminus of the previous Okazaki fragment, it continues replicating by displacement of the RNA primer, forming a 5′ flap, which is then cut by Fen1 (Kunkel and Erie, 2015). In order to entirely eliminate the RNA primer, it has been proposed that repetitious Pol δ strand displacement and Fen1 cleavage is required, a process called nick translation (Garg et al., 2004). The forward movement of Pol δ that leads to strand displacement is countered by the exonuclease activity of Pol δ: for example, after limited strand displacement, Pol δ degrades several nucleotides from the 3'-terminus of the nascent strand, using its exonuclease activity, back to the nick position, in a process called idling (Garg et al., 2004). This allows the 5′-displaced strand of the adjacent Okazaki fragment to realign and generate a ligatable nick. Idling helps to maintain the position of the nick in the absence of other processing activities (Prindle and Loeb, 2012). It has been proposed that without idling, unregulated strand-displacement synthesis creates problematic long flaps that require alternative processing mechanisms (Garg et al., 2004). In the event of excess flaps, Dna2, an exonuclease and helicase, intervenes in Okazaki fragment maturation and, unlike Fen1, it is an essential protein for cell survival in yeast (Garg and Burgers, 2005). Extensive strand displacement synthesis by Pol δ causes the formation of long flaps (~30 nucleotides) that are substrates for Dna2 nuclease activity, not Fen1 nuclease activity (Garg and Burgers, 2005). Thus, Dna2 trims the flaps so that they can be processed by Fen1 (Tsutsui et al., 2005).

Figure 1.3

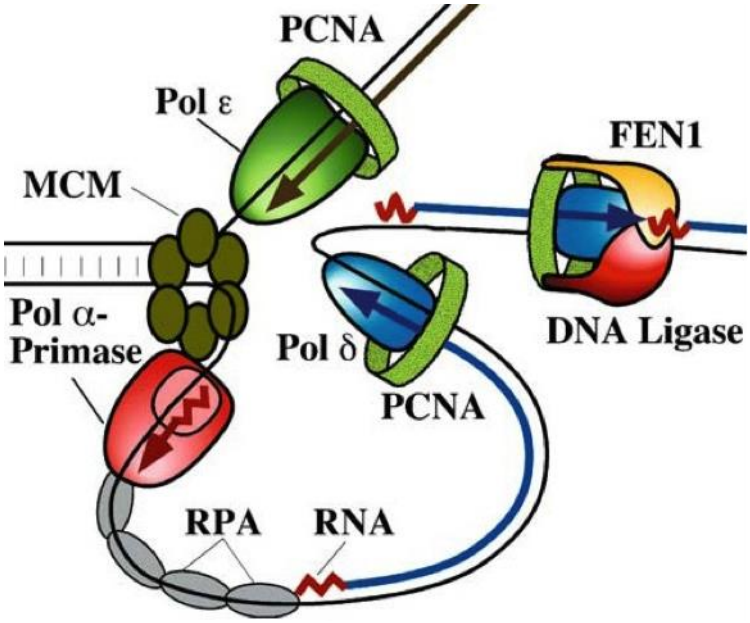


Figure 1.3: The eukaryotic DNA replication fork. Displayed are the main set of proteins and enzymes needed for replication fork propagation. During initiation of replication, the minichromosome maintenance (MCM) complex is loaded onto DNA by various different factors to unwind the helix and create single-stranded DNA (ssDNA). It is part of the pre-replication complex (Sclafani and Holzen, 2007) (other proteins and co-factors, not shown above, are involved in the loading of Pol ε onto the replication fork). Polymerase switching from Pol α to Pol δ on the lagging strand is facilitated by replication protein A (RPA), replication factor C (RFC) and proliferating cell nuclear antigen (PCNA) (Waga and Stillman, 1998). RPA coats ssDNA and prevents it from winding back in on itself and forming secondary structures (Pavlov et al., 2006b). On the leading strand, polymerase switching only occurs once. On the lagging strand, switching is required each time Pol α forms a segment of the Okazaki fragment. Synthesis by Pol δ terminates when it clashes with the 5′ terminus of the preceding Okazaki fragment (Cotterill and Kearsey, 2009). Accessory factors such as the Flap endonuclease/exonuclease 1 (Fen1), Dna2 exonuclease and DNA ligase are needed to remove the RNA primer (synthesised by Pol α) and to seal the nick between the 3’ end of the newly synthesized strand and the 5’ end of the previous Okazaki fragment, allowing completion of DNA synthesis. (Cotterill and Kearsey, 2009; Reha-Krantz, 2010). Image adapted from Garg and Burgers (2005).

In addition to lagging-strand replication and Okazaki fragment maturation, it is possible that Pol δ takes over leading-strand synthesis in some circumstances because the N-terminal exo-pol domain of Pol ε is non-essential (Kesti et al., 1999). The latter model is supported by a study that implies Pol δ initiates leading-strand synthesis before it is displaced by Pol ε at certain replicons in the genome (Daigaku et al., 2015). Furthermore, it has been reported in fission yeast that Pol δ replicates both the leading and lagging strands after homologous recombination (HR)-dependent fork restart (Miyabe et al., 2015).

Table 1.1 : The genes and subunit sizes of Pols α, ε, and δ across different species

	Pol α-primase	**Pol ε**	**Pol δ**
S. pombe	Pol1 - 159 kDa	Pol2 (Cdc20) - 253 kDa	Pol3 (Cdc6) - 124 kDa
	Pol12 (Spb70) - 64 kDa	Dpb2 - 67 kDa	Cdc1 - 51 kDa
	Pri1 (Spp1) - 52 kDa	Dpb3 - 22 kDa	Cdc27 - 42 kDa
	Pri2 (Spp2) - 53 kDa	Dpb4 - 24 kDa	Cdm1 - 19 kDa
S. cerevisiae	Pol1 - 167 kDa	Pol2 - 256 kDa	Pol3 - 125 kDa
	Pol12 - 79 kDa	Dpb2 - 78 kDa	Pol31 - 55 kDa
	Pri1 - 48 kDa	Dpb3 - 23 kDa	Pol32 - 40 kDa
	Pri2 - 62 kDa	Dpb4 - 22 kDa	N/A
H. sapiens	PolA1 - 166 kDa	PolE - 261 kDa	PolD1 - 124 kDa
	PolA2 - 68 kDa	PolE2 - 59 kDa	PolD2 - 51 kDa
	Prim1 - 48 kDa	PolE3 - 17 kDa	PolD3 - 66 kDa
	Prim2A - 58 kDa	PolE4 - 12 kDa	PolD4 - 12 kDa

Table 1.1 is modified from Kunkel and Burgers (2008). N/A – Not Applicable.

1.3.5 Pol ε versus Pol δ

The two polymerases show sequence similarity over their exonuclease domains and share high levels of evolutionary conservation across various species (Heitzer and Tomlinson, 2014).

While studies in yeast have shown that Pol ε replicates the leading strand and Pol δ replicates the lagging strand (McElhinny et al., 2008; Shcherbakova and Pavlov, 1996; Morrison and Sugino, 1994; Miyabe et al., 2011), it is yet to be ascertained whether this defined pattern of

replication always occurs. There is evidence to suggest that polymerase switching from Pol ε to Pol δ takes place if the replication fork stalls on the leading strand (Morrison et al., 1993; Miyabe et al., 2015). The latter may be possible, particularly upon inactivation of Pol ε proofreading. Overall, the division of labour is broadly maintained across the entire genome, however, as previously mentioned, it has been reported in yeast that Pol δ initiates leading-strand synthesis, followed by exchange for Pol ε at particular replicons in the genome in unperturbed DNA replication (Daigaku et al., 2015).

1.3.6 Polymerase fidelity, exonuclease activity and other DNA repair roles

Both Pols ε and δ show a high fidelity of synthesis with an error rate of 10^{-7} (**Table 1.2**) (Heitzer and Tomlinson, 2014). This is due to discrimination inherent to nucleotide selectivity during DNA synthesis (reviewed in Ganai and Johansson, 2016), and intrinsic proofreading activity (Shcherbakova et al., 2003b; Fortune et al., 2005; Bebenek and Kunkel, 2004) (see **Figure 1.1**).

Table 1.2: Fidelity rate and key functions of replicative polymerases

Polymerase	Fidelity (Error per bp)	3'-5' Exonuclease activity	Function
α	10^{-4}	No	Synthesises RNA primers (7 bp) and extends them with dNTPs (20-40 bp). Primes Pol ε to leading strand and Pol δ to lagging strand.
ε	10^{-7}	Yes	Proposed leading-strand DNA synthesis. Replisome assembly. Replication checkpoint.
δ	10^{-7}	Yes	Proposed lagging-strand DNA synthesis (120-250 bp per fragment). DNA repair e.g. NER, BER.

McCulloch and Kunkel, (2008); Pavlov et al., (2006b); Kunkel and Burgers, (2008).

A correct nucleotide favours continued DNA synthesis in the polymerase site and an incorrect nucleotide stalls DNA synthesis and the mismatched primer terminus is transferred to the exonuclease site. When a misincorporated nucleotide(s) is added to the growing 5'-3' DNA strand, this causes misalignment of the 3'OH primer and slows polymerisation (Reha-Krantz, 2010). This provides time for the 3' terminus of the nascent strand to flip to the intrinsic exonuclease active site, 40 Å away from the polymerase active site, to have the incorrectly incorporated nucleotide(s) removed. When this occurs, the DNA is no longer in contact with the PALM (polymerisation) domain but still remains attached to the polymerase via the thumb domain (**Figure 1.4**) (Cotterill and Kearsey, 2009). This elegant rotation of the DNA back and forth between the two catalytic sites enhances the fidelity and processivity of the polymerase reaction. Amino acid substitutions that affect this switch between these two distinct domains affect the fidelity of DNA polymerases (Reha-Krantz, 2010). For an in-depth review on this topic, please see Reha-Krantz (2010). The ability to extend a mismatched primer terminus also determines the fidelity of the DNA polymerase. If it is unable to extend the mismatch, the DNA polymerase will either transfer the 3' end to the intrinsic exonuclease site, or the polymerase stalls, dissociates from the replisome and exposes the 3' end to other proteins that can correct the error (**Figure 1.2A-C**) (Ganai and Johansson, 2016). Proof for the latter mechanism originates from yeast studies showing that errors made by Pol α and Pol ε can be proofread by Pol δ (Pavlov et al., 2006a; Flood et al., 2015; Bulock et al., 2020a; b).

The mismatch repair pathway plays a crucial role in preventing genomic instability because it repairs many replication errors, including mismatches that have escaped the surveillance of polymerase proofreading (**Figure 1.2D-E**) (Li et al., 2005; Kunkel and Erie, 2005; Fukui, 2010). With functional MMR in budding yeast, the mutation rate per diploid genome per generation is 0.004, and the average substitution rate per base pair per generation is 1.7×10^{-10}

(Lujan et al., 2014). Ganai and Johansson (2016) further explains that the presence of DNA lesions in the DNA template and altered dNTP pools can have an effect on replication fidelity.

Mismatch repair (MMR) is a DNA repair system which involves a subset of proteins that rectify the errors that have evaded the replicative DNA polymerases' proofreading functions (reviewed in Kunkel and Erie, 2015). There are several proteins involved in the MMR pathway, such as: MSH2, MSH6, MSH3, MLH1, PMS1/2, and EXO1, and they are divided up into separate categories depending on their specific roles and type of replication errors (mismatches, insertions and deletions) they detect or repair (Ganai and Johansson, 2016; Lange et al., 2011). After the replication error has been detected, MMR must identify which strand to correct in a process called strand discrimination (Kunkel and Erie, 2015). The template strand should be left intact and a nick must be created on the nascent strand that contains the replication error. In eukaryotes, replication errors are detected by MutSα (Msh2/Msh6) and MutSβ (Msh2/Msh3) complexes, and MutLa (Mlh1/Pms1 in yeast or Mlh1/Pms2 in humans) complex cleaves the strand with the replication error on either side of the mismatch with the aid of several other factors such as PCNA and RFC (Kunkel and Erie, 2015; Ganai and Johansson, 2016). After an exonuclease, Exo1, has excised the replication error, Pol ε or Pol δ fills the gap, and a DNA ligase seals the nick (Ganai and Johansson, 2016; Tran et al., 1999b). However, Pol δ is primarily responsible for filling the gap in the DNA at the end of mismatch repair (MMR) and it has been suggested to actively take part in DNA repair during MMR (Longley et al., 1997; Kadyrova and Kadyrov, 2016). Additionally, nicks that separate Okazaki fragments on the lagging strand have been implied to act as a strand discrimination signal for MMR (McElhinny et al., 2010a). Furthermore, MMR rectifies errors made during DNA replication with varying efficiency at different locations in the genome. Errors in the lagging strand are more efficiently repaired by MMR compared to those in the leading strand because it is believed that the high density of 5' ends at Okazaki fragments and the higher density of PCNA on the lagging strand

might trigger MMR activity (Pavlov et al., 2003). Comparably, in vitro and in vivo studies have shown that Pol ε has higher fidelity than Pol δ compensating for less efficient MMR on the leading strand; whereas the moderately lower fidelity of Pol δ is compensated for by more efficient MMR on the lagging strand (Fortune et al., 2005; St Charles et al., 2015).

There is synthetic lethality between exonuclease-dead polymerase mutations and MMR deficient mutations. The failure of both Pol δ proofreading and MMR, for example Pms1, causes lethality in haploid yeast (Morrison et al., 1993). This was consolidated in mouse studies whereby homozygous defects in either Pol ε or Pol δ exonuclease activity and MMR, for example *msh2Δ* or *mlh1Δ*, caused embryonic lethality (Albertson et al., 2009). This highlights the fact that these error-detecting pathways, i.e. proofreading and post-replication MMR, act in series and behave synergistically to prevent spontaneous mutation and cancer. Moreover, mice with homozygous defects in both Pol ε and δ proofreading died significantly younger from thymic lymphoma than mice with either Pol ε or δ defects alone (Albertson et al., 2009). Additionally, a synergistic mutational relationship was observed in diploid budding yeast completely lacking Pol ε and δ exonuclease activities (Morrison and Sugino, 1994).

Pols ε and δ have other cellular roles apart from DNA replication that are important in the overall maintenance of genome stability (Pavlov et al., 2006b). Firstly, Pol δ is involved in different types of DNA repair other than MMR, for example: it synthesises DNA to fill the gap of approximately 30 nucleotides that is created during nucleotide excision repair (NER) (Shivji et al., 1995; Ogi et al., 2010; Nishida et al., 1988; Lehmann, 2011); Pol δ carries out DNA re-synthesis in long-patch base excision repair (BER) (Blank et al., 1994; Stucki et al., 1998; Robertson et al., 2009); it functions in DNA re-synthesis after break-induced replication (BIR), a pathway that repairs one-ended double-strand breaks (DSBs), and Pol δ has been shown to directly initiate BIR (Costantino et al., 2014; Lydeard et al., 2007). Pol ε may act as a sensor of

DNA damage as it appears to activate the checkpoint pathways needed to deal with the consequences of replication fork stalling (Pursell and Kunkel, 2008). For example, specific mutations in Pol ε render a defect in the intra-S-phase checkpoint in *S. cerevisiae* (Dua et al., 1998; Navas et al., 1995).

Figure 1.4

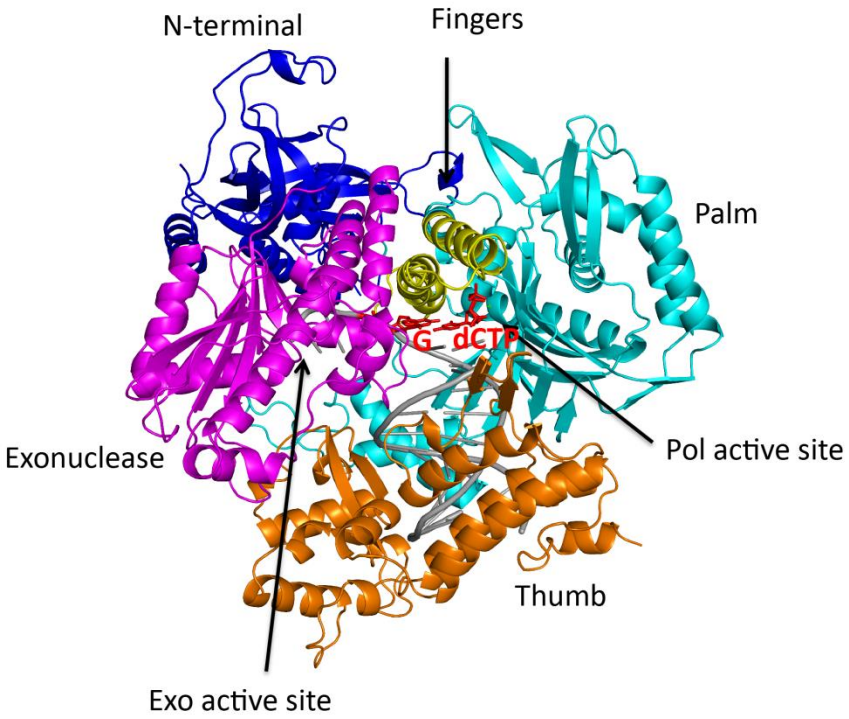


Figure 1.4: Crystal structure of *S. cerevisiae* Pol ε catalytic domain. Pol2 palm, fingers, thumb, exonuclease and N-terminal domains are shown in cyan, yellow, orange, magenta and blue, respectively. DNA is in grey, and the templating G and incoming dCTP are in red. The polymerase (Pol) and exonuclease (Exo) active sites are labelled. Both the polymerase (cyan) and exonuclease (magenta) domains are within the same catalytic subunit. The 3' end of the nascent DNA strand can readily flip between the two active sites of Pol and Exo for excision of incorrectly incorporated nucleotides and subsequently, for polymerisation to resume (Reha-Krantz, 2010). The two active sites are 30-40 Å apart (Cotterill and Kearsey, 2009). Image and legend adapted from Jain et al (2014).

1.4 EXONUCLEASE DOMAIN MUTATIONS (EDMs) AND CANCER

1.4.1 EDMs increase mutation rates

It has been demonstrated in yeast that proofreading by Pol ε and δ is as significant as MMR for managing the mutational burden in the cell (Morrison and Sugino, 1994). Defects in Pols ε and δ give rise to a strong mutator phenotype in yeast strains, more so in exonuclease-null Pol δ (approximately up to hundred-fold increase in mutation rate) (Morrison et al., 1991; Simon et al., 1991; Morrison et al., 1993). These are point mutations inactivating key catalytic residues within the exonuclease active site of the polymerases and, additionally, it is believed that exonuclease deficient T4 DNA polymerases in bacteriophages reduce DNA replication activity two to three-fold in vivo (Reha-Krantz and Nonay, 1993). Thus, defective proofreading limits polymerase activity because the mutant polymerases can no longer excise terminal mismatches which, in turn, delays further primer extension (Reha-Krantz, 2010).

If defective proofreading can reduce replication fidelity, we can imagine that other mutations within the exonuclease domain, not necessarily directly affecting key catalytic residues, could also have a detrimental effect on proofreading and overall genome stability. One of the reasons for an increased mutation rate caused by exonuclease domain mutant (EDM) polymerases could be partly due to the exonuclease-defective polymerase inserting more incorrect nucleotides than wild type (Wt) and, subsequently, overwhelming the ability of MMR to correct all mismatched nucleotides (Pavlov et al., 2003). Moreover, proofreading-defective polymerases might dissociate from the progressing replication fork more frequently than normal, resulting in increased fork stalling events.

It has been proposed that DNA Pol δ has the added responsibility to extrinsically proofread replication errors made by defective Pol α or Pol ε; therefore, if Pol δ has deficient proofreading

capability, it fails to efficiently process Okazaki fragments and to remove mismatches on the leading strand, prompting mutagenesis and genomic instability. This hypothesis is supported by studies in yeast: firstly, a Pol α mutant with low replication fidelity had an accumulative mutation rate when 3'-5' exonuclease activity was inactivated in Pol δ, but not when it was inactivated in Pol ε (Pavlov et al., 2006a); secondly, the mutation rate increased synergistically when a Pol ε defective allele in nucleotide selectivity was combined with a Pol δ proofreading defective allele (Bulock et al., 2020a). Conversely, in the same study, a combination of Pol δ nucleotide selectivity and Pol ε proofreading deficiencies produced no synergy. Thus, this indicates that Pol δ can correct replication errors made by Pol ε but not the other way around. In vitro replication assays further demonstrated that Pol δ can remove mismatches made by exonuclease-deficient Pol ε (Bulock et al., 2020a). This is perhaps one reason why defective DNA Pol δ can lead to tumour development and fatality within the first year of life in mice (Goldsby et al., 2001). Mice homozygous for exonuclease-null *Pole* alleles also displayed tumours, however, the tumour spectrum differed between exonuclease-null *Pole* alleles versus exonuclease-null *Pold1* alleles (Albertson et al., 2009; Goldsby et al., 2002). Since both Pols ε and δ (but predominantly Pol δ) may be involved in the gap-filling step of mismatch repair (Tran et al., 1999b), not only is proofreading compromised but so is post-replicative DNA repair, accounting for increased mutagenesis.

Earlier work in budding yeast showed that a mutagenic exonuclease null Pol δ (*pol3-01*) strain activates error-prone repair, namely translesion synthesis (TLS), via a checkpoint pathway that elevates dNTP levels upon DNA damage signalling (Datta et al., 2000). Interestingly, in the report, preventing checkpoint activation reduces the mutation rate of the *pol3-01* strain, indicating that events downstream of checkpoint activation, rather than just reduced proofreading per se, contribute to the mutator phenotype (Datta et al., 2000). It is assumed that mismatched termini that cannot be repaired by abolished 3'-5' exonuclease activity of Pol δ

trigger the S phase DNA damage checkpoint pathway. Furthermore, Williams et al (2015) and Mertz et al (2015) confirm that raised levels of dNTPs caused by checkpoint activation account for the mutator phenotypes of some polymerase active site mutations that affect base selectivity in DNA Pols ε and δ, respectively. It remains unknown, however, whether dNTP pool levels play a major role in the development of tumours due to Pol ε or Pol δ EDMs.

To conclude, mutations affecting exonuclease function can enhance the overall mutator phenotype via mechanisms other than proofreading deficiency and this could be independent of S phase since these polymerases do have additional roles (Jin et al., 2005; Tseng et al., 2008).

1.4.2 EDMs cause cancer predisposition

Mice with homozygous germline Pols ε and/or δ mutations inactivating exonuclease activity show a number of distinct but overlapping tissue specific tumour phenotypes. *Pole*-mutant mice mainly developed intestinal adenomas or nodal lymphomas, whereas *Pold1*-mutant mice predominantly had thymic lymphomas or lung adenomas (Albertson et al., 2009). Double knockout animals died within six months mainly from thymic lymphomas (Albertson et al., 2009). Note that some of the tissues affected by these EDMs have a high rate of cell turnover (Goldsby et al., 2001, 2002).

1.4.2.1 Germline POLD1 S478N and POLE L424V exonuclease domain mutations

Polymerase mutations may also be linked to human cancer predisposition. The 2012 Cancer Genome Atlas exome sequencing study of 224 sporadic CRCs identified a subset of micro-satellite stable (i.e. MMR-proficient) cancers that possessed hypermutating somatic mutations in the POLE exonuclease domain (The Cancer Genome Atlas Network, 2012). A similar analysis was conducted in 72 CRC exomes, and had similar findings to the former study (Seshagiri et al., 2012). Further studies using whole-genome sequencing, pedigree and linkage

analyses of 15 probands who had already developed colorectal adenomas by 60 years of age without known predisposition mutations, led to the discovery of two autosomal heterozygous germline mutations located in the POLE and POLD1 exonuclease domains, respectively (Palles et al., 2013). *POLE* L424V and *POLD1* S478N variants are dominantly inherited and carry a high-penetrance predisposition to large or multiple colorectal adenomas or early-onset CRC (Palles et al., 2013). Uniquely, seven carriers of the *POLD1* S478N mutations had developed endometrial carcinoma (Palles et al., 2013). Although *POLE* L424V has been predominantly associated with CRC predisposition, it also predisposes to endometrial cancer (EC), gastric and brain cancers (Rayner et al., 2016). Both mutations are situated in highly evolutionarily conserved motifs of the exonuclease domain but neither affect key catalytic residues essential for proofreading activity (**Figures 1.5** & **1.6**) (Palles et al., 2013). To assess the likely pathogenicity of these two variants, equivalent mutations were constructed in *S. pombe*: the *POLD1* variant had a 12-fold increase in mutation rate compared to that of the wild type (Palles et al., 2013). The *POLE* L424V mutant shared a similar mutation rate to the *POLD1* variant (Palles et al., 2013). Moreover, *POLE* L424V had a mutation rate approximately half of that of an exonuclease null *POLE* mutant (D276A, E278A) which implies that its proofreading ability is defective but not entirely inactive (Shinbrot et al., 2014). Both *POLD1* S478N and *POLE* L424V mutations were predicted to have functional consequences for nuclease activity based on their locations in the exonuclease domain (Palles et al., 2013). Finally, the exonuclease polymerase variants have been shown to affect proofreading ability and cause a relatively moderate mutator phenotype in fission yeast (Palles et al., 2013).

These germline mutations in polymerase exonuclease domains are believed to generate tolerated mutator phenotypes which eventually lead to random second hits in oncogenes or tumour suppressors. Second hits, in terms of loss of heterozygosity (LOH) involving the germline *POLE* L424V and *POLD1* S478N mutations, were found in few colorectal tumours

and in the case of endometrial cancer (EC), no tumour was identified with LOH (Palles et al., 2013; Church et al., 2013). Future work is required to ascertain whether loss of the wild-type allele is required for tumourigenesis. It remains to be seen whether mutations affecting polymerase exonuclease function can induce genome instability via mechanisms other than proofreading deficiency per se, as outlined in **Chapter 1.4.1**.

Several studies have reviewed and suggested that germline *POLE* and *POLD1* mutations are present in 0.5-2% of patients in intestinal polyposis and CRC cohorts enriched for hereditary disease (Rayner et al., 2016; Bellido et al., 2016; Spier et al., 2015; Chubb et al., 2015). According to the literature, the most frequent deleterious germline, exonuclease domain mutation (EDM) to date is the *POLE* L424V variant allele; it was identified in 21 independent carriers (Spier et al., 2015; Valle et al., 2014; Elsayed et al., 2015). Note that the Pol ε residue L424 is the site of both germline and somatic mutations (Rayner et al., 2016). Most cancer cells expressing *POLE* or *POLD1* proofreading domain mutations are microsatellite-stable (MSS), i.e. mismatch-repair proficient, albeit some have been found to be microsatellite-unstable (MSI), i.e. mismatch-repair deficient (Palles et al., 2013; Elsayed et al., 2015; Shlien et al., 2015). The existence of both *POLE/POLD1* EDMs and MSI is rare in tumours; however, when they do occur together the mismatch repair genes predominantly affected are *MSH6* or *MSH2* in hereditary or sporadic *POLE* EDM tumours, respectively (Rayner et al., 2016; Williams et al., 2013; Heyer et al., 1999). The only analysis of mutation spectrum that has been undertaken thus far on germline EDMs is on *POLE* L424V and *POLD1* S478N tumours, which phenotypically express a large number of missense substitutions and relatively few frameshift mutations (Palles et al., 2013).

1.4.2.2 POLD1 EDMs: P327L, L474P, D316N and G321S

In addition to the *POLD1* S478N variant, Palles et al (2013) discovered another germline cancer-predisposing mutation in *POLD1*: the P327L variant was detected in a 70-year-old with multiple colorectal adenomas. It is believed to have functional consequences because the residue is highly conserved and is situated on the DNA-binding interface next to the exonuclease catalytic site (**Figures 1.5** & **1.6**) (Briggs and Tomlinson, 2013). Intriguingly, the equivalent mutation in the bacteriophage T4 polymerase, Pro123Leu, has a mutation rate approximately 40 times higher than the wild type (Reha-Krantz, 1988), making the human equivalent mutation a strong predictor for pathogenicity. Furthermore, the homologous mutation to *POLD1* P327L in *S. cerevisiae* Pol2, *P301L*, has a hypermutator phenotype; in other words, its mutation rate exceeds that of the exonuclease-null Pol2 (Hamzaoui et al., 2020). This mutation has not yet been modelled and assessed in *S. pombe*.

Ever since the Palles et al (2013) study was published, a small number of newer pathogenic non-synonymous *POLD1* EDMs have been identified: *POLD1* L474P (Bellido et al., 2016; Valle et al., 2014; Rayner et al., 2016), *POLD1* D316N (The Cancer Genome Atlas Network, 2014; Rayner et al., 2016) and *POLD1* G321S (**Figure 1.5**) (Gong et al., 2017; Palles et al., 2018; Weren et al., 2017).

The *POLD1* L474P germline mutation involves a highly conserved residue located within the proofreading domain of DNA Pol δ and it affects the equivalent residue to the recurrently reported Pol ε EDM, *POLE* L424V (**Figures 1.5** & **1.6**). The *POLD1* L474P variant allele was first described as a *de novo* mutation in Valle et al (2014): 858 familial/early onset CRC and polyposis patients were screened. Mutation screening was performed by KASPar genotyping assays and Sanger sequencing of the involved exons, and as a result, *POLD1* L474P was discovered in a MMR-proficient, Amsterdam II-criteria family (mean age at diagnosis was 40

years) (Valle et al., 2014). Bear in mind that the Amsterdam criteria are used in the diagnosis of hereditary non-polyposis colorectal cancer, including Lynch Syndrome, and the exclusion of familial adenomatous polyposis (FAP), based on the number of first or second degree relatives affected and cancer histopathology (Park et al., 2002; Llor et al., 2005). The *POLD1* L474P mutation is predicted to be pathogenic because it co-segregates in the family with cancer predisposition; it is positioned in a region of the exonuclease domain that can have structural implications for the holoenzyme and it has been previously reported to have a mutator phenotype in *S. cerevisiae* (Valle et al., 2014; Murphy et al., 2006). The *POLD1* L474P germline mutation is predominantly associated with CRC and possibly EC development and has been found in a number of non-polyposis cases (Valle et al., 2014; Bellido et al., 2016). Polyposis is the presence of multiple polyps that increase the risk of cancer at a young age (30 to 40 years), namely CRC, that may be due to a germline mutation in a known predisposition gene, for example, adenomatous polyposis coli (*APC*) – tumour suppressor gene involved in the Wnt signalling pathway, or *MUTYH* – a base excision repair gene (Rayner et al., 2016). Familial adenomatous polyposis (FAP) is a rare inherited cancer predisposition specifically caused by mutations in the *APC* gene. The histopathology of *POLD1* L474P tumours is in contrast to other CRC-associated *POLE* and *POLD1* EDM tumours whose phenotypes had more similarities with those of germline mutations in the *APC* and in *MUTYH* genes. (Briggs and Tomlinson, 2013; Palles et al., 2013). Since most patients with *POLE* or *POLD1* CRCs present a multitude of polyps, they have been referred to as having the disease: polymerase proofreading associated polyposis (PPAP) (Heitzer and Tomlinson, 2014). However, this terminology to describe the disease can be misleading because as previously mentioned, some CRC-associated *POLE*/*POLD1* tumours, such as L474P, were not characterised by a large number of intestinal polyps. Furthermore, Bellido et al (2016) implicates a correlation between *POLD1* L474P (and other *POLD1* variants) and the development of brain and breast tumours.

Figure 1.5

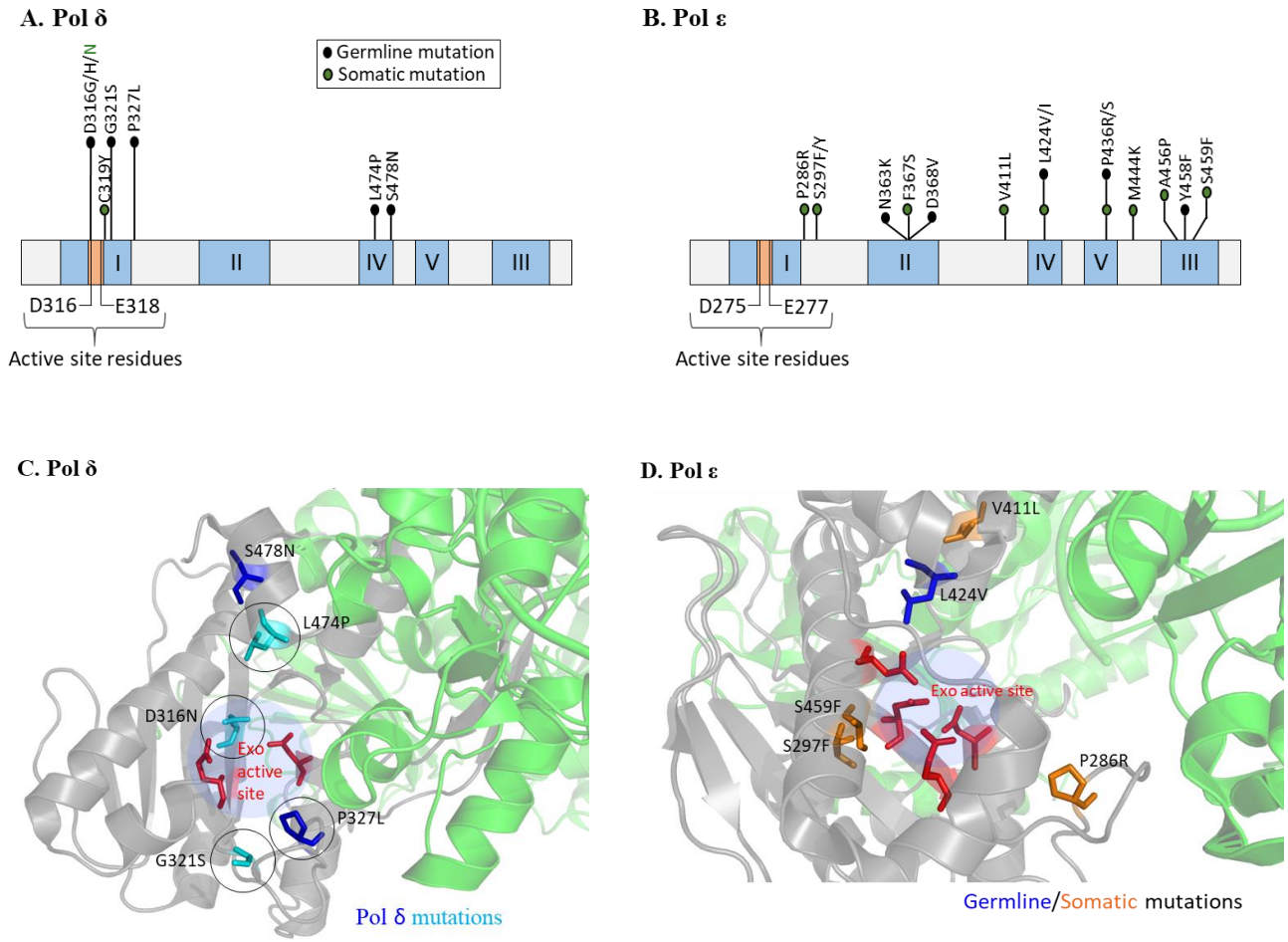


Figure 1.5: The location of germline and somatic Pol δ and ε exonuclease domain mutations associated with cancer. (A) Localisation of germline and somatic *POLD1* mutations within the exonuclease domain. Conserved exo I – V motifs are highlighted in dark blue, and the exo I motif active sites at codons 316 and 318 are highlighted in pink. The exo motifs I – V encompass the Pol δ exonuclease domain. Note that there are very few somatic Pol δ proofreading domain mutations. *POLD1* D316N (the "N" is highlighted in green) is a somatic mutation, whereas *POLD1* D316G/H are germline mutations. **(B)** Localisation of germline and somatic *POLE* mutations within the exonuclease domain. Conserved exo I – V motifs are highlighted in dark blue, and the exo I motif active sites at codons 275 and 277 are shown in pink. The exo motifs 1 – V comprise the Pol ε exonuclease domain. Black circles denote germline mutations; green circles denote somatic mutations (see key). Also, Pol ε residues L424V and P436R/S are the sites of both germline and somatic mutations. Note that there are many more somatic Pol ε proofreading domain mutations compared to Pol δ. **(C)** The positions of the exonuclease domain mutations (cyan and blue) are mapped to *S. cerevisiae* Pol δ exonuclease domain structures using PYMOL. The exo I motif active site residues are highlighted in red with the exception of mutated Pol δ active site residue D316, which is also the site of germline and somatic mutations, as previously mentioned. The germline mutations circled represent the mutations explored further in this study. **(D)** The positions of some key germline (blue) and somatic (orange) exonuclease domain mutations are mapped to *S. cerevisiae* Pol ε exonuclease domain structures using PYMOL. The exo I motif active site residues are shown in red. Figure adapted and modified from Rayner et al (2016).

Figure 1.6

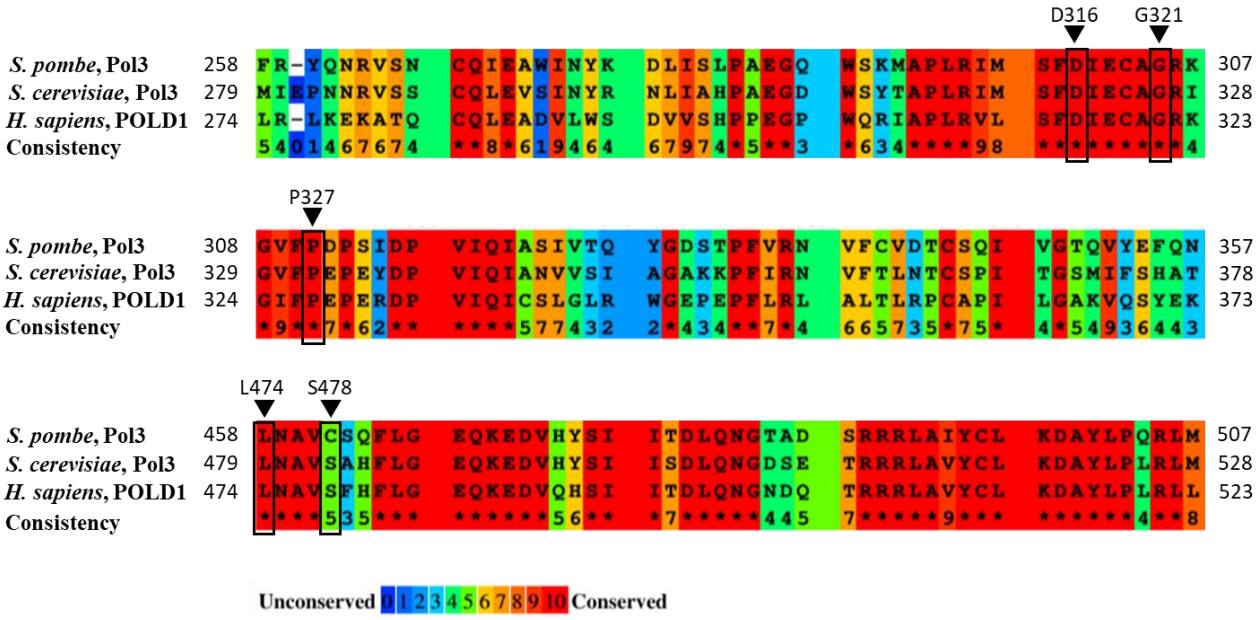


Figure 1.6: Sequence alignment of *POLD1* exonuclease domain mutations in different species. Asp316, Gly321, Pro327 and Leu474 are invariant in POLD1 orthologues. Ser478 is partially evolutionarily conserved in eukaryotes including *S. cerevisiae*, although in *S. pombe*, the homologous amino acid is the structurally similar cysteine. The results are colour-coded for amino acid conservation. Alignment produced using PRALINE (http://zeus.few.vu.nl/programs/pralinewww/).

POLD1 L474P has not been modelled yet in *S. pombe*, so it would be interesting to see if the fission yeast version of the mutation will have similar mutagenicity to the equivalent mutation in budding yeast (Murphy et al., 2006).

POLD1 D316N is a somatic mutation affecting a key catalytic residue in the exonuclease active site of Pol δ, therefore, simply based on its location and affected residue, it is expected to be highly mutagenic (**Figures 1.5** & **1.6**) (Bellido et al., 2016). There has not been much published work on this mutation; it was identified once in a highly mutated sporadic gastric cancer with a mutation spectrum largely consisting of insertions and deletions (indels) (The Cancer Genome Atlas Network, 2014; Rayner et al., 2016). A similar germline mutation, *POLD1* D316G, was associated with malignancy in 4 of 4 middle-aged carriers with a propensity for CRC, EC and breast cancer (BrC) (Bellido et al., 2016). *POLD1* D316H germline mutation was also reported in the latter study and was identified in 60-year-old carriers having either CRC or BrC and there was an isolated case of mesothelioma in a carrier. Note that affected individuals with the D316G/H substitution mutation had MSS EC or CRC, i.e. the tumours were MMR-proficient (Bellido et al., 2016).

Yeast fluctuation assays, i.e. mutation rate assays, have implicated the negative functional and pathogenic effects of the D316N missense mutation in Pol δ of budding yeast (Sc. *pol3-D321N*) (Murphy et al., 2006). The *POLD1* D316N mutation has not been constructed or assessed in *S. pombe* yet.

Whole-genome sequencing data revealed a novel exonuclease domain missense mutation in Pol δ, *POLD1* G321S, which is also autosomal dominantly inherited (Weren et al., 2017). It was found in a family of 6 who either developed adenomatous polyposis or CRC (mean age of 40 years) and those who had colorectal tumours were MSS (Weren et al., 2017; Palles et al., 2018). Therefore, this mutant may be another germline EDM, like *POLE* L424V and *POLD1* S478N,

that is responsible for the disease PPAP (Weren et al., 2017; Palles et al., 2013). The *POLD1* G321S variant is predicted to decrease the proofreading fidelity of the enzyme because it affects a highly conserved amino acid residue in the exo I motif (**Figures 1.5** & **1.6**) (Weren et al., 2017). No homologous yeast mutation has been made or studied, thus far.

1.4.2.3 Somatic POLE/POLD1 EDMs

In light of the recent Cancer Genome Atlas (TCGA) projects, somatic Pol ε EDMs were detected in 1-2% of sporadic CRCs (The Cancer Genome Atlas Network, 2012; Seshagiri et al., 2012). Subsequently, these somatic hypermutating mutations were found to predominantly express a base substitution mutator phenotype with an increased proportion of C→T transitions and C→A transversions (Shinbrot et al., 2014; Rayner et al., 2016; Soriano et al., 2021). *POLE* EDMs have also been found, albeit rarely, in brain, pancreas, ovary, breast, stomach, lung and prostate cancers (Barbari and Shcherbakova, 2017; Rayner et al., 2016). Further research showed that somatic *POLE* EDMs were present in 7-12% of sporadic endometrial cancers (ECs) (Church et al., 2013; The Cancer Genome Atlas Network, 2013; Church et al., 2015). Similar to CRCs, *POLE* EDMs in ECs were MSS, 'ultra-hypermutated' and largely characterised by base substitution mutations (Donehower et al., 2013; Briggs and Tomlinson, 2013; Palles et al., 2013). This is in contrast to the MSI seen in Lynch Syndrome (De la Chapelle, 2004). Sporadic *POLE* EDMs are similar to tumours in germline-variant carriers where they show few copy number changes and are generally MSS despite mutations in MMR genes (The Cancer Genome Atlas Network, 2012; Church et al., 2013; Seshagiri et al., 2012; The Cancer Genome Atlas Network, 2013). Tumours with somatic *POLE* proofreading domain mutations tend to occur in young patients (i.e. <50 years), have a high tumour grade and, under the microscope, they have an abundance of multinucleated giant cells with abnormal

morphology (Rayner et al., 2016). This is probably linked to somatic *POLE* EDMs' hypermutated phenotype.

Somatic *POLD1* mutations are not commonly found in CRCs and ECs (**Figure 1.5**) (Church et al., 2013; The Cancer Genome Atlas Network, 2013; Palles et al., 2013). This could be due to MMR preferentially correcting mismatch errors on the lagging strand rather than the leading strand (Pavlov et al., 2003; Tran et al., 1999b). **Figure 1.5** displays the locations of the somatic and germline *POLE* and *POLD1* EDMs. One somatic *POLD1* proofreading domain variant, C319Y, was identified in an ultramutated paediatric glioblastoma with MSI due to a heterozygous mutation in the MMR gene, *MSH6* (Shlien et al., 2015). The second somatic mutation identified is the aforementioned *POLD1* D316N which will be investigated later in this study.

The most prevalent heterozygous somatic *POLE* EDM found in predominantly sporadic colorectal and endometrial carcinomas alters a highly conserved proline residue in the Exo I motif: *POLE* P286R (**Figure 1.5**) (The Cancer Genome Atlas Network, 2012; Seshagiri et al., 2012; Church et al., 2013). Pro286 is evolutionarily conserved, lies on the DNA-binding interface of the POLE exonuclease domain and is predicted to compromise proofreading activity by perturbing DNA binding (**Figure 1.6**) (Palles et al., 2013; Church et al., 2013). The analogous mutation in *S. cerevisiae* has a strong mutator phenotype, fifty times higher than the mutation rate of proofreading-defective mutants (Kane and Shcherbakova, 2014; Barbari et al., 2018). The latter mutation has recently been modelled in *S. pombe* (*pol2(e)P287R*) and has a mutation rate approximately 60-70 times higher than wild type and ten-fold higher than the exonuclease inactive mutant, *pol2(e)D276E/A278E,* which is not a clinical mutation (Soriano et al., 2021). This consolidates the idea that *POLE* P286R increases the mutation rate and enhances genomic instability via pathways other than proofreading insufficiency per se. It has

come to light recently that somatic *POLE* EDMs, namely *POLE* P286R, have favourable prognosis in EC (Rayner et al., 2016; Church et al., 2015; Billingsley et al., 2014); this is probably due to the plethora of mutations found in these cancers causing an abundance of antigenic neoepitopes. These novel epitopes, created by somatic Pol ε mutations in tumours, are capable of triggering an antitumour immune response – a cytotoxic T-cell response (Van Gool et al., 2015; Howitt et al., 2015).

Furthermore, the cancer-associated germline *POLD1* P327L mutates the same relative position as the hypermutating somatic *POLE* P286R mutation in an alignment of Pols δ and ε (**Figure 1.5**), and so it will be relatively simple to model in fission yeast.

1.5 AIMS OF THE PROJECT

The main purpose of this study is to determine whether polymerase cancer-associated mutations present in *POLD1* are likely to be pathogenic by modelling the equivalent mutations in *S. pombe*. The focus is on the *POLD1* EDMs: P327L, L474P, D316N and G321S because their phenotypes have not yet been assessed in fission yeast, let alone in mammals. In addition to performing mutation rate assays, I will test whether the *pol3(d)* mutants are sensitive or resistant to various DNA-damaging compounds and explore the mechanism if there are any notable phenotypes. Thirdly, I will ascertain whether the DNA damage checkpoint pathway is activated and required for cell viability in the mutant strains and whether the levels of Pol δ are compromised in these variants.

Since Sp. *pol2(e)P287R* (human *POLE* P286R) has a hypermutator phenotype, I will model the equivalent mutation in *pol3* to create the Sp. *pol3(d)P311R* mutation. This is to see if similarly high mutation rates are observed in the *pol3* mutant strain and to shed light on how EDMs have different effects on mutagenicity in Pol ε versus Pol δ.

The final purpose of this study is to acquire a more profound understanding of what genes are relevant to the function of Pol δ in the cell. Synthetically sick/lethal (SSL) interactions report on the extent to which the viability of a mutant depends on the function of a second gene (Roguev et al., 2007). By crossing the most reported germline Pol δ EDM, *POLD1* L474P with some 'suspect' genes, we may uncover the mechanisms of how this germline Pol δ variant proceeds to manifest cancer, and perhaps we can unveil some potential drug-targeted therapies. *S. pombe* is an ideal model organism to observe these SSL interactions on a basic molecular level and the study of synthetic lethality is not uncommon in this type of yeast (Roguev et al., 2018a; c). A schematic summarises the aims of the project in **Figure 1.7**.

The ultimate goal is to inform genetic testing of clinically established EDMs and potentially to inform gene therapy by discovering novel drug targets.

Figure 1.7

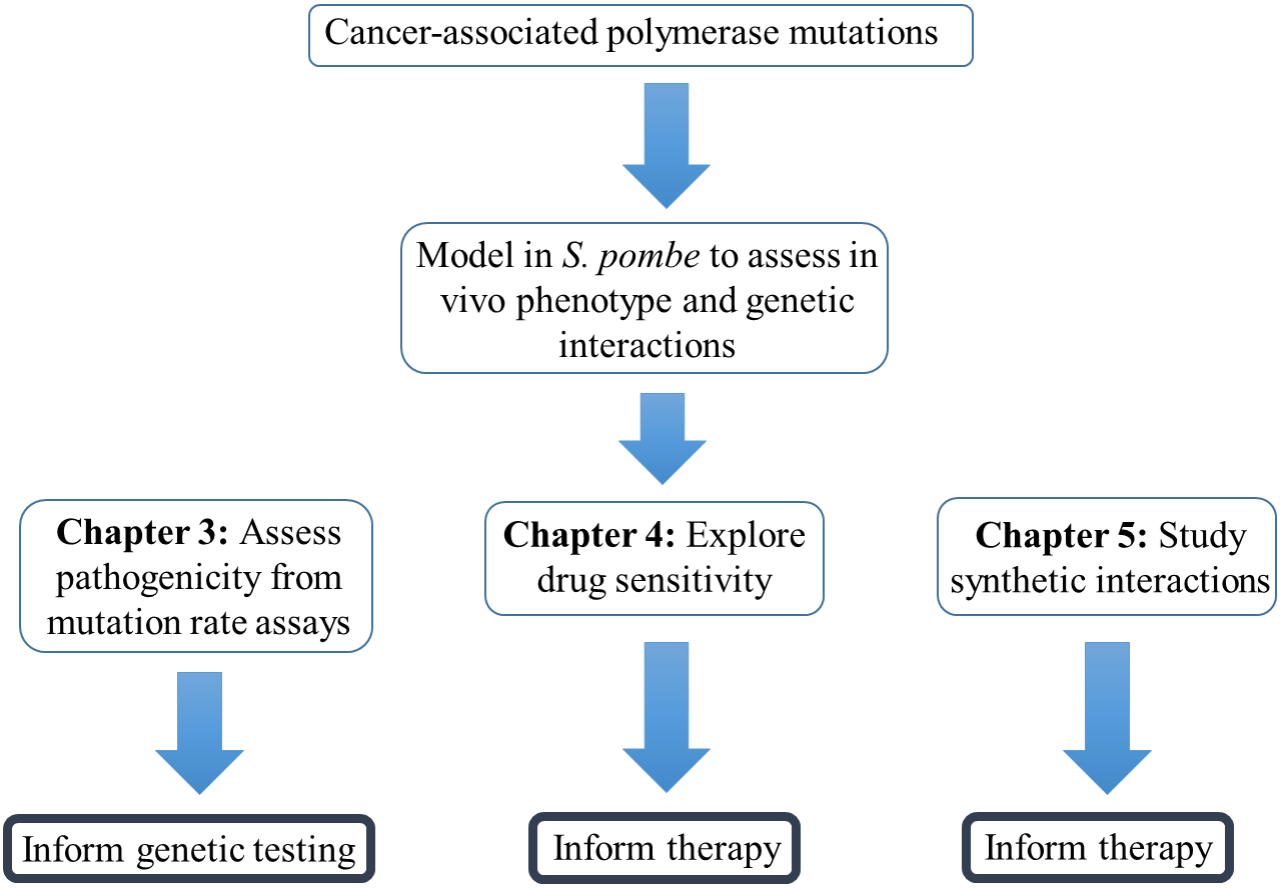


Figure 1.7: Schematic outlining the main aims of the project.

Chapter 2 Materials and Methods

2.1 *S. pombe* METHODS

2.1.1 General methods

The yeast strains in this study are catalogued in **Table 2.1**. Additional supplements, such as adenine, leucine, uracil, lysine, histidine and/or arginine, were added to the standard media. For solid media, 2% Bacto-agar was added prior to autoclaving. Standard media was used for the growth of *S. pombe* strains (Moreno et al., 1991):

Yeast extract 3 or 6 supplements (YE3/6S)

170 mM glucose, 5 g/L yeast extract (Sigma), and 225 mg/L of the necessary supplements. Selective agents were used at the following concentrations: G418 200 µg/ml; hygromycin 200 µg/ml; cycloheximide 100 µg/ml. Hydroxyurea (HU) was used at 10-24 mM, depending on the experiment, in liquid media.

Edinburgh minimal medium (EMM)

110 mM glucose; 93.5 mM ammonium chloride; 15.5 mM di-sodium hydrogen phosphate; 14.7 mM potassium hydrogen phthalate; 1 × salts stock; 1 × vitamins stock; 1 × minerals stock; 150 mg/L of each supplement required.

Pombe glutamate media (PMG)

110 mM glucose; 20 mM L-glutamic acid; 15.5 mM di-sodium hydrogen phosphate; 14.7 mM potassium hydrogen phthalate; 1 x salts stock; 1 x vitamins stock; 1 x minerals stock; 150 mg/L

per supplement. Canavanine (Can) was added at 70 μg/ml to PMG for the purpose of Can^r fluctuation analysis.

SPAS

55.5 mM glucose, 7.3 mM potassium di-hydrogen phosphate, 1 × vitamin stock, and 45 mg/L each supplement required. SPAS plates were used for mating *S. pombe* strains.

Strains were generally grown in YES liquid at 30-32°C, except for those that were temperature-sensitive, which were grown at 25°C. For short term storage, strains were kept as patches on appropriate agar plates at 4°C for up to two months. *S. pombe* strains were stored in 50% glycerol at -80°C long-term. The absorbance at 600 nm (optical density, OD_{600}) in a Pharmacia Biotech Ultraspec 2000 was used to provide approximate concentration of the cells: OD is a measure of cell mass, not cell number. An OD_{600} of 1.0 being ~1.5 x 10^7 cells/ml. Liquid cultures were prepared from a fresh single colony, inoculated into 10-20 ml of YES and were incubated overnight at an appropriate temperature until cells were in early stationary phase (OD_{600} 0.8-1.0); this saturated culture was used to inoculate a larger culture, as needed. For most experiments, cells were maintained in exponential growth (OD_{600} 0.2-0.8).

For more information on media composition and general conditions and methods applied to fission yeast, please refer to PombeNet and the Forsburg Laboratory: https://dornsife.usc.edu/pombenet/.

The *S. pombe* haploid strains utilised during this study are listed below in **Table 2.1**.

Table 2.1: Strains used in this study

Strain Number	Genotype	Also Known As
1617	*h⁺ rad3::ura4, leu1-32, ura4-D18*	*rad3*Δ
1918	*h⁺ uve1::LEU2, rad13::ura4, leu1-3, ura4-D18, ade-*	*uve1*Δ*rad13*Δ
2067	*h⁻ pol1-5FLAG::kanMX6*	*pol1-5FLAG*
2839	*h⁻ ade6-704, leu1-32, ura4-D18, rad3ts*	*rad3ts*
2840	*h⁻ ade6-485*	Wt
3169	*h⁺ ade6-424, msh2::his3, his3-D1*	*msh2*Δ
3176	*h⁻ pol3+::kanMX6, ade6-485*	Wt-*kanMX6*
3194	*h⁻ ade6-[(GT)₈ -1397], his3-D1, leu1-32, ura4-D18*	Wt, *ade6-(GT)₈*
3199	*h⁻ pol2(e)D276A/E278A::kanMX6, ade6-485* (ex 2840)	Exo-null *pol2(e)*
3200	*h⁻ pol2(e)D276A/E278A::kanMX6, ade6-485* (ex 2840)	Exo-null *pol2(e)*
3251	*h⁻ top1::LEU1, leu1-32, ura4-D18*	*top1*Δ
3273	*h⁻ pol3(d)D386A::kanMX6, ade6-485*	Exo-null *pol3(d)*
3285	*h⁺ cdc22-D57N*	*cdc22-D57N*
3292	*h⁻ pol3D386A::kanMX6, ade6-704, leu1-32, ura4-D18, rad3ts*	*pol3D386A, rad3ts*
3311	*h? msh2*Δ*::his3, ade6-[(GT)₈ -1397], his3-, leu1-, ura4-* (3194 x 3169)	*msh2*Δ *ex ade6-(GT)₈*
3500	*h⁻ ade6-485*	Wt (2840 restored)
3622	*h⁻ pol2(e)P287R ::kanMX6, ade6-485* (ex 2840)	*pol2(e)P287R*
3758	*h⁻ pol2P287R::kanMX6, ade6-485* (ex 2840)	*pol2(e)P287R*
TH 1483	*h⁺ mus81::kanMX6, ade6-704, leu1-32, ura4-D18*	*mus81*Δ
TH 1846	*h⁺ rad51::his3, ade7-152, his3-D1*	*rad51*Δ
TH 2093	*h⁺ arg3-D4, ade6-D1, ura4-D18, leu1-32, his3-D1*	Wt *(h⁺)*
TH 3181	*h⁻ ade6-M210; leu1-32; ura4-D18; mat1_m_cyh^S, smt0; rpl42::cyh^R (sP56Q)*	Parental PEM2 strain
TH 5346	*h⁺ rad32 (mre11)::kanMX6*	*mre11*Δ (*rad32*Δ)
U2-54-D-08	*h⁺ rad3::kanMX6, ade-, leu-, ura-*	*rad3*Δ. Bioneer.
U2-55-E-08	*h⁺ nse5::kanMX6*	*nse5*Δ. Bioneer.
V2-04-A-08	*h⁺ mms19::kanMX6*	*mms19*Δ. Bioneer.
V2-05-B-05	*h⁺ rad1::kanMX6*	*rad1*Δ. Bioneer.
V2-08-H-07	*h⁺ ctf18::kanMX6*	*ctf18*Δ. Bioneer.
V2-09-C-02	*h⁺ rhp7::kanMX6*	*rhp7*Δ (*rad7*Δ). Bioneer.
V2-09-D-04	*h⁺ ago1::kanMX6*	*ago1*Δ. Bioneer.
V2-09-F-09	*h⁺ rrp2::kanMX6*	*rrp2*Δ. Bioneer.
V2-09-G-09	*h⁺ rhp18::kanMX6*	*rhp18*Δ (*rad18*Δ). Bioneer.
V2-10-C-10	*h⁺ top1::kanMX6*	*top1*Δ. Bioneer.
V2-10-D-05	*h⁺ hip4::kanMX6*	*hip4*Δ. Bioneer.
V2-11-E-09	*h⁺ msh6::kanMX6*	*msh6*Δ. Bioneer.
V2-16-G-12	*h⁺ cdt2::kanMX6*	*cdt2*Δ. Bioneer.
V2-17-B-12	*h⁺ thp1::kanMX6*	*thp1*Δ. Bioneer.
V2-22-B-11	*h⁺ exo1::kanMX6*	*exo1*Δ. Bioneer.
V2-23-F-11	*h⁺ cmb1::kanMX6*	*cmb1*Δ. Bioneer.
V2-26-D-11	*h⁺ bdc1::kanMX6*	*bdc1*Δ. Bioneer.
V2-28-B-05	*h⁺ pst2::kanMX6*	*pst2*Δ. Bioneer.
V2-32-F-02	*h⁺ dre4::kanMX6*	*dre4*Δ. Bioneer.

V2R-43-D-02	h^+ *dpb4::kanMX6*	*dpb4*Δ. Bioneer.
V2R-44-B-05	h^+ *raf2::kanMX6*	*raf2*Δ. Bioneer.
V2R-44-C-04	h^+ *mre11::kanMX6, ade-, leu-, ura-*	*mre11*Δ (*rad32*Δ). Bioneer.
V2R-44-F-03	h^+ *lsd1::kanMX6*	*lsd1*Δ. Bioneer.
V3R-45-B-11	h^+ *cbf11::kanMX6*	*cbf11*Δ. Bioneer.
V4R-46-C-05	h^+ *rad50::kanMX6*	*rad50*Δ. Bioneer.
V4R-46-D-06	h^+ *rad22::kanMX6*	*rad22*Δ (*rad52*Δ). Bioneer.
V4R-46-F-02	h^+ *wee1::kanMX6*	*wee1*Δ. Bioneer.
V4R-46-G-06	h^+ *liz1::kanMX6*	*liz1*Δ. Bioneer.
V4R-47-D-12	h^+ *rad2::kanMX6*	*rad2*Δ (*fen1*Δ) Bioneer.
V4R-50-A-02	h^+ *arb1::kanMX6*	*arb1*Δ. Bioneer.
3354	h^- *pol3(d)P311L::kanMX6, ade6-485* (ex 2840)	*pol3(d)P311L*
3355	h^- *pol3(d)P311L::kanMX6, ade6-485* (ex 2840)	*pol3(d)P311L*
3416	h^- *pol3P311L::kanMX6, ade6-704, leu1-32, ura4-D18, rad3ts* (ex 2839)	*pol3P311L, rad3ts*
3419	h^- *pol3(d)P311R::kanMX6, ade6-485* (ex 2840)	*pol3(d)P311R*
3421	h^- *pol3(d)D386A::kanMX6, ade6-485* (ex 2840)	Exo-null *pol3*
3426	h^- *pol3(d)P311R::kanMX6, ade6-485* (ex 2840)	*pol3(d)P311R*
3941	h^- *pol3G305S::kanMX6, ade6-485* (ex 3500)	*pol3(d)G305S*
3942	h^- *pol3G305S::kanMX6, ade6-485* (ex 3500)	*pol3(d)G305S*
3943	h^- *pol3L458P::kanMX6, ade6-485* (ex 3500)	*pol3(d)L458P*
3944	h^- *pol3L458P::kanMX6, ade6-485* (ex 3500)	*pol3(d)L458P*
3945	h^- *pol3D300N::kanMX6, ade6-485* (ex 3500)	*pol3(d)D300N*
3946	h^- *pol3D300N::kanMX6, ade6-485* (ex 3500)	*pol3(d)D300N*
3947	h^- *pol3P311L::kanMX6, ade6-(GT)$_8$* (ex 3194)	*pol3P311L ex ade6-(GT)$_8$*
3948	h^- *pol3P311L::kanMX6, ade6-(GT)$_8$* (ex 3194)	*pol3P311L ex ade6-(GT)$_8$*
3949	h^- *polG305S::kanMX6, ade6-(GT)$_8$* (ex 3194)	*pol3G305S ex ade6-(GT)$_8$*
3950	h^- *polG305S::kanMX6, ade6-(GT)$_8$* (ex 3194)	*pol3G305S ex ade6-(GT)$_8$*
3951	h^- *pol3L458P::kanMX6, ade6-(GT)$_8$* (ex 3194)	*pol3L458P ex ade6-(GT)$_8$*
3952	h^- *pol3L458P::kanMX6, ade6-(GT)$_8$* (ex 3194)	*pol3L458P ex ade6-(GT)$_8$*
3953	h^- *pol3D300N::kanMX6, ade6-(GT)$_8$* (ex 3194)	*pol3D300N ex ade6-(GT)$_8$*
3954	h^- *pol3D300N::kanMX6, ade6-(GT)$_8$* (ex 3194)	*pol3D300N ex ade6-(GT)$_8$*
3955	h^- *pol3D386A::kanMX6, ade6-(GT)$_8$* (ex 3194)	*pol3D386A ex ade6-(GT)$_8$*
3956	h^- *pol3D386A::kanMX6, ade6-(GT)$_8$* (ex 3194)	*pol3D386A ex ade6-(GT)$_8$*
3957	h^- *pol3G305S::kanMX6, ade6-704, leu1-32, ura4-D18, rad3ts* (ex 2839)	*pol3G305S, rad3ts*
3958	h^- *pol3L458P::kanMX6, ade6-704, leu1-32, ura4-D18, rad3ts* (ex 2839)	*pol3L458P, rad3ts*
3959	h^- *pol3D300N::kanMX6, ade6-704, leu1-32, ura4-D18, rad3ts* (ex 2839)	*pol3D300N, rad3ts*
3960	h^- *pol3-5FLAG::hphMX6, ade6-485* (ex 3176)	*pol3-5FLAG-hphMX6* (Wt-tagged)
3961	h^- *pol3-5FLAG::hphMX6, ade6-485* (ex 3176)	*pol3-5FLAG-hphMX6* (Wt-tagged)
3962	h^- *pol3P311L-5FLAG::hphMX6, ade6-485* (ex 3354)	*pol3P311L-5FLAG-hphMX6*
3963	h^- *pol3P311L-5FLAG::hphMX6, ade6-485* (ex 3354)	*pol3P311L-5FLAG-hphMX6*
3964	h^- *pol3G305S-5FLAG::hphMX6, ade6-485* (ex 3941)	*pol3G305S-5FLAG-hphMX6*
3965	h^- *pol3G305S-5FLAG::hphMX6, ade6-485* (ex 3941)	*pol3G305S-5FLAG-hphMX6*
3966	h^- *pol3L458P-5FLAG::hphMX6, ade6-485* (ex 3943)	*pol3L458P-5FLAG-hphMX6*

3967	*h⁻ pol3L458P-5FLAG::hphMX6, ade6-485* (ex 3943)	*pol3L458P-5FLAG-hphMX6*
3968	*h⁻ pol3D300N-5FLAG::hphMX6, ade6-485* (ex 3945)	*pol3D300N-5FLAG-hphMX6*
3969	*h⁻ pol3D300N-5FLAG::hphMX6, ade6-485* (ex 3945)	*pol3D300N-5FLAG-hphMX6*
3970	*h⁻ pol3D386A-5FLAG::hphMX6, ade6-485* (ex 3273)	*pol3D386A-5FLAG-hphMX6*
3971	*h⁻ pol3D386A-5FLAG::hphMX6, ade6-485* (ex 3273)	*pol3D386A-5FLAG-hphMX6*
3972	*h⁺ mus81::hphMX6, ade6-704, leu1-32, ura4-D18* (ex TH 1483)	*mus81Δ*
3973	*h? pol3P311L::kanMX6, mus81::hphMX6, leu1-32, ura4-D18* (3354 x 3975)	*pol3P311L, mus81Δ*
3974	*h? pol3G305S::kanMX6, mus81::hphMX6, leu1-32, ura4-D18* (3941 x 3975)	*pol3G305S, mus81Δ*
3975	*h? pol3L458P::kanMX6, mus81::hphMX6, leu1-32, ura4-D18* (3943 x 3975)	*pol3L458P, mus81Δ*
3976	*h? pol3D386A::kanMX6, mus81::hphMX6, leu1-32, ura4-D18* (3273 x 3975)	*pol3D386A, mus81Δ*
3977	*h⁺ pol3P311L::kanMX6, ade6-485, cdc22-D57N* (3354 x 3285)	*pol3P311L, cdc22-D57N*
3978	*h⁺ pol3G305S::kanMX6, ade6-485, cdc22-D57N* (3941 x 3285)	*pol3G305S, cdc22-D57N*
3979	*h⁺ pol3L458P::kanMX6, ade6-485, cdc22-D57N* (3943 x 3285)	*pol3L458P, cdc22-D57N*
3980	*h⁺ pol3D386A::kanMX6, ade6-485, cdc22-D57N* (3273 x 3285)	*pol3D386A, cdc22-D57N*
3981	*h⁺ pol3D386A::kanMX6, ade6-485, cdc22-D57N* (3273 x 3285)	*pol3D386A, cdc22-D57N*
3982	*h⁻ pol3L458P::hphMX6, ade6-485* (ex 3943)	*h⁻ pol3L458P::hphMX6*
3983	*h⁺ pol3L458P::hphMX6, ade6-485, arg3-D4, ade6-D1, ura4-D18, leu1-32, his3-D1* (3982 x TH 2093)	*h⁺ pol3L458P::hphMX6*
3984	*h⁻ pol3L458P::hphMX6; ade6-485; arg3-D4; ade6-D1; ura4-D18; leu1-32; his3-D1; ade6-M210; mat1_m_cyh^S, smt0; rpl42::cyh^R (sP56Q)* (3983 x 3181)	*pol3L458P* ex *PEM-2 strain*
3985	*h? pol3L458P::hphMX6, rad3::kanMX6, ade6-485* (3985 x U2-54-D-08)	*pol3L458P, rad3Δ*

Strains highlighted in dark green were sourced from Stephen Kearsey's laboratory, while those highlighted in blue were made for the purposes of this study. Any strains preceded by 'TH' were sourced from Tim Humphrey's strain collection (faintly green). Strains highlighted in orange were from the Bioneer deletion library stored in T. Humphrey's lab. All the Bioneer strains were Ade-, Leu- and Ura- and G418 resistant (G418^R). Mating types are shown where possible; mating type is not shown where multiple isolates were constructed and consequently h^+ and h^- strains exist.

2.1.2 Genetic crosses

Genetic crosses were carried out by mixing two freshly growing strains of opposite mating type (h^+ and h^-) on SPAS plates with the appropriate supplements and incubating them at room

temperature for 5-6 days. For a faster cross, some plates were incubated at 25-32°C (depending on the presence of temperature-sensitive alleles) for 1-2 days. Spores can be prepared from sporulated mating-mixes between haploid strains (zygotic asci) or from sporulated diploids (azygotic asci). Asci produced by the sporulation of diploids (azygotic asci) are easily distinguished from asci produced by the sporulation of zygotes (zygotic asci) by microscopic examination. Diploid cells are fatter than haploid cells and form linear and compact azygotic asci (Ekwall and Thon, 2017a), whereas zygotic asci, resulting from the cross of two haploid cells with opposite mating types, are banana-shaped and the tetrads are not so compact (Escorcia and Forsburg, 2018). Light microscopy was also used to check for the presence of asci in the h^+ parental strain, which is less stable than h^- strains, to rule out self-mating (Forsburg, 2003). The spores of the desired genotype were isolated using random spore analysis or tetrad analysis.

2.1.2.1 Random spore analysis

1 ml of sterile deionised water was inoculated with some of the cross mixture. 5 µl of Helicase (Helix pomatia juice, Sepracor, France) was added and incubated overnight at room temperature to break down the ascus wall and kill vegetative cells. The spores were centrifuged at 4,000 rpm (Heraeus centrifuge) for 5 minutes and resuspended in 1 ml of 30% ethanol to kill any remaining vegetative cells. The 1 ml mixture was vortexed repeatedly to break up spore clumps. The appropriate dilutions were plated out on appropriate media based on the following approximation: 100 µl of 1/1000 dilution of a cross that has many asci will give around 200 colonies per plate. The plates were then incubated for 2-3 days at 30°C until colonies formed. Depending on the cross, colonies of the desired genotype were selected by replica plating to selective media or by screening with colony PCR.

2.1.2.2 Tetrad analysis

A 1-2 day cross at 30°C was usually used for tetrad analysis. 1 ml of sterile deionised water was inoculated with some of the cross mixture and 5 µl of Helicase (Helix pomatia juice, Sepracor, France) was added and left to stand for up to 30 minutes. The asci were streaked on to a YES plate and the four spores in each ascus were separated out using a micromanipulator (Singer Instruments, MSM) to give a vertical line or column of four isolated spores. They were then incubated at an appropriate temperature for the cross for 4-5 days until colonies formed. Colonies of the desired genotype were selected by replica plating to selective media or by screening with colony PCR. Each colony was scored for its specific genotype.

2.1.3 Yeast transformation

The Lithium Acetate (LiAc) method was used for yeast transformation (Bahler et al., 1998).

2.1.4 Colony PCR

Colony PCR was used to genotype yeast strains produced by transformation etc. The primers used for colony PCR analysis are shown in **Table 2.2** to identify the deleted, mutated or tagged genes. Positive and negative controls were used. The PCR reactions were run in a GeneAmp PCR system 9700 (Applied Biosystems). Each colony to be screened was suspended in 20 µl VWR Red Taq Ready Mix (Thermo Scientific) and the following cycling conditions were employed: 94°C for 5 minutes, 35 cycles of denaturation at 94°C for 30 seconds, annealing at 55°C for 1 minute, extension at 68°C for 3-6 minutes (depending on the size of synthesized DNA fragments), and held at 68°C for 7 minutes. PCR products were checked by DNA electrophoresis (8 µl loaded onto gel).

The primer pair used in the colony PCR of *E.coli* transformants (see **Section 2.2.1.4.2**) during the construction of the germline variants was 1075 and 1121. The following primer pairs were used in colony PCR of yeast transformants: 1183 & 1088 for the *pol3P311* mutants, *pol3D300N*, *pol3L458P* and *pol3G305S* mutants, and 1087 & 1088 for the *pol3D386A* mutant. The subsequent PCR products were digested with the appropriate enzymes and analysed by gel electrophoresis (see **Section 2.2.2**). The following restriction enzymes: BglI, BsmI, NruI, NruI SspI-high fidelity (HF) and XbaI, were used to digest colony PCR products of *pol3G305S*, *pol3L458P*, *pol3P311R*, *pol3D386A*, *pol3D300N*, and *pol3P311L* mutant strains, respectively, as per New England Biolabs (NEB) manufacturer's guidelines.

The primer pairs used in colony PCR for the characterisation of the *cdc22-D57N* mutation in the Pol δ double mutants were 989 and 997. The PCR product was digested with DdeI and analysed on agarose gel.

The primers used to identify the mating type of haploid strains were: 738, 739 and 740. h^- strains produced a band size of approximately 750 bp, and h^+ strains produced a band size of approximately 1000 bp on agarose gel. The primer pairs used to confirm the presence of the cyh^S (cycloheximide-sensitive) and cyh^R (cycloheximide-resistant) alleles in the *pol3L458P PEM-2* strain (#3987 – **Table 2.1**) were 304 & 305, and 306 & 307, respectively.

The primers used during this study are described in **Table 2.2**.

Table 2.2: Primers used during the course of mutant construction, colony PCR and sequencing of plasmids and genomic *S. pombe* DNA

Primer	Sequence (5'-3')	Name
736	5'-GAATTCGAGCTCGTTTAAAC-3'	*pFA6a-5FLAG-hphMX6* tagging in *pol3* mutant strains. Reverse primer for *pFA6a* vectors, reads into Ttef, selectable marker.
738	5'-AGAAGAGAGAGTAGTTGAAG-3'	For mating type determination. Common forward primer MT1.
739	5'-ACGGTAGTCATCGGTCTTCC-3'	For mating type determination. Mat1-P specific, reverse primer.
740	5'-TACGTTCAGTAGACGTAGTG-3'	For mating type determination. Mat1-M specific, reverse primer.
989	5'-TTTGGATCCATGTTTGTATACAAAAGAGGTATGAAACAGG-3'	*cdc22-D57N*, forward primer. Used in colony PCR.
997	5'-GGACGAGGAGTACCGGCATTG-3'	*cdc22-D57N*, reverse primer. Used in colony PCR.
1075	5'-tttggatccTTGAATGCGCAGGTCGCAAAGGCG-3'	*pol3(d)* open reading frame (ORF), forward. Used in colony PCR for *pol3P311 E.coli* transformants.
1076	5'-tggcgcgccCCATCTTTTTCACCAGGACATTTCATCAAATC-3'	*pol3(d)* ORF, reverse. Flanking primer used in site-directed mutagenesis for construction of *pol3P311*, *pol3D300N*, *G305S* & *L458P* mutants.
1080	5'-GCAGTCTctTCTCAGTTTCTAGGCGAGCAAAAAGAAG-3'	*pol3(d)* ORF, forward. Sequencing of *pol3* mutant *E.coli* transformants.
1081	5'-TAACGCAGTATGGAGACTCCACTCC-3'	*pol3(d)* ORF, forward. Sequencing of *pol3* mutant *E.coli* transformants. Sequencing of *pol3L458P* yeast transformants.
1087	5'-CCCCACTGAGGATCATGAGCTTTG-3'	*pol3(d)* ORF, forward. Used in colony PCR of D386A yeast transformants.

1088	5’-gGTGACCCGGCGGGGAC-3’	*pFA6a* ORF, reverse. Used in colony PCR of *pol3P311* and *pol3D386A* yeast transformants.
1121	5’-CGTCTTCTAGAATCGGCAGTGCC-3’	*pol3(d)* ORF, reverse. Used in colony PCR of P311 *E.coli* transformants. Sequencing of *pol3D386A* yeast transformants.
1122	5’-CACTTTATCCTTCGATTATGCAAGCCc-3’	*pol3(d)* ORF, forward. Sequencing of *pol3* mutant *E.coli* transformants.
1123	5’-GAAACTGTCAGAAGAGATAACTGTCCtc-3’	*pol3(d)* ORF, forward. Sequencing of *pol3* mutant *E.coli* transformants.
1124	5’-GGGACGAGGCAAGCTAAACAGATC-3’	*pFA6a* ORF, reverse. Sequencing of *pol3* mutant *E.coli* transformants.
1148	5’-tttggatccGGGTGTGATCGATCATTGCATTATAGAG-3’	*pol3(d)* ORF, forward. Flanking primer used in site-directed mutagenesis for construction of *pol3P311*, *pol3D300N*, *G305S* & *L458P* mutant strains. Sequencing of *pol3* mutant *E.coli* transformants. Sequencing of *pol3P311*, *G305S* & *D300N* yeast transformants.
1165	5’-GAGCACGCTGTTGAATTGAGAAGGG-3’	*ade6-(GT)$_8$*, reverse primer. Used to sequence *ade6* with incorporated GT_8 repeat run.
304	5’-AATTGGTTTTGAAGCGTTGC-3’	*Cyh^S*, forward primer. Used in colony PCR for detecting *cyh^S* allele in PEM-2 strain.
305	5’-TGGAGAGGATGTGATCTGAG-3’	*Cyh^S*, reverse primer. Used in colony PCR for detecting *cyh^S* allele in PEM-2 strain.
306	5’-CACCGTGTTACTCAGTATAAG-3’	*Cyh^R*, forward primer. Used in colony PCR for detection of *cyh^R* allele in PEM-2 strain.

307	5’-AAGATGTGCCCATCGACGTA-3’	*Cyh^R*, reverse primer. Used in colony PCR for detection of *cyh^R* allele in PEM-2 strain.
512	5’-CGGATCCCCGGGTTAATTAAGGCG-3’	*pFA6a-hphMX6*, forward primer. For amplification of hphMX6 (HYG) cassette from p116 for marker swap using pTEF/tTEF as homology. Amplified HYG used in yeast transformation.
513	5’GAATTCGAGCTCGTTTAAACACTGGATGGCGGCGTTAGTATCG-3’	*pFA6a-hphMX6*, reverse primer. For amplification of hphMX6 (HYG) cassette from p116 for marker swap using pTEF/tTEF as homology. Amplified HYG used in yeast transformation.
1176	5’-AGGGATCtaGAAAAACGCCTTTGCGACCTGCGCATTC-3’	*pol3(d)P311L*, reverse. Mutagenic primer used to construct *pol3P311L* mutant plasmid.
1177	5’-TTCtaGATCCCTCTATTGACCCTGTAATTCAAATTGC-3’	*pol3(d)P311L*, forward. Mutagenic primer used to construct *pol3P311L* mutant plasmid.
1183	5’-GATTTAGATGCTACTTGTAATGGgg-3’	*pol3(d)*, forward. Used in colony PCR of *pol3* mutant yeast transformants.
1192	5’-AGGGATCgcGAAAAACGCCTTTGCGACCTGCGCATTC-3’	*pol3(d)P311R*, reverse. Mutagenic primer used to construct *pol3P311R* mutant plasmid.
1193	5’-TTCgcGATCCCTCTATTGACCCTGTAATTCAAATTGC-3’	*pol3(d)P311R*, forward. Mutagenic primer used to construct *pol3P311R* mutant plasmid.
1206	5’-CTTTaATATTGAATGCGCAGGTCGCAAAGGCG-3’	*pol3D300N*, forward. Mutagenic primer used to construct *pol3D300N* mutant plasmid.
1207	5’-CATTCAATATtAAAGCTCATGATCCTCAGTGGG-3’	*pol3D300N*, reverse. Mutagenic primer used to construct *pol3D300N* mutant plasmid.
1208	5’-GCGCAaGcCGCAAAGGCGTTTTTCCTGATCCCTC-3’	*pol3G305S*, forward. Mutagenic primer used to construct *pol3G305S* mutant plasmid.

1209	5’-GCGgCtTGCGCATTCAATATCAAAGCTCATGA-3’	*pol3G305S*, reverse. Mutagenic primer used to construct *pol3G305S* mutant plasmid.
1210	5’-CTCTccgAATGCAGTCTGCTCTCAGTTTCTAGG-3’	*pol3L458P*, forward. Mutagenic primer used to construct *pol3L458P* mutant plasmid.
1211	5’-ATTcggAGAGTAAGATCGAAGCTTAAAATCACG-3’	*pol3L458P*, reverse. Mutagenic primer used to construct *pol3L458P* mutant plasmid.
1340	5’-TGTACCAGTAGAGACTGCCCCATATTTTATATGCGAATTGCAGAACACAAGAAACTTCAGCAATCTGTTGACTTACTGAAAAGATTTGATGAAATGTCCTGGCGGATCCCCGGGTTAATTAA-3’	5’ -(gene-specific sequence)-CGGATCCCCGGGTTAATTAA-3’ *pFA6a-5FLAG-hphMX6* tagging in *pol3* mutant strains. Forward primer. Primer used to construct *pol3 mutant-5FLAG-hphMX6* tagged strains to measure Pol3 levels in each mutant.

Primers highlighted in green were obtained from existing stock in S. Kearsey’s Laboratory; those highlighted in pink were from existing stock in T. Humphrey’s Laboratory; those highlighted in blue were designed for the purposes of this study. The names of the primers given reflect their use(s) in the experiments.

2.1.5 Fluctuation assays

Mutation rates were assessed using fluctuation analyses (Foster, 2006; Sarkar et al., 1992). Briefly, 12 cultures were set up with an initial cell density of 10^4 cells per ml and grown to saturation. The final cell density was assessed by plating 10^{-4} dilutions of the saturated cultures onto YES plates and incubating the plates at 30°C for 2-3 days. For all the assays, 150 µl of each culture was spotted onto the relevant plates which were previously dried with Grade 3, 70 mm Whatman Paper (Lang and Murray, 2008). Mutation rates were calculated using the Ma-Sandri-Sarkar Maximum Likelihood Estimator (MSS-MLE) method (Sarkar et al., 1992). Each experiment was carried out in triplicate i.e. a total of at least 36 cultures.

For further information about the MSS-MLE statistical method please refer to: http://genomics.brocku.ca/FALCOR/FALCOR_old.html

For canavanine resistance fluctuation assays, saturated cultures were spotted onto PMG plates containing 70 μg/ml canavanine and plates were incubated for 12 days before counting the number of canavanine-resistant (Can^r) colonies using the naked eye.

For *ade-* to *ade+* reversion fluctuation assay, saturated cultures were spun down and washed twice in 1 ml sterile water before doing the dilutions and before spotting onto dried EMM plates. Plates were incubated for 8 days. Note that the saturated cultures were diluted 1:100 before spotting onto EMM plates to ease the counting of adenine revertant colonies. The dilution was accounted for in the calculation of the mutation rate.

2.1.6 Spot tests

Strains were grown to log phase and diluted to an OD of 0.5. Cultures were serially diluted five-fold with the first well undiluted. Each well was spotted onto partially dried YES plates using a 6 by 8 hedgehog device. Plates were incubated for 2-6 days under the conditions indicated. In the case of drug spot tests, each well was spotted onto YES plates containing no drug or onto YES plates containing either 2 or 7.5 mM hydroxyurea (HU), 9-15 μM camptothecin (CPT), 0.5 μg/ml bleomycin, 0.5 μM 4-nitroquinoline 1-oxide (4NQO) and 0.005% v/v methyl methanesulfonate (MMS). For irradiation of cells spotted onto YES agar, the plate was irradiated with a UV-C dose of 200 J/m^2 using a XL-1500 crosslinker (Spectronics Corporation).

2.1.7 Microscopy

2.1.7.1 Ethanol fixation

Approximately 1.5 x 10^7 cells (i.e. 1.0 OD_{600} unit) were harvested from an exponentially growing culture and centrifuged at 2,000 rpm for 5 minutes (5810R centrifuge). Cell pellets were resuspended in 1 ml cold 70% v/v ethanol and stored at 4°C (cells keep indefinitely). Samples were stained with DAPI to visualise the nucleus, with calcofluor to visualise the septa, or processed for FACS analysis (**Chapter 2.1.8**).

2.1.7.2 DAPI (4'6'-diamidino-2-phenylindole) staining nuclei

Cell samples were harvested and fixed in 1 ml 70% ethanol. 200 µl of fixed cells were centrifuged (4,000 rpm, 2 minutes, Heraeus centrifuge), and most of the supernatant removed leaving a small amount (approximately 20 µl) of 70% ethanol covering the pellet. The pellet was vortexed several times before suspending it in 1 ml acetone. To mount the cells, they were first briefly sonicated (10 amps for 10 seconds), centrifuged (3,000 rpm, 5 minutes, Heraeus centrifuge), and most of the supernatant was extracted leaving approximately 20 µl acetone so that the cells were concentrated. 10-20 µl of vortexed cells was spread on a pre-warmed glass slide as a monolayer of cells. When the ethanol had evaporated, an equal volume (10-20 µl) of molten DAPI mountant (kept in dark, -20°C) (100-125 ng/ml DAPI, 0.6 % w/v high purity low melting temperature agarose (GRS Agarose LMT – Grisp Research Solutions)) to 10 mls 0.1M Tris-acetate (pH 8.5) was applied. A cover slip was placed on top and pressed moderately hard with a pipette tip. The DAPI mountant was left to set on the slide for 30-60 minutes. The slides were examined using a Zeiss Axioskop microscope and images recorded from the DAPI (DNA) channel. Images were analysed using NIH image software (ImageJ). At least 250 cells were counted for each data point.

2.1.7.3 Septum staining with calcofluor

Calcofluor can be used to stain live or fixed cells, as described above for DAPI. A 5 mg/ml stock was made up in 50 mM sodium citrate, 100 mM sodium phosphate and stored in the dark at -20°C. A working stock was diluted to 50 µl/ml with 50% glycerol. 10-20 µl of fixed cells was spread onto a glass slide and 10-20 µl of calcofluor working stock was applied. The slides were examined with a Zeiss Axioskop microscope using a DAPI channel to visualise stained septum. At least 250 cells were counted for each data point.

2.1.8 Flow Cytometry

To process the cells, 0.3mls of fixed cells (approximately 2-3 x 10^6 cells) were washed in 4.5ml 10mM ethylenediamine tetra-acetic acid (EDTA) (pH 8) and centrifuged at 2000 rpm 5 minutes (5810R centrifuge). The cell pellet was resuspended in 0.5 ml of 10 mM EDTA containing 0.1 mg/ml RNase A (Roche Diagnostics Ltd) and incubated for 2 hours at 36°C. For DNA staining, 0.5 mls 10mM EDTA containing 2 µM Sytox Green nucleic acid dye (Life Technologies) was added to each sample so that the final concentration in the sample was 1 µM. The cells in each tube were briefly sonicated. The DNA content of whole *S. pombe* cells was analysed using a FACSCalibur flow cytometer (BD Biosciences). Analysis was carried out using Flowjo software (https://www.flowjo.com/solutions/flowjo/downloads).

2.1.9 Growth rate assays

Cells were grown to log phase and diluted to OD_{600} 0.2 in 3 mls of YES. 250 µl of each diluted sample was dispensed into the appropriate wells of a honeycomb 100-well microplate. Seven replicates (i.e. 6 technical repeats) were dispensed for each strain per experiment. Note that 250 µl of YES was dispensed into the first seven wells, as these were the blanks of the experiment. The growth rate of each strain was measured by the Bioscreen C automated system (Oy Growth

Curves Ab Ltd) which works similarly to a spectrophotometer when measuring the optical density (OD) of each well. The microplate was placed inside the Bioscreen C instrument and was run under the Bioscreen 3D Program for 22 hours shaking at 30°C. The OD_{600} of each well was measured every 20 minutes. After 22 hours, the results were exported as a Microsoft Excel file.

2.1.10 Bioneer cross

Genetic interaction mapping in fission yeast was conducted using the pombe epistasis mapper (PEM) system and a ROTOR HDA colony replicating robot (Singer Instruments) in a 384 array format, as per detailed in Roguev et al (2018c). The *S. pombe* haploid deletion library of strains (G418 resistant, i.e. the Bioneer library) were stored in 96 well plates at -80°C. In the first instance of the screen, the library in a 96-well format was woken up and pin-plated in 384 array format onto non-selective YE6S plates; every strain was present in quadruple spots, i.e. three technical repeats per genetic cross. Subsequently, colonies were replica-plated onto YE6S plates containing G418. A 50 ml saturated culture of *pol3L458P* PEM-2 strain was spotted onto YE6S plates containing hygromycin (HYG) in 384 array format. Both sets of plates were incubated for 3 days at 30ºC. The PEM-2 and library arrays were combined on SPAS plates and incubated for 4 days at 25ºC. Colonies were pinned onto YE6S + cycloheximide (CYC) (100 µg/ml) + G418 (200 µg/ml) and incubated for 2-3 days at 32ºC in two rounds to facilitate germination, anti-diploid selection (ADS) and mating type selection (MTS) (see **Chapter 5**). Colonies were finally pinned onto plates selective for both the PEM-2 and library strains' deletion markers , i.e. YE6S + CYC + G418 + HYG (200 µg/ml). The *S. pombe* query strain is the *pol3L458P* mutation (marked by Hyg^R) in the PEM-2 genetic background (#3984 – **Table 2.1**).

2.2 DNA METHODS

2.2.1 Cloning

Standard methods were used for site-directed mutagenesis, plasmid preparation, in vitro restriction and ligation, and transformation into *E.coli* (see **Chapter 2.2.1.4**) (Kunkel et al., 1985; Rothstein, 1983; Sambrook et al., 1989; Moreno et al., 1991).

For gene cloning purposes, the QiAgen PCR purification kit was used to clean up (digested) colony PCR DNA product. Exceptionally, the PCR fragments yielded from the first round of PCR (site-directed mutagenesis) in the initial construction of the *pol3* mutants were cleaned via the QiAgen Gel Extraction Kit. Note that for gel extraction, DNA samples containing 1 µl of 1:1000 dilution of Syber Gold (ThermoFisher) (working stock is 10,000X concentrated in DMSO, kept at -20°C) were run on 1-2% agarose gel (Gibco BRL) at 90 V for 15-20 minutes and the DNA fragment of the required size was excised from the agarose gel under blue light. The purified DNA was verified by DNA agarose electrophoresis previous to cloning.

In order to amplify the hygromycin cassette from plasmid, *pFA6a-hphMX6* (p116 – **Table 2.3**), a 500 µl PCR reaction consisting of Phusion high fidelity (HF) PCR Master Mix with HF buffer 2x concentrate (Biolabs), primers 512 (10 µM) and 513 (10 µM), and 100 ng of p116, was run with the aforementioned 'colony PCR' cycling conditions (see **Section 2.1.4**). The final PCR fragment (1.7 kbp) was cleaned up using QiAgen PCR Purification Kit and, subsequently, used in yeast transformation to swap the kanMX6 cassette (conferring G418 resistance), that marks the *pol3* gene, to the hphMX6 cassette (conferring hygromycin resistance).

Comparably, in order to amplify the 5FLAG-hphMX6 cassette from the *pFA6a-5FLAG-hphMX6* plasmid (#997 – **Table 2.3**), for pol3-tagging in the mutant strains (via yeast transformation), a PCR reaction using VWR Red Taq Ready Mix was set up including 10 ng

of plasmid and 100 μM each of primers 1350 and 736. The same cycling conditions used for colony PCR were used for this reaction and the final PCR fragment (2175 bp) was purified.

2.2.1.1 Plasmids

The plasmids used or generated during this study are outlined in **Table 2.3**.

Table 2.3: Plasmids used and constructed in this study

Plasmid No.	Genotype	Source
958	*pFA6a-kanMX6*	Laboratory stock
969	*pFA6a-kanMX6-pol3(d)D386A*	Laboratory stock
983	*pFA6a-kanMX6-pol3(d)P311L*	This study
984	*pFA6a-kanMX6-pol3(d)P311R*	This study
997	*pFA6a-5FLAG-hphMX6*	Laboratory stock
1012	*pFA6a-kanMX6-pol3(d)G305S*	This study
1013	*pFA6a-kanMX6-pol3(d)D300N*	This study
1014	*pFA6a-kanMX6-pol3(d)L458P*	This study
p116	*pFA6a-hphMX6*	Laboratory stock

Plasmids 983, 984, 1012-1014 were sourced from empty cut vector, 958. Plasmid 969 was used to make more *pol3(d)D386A* strains (devoid of any exonuclease activity) for use in further experiments. The plasmid highlighted in pink was from T. Humphrey's plasmid collection.

2.2.1.2 Restriction digestion

Initially, in the construction of the Pol δ exonuclease domain mutants (EDMs), the final PCR product yielded from site-directed mutagenesis and the plasmid *pFA6a* vector (#958 in **Table 2.3**) were both cut with restriction enzymes BamHI-HF (NEB) and AscI (NEB), with the supplied buffers (NEB) according to the manufacturer's specifications. The digested vector was cleaned using QiAgen PCR Purification Kit following verification by DNA agarose

electrophoresis (see **Section 2.2.2**). The digested PCR product was cleaned via the QiAgen Gel Extraction Kit and verified by DNA agarose electrophoresis.

Plasmids 983, 984, 1012, 1013 and 1014 were linearised with XhoI restriction enzyme (NEB) and Plasmid 969 was linearised with CspCI restriction enzyme (NEB) prior to yeast transformation using the LiAc method (**Section 2.1.3**).

2.2.1.3 DNA ligation

The digested DNA fragment (insert) was cloned into the pre-cut *pFA6a-kanMX6* vector using T4 DNA Ligase (NEB), as per the manufacturer's instructions for ligation. Briefly, 200 ng of pre-cut vector was mixed with DNA insert to give a vector : insert ratio of 1 : 3 in a 20 µl reaction volume. The DNA ligation was incubated at room temperature for at least 4 hours or at 4°C overnight. After the reaction, the ligation mix was transformed into bacteria, described below.

2.2.1.4 E. coli general methods

The plasmids used and made during the course of this project are shown in **Table 2.3**. *E.coli* was grown to log phase in standard media, Luria-Bertani (LB) (0.17 M sodium chloride, 10 g/L Bacto-tryptone and 10 g/L Bacto-yeast extract) at 37°C (Sambrook et al., 1989). To select for carbenicillin/ampicillin resistance, carbenicillin was added to LB liquid at a final concentration of 50-100 µg/ml or to LB + agar to make plates containing carbenicillin.

2.2.1.4.1 E.coli transformation

The Calcium Chloride ($CaCl_2$) method, using either freshly prepared competent cells or a frozen stock of competent cells, was used for *E.coli* transformation (Sambrook et al., 1989).

2.2.1.4.2 Plasmid preparation

After *E.coli* transformation of the ligation mix, transformants were initially screened by colony PCR and, subsequently, by restriction enzyme digestion of mini-preps (see **Chapter 2.1.4**). Note that QiAgen Plasmid Midi/Maxi Prep was used to obtain purified plasmid (mini-prep) as per the manufacturer's instructions. Plasmids were stored at -20°C.

2.2.2 DNA analysis by gel electrophoresis

DNA samples were mixed with DNA loading buffer prior to loading on an agarose gel. The concentration of gels made were between 1 to 1.8% w/v of agarose in 1x TAE (0.04 M Tris acetate, 0.01 M EDTA, pH 8) buffer. Small gel electrophoresis tanks and mini combs were used in which 30 ml of molten agarose, containing 500 ng/ml ethidium bromide (stock concentration 10 mg/ml, Invitrogen) was poured. 10 µl of 1 kilobase (kb) Generuler (Thermo Fisher) was used as a marker of DNA fragment sizes. The electrophoresis was run at 100 V for 30-40 minutes depending on the size of DNA analysed. DNA was visualised using 365 nm UV light from a transilluminator. Images were taken using a charge-coupled-device (CCD) camera (Alpha Innotech Corporation) or they were captured using Quantity-One (BioRad).

2.2.3 Quantification of DNA samples

DNA concentration was determined using a Nanodrop 1000 spectrophotometer (Thermo Scientific). Samples were diluted in TE buffer to appropriate concentrations and absorbance was measured at 260 nm and 280 nm. Concentration was calculated in ng/µl.

2.2.4 Construction of *pol3(d)* mutant plasmids by PCR

Site-directed mutagenesis (two-step PCR) was used to construct the *pol3* mutant plasmids (983, 984, 1012-1014 – **Table 2.3**). For the amplification of gene fragments, a high fidelity enzyme,

phusion DNA polymerase (0.02 U/µl, Thermo Scientific), was used in two reactions including the flanking primers (1148 and 1076, 100 µM each) and the two mutagenic primers (100 µM), which varied for different mutations. The first-round of PCR was carried out in 1 x High Fidelity buffer (Thermo Scientific); primers (1148, 1076, and the two mutagenic primers), stock concentration at 100 uM; dNTPs at 10 mM (Thermo Scientific); 3% DMSO (100% concentrated, Thermo Scientific) and 100 ng of *S. pombe* genomic (template) DNA in a total volume of 50 µl. The following cycling conditions were used for the first round of PCR: 5 minutes at 94°C, 30 cycles of denaturation at 94°C for 30 seconds, annealing at 55°C for 1 minute, extension at 68°C for 3 minutes, and hold for 7 minutes at 68°C. The two PCR fragments were cleaned up by gel purification using a QiAgen Gel Purification Kit as per manufacturer's instructions. Note that the mutagenic primers used in the construction of the *pol3P311L/R*, *G305S*, *L458P* and *D300N* variants are recorded in **Table 2.2**.

The concentrations of the two PCR fragments were measured using the Nanodrop. For the second round of PCR in gene mutagenesis, the two PCR fragments of varying lengths were mixed in equimolar quantities and annealed together at 95°C for 30 seconds and then held at 25°C for 10 minutes. Subsequently, the annealed PCR product was diluted 1:100 and 1 µl of that was extended with 50 µl of Master Mix Phusion (consisting of phusion polymerase, 10mM dNTP mix and other reagents, as listed above) for 10 minutes at 72°C. After extension PCR, the flanking primers 1148 and 1076 (**Table 2.2**) were added to the reaction and run on the same cycling conditions used in the first round of PCR. The final PCR fragment was cleaned up using QiAgen PCR Purification Kit.

2.2.5 Sequencing

Sanger Sequencing Services (Source Bioscience) sequenced all plasmids, made for the purposes of the study, and PCR products. The primers used for sequencing the plasmid mini-

preps and the yeast transformants are outlined in **Table 2.2**, and the plasmids are outlined in **Table 2.3** (983, 984, 1012, 1013, 1014). The following primers were used to sequence the Pol3 reading frame of the *pol3* mutant plasmids: 1148, 1080, 1081, 1122, 1123 and 1124.

Colony PCR was performed on at least two successful yeast transformants and following clean-up by QiAgen PCR Purification Kit, they were sequenced to confirm the presence of the desired mutation. Primer 1148 was used to sequence the region consisting of the desired mutation in the *pol3P311L/R*, *pol3G305S* and *pol3D300N* yeast transformants, and primers 1081 and 1121 were used to sequence the region consisting of the desired mutation in the *pol3L458P* and *pol3D386A* yeast transformants, respectively.

2.3 PROTEIN METHODS

A summary table of the antibodies used in western analysis is listed in **Table 2.4**. Protein extracts were made by TCA extraction and then analysed by western blotting. Pol3-5FLAG was detected using anti-FLAG primary mouse antibody F1804 (Sigma) at a dilution of 1/1000 and anti-mouse as a secondary antibody (1/10,000). As a loading control, α-tubulin was detected with antibody T5168 (Sigma) at a dilution of 1/10,000 and anti-mouse (1/10,000) as a secondary antibody.

Table 2.4: Antibodies used in this study

Antibody	Use	Type	Dilution	Source
anti-FLAG	Primary antibody	Mouse monoclonal	1:1000	M2, F1804, Sigma
α-tubulin	Anti-tubulin antibody	Mouse monoclonal	1:10,000	T5168, Sigma
anti-mouse IgG-Peroxidase	Secondary antibody	Rabbit polyclonal (IgG)	1:10,000	A9044, Sigma

2.3.1 TCA protein extraction

Whole cell protein extracts were prepared by trichloroacetic acid (TCA) precipitation. 100 ml of cells were grown to log phase in appropriate media followed by centrifugation at 3000 rpm for 5 minutes (5810R centrifuge), then resuspended in 1 ml of 1.2 M sorbitol and transferred to a 2 ml Eppendorf tube. The tube was centrifuged for 30 seconds at 13,000 rpm (Heraeus centrifuge) to pellet the cells. The pellet was resuspended in 100 µl 20% TCA. 500 µl of glass beads were added to the tube then vortexed for 5 minutes at 4°C. The tube was left to stand for 1 minute at 4°C and then vortexed again for 1 minute at 4°C. 900 µl of 5% TCA was added, followed by a brief vortex. 800 µl of the extract was transferred to a clean 2 ml Eppendorf tube then centrifuged at 3,000 rpm for 10 minutes (Heraeus centrifuge). The protein pellet was resuspended by pipetting in 250 µl 1x Laemmli buffer (62.5 mM Tris-HCl pH 6.8, 5% v/v betamercaptoethanol, 2% w/v sodium dodecyl sulphate (SDS), 0.1% w/v bromophenol blue, 10% v/v glycerol) and boiled for 5 minutes, followed by centrifugation for 10 minutes at 3000 rpm (Heraeus centrifuge). The supernatant containing the protein extract was transferred to a fresh tube and stored at -20°C.

2.3.2 SDS-polyacrylamide gel electrophoresis (SDS-PAGE)

SDS-PAGE was performed using a mini-gel electrophoresis apparatus (Biorad). The protein gel used was PROTEAN TGX 4-12% precast mini-gel (Biorad). The gel was then placed in an electrophoresis chamber containing 1x running buffer (10 g/l SDS, 30 g/l Tris-HCl, 144 g/l glycine). Protein samples were boiled in a water bath for 5-7 minutes then centrifuged for 30-60 seconds at 13,000 rpm (Heraeus centrifuge). Subsequently, 16 µl of protein supernatant was loaded per lane. One lane was loaded with 6 µl of pre-stained protein molecular weight marker (Thermo Scientific PageRuler Plus) ranging from 10 kDa to 250 kDa. The gel was run at 150 volts (V) for 30-40 minutes in running buffer.

2.3.3 Western blotting

Proteins were transferred from the gel to the membrane using a semi-dry western blotting system. A pre-assembled package of 10, 7 x 8.5 cm pre-cut blotting mini transfer pack (Biorad) was used comprising: filter paper, buffer and 0.2 µm nitrocellulose membrane for use with Trans-Blot Turbo Transfer System (Biorad) – a semi-dry blotting apparatus. The gel was placed on top of the membrane and sandwiched between layers of soaked filter paper. Air bubbles were rolled out carefully using a roller. The proteins were transferred to the membrane by blotting with the high molecular weight (MW) BioRad pre-programmed protocol: up to 25 V and 1.3 A for 10 minutes. After electro-blotting, transferred proteins were checked by ponceau staining (0.1% ponceau S, 5% acetic acid). The membrane was de-stained with 1 x phosphate buffered saline (PBS) (PBS tablets, OXOID). The membrane was then blocked with 5% skimmed milk (Sigma) in 1 x PBS, 0.1% Tween (PBS-T) for 30-60 minutes at room temperature with shaking. The membrane was incubated in 5% skimmed milk and 1 x PBS-T with 1:1000 dilution of primary antibody, as detailed in **Table 2.4**. Primary antibody incubation was carried out at 4°C overnight on a rotating plate. Membranes were washed three times (5 minutes per wash) in 1 x PBS-T and incubated in 5% skimmed milk, 1 x PBS-T containing 1:10,000 secondary antibody at room temperature for 1-2 hours. The washing steps were repeated and the ECL prime western blotting system (GE Healthcare) was used for chemiluminescent detection as per the manufacturer's instructions. The protein levels were then visualised using a UV transilluminator and an image captured using Quantity-One (BioRad).

2.3.4 Western blot stripping

To strip blots, the blot was incubated, shaking in stripping buffer (0.1 M Glycine - HCl, pH 2.5-3) for 15-30 minutes at room temperature.

Chapter 3 The construction and characterisation of *pol3* exonuclease domain mutations in *S. pombe*

3.1 INTRODUCTION

In the last century, *S. pombe* has become an ideal laboratory model organism for studying eukaryotic molecular and cellular processes. In comparison to *Saccharomyces cerevisiae*, *Schizosaccharomyces* possesses more biological pathways that are conserved in higher eukaryotes, such as 67% of its protein-coding genes are conserved in humans (Hayles and Nurse, 2016; Wood et al., 2002). For these reasons, fission yeast has become an excellent model organism for preliminarily investigating biological mechanisms involved in mitotic and meiotic cell cycles, chromosome biology, and DNA replication, damage and repair.

3.1.1 Aims of Chapter 3

The predominant purpose of this chapter is to determine whether the cancer-associated mutations present in *POLD1* are likely to be mutagenic by modelling the equivalent mutations in *S. pombe*.

The aims of the chapter are as follows:

- Construction of *pol3* mutants in fission yeast via gene cloning methods.
- Calculation of the mutation rates of various *pol3* variants to assess their inherent mutagenicity.
- Assessment of dinucleotide repeat stability in *pol3* variants via mutation rate analyses.
- Measurement of the growth rates of the *pol3* mutant strains versus wild type.
- Determining whether the *pol3* variants show other phenotypes, such as sensitivity to DNA-damaging agents.

3.2 RESULTS

3.2.1 Construction of *pol3* yeast mutants

3.2.1.1 Construction of equivalent POLD1 exonuclease domain mutants (EDMs) in fission yeast

The scheme for site-directed mutagenesis is summarised in **Figure 3.1**. Primers 1148 and 1076 are the forward and reverse flanking primers that amplify the whole Pol3 reading frame. Point mutations were created by designing a mismatch in the mutagenic primers and the desired variant is located in the centre of the overlapping region of the two mutagenic primers (**Figure 3.1A**). The mutagenic primer pairs used were: 1176 & 1177 (for *pol3P311L*), 1206 & 1207 (for p*ol3D300N*), 1208 & 1209 (for *pol3G305S*), and 1210 & 1211 (for *pol3L458P*) (**Table 2.2**). Each mutation generates a specific restriction site, summarised in **Figure 3.1B**.

Constructing the mutation involved two rounds of PCR. The first round of PCR involved two reactions with primer 1148 (forward) and the mutagenic primer (reverse); and primer 1076 (reverse) and the other mutagenic primer (forward), with *S. pombe* DNA as template. After the first round of PCR, two separate fragments were formed (**Figure 3.1C**): the first fragment (the 'L' fragment) was ~ 437 base pairs (bp) and the second fragment (the 'R' fragment) was 2337 bp for the *P311L* mutation. The L fragments for *D300N*, *G305S* and *L458P* mutations were 414, 424 and 883 bp, respectively, and the R fragments were 2377, 2363 and 1903 bp, respectively. The fragments were gel purified. The second round of PCR used template generated by annealing and extending the 'L' and 'R' fragments together as described in **Section 2.2.4**. After annealing and extension, the annealed fragments were used as a PCR template for primers 1148 and 1076 (**Figure 3.1D**). The product was digested with its respective unique restriction enzyme to ensure that it contained the desired mutation.

The PCR product (~ 2.8 kbp) was cut with BamHI and AscI, ligated into a similarly cut plasmid *pFA6a-kanMX6* vector (#958 – **Table 2.3**) and, subsequently, transformed into *E. coli* (**Figure 3.2**). *E. coli* transformants were screened by colony PCR; positive transformants yielded a DNA fragment size of 571 bp using oligos 1121 and 1075 (see **Table 2.2**; **Figure 3.2C**). Plasmid from a positive transformant was purified and then sequenced to confirm that the insert contained the desired mutation and that no additional mutations were introduced by PCR amplification, as described in **Chapter 2.2.5**. This created the new plasmids: *pFA6a-kanMX6-pol3P311L* (#983), *pFA6a-kanMX6-pol3G305S* (#1012), *pFA6a-kanMX6-pol3D300N* (#1013) and *pFA6a-kanMX6-pol3L458P* (#1014) (see **Table 2.3**).

After *E. coli* transformation, plasmid purification and sequencing, the *pFA6a-kanMX6-mutant* plasmids were linearised using the restriction enzyme XhoI and transformed into *S. pombe* (Strain #3500 – see **Table 2.1**; **Figure 3.3**). Colonies were selected for G418 resistance.

Transformants were screened by colony PCR (using primers 1183 and 1088) to determine if integration had occurred at the *pol3* locus, and the PCR amplified DNA was digested with its corresponding unique restriction enzyme to determine whether the designated mutation had been successfully retained. The desired fragment sizes and total number of positive yeast transformants (average 50% transformation efficiency) for the varying mutations after colony PCR and restriction digestion are displayed on agarose gels in **Figure 3.4**. Two *pol3P311L/G305S/L458P/D300N* strains were thus identified and selected, i.e. two biological replicate strains were isolated for each mutation, to observe whether two strains, supposedly with the same genotype, express a similar phenotype in the experimental assays. Finally, the yeast transformants were sequenced to confirm that the sequences were as expected (**Figure 3.5**). This yielded the *S. pombe* strains: 3354, 3355, 3941, 3942, 3943, 3944, 3945 and 3946 (**Table 2.1**).

Figure 3.1

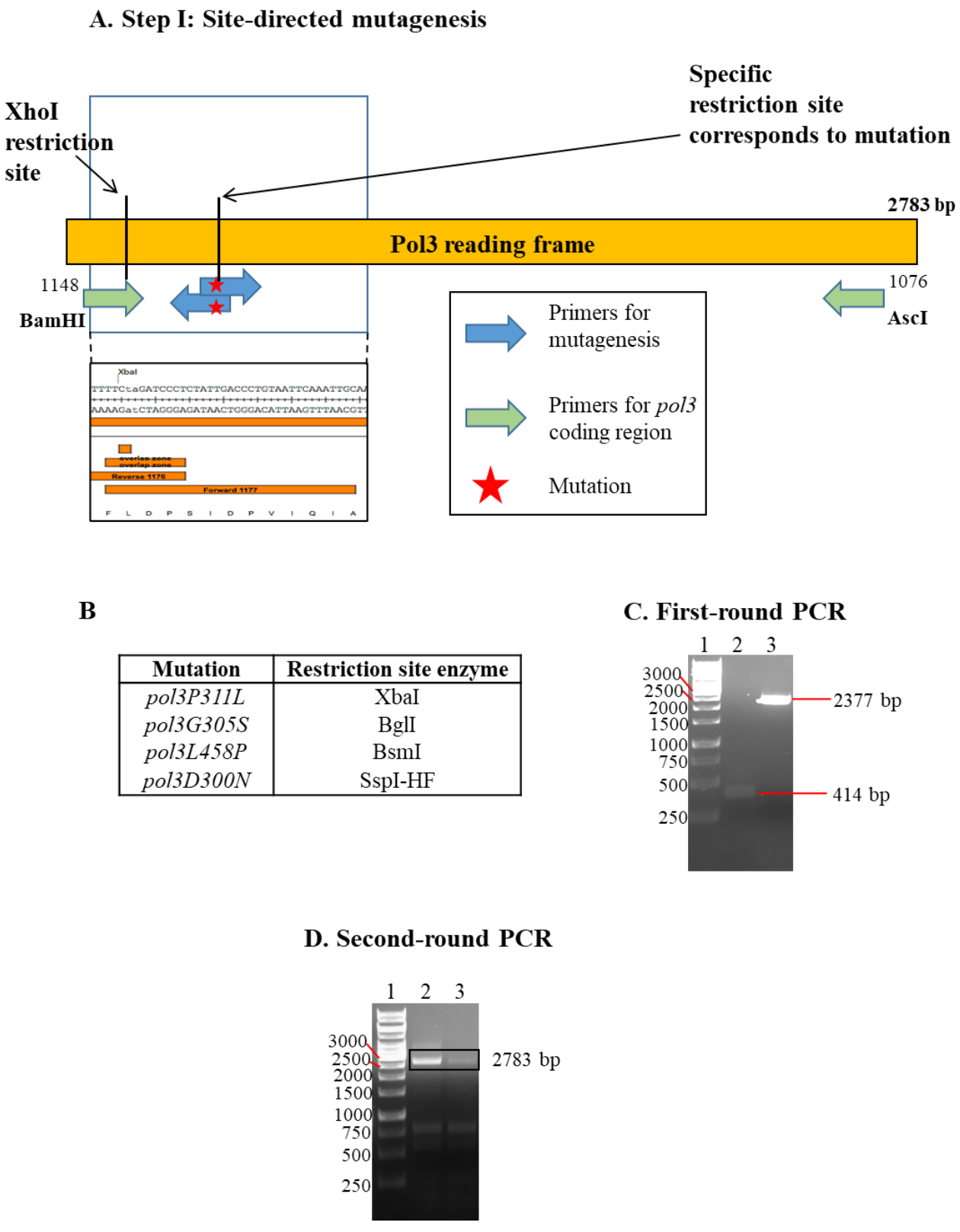

A. Step I: Site-directed mutagenesis
XhoI restriction site
Specific restriction site corresponds to mutation
2783 bp
Pol3 reading frame
1148
BamHI
1076
AscI
Primers for mutagenesis
Primers for pol3 coding region
Mutation
XbaI
overlap zone
overlap zone
Reverse 1176
Forward 1177
F L D P S I D P V I Q I A
B
Mutation
Restriction site enzyme
pol3P311L
XbaI
pol3G305S
BglI
pol3L458P
BsmI
pol3D300N
SspI-HF
C. First-round PCR
1 2 3
3000
2500
2000
1500
1000
750
500
250
2377 bp
414 bp
D. Second-round PCR
1 2 3
3000
2500
2000
1500
1000
750
500
250
2783 bp

Figure 3.1: The first step in constructing the exonuclease domain mutations (EDMs) in *S. pombe* is via site-directed mutagenesis: (A) A schematic outlining Step I in the construction of the mutations, site-directed mutagenesis. The location of the mutation is emphasised by red stars on overlapping regions of the primers for mutagenesis (blue arrows), which vary in sequence for each mutation. The mutagenic primers create two fragments of DNA containing the desired mutation during the first-round of PCR; the diagram panel below the blue arrows is an example of how mutagenic primers, 1176 and 1177, create the 'ta' mutation in *pol3P311L*, with the specific restriction site, XbaI. Primers 1148 (forward) and 1076 (reverse), for the *pol3* coding region, are depicted by light green arrows on either side of the Pol3 reading frame. XhoI restriction enzyme is used to linearise the plasmid before yeast transformation. **(B)** Each mutation generates a unique restriction site. **(C)** Gel showing the DNA fragments formed after the first-round of PCR in the construction of the *pol3D300N* mutation. Lane 1 is the 1 kb DNA molecular marker; Lane 2 is the DNA fragment (414 bp) formed by primers 1148 (forward) and 1207 (reverse mutagenic primer); Lane 3 is the DNA fragment formed by primers 1206 (forward mutagenic primer) and 1076 (reverse). **(D)** Agarose gel showing the annealed DNA fragment (2783 bp) post extension and second-round PCRs. Lane 1 is the 1 kb DNA molecular marker; Lanes 2 and 3 are the PCR products of the annealed fragment, 1:10 and 1:100 dilution, respectively.

Figure 3.2

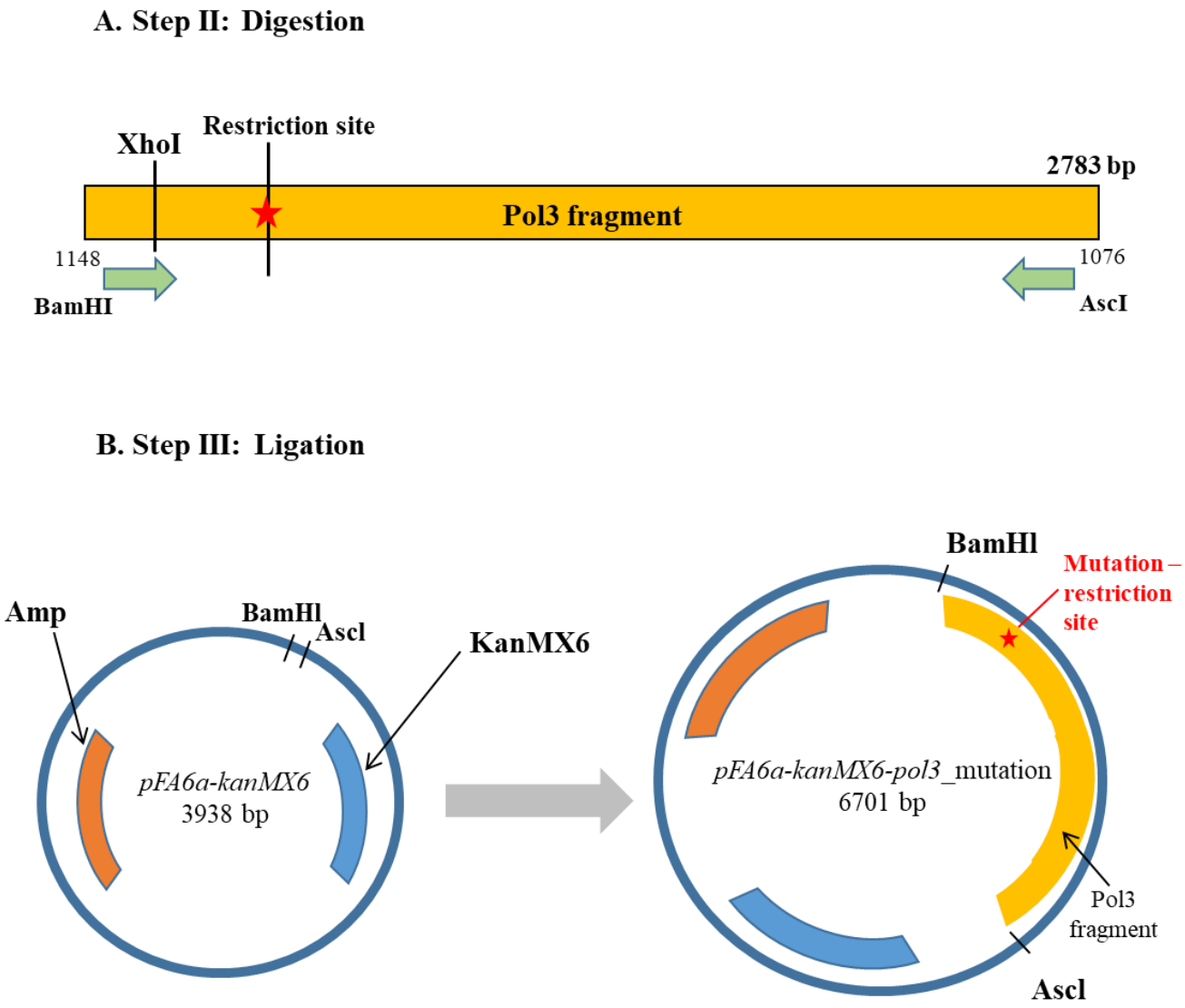
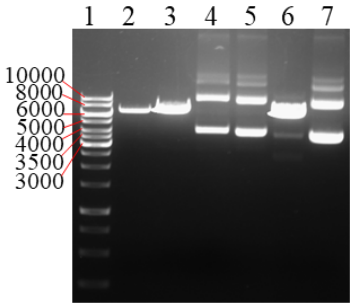

A. Step II: Digestion
XhoI
Restriction site
2783 bp
Pol3 fragment
1148
1076
BamHI
AscI
B. Step III: Ligation
Amp
BamHI
AscI
KanMX6
pFA6a-kanMX6
3938 bp
BamHI
Mutation – restriction site
pFA6a-kanMX6-pol3_mutation
6701 bp
Pol3 fragment
AscI
C. Step IV: E. coli Transformation
3000
2500
2000
1500
1000
750
500
250
571 bp
Purification of mutant plasmid from positive E. coli transformant(s)

Figure 3.2: Steps II, III and IV in the construction of the EDMs. Digestion and ligation of the vector and insert, followed by transformation of the vector-insert construct into *E. coli*. (A & **B)** Primers 1148 (forward) and 1076 (reverse) are depicted by light green arrows on either side of the Pol3 reading frame. Restriction enzymes BamHI and AscI are used to create sticky ends on the fragment, ready for cloning into the similarly BamHI- and AscI-cut plasmid vector. The plasmid vector possesses both ampicillin (Amp - orange) and kanamycin/G418 (KanMX6 – blue) resistance. The red star in the pol PCR insert of the ligated vector-insert construct represents the region of the Pol3 fragment (yellow) that has the desired mutation, which is specific to unique enzymatic digestion as described in **Figure 3.1**. **(C)** Diagnostic gel showing bacterial transformants that have successfully incorporated the vector-insert construct, producing a desired band of 571 bp after colony PCR with primers 1121 and 1075. The successful bacterial transformant colonies are then purified to obtain the mutant plasmid. Lane 1 is the 1 kb molecular marker.

Figure 3.3

A. Step V: Linearisation of plasmid with XhoI



B. Step VI: Integration into *S. pombe* via HR

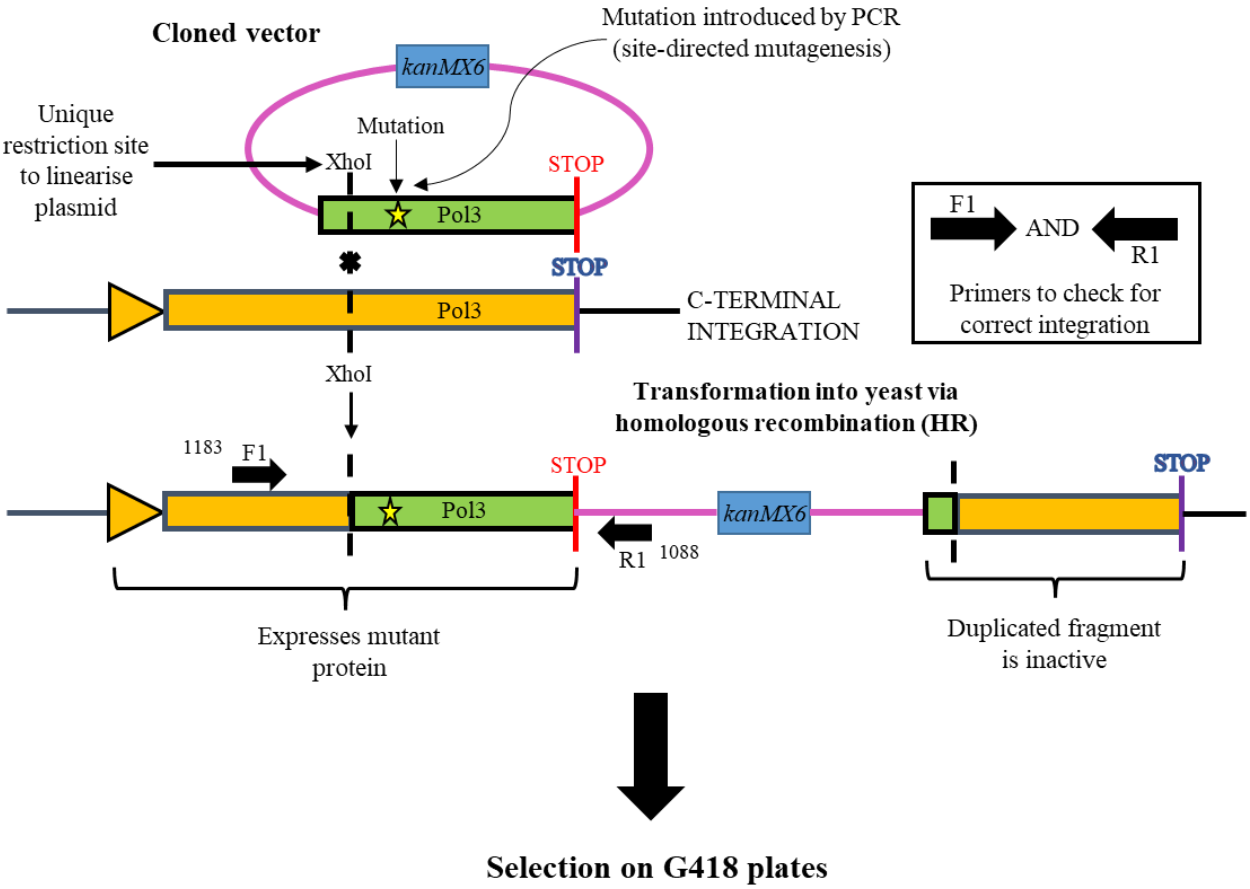
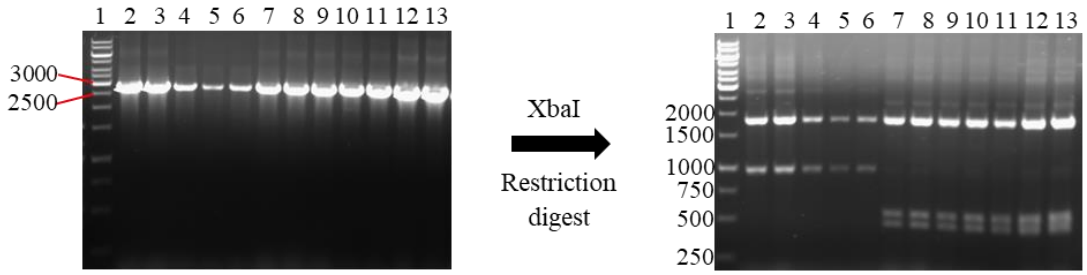


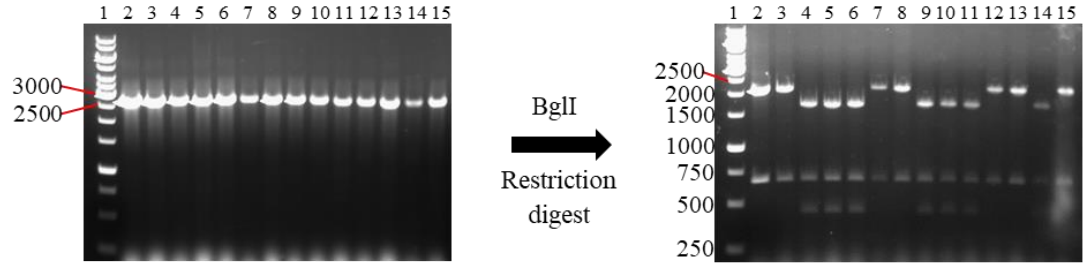
Figure 3.3: The final two steps (V and VI) in the construction of EDMs in *S. pombe*. Linearisation of the mutant plasmid is required prior to yeast transformation. (A) Gel showing mutant plasmids pre- and post-linearisation with restriction enzyme XhoI. Lane 1 is the 1 kb molecular marker; Lanes 2, 3 and 6 are the XhoI-cut plasmids, *pFA6a-kanMX6-pol3D300N*, *pFA6a-kanMX6-pol3G305S* and *pFA6a-kanMX6-pol3L458P*, respectively, producing a band of 6701 bp. Lanes 4, 5 and 7 are uncut *pFA6a-kanMX6-pol3D300N*, *G305S* and *L458P* plasmids, respectively, producing the typical supercoiled, nicked and diamond plasmid DNA structures observed. **(B)** Transformation of the linearised *pol3* mutant plasmid into *S. pombe* genomic DNA. The Pol3 fragment of the cut plasmid possessing the desired mutation (green with yellow star) integrates with part of the Pol3 reading frame from the genomic yeast DNA (orange), forming a new Pol3 coding domain that includes the mutation. The other duplicated Pol3 fragment becomes inactive and is not expressed. Since the whole plasmid becomes integrated, then the new strain now expresses G418 resistance (Figure 3.2). Thus, the yeast colonies carrying the desired mutation are selected on G418-containing plates. The F1 and R1 primers represent 1183 and 1088 primers, respectively, and they check that the plasmid has been correctly integrated in the yeast genome, via colony PCR.

Figure 3.4

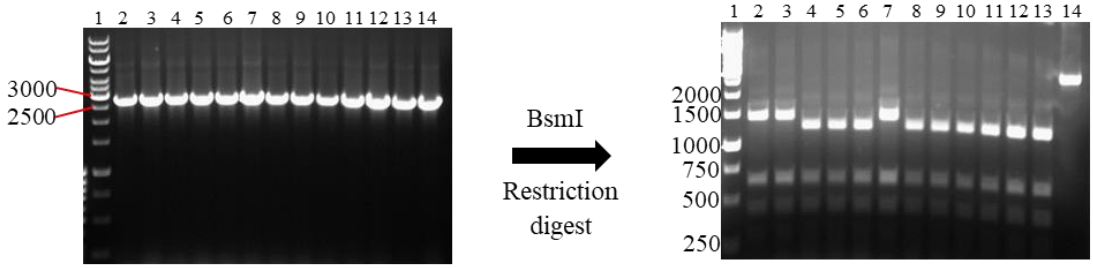
A. *pol3P311L*: Colony PCR



B. *pol3G305S*: Colony PCR



C. *pol3L458P*: Colony PCR



D. *pol3D300N*: Colony PCR

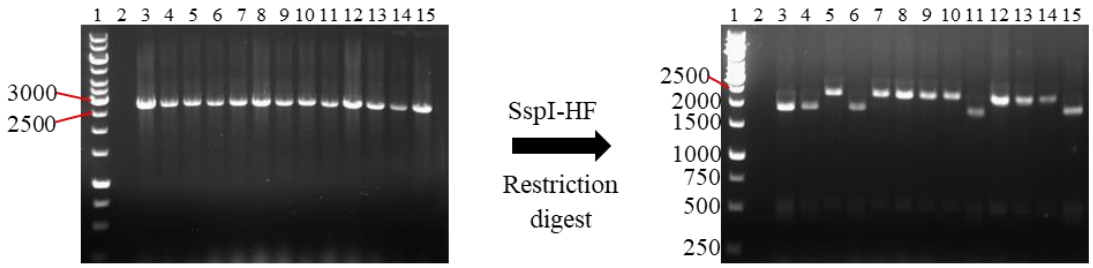


Figure 3.4: Characterisation of yeast transformants' genotype via colony PCR and restriction digestion. Left panel: colony PCR was carried out on yeast transformant single colonies using the primer pair 1183 and 1088. Correct integration of the mutant plasmid into the yeast DNA yields a 2.8 kbp band on agarose gel. For all gels, lane 1 is the 1 kb molecular marker. **(A)** The colony PCR fragments were digested with XbaI restriction enzyme (right panel). If the *pol3P311L* mutation is present, XbaI cuts twice forming 3 bands: 1798 bp, 532 bp and 463 bp. If the mutation is not present then XbaI cuts once forming 2 bands: 1798 bp and 968 bp. Therefore, lanes 7-13 are positive yeast transformants. **(B)** The colony PCR fragments were digested with BglI restriction enzyme (right panel). If the *G305S* mutation is present, BglI cuts twice forming 3 bands: 1721 bp, 673 bp and 451 bp. If the mutation is not present then BglI cuts once forming 2 bands: 2172 bp and 673 bp. Therefore, lanes 4-6, 9-11 and 14 are positive yeast transformants. **(C)** The colony PCR fragments were digested with BsmI restriction enzyme (right panel). If the *L458P* mutation is present, BsmI cuts four times forming 5 bands: 1292 bp, 642 bp, 441 bp, 283 bp and 187 bp. If the mutation is not present then BsmI cuts three times forming 4 bands: 1479 bp, 642 bp, 441 bp and 283 bp. Therefore, lanes 4-6 and 8-13 are positive yeast transformants. **(D)** The colony PCR fragments were digested with SspI-HF restriction enzyme (right panel). If the *D300N* mutation is present, SspI-HF cuts twice forming 3 bands: 1915 bp, 499 bp and 431 bp. If the mutation is not present then SspI-HF cuts once forming 2 bands: 2346 bp and 499 bp. Therefore, lanes 3, 4, 6, 11 and 15 are positive yeast transformants.

Figure 3.5

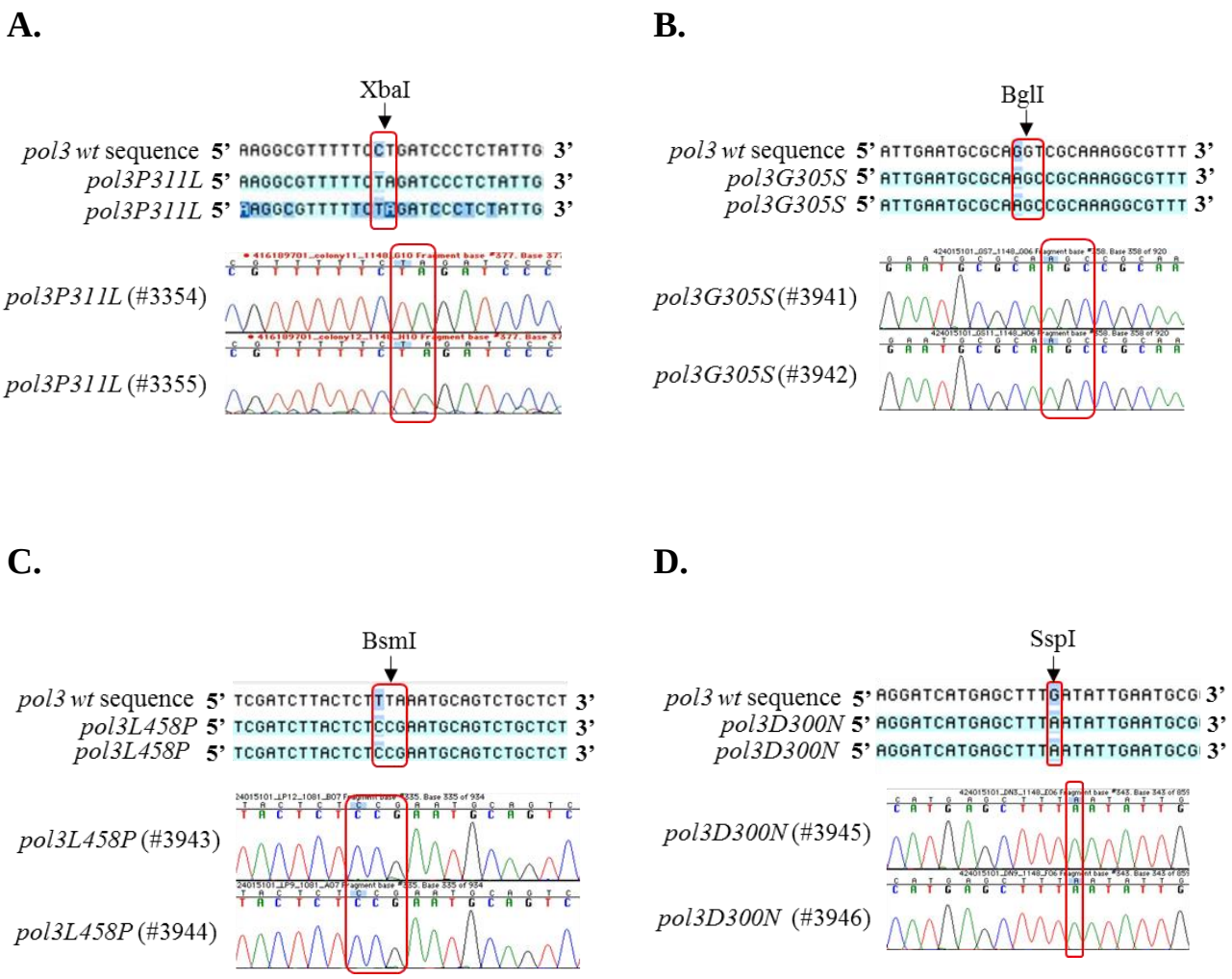


Figure 3.5: Yeast strains contain the desired *pol3* mutations. Sequencing results of *pol3P311L* **(A)**, *pol3G305S* **(B)**, *pol3L458P* **(C)**, and *pol3D300N* **(D)** mutant strains display the desired base substitution mutations (in red boxes) at the restriction sites of Xbal, BglI, BsmI and SspI enzymes, respectively. The resulting strain numbers are in brackets.

3.2.1.2 Construction of fission yeast strain expressing pol3(d)D386A mutation: an exonuclease null pol3 strain

The *pol3D386A* yeast mutation was not modelled from a clinical *POLD1* variant in humans. Instead, it behaves as a control in all the experiments; it is an *S. pombe* strain where a key catalytic residue, Asp386, in the exonuclease active site of Pol3 has been substituted to alanine (p.Asp386Ala) (**Figure 3.6A**), and equivalent mutations constructed in mice and ϕ29 DNA polymerase (from the bacteriophage ϕ29) have been shown to lack proofreading (Goldsby et al., 2002; Bernad et al., 1989).

There was an existing *pol3D386A* strain (#3273 – **Table 2.1**) in the lab, however, in order to produce a second biological replicate of the D386A variant, the *pFA6a-kanMX6-pol3D386A* plasmid (#969 – **Table 2.3**) was linearised using the restriction enzyme CspCI prior to yeast transformation into a Wt strain (#3500). Transformants were screened by colony PCR, using the primer pair 1087 and 1088, and the PCR amplified DNA was incubated with the restriction enzyme, NruI (**Figure 3.6B**). Six out of nine yeast transformants tested positive for the *pol3D386A* mutation and one successful transformant was sequenced with primer 1121 to confirm that the sequence was as expected (**Figure 3.6C**). This created the strain 3421 (**Table 2.1**).

3.2.1.3 Construction of fission yeast strain expressing pol3(d)P311R mutation

Previous work has shown that an *S. cerevisiae* strain expressing *pol2(e)P301R*, equivalent to the human *POLE* P286R somatic mutation, has a very high Can^r mutation rate; 150 fold increase over Wt, and 50 times higher than that of the exonuclease null Pol ε strain (Kane and Shcherbakova, 2014). Thus, mutation of this highly conserved proline residue in Pol ε causes a very strong mutator phenotype (**Figure 3.7B**). The location of *POLD1* P327L (Sp. *pol3P311L*) is homologous to *POLE* P286R (Sp. *pol2P287R*) in the exonuclease domain (**Figure 3.7A**);

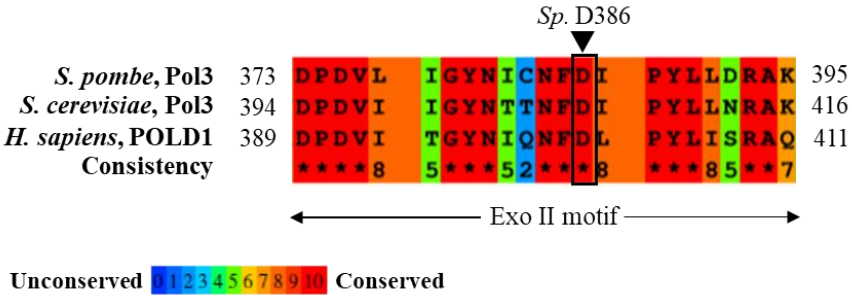
therefore, it would be interesting to observe if the same missense mutation (proline to arginine amino acid change) in Pol δ at the homologous position would have an equally high mutation rate, in an attempt to understand the effects of Pol ε and Pol δ malfunction on leading and lagging strands, respectively. To address this question, the equivalent mutation in *pol3* was constructed, followed by mutation rate analysis (Can^r fluctuation assay). Note that *pol3P311R* is not a clinically found mutation.

This strain was made identically to the germline *pol3* mutants (**Section 3.2.1.1**) with some adjustments: during gene mutagenesis (first round PCR), the two mutagenic primers used were 1192 and 1193 (**Table 2.2**); the flanking primers, 1148 and 1076, remained the same. Secondly, the *P311R* mutation generated a specific NruI restriction site that cut only once within the Pol3 reading frame.

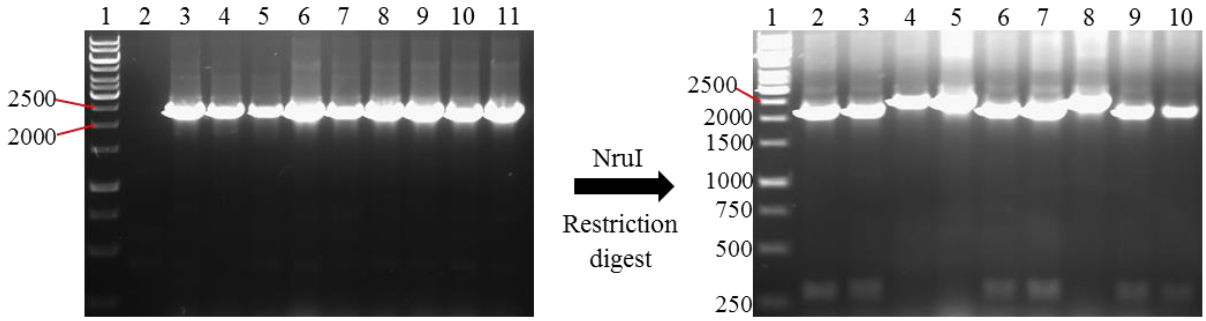
After yeast transformation, transformants were screened by colony PCR to determine if correct integration had occurred and the PCR amplified DNA was incubated with NruI to determine whether the mutation had been successfully incorporated (**Figure 3.7C**). Out of 12 colonies screened, 4 had successfully been integrated at the *pol3* locus containing the desired mutation. Two *pol3P311R* transformants were thus selected and sequenced with primer 1148 to confirm that the sequence was as expected (**Figure 3.7D**). This produced the strains 3419 and 3426 (**Table 2.1**).

Figure 3.6

A.



B. *pol3D386A*: Colony PCR



C.



Figure 3.6: Confirmation of introduction of the *pol3D386A* mutation in *S. pombe*. (A) The Sp. *pol3D386A*/ Sc. *pol3D407A* mutation affects a highly conserved aspartate residue in the Exo II motif of the exonuclease domain. Results are colour-coded for amino acid conservation. Alignment produced using PRALINE. **(B)** Colony PCR of yeast transformant single colonies using the primer pair 1087 and 1088 (left panel). Correct integration of the mutant plasmid into the yeast DNA yields a 2.4 kbp band on agarose gel. The colony PCR fragments were digested with NruI restriction enzyme (right panel). If the D386A mutation is present, NruI cuts once forming 2 bands: 2159 bp, and 303 bp. If the mutation is not present then NruI does not cut, leaving the PCR fragment intact (2.4 kbp). Thus, lanes 2, 3, 6, 7, 9 and 10 are positive yeast transformants. Lane 1 is the 1 kb molecular marker. **(C)** Sequencing results of *pol3D386A* mutant strain display the desired base substitution mutations (in red boxes) at the restriction site of NruI. The yeast strain number is in brackets.

Figure 3.7

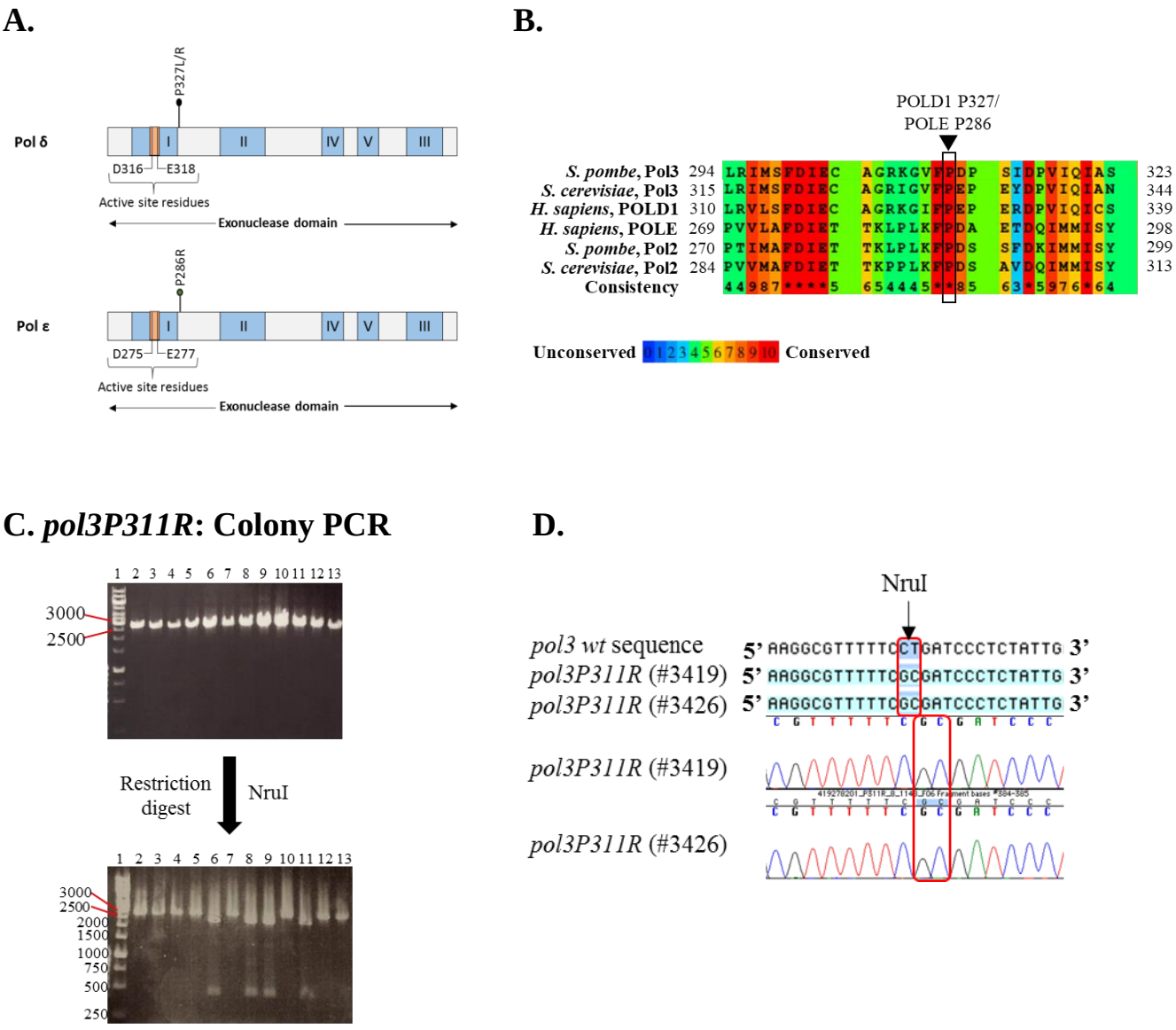


Figure 3.7: *Pol3P311L/R* is homologous to *pol2P287R*, which affects a conserved proline residue required for proofreading. The *pol3P311R* mutation in strains is confirmed. (A) The location of the human *POLD1* P327 (Sp. *pol3P311*) mutation in the exonuclease domain of Pol δ is homologous to the location of the human somatic *POLE* P286R (Sp. *pol2P287R*) mutation in the exonuclease domain of Pol ε. Conserved exo I – V motifs are highlighted in dark blue, and the exo I motif active site residues are highlighted in pink. Image modified from Rayner et al (2016) **(B)** Sequence alignment (using PRALINE) demonstrates that human Pro286 (Sp. Pro287) and human Pro327 (Sp. Pro311) are invariant in POLE and POLD1 orthologues, respectively. Results are colour-coded for amino acid conservation. **(C)** Colony PCR of yeast transformant single colonies using the primer pair 1183 and 1088 (upper panel). Correct integration of the mutant plasmid into the yeast DNA yields a 2.8 kbp band on agarose gel. The colony PCR fragments were digested with NruI restriction enzyme (lower panel). If the *pol3P311R* mutation is present, NruI cuts once forming 2 bands: 2337 bp, and 446 bp. If the mutation is not present then NruI does not cut leaving the PCR fragment intact (2.8 kbp). Thus, lanes 6, 8, 9 and 11 are positive yeast transformants. Lane 1 is the 1 kb molecular marker. **(D)** Sequencing results of *pol3P311R* mutant strains display the desired base substitution mutations (in red boxes) at the restriction site of NruI. Strain numbers are in brackets.

3.2.2 Mutation rate assays

Mutation rates were assessed by fluctuation analysis of canavanine-resistant (Can^r) mutants in replica cultures (Foster, 2006) and were calculated using the Ma-Sandri-Sarkar Maximum Likelihood Estimator (MSS-MLE) method (Sarkar et al., 1992; Rosche and Foster, 2000). **Figures 3.8A** & **B** depict a step-by-step flow chart of the fluctuation assay method. In detail, two independent freshly grown colonies per genotype were grown in 10 ml YES at 30°C.

The following morning each culture was diluted to 10^4 cells per ml and divided into twelve 1 ml replica cultures grown in a sterile flat-bottom 24-well polypropylene microtitre plate with a low-evaporation lid. After 2 days of growth at 30°C, the cells were suspended by vigorous vortexing. 150 µl of twelve replica cultures for each isolate were 'spotted' on canavanine selection plates (6 spots per plate). It is important to add that each well was spotted twice onto PMG + Can plates to gain repeats and to allow for potential contamination. Can^r mutants (r) were counted after 12 days of growth at 30°C. This way 'r', the total number of mutants per culture, can be calculated. Next, since it can be assumed that all saturated cultures have approximately the same final density, 10^{-4} dilutions of two cultures per isolate were transferred onto two YES plates separately in order to determine the total number of viable cells per culture (Nt). YES plates were incubated for 2-3 days at 30°C. The data were imported into FALCOR to calculate the mutation rates (M) using the statistical method MSS-MLE (see **Chapter 2.1.5**).

The mechanism of resistance to the arginine analogue L-canavanine, and of arginine uptake in fission yeast were examined in Fantes and Creanor (1984). Canavanine resistance in cells is achieved by gaining a minimum of two mutations, one of these being a loss-of-function mutation in the *can1* gene, meaning that the cells cannot import the drug; the other mutation occurs in a gene that remains unknown till this day (Fantes and Creanor, 1984).

Figure 3.8C displays how the spotting method used in fluctuation analyses appears for some of these strains after 12 days incubation at 30°C. There are very few visible canavanine-resistant (Can^r) colonies that have grown on the spots of the Wt strain, as expected, and *pol3P311L* strain (**Figures 3.8C I** & **IV**). This implies that *pol3P311L* has a low mutator phenotype. *Pol2P287R* is highly mutagenic according to Kane and Shcherbakova (2014) and thus, as predicted, it has many Can^r colonies (**Figure 3.8C II**). *Pol2(e)D276A/E278A* is an exonuclease null *pol2* strain and has numerous Can^r colonies (**Figure 3.8C III**), but not as many as *pol2P287R*.

3.2.2.1 Mutation rates of pol3 EDMs

Fluctuation analysis was conducted on the *pol3* variants to ascertain their mutation rates and to compare them to the *pol3D386A* mutant that lacks proofreading activity.

The mutation rates of the *pol3P311L* and *pol3G305S* strains did not significantly differ from wild type (**Figures 3.9A** & **B**; **Table 3.1**); hence, they do not have strong mutator phenotypes which may be the same for the human equivalent germline mutations *POLD1* P327L and *POLD1* G321S.

The mutation rate of the exonuclease dead *pol3* mutant (*pol3D386A*) was approximately 30 times higher than that of wild type which is expected for a strain that is completely defective in proofreading (**Figure 3.9E; Table 3.1**). Residue D386 is highly conserved and the equivalent Pol δ mutations in budding yeast (D407A) and mice (D400A) were previously characterised as strong mutators (Murphy et al., 2006; Simon et al., 1991; Jin et al., 2001; Goldsby et al., 2001, 2002). The *pol3-D407A* strain was reported to have a Can^r mutation rate 26 times higher than wild type, similar to the relative mutation rate of *pol3D386A* observed in *S. pombe* (Herr et al., 2011).

It was predicted that *pol3D300N* would have a strong mutator phenotype because *D300N* affects a highly conserved key catalytic residue in the Exo I motif of the exonuclease active site (see **Figures 1.5** & **1.6**) (Murphy et al., 2006). As expected, *pol3D300N* had a significantly elevated relative mutation rate, comparable to exonuclease null Pol3 (**Figure 3.9D; Table 3.1**). In addition, mutation of the corresponding residue in *S. cerevisiae*, D321 inactivated exonuclease activity and increased the mutation rates 90-370 fold over Wt (Simon et al., 1991; Jin et al., 2001). Therefore, it appears that mutations of highly conserved residues in the Exo I motif are just as mutagenic as mutations of equally conserved residues in the Exo II motif of Pol δ, such as Sp. *pol3D386A* (Sc. *pol3-D407A*) (Simon et al., 1991; Murphy et al., 2006).

The relative mutation rate of *pol3L458P* was significantly different to Wt (**Figure 3.9C; Table 3.1**): it was 9 times higher than that of Wt, suggesting that *pol3L458P* has compromised, but not entirely lacking, proofreading activity. Murphy et al (2006) conducted mutation rate assays on an *S. cerevisiae* strain expressing a different missense mutation at the analogous amino acid residue, p. Leu479Ser: it was highly error-prone and had a comparable mutator phenotype to a strain completely devoid of any Pol δ proofreading activity (approximately 30-fold increase over Wt for the Can^r mutation rate). This did not quite correspond with the considerably weaker mutator phenotype observed for the *pol3L458P* mutation in *S. pombe*. In concordance with the former study, Sattar et al (1996) revealed that an alanine substitution for L287 in T4 DNA polymerase (Sp. L458) produces mutants with significantly impaired exonuclease activity (Sattar et al., 1996).

Table 3.1 lists the mean mutation rate values per 10^8 cell divisions for each *pol3* genotype.

Figure 3.8

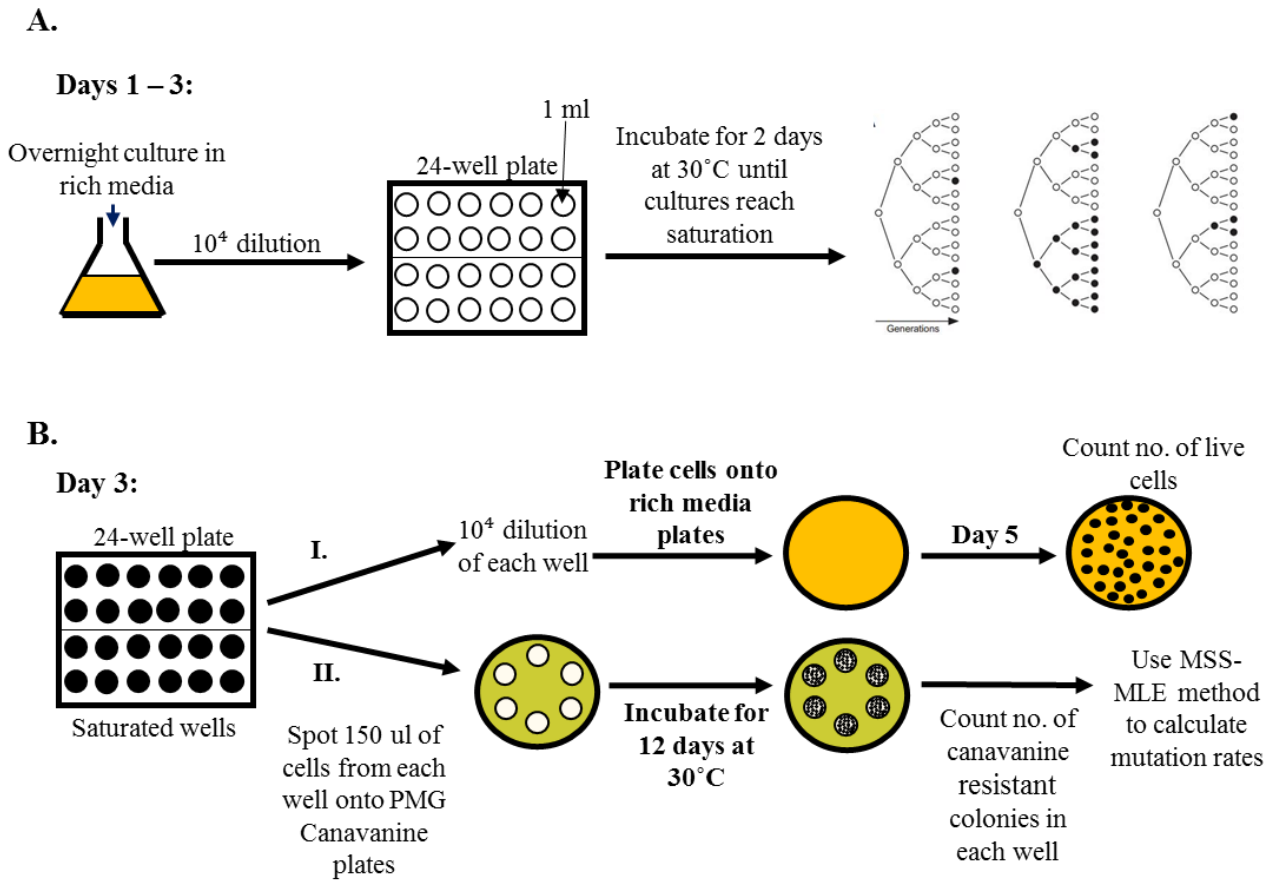

A.
Days 1 – 3:
Overnight culture in rich media
10⁴ dilution
24-well plate
1 ml
Incubate for 2 days at 30˚C until cultures reach saturation
Generations
B.
Day 3:
24-well plate
Saturated wells
I.
II.
10⁴ dilution of each well
Spot 150 ul of cells from each well onto PMG Canavanine plates
Plate cells onto rich media plates
Incubate for 12 days at 30˚C
Day 5
Count no. of live cells
Count no. of canavanine resistant colonies in each well
Use MSS-MLE method to calculate mutation rates
C.
I
II
III.
IV.

Figure 3.8: Diagrams outlining the canavanine resistance fluctuation assay method. (A) Cells were grown overnight in YES and diluted to 10^4 cells per ml per well in a 24-well plate. Twelve wells per strain with an initial cell density of 10^4 cells were grown to saturation for 2 days at 30˚C. This is so the cells can be subjected to many generations of growth and division to allow for a mutation/s to occur during the growth of a culture. If mutagenesis is spontaneous, occasional mutations occurring early in the 24-well plates would give rise to 'jackpots' of resistance on the selective plates (Sarkar et al., 1992). **(B.I)** 10^{-4} dilutions of saturated cultures were plated onto YES. Colonies were counted after 2 days at 30˚C. This is the total number of cells present in the culture before plating onto selective media. **(B.II)** 150 µl of each saturated well was spotted onto canavanine-containing PMG plates (6 spots per plate), allowed to dry and incubated at 30˚C for 12 days. Mutant cells prosper to form visible colonies on the plate and the number of such colonies is equal to the number of mutant cells present in the corresponding culture at the time of plating. The number of canavanine-resistance (Can^r) colonies were counted with the naked eye. Mutation rates were calculated using the Ma-Sandri-Sarkar Maximum Likelihood Estimator (MSS-MLE) method (Sarkar et al., 1992). **(C)** Spotting method in Can^r fluctuation assay. Saturated cultures were spotted onto PMG + 70 µg/ml Can plates. Colonies were counted after 12 days of growth. The white colonies are Can^r colonies. Each plate represents a different strain spotted: **I.** *pol3(d)P311L*, **II.** *pol2(e)P287R*, **III.** *pol2(e)D276A/E278A* (i.e. exonuclease defective Pol e) and **IV.** Wild type (Wt).

Figure 3.9

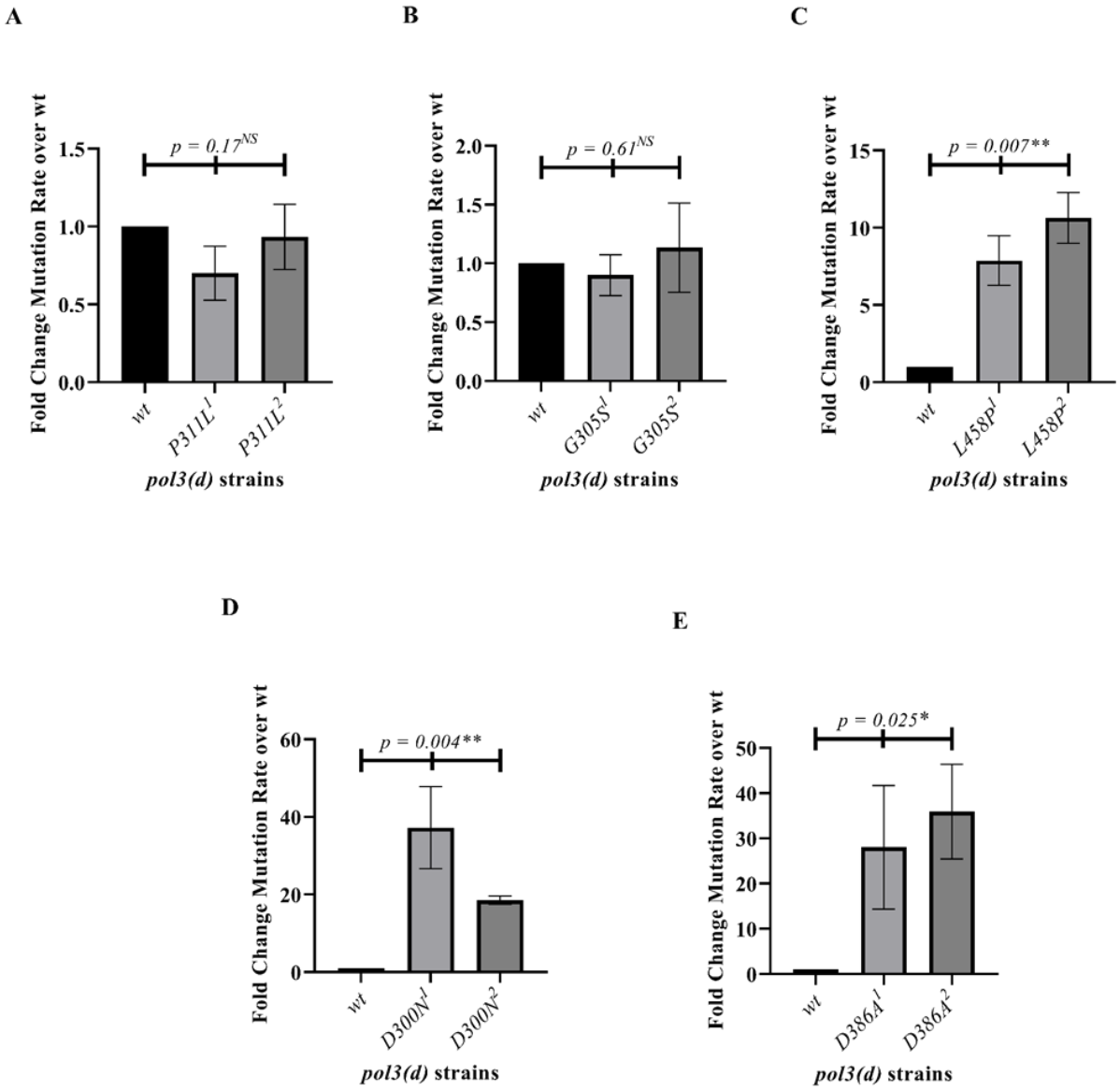


Figure 3.9: Can^r mutation rates of the indicated strains relative to wild type, determined by fluctuation analysis. (A-E) Mutation rates (x 10^{-8}) were calculated using the MSS-MLE method and the fold change shown is the fold difference in the Can^r mutation rate between the haploid wild type and *pol3* variants. Two biological replicate strains were used for each mutant genotype. The strains used were: 3500 (Wt), 3354 (*P311L*^{1}), 3355 (*P311L*^{2}), 3941 (*G305S*^{1}), 3942 (*G305S*^{2}), 3943 (*L458P*^{1}), 3944 (*L458P*^{2}), 3945 (*D300N*^{1}), 3946 (*D300N*^{2}), 3273 (*D386A*^{1}), and 3421 (*D386A*^{2}). *Pol3(d)D386A* is a *pol3* mutant devoid of exonuclease activity. Data are shown as mean ± SD (n = 3). P-values were calculated using the Kruskal-Wallis test: ^{NS} p > 0.05, * p < 0.05, ** p < 0.01. NS = Not Significant. Numerical data are in **Table 3.1**.

Table 3.1: Rate of spontaneous mutation in haploid *pol3* mutants

	Can^r mutation	
Genotype	**Mutation Rate (x10^{-8})**	**Fold increase**
Wild-type	12.1 (5.3)	1
pol3P311L	9.4 (2.8)	0.8
pol3G305S	12.4 (6.7)	1
pol3L458P	114.8 (55.5)	9.5
pol3D300N^1	439.9 (216)	36.4
pol3D300N^2	226 (108.1)	18.7
pol3D386A	345.5 (69.7)	28.6

Can^r mutation rates are given as the mean values of all the mutation rates for both replicate strains per mutant genotype (n=3); except *pol3D300N^1* and *pol3D300N^2* biological replicate strains are presented individually because they had a large difference in mutation rate (n=3). Standard deviation (SD) is given in the parentheses. The fold increase shown is the fold difference in the Can^r mutation rate between the wild type and *pol3* mutants (see **Figure 3.9**).

3.2.2.2 Mutation rate of strain expressing pol3P311R

Can^r fluctuation analysis was carried out on a non-clinical mutation in DNA Pol δ, the *pol3(d)P311R* strain, to discern its mutation rate and compare it to the mutation rate of the analogous *S. pombe* variant in Pol ε, *pol2(e)P287R* (**Figure 3.10**). The mean mutation rate of *pol3P311R* was 28.1 x 10^{-8} per generation, two- to three-fold higher than that of Wt. Unlike the *pol2(e)* homologous mutation, *pol3P311R* had a very low mutation rate in comparison (30 times lower). Thus, this particular mutation has a more dramatic effect on Pol ε function than on Pol δ function.

Pol2D276A/E278A is a double mutant yeast strain affecting two highly conserved catalytic residues in the Exo I motif of the Pol ε exonuclease domain and it inactivates proofreading

activity. Mice that carry the analogous double *Pole* mutations (D272A/E274A) also have impaired exonuclease activity (Albertson et al., 2009; Preston et al., 2010). The fact that the clinical P286R mutation (Sp. *pol2P287R*) had a mutation rate an order of magnitude higher than the proofreading deficient Pol ε strain (*pol2D276A/E278A*) indicates that it enhances mutagenicity and elevates cancer risk via some process other than exonuclease deficiency per se (**Figure 3.10**) (Church et al., 2013; Shinbrot et al., 2014; Church et al., 2015). The latter result is consistent with the data on the analogous substitution of human P286R in budding yeast, *pol2-P301R* (Kane and Shcherbakova, 2014).

3.2.3 Guanine-thymine (GT) repeat stability in the *pol3* mutant strains

Simple repeat sequences (≥8 nucleotides) in coding sequences are hot spots for frameshift and insertion and deletion mutations (indels) that can lead to cancer in humans with mismatch repair (MMR) deficiency (Tran et al., 1997; Liu et al., 1999; Pena-Diaz and Rasmussen, 2016). MMR proteins in yeast and mammalian cells, e.g. Msh2, Msh6 and Pms1/2, have been shown to play an important role in preventing tract length variations in mono-, di- and tri-nucleotide repeats, such as the poly (GT) tract, which is the most common simple repeat found in the majority of eukaryotes (Mansour et al., 2001; Tran et al., 1997; Kunkel and Erie, 2015; Strand et al., 1993; Kim et al., 2013; Hamada et al., 1982). Since proficient exonuclease activity and mismatch repair are both required in maintaining DNA replication fidelity and genomic stability (Kunkel and Erie, 2015; Ganai and Johansson, 2016), the Pol δ proofreading domain mutants may have an increased tendency for strand slippage when they encounter homopolymeric or repeat sequences, enhancing indel mutagenesis if not repaired efficiently, as indicated in the following in vivo and in vitro yeast studies (Liu et al., 1999; Kokoska et al., 2000; Fortune et al., 2005). In response to this hypothesis, adenine reversion fluctuation assays were conducted on the *pol3* mutations in a background strain, which consists of eight GT repeat units in the *ade6* gene,

making the strains auxotrophic for adenine (Ade-) (Mansour et al., 2001). If the *pol3* mutations cannot accurately replicate the GT repeat sequence then this can generate a frame shift that can revert the strain to adenine prototrophy (Ade+) (Mansour et al., 2001) (**Figure 3.11A**).

Adenine reversion fluctuation assays were carried out similarly to Can^r fluctuation analyses (see **Section 3.2.2**), except saturated cultures were spotted onto EMM minus-adenine plates. Additionally, saturated cultures grown in rich media were washed twice with sterile deionised water before spotting on EMM solid media in order to wash out amino acid supplements, particularly adenine. EMM plates were incubated at 30˚C for 8 days until colonies formed (refer to methods in **Chapter 2.1.5**).

3.2.3.1 Construction of fission yeast pol3 strains with GT repeats in the ade6 marker gene

The *pFA6a-kanMX6-pol3* mutant plasmids (#969, #983, #1012, #1013 and #1014 – **Table 2.3**) were linearised by Xho1 prior to transformation into the *S. pombe ade6-(GT)$_8$* strain (#3194 – **Table 2.1**). Note that initially, the latter strain was sequenced with primer 1165 (**Table 2.2**) to confirm the presence of the $(GT)_8$ repeat in the *ade6* locus (**Figure 3.11A**). Transformants were selected for on G418-plates. Correct integration was then determined by colony PCR and, subsequently, restriction digestion of the PCR fragments (as described in **Chapter 2.1.4**). Two independent strains with a $(GT)_8$ repeat in *ade6* were isolated for each *pol3* mutant genotype, giving rise to the following strains: 3947-56 (see **Table 2.1**).

3.2.3.2 Mutation rates of pol3 mutants with (GT)$_8$ repeat in ade6.

Adenine reversion fluctuation analyses determined the level of GT repeat stability in the following EDMs: *pol3P311L*, *G305S*, *L458P*, *D300N* and *D386A* mutants had 1.5, 1.7, 1.1, 1.0 and 1.5 fold increase mutation rate over wild type, respectively (**Figure 3.11B**). The differences in the various mutation rates were insignificant ($p > 0.05$), implying that the *pol3* mutants do

not have problems replicating GT repeat sequences accurately and, thus, do not generate frameshift mutations in this type of repeat at a higher rate than Wt. This could be due to two reasons: either slippage of the nascent strand at the poly (GT) tract does not frequently occur in these *pol3* variants or the MMR system is more than ample to accurately rectify these frameshift mismatches that escape polymerase proofreading (Greene and Jinks-Robertson, 1997; Harfe and Jinks-Robertson, 2000; Sia et al., 1997).

The Ade+ reversion (mutation) rate of wild type was much higher than previously reported: its average mutation rate in this study was 11.6 per 10^8 cell divisions, whereas its mutation rate in the literature was 0.34 per 10^8 divisions (Mansour et al., 2001). This difference could be for many reasons such as technical ones (e.g. the length of time the plates were incubated), however, mutation rates were presented as fold increase over Wt, limiting these discrepancies.

The strain, *msh2*Δ *ade6-(GT)*$_8$ (#3311 – **Table 2.1**), was used as a positive control in the experiment; it is known that *msh2*Δ has a high rate of GT repeat instability in *S. pombe* (Mansour et al., 2001). In this study, the mean Ade+ reversion rate was 5141 per 10^8 cell generations (**Figure 3.11C**), which is in agreement with the aforementioned literature.

To conclude, *pol3* EDMs do not appear to have increased GT repeat instability during replication, however, this does not mean that they will behave similarly when replicating other length variations of nucleotide repeats.

3.2.4 Growth rate of the *pol3* exonuclease domain mutants (EDMs)

The growth rates of the *pol3* EDM strains were determined to see if the strains had any significant growth disadvantages compared to wild type. Growth rates were determined by an advanced automated spectrophotometer, Bioscreen C, which operates by measuring the OD_{600} values of each strain (grown in a 100-well honeycomb microplate in rich media, agitated at

30°C) every 20 minutes for up to 22 hours (see **Chapter 2.1.9**). After 22 hours, the results were exported as an Excel file and the doubling times (in minutes) were calculated via the exponential growth equation (least squares fit) on GraphPad Prism. The subsequent data show the rates of growth up to 14 hours (840 minutes); thereafter, for all the yeast strains involved, the growth rates plateaued (**Figure 3.12**).

The doubling times for the strains are shown in tables in **Figure 3.12**. The results show no significant differences between the growth of the strains, suggesting that the variant polymerases do not dramatically extend S phase or cause full activation of checkpoint mechanisms that might delay cell division under physiological conditions. In summary, the rates of growth of the *pol3* mutant strains were similar to Wt.

Figure 3.10

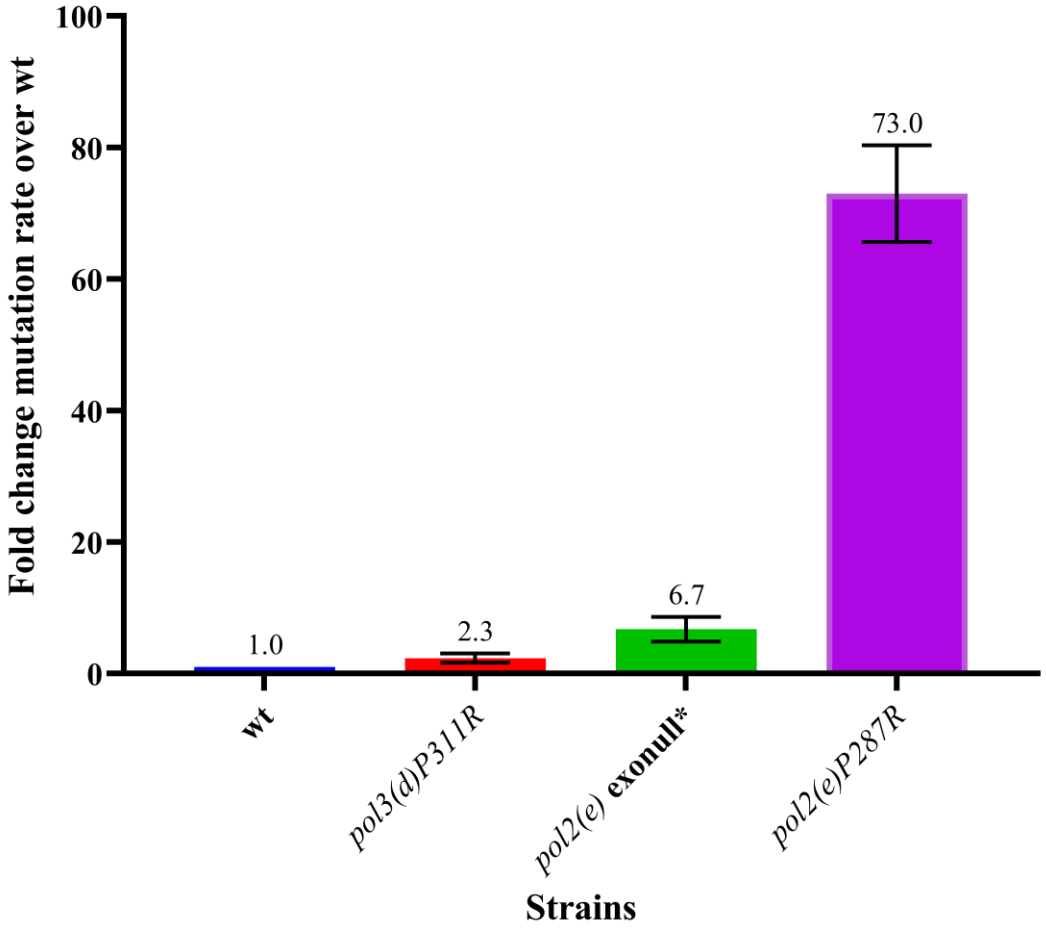
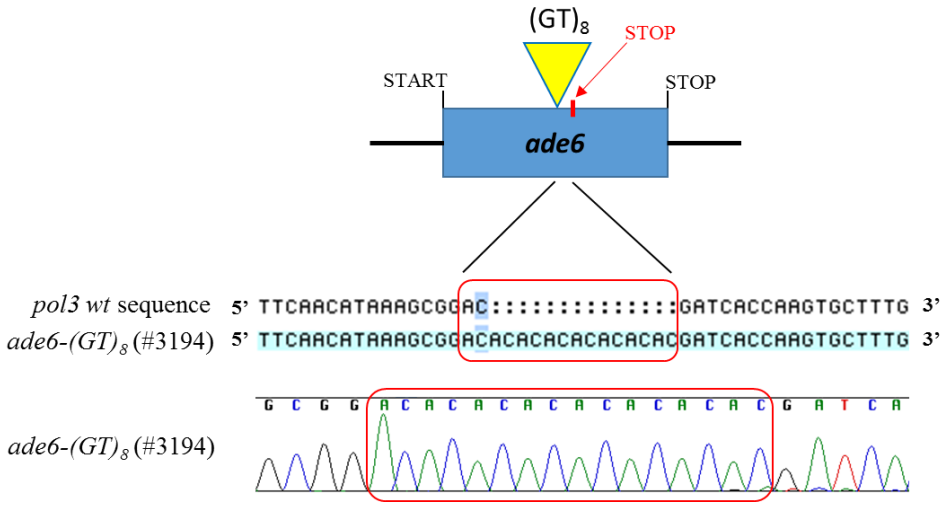


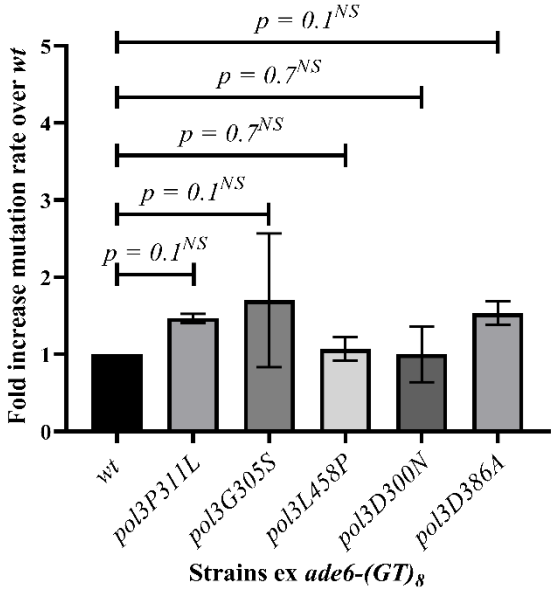
Figure 3.10: *Pol2P287R* has a mutation rate 30-40 times higher than that of *pol3P311R*. Mutation rates (x 10^{-8}) were calculated using the MSS-MLE method and the fold change shown is the fold difference in the Can^r rate between the wild type and *pol3/pol2* haploid variants. **Pol2(e)D276A/E278A* (exo-null *pol2(e)*) is a mutant devoid of exonuclease activity. Two biological replicates were used for each mutant genotype. Data are shown as mean ± SD (n = 2). The strains used were: 3500 (Wt), 3419 & 3426 (*pol3P311R*, respectively), 3199 & 3200 (exo-null *pol2*, respectively), and 3622 & 3758 (*pol2P287R*, respectively).

Figure 3.11

A.



B.



C.

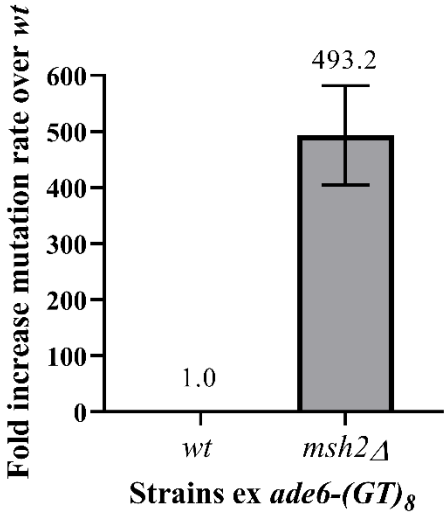
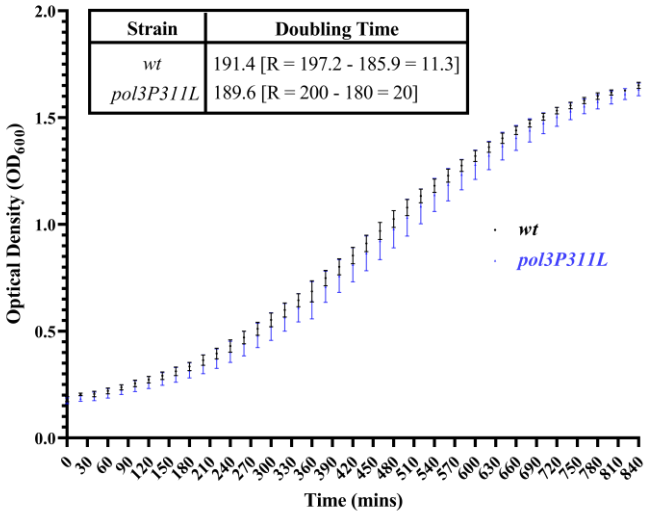


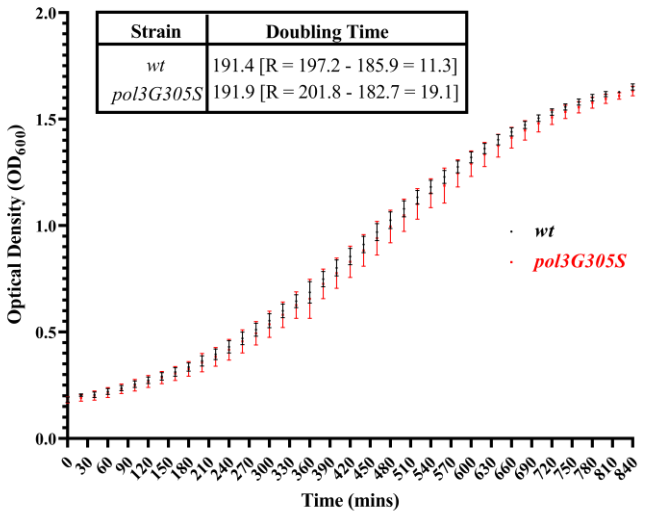
Figure 3.11: The *pol3* EDMs do not have increased replicative slippage when synthesising GT repeat sequences. (A) Schematic of test system for GT repeat stability (strain #3194): GT repeats (yellow triangle) were introduced at an existing GT site of the *ade6* gene (blue box), causing a frame shift and an in-frame stop codon downstream (in red); thus, rendering adenine auxotrophy. Figure modified from Mansour et al (2001). **Sequencing results:** the region consisting of the $(GT)_8$ repeats, outlined in red, was sequenced with primer 1165 to confirm the strain's genotype. (**B** & **C).** Ade reversion rates (x 10^{-8}) were calculated and the fold increase over Wt is shown for each strain. The positive control used was *msh2 ex ade6-(GT)₈* strain (#3311). Two biological replicate strains were used for each *pol3* mutation. Data are shown as mean ± SD (n=3). P-values were calculated using the two-tailed Mann-Whitney test: ^{NS} $p > 0.05$. NS = Not Significant. The strains used were: 3500 (Wt), 3311 (positive control), 3947-56 (*pol3* mutants ex GT_8).

Figure 3.12

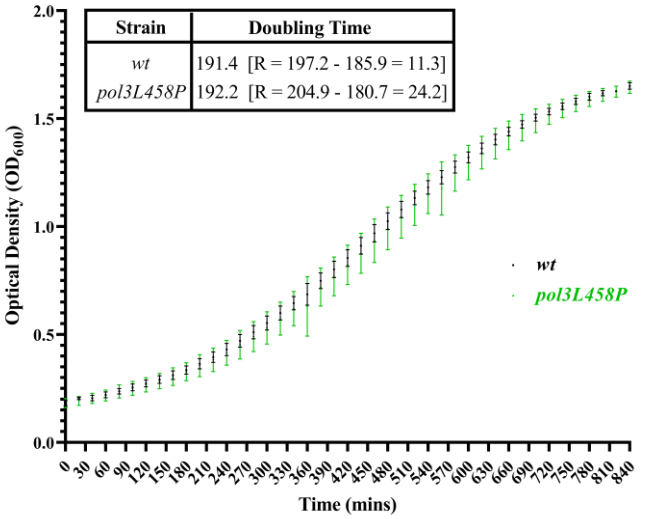
A. *pol3P311L*



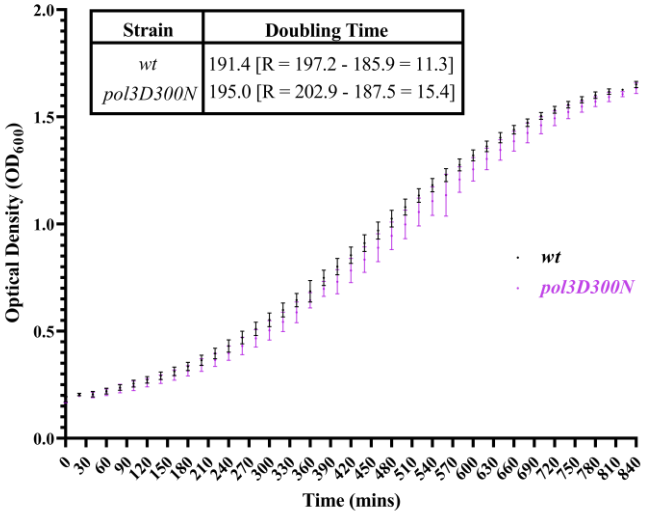
B. *pol3G305S*



C. *pol3L458P*



D. *pol3D300N*



E. *pol3D386A*

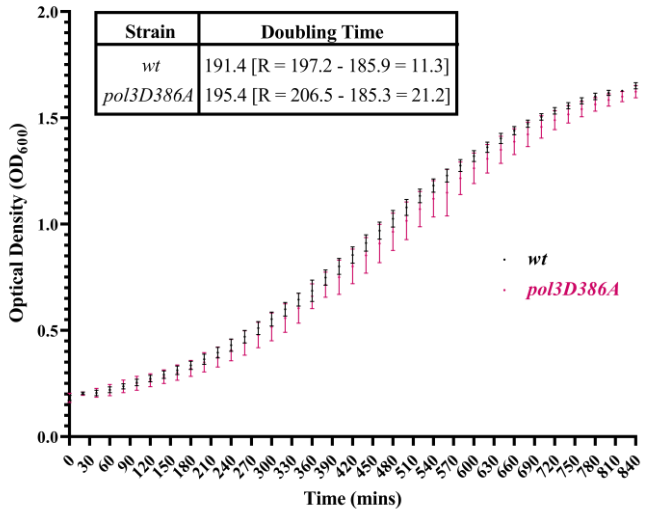


Figure 3.12: The *pol3* proofreading domain mutations do not have growth defects. (A–E) Growth rate curves displaying the optical densities (OD_{600}) (light absorbance at 600 nm) for each *pol3* variant strain grown at 30°C, measured at 20 minute intervals for up to 14 hours. The doubling times (in minutes) of the strains were calculated via non-linear regression, and are tabulated. 'R' represents the range of the doubling times (n=2). The strains used were: 3500, 3273, 3354, 3941, 3943 and 3945.

3.2.5 *Pol3P311L* and *pol3G305S* strains exhibit growth defects under replication stress

Prior data suggest that the *pol3P311L* and *pol3G305S* mutations do not have a mutator phenotype, particularly under normal cellular conditions, however, they may display a different phenotype under stress. To assess this, spot-dilution assays were carried out (**Chapter 2.1.6**) in which the *pol3* mutant strains were challenged with various DNA-damaging agents that cause some form of replicative stress via different mechanisms of action (**Figure 3.13**).

Methyl methanesulfonate (MMS) is an alkylating agent that causes methylation of N7-deoxyguanine and N3-deoxyadenine (Lee et al., 1989). DNA methylation can lead to single-strand breaks (SSBs) following base excision repair (BER). MMS lesions can be repaired by nucleotide excision repair (NER) but the MMS-DNA methylated complex can cause replication fork stalling and stalled forks can lead to double strand breaks (DSBs) if homologous recombination is deficient in cells (Lundin et al., 2005). Bleomycin is a radiomimetic drug that binds to DNA directly. The drug possesses a metal binding region that generates reactive oxygen species (ROS), which react with DNA, directly causing SSBs and DSBs (Chen and Stubbe, 2005; Povirk, 1996).

Camptothecin (CPT) inhibits DNA topoisomerase 1 (Top1), which is an enzyme that alleviates topological constraints of DNA, such as the unwinding of DNA supercoils, during replication and transcription (Tsao et al., 1993). Top1 cuts DNA at one strand creating a temporary nick, which alleviates the torsional strand, and then later reseals it. CPT inhibits Top1 by forming an intermediate with the enzyme at the nick, blocking the release of the enzyme. This creates a barrier to the oncoming replication fork, ultimately resulting in fork stalling and collapse, and the formation of replication-dependent DSBs (Svejstrup et al., 1991). Hydroxyurea (HU) is a ribonucleotide reductase inhibitor that results in reduced deoxyribonucleoside triphosphate (dNTP) pools (Krakoff et al., 1968; Tyrsted, 1982). HU quenches the tyrosyl free radical in the

active site of ribonucleotide reductase (RNR), inactivating the enzyme and compromising DNA synthesis (Bianchi et al., 1986). The depletion of dNTP pools enhances nucleotide misincorporation, increases replication fork stalling and collapse, and promotes DSBs at replication sites (Petermann et al., 2010).

4-nitroquinoline 1-oxide (4NQO) is a quinolone derivative that mimics the effects of ultraviolet (UV)-induced DNA damage because it forms molecular lesions that are usually resolved by NER (Janner et al., 1979). 4NQO forms stable DNA base adducts which, if left unrepaired, lead to transversions of guanines to thymines (Bailleul et al., 1981; Janner et al., 1979). UV-induced photolesions include, for instance, cyclobutane pyrimidine dimers and 6-4 photoproducts (Hannah and Zhou, 2009).

Spot-dilution assays were conducted and the *pol3* strains were treated with HU, CPT, MMS, bleomycin, UV and 4-NQO. The *pol3P311L*, *G305S*, *D300N*, *D386A* strains displayed no phenotypes on YES + UV and YES + 4-NQO plates (**Figure 3.14**). It is important to mention that in **Figure 3.15**, the *pol3L458P* variant displayed slight temperature-sensitivity (ts) under normal conditions (i.e. on YES at 36˚C). There were no other obvious phenotypes observed with this strain. Strikingly, *pol3P311L* and *G305S* conferred sensitivity to HU (**Figure 3.16**). A reduction of dNTPs during DNA replication slows down the replication fork, potentially causing the polymerase to stall and dissociate from the replisome (Reha-Krantz, 2010). Therefore, it appears that the *pol3P311L* and *G305S* variants do not cope well in an environment with compromised dNTP levels. Interestingly, the exonuclease null version of Pol δ (*pol3D386A*) and *pol3D300N* grew normally, relative to the wild-type, after the application of exogenous DNA damage, presented in this study (**Figure 3.17**).

Figure 3.13

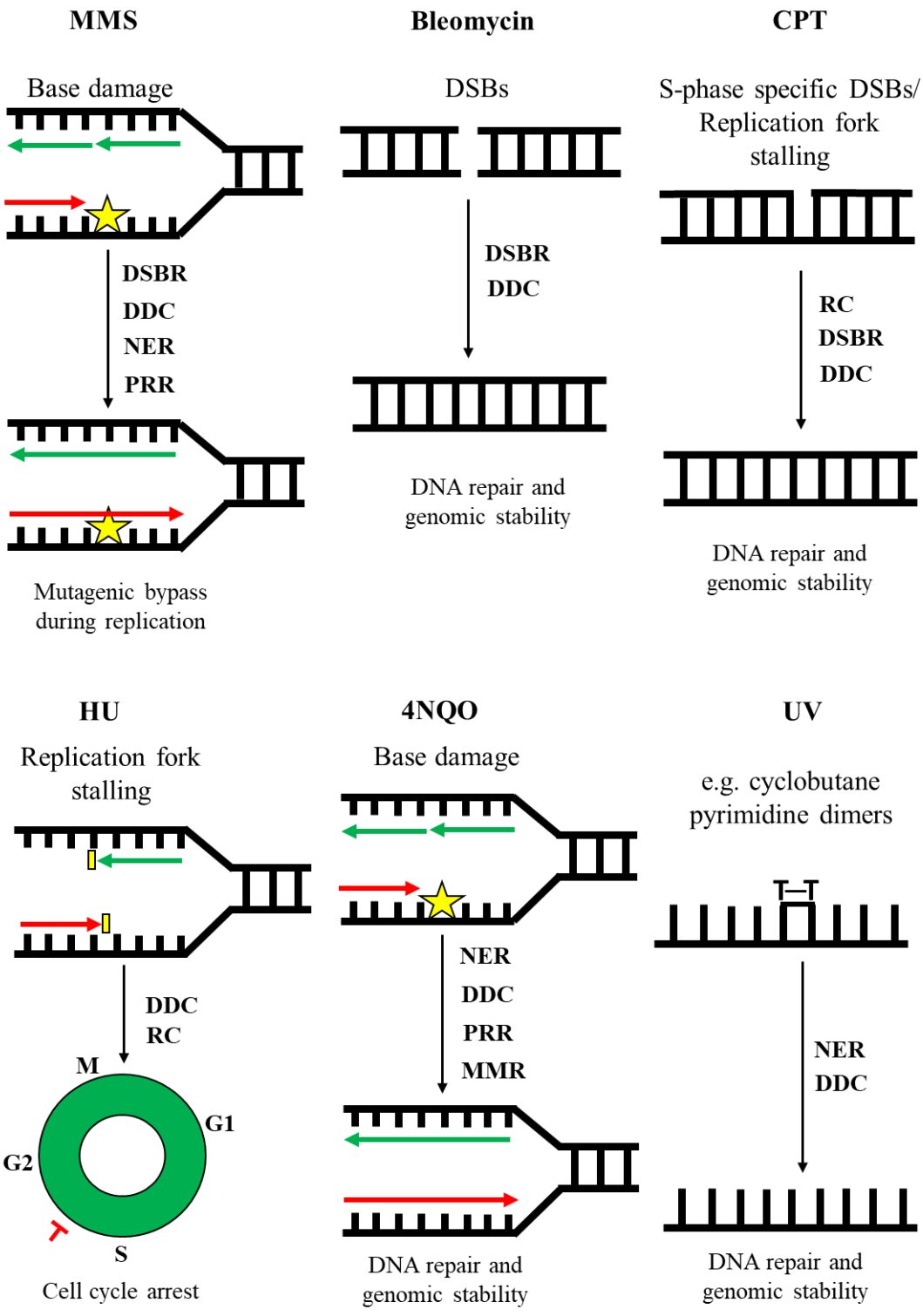


Figure 3.13: DNA damaging agents. Illustration of applied damage and the respective DNA repair pathways for a variety of DNA damage inducing agents used in this study. DSBs (double-strand breaks), DSBR (double-strand break repair), DDC (DNA damage checkpoint), RC (replication checkpoint), NER (nucleotide excision repair), PRR (post-replication repair), MMR (mismatch repair). Image adapted from Kasparek (2013).

Figure 3.14

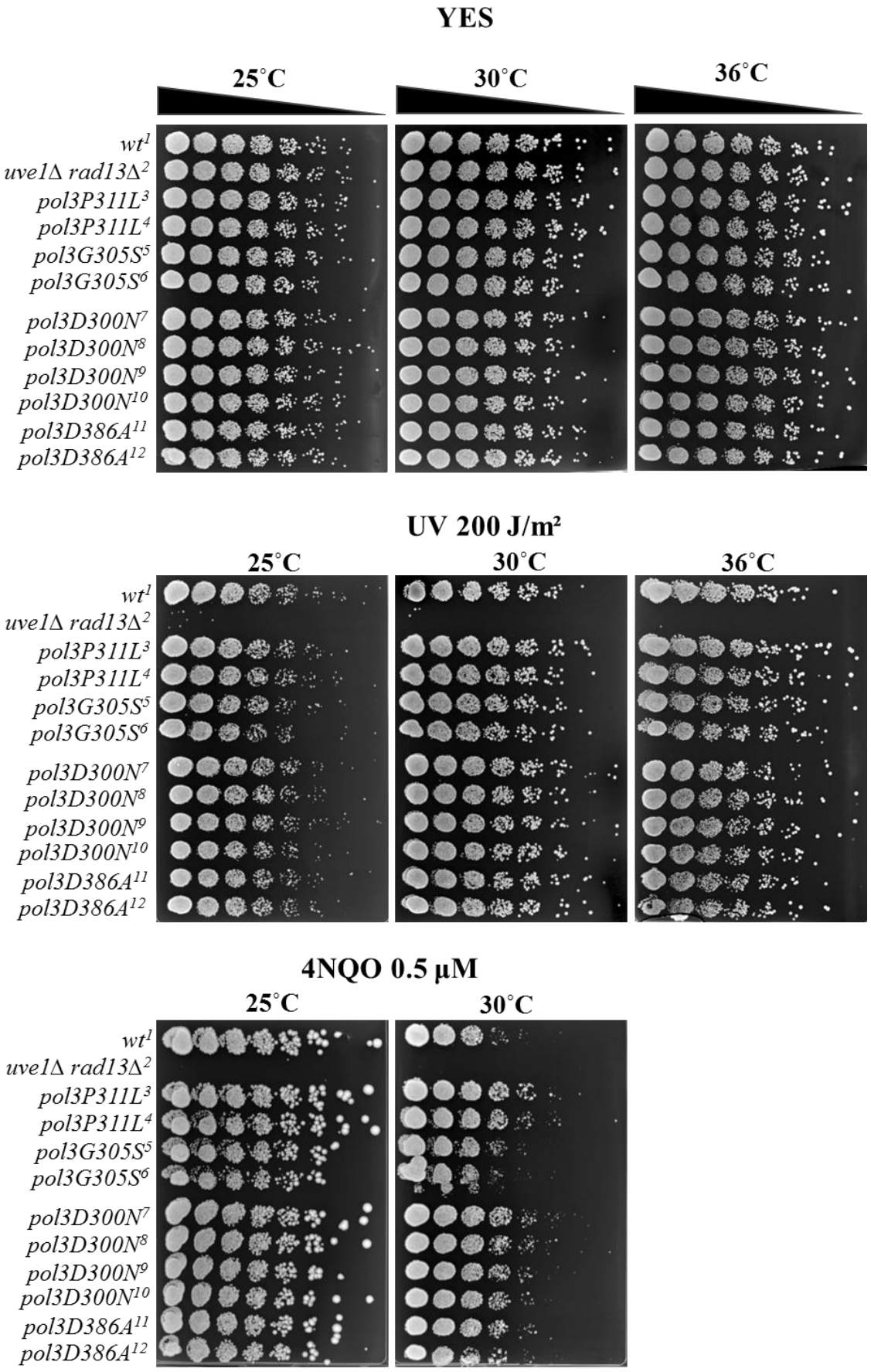

YES
25˚C
30˚C
36˚C
wt[1]
uve1Δ rad13Δ[2]
pol3P311L[3]
pol3P311L[4]
pol3G305S[5]
pol3G305S[6]
pol3D300N[7]
pol3D300N[8]
pol3D300N[9]
pol3D300N[10]
pol3D386A[11]
pol3D386A[12]
UV 200 J/m²
25˚C
30˚C
36˚C
wt[1]
uve1Δ rad13Δ[2]
pol3P311L[3]
pol3P311L[4]
pol3G305S[5]
pol3G305S[6]
pol3D300N[7]
pol3D300N[8]
pol3D300N[9]
pol3D300N[10]
pol3D386A[11]
pol3D386A[12]
4NQO 0.5 µM
25˚C
30˚C
wt[1]
uve1Δ rad13Δ[2]
pol3P311L[3]
pol3P311L[4]
pol3G305S[5]
pol3G305S[6]
pol3D300N[7]
pol3D300N[8]
pol3D300N[9]
pol3D300N[10]
pol3D386A[11]
pol3D386A[12]

Figure 3.14: The *pol3* mutants are not sensitive to UV or 4NQO DNA damage. Spot-dilution assay of *pol3P311L*, *G305S*, *D300N* and *D386A* (exo-null *pol3(d)*) mutants. Strains were serially diluted five-fold and challenged with UV and 4NQO at indicated exposure/concentration and temperatures. 3500[1] (Wt) and 1918[2] (*uve1*Δ *rad13*Δ) strains were used as negative and positive controls, respectively. Two biological replicates were used for each *pol3* variant. The rest of the strains used were: 3354[3], 3355[4], 3941[5], 3942[6], 3945[7,9], 3946[8,10], 3273[11] and 3421[12]. Note that 4NQO was not compatible with temperatures above 32˚C (i.e. no strains, not even Wt, grew on 4NQO plates above 32ºC).

Figure 3.15

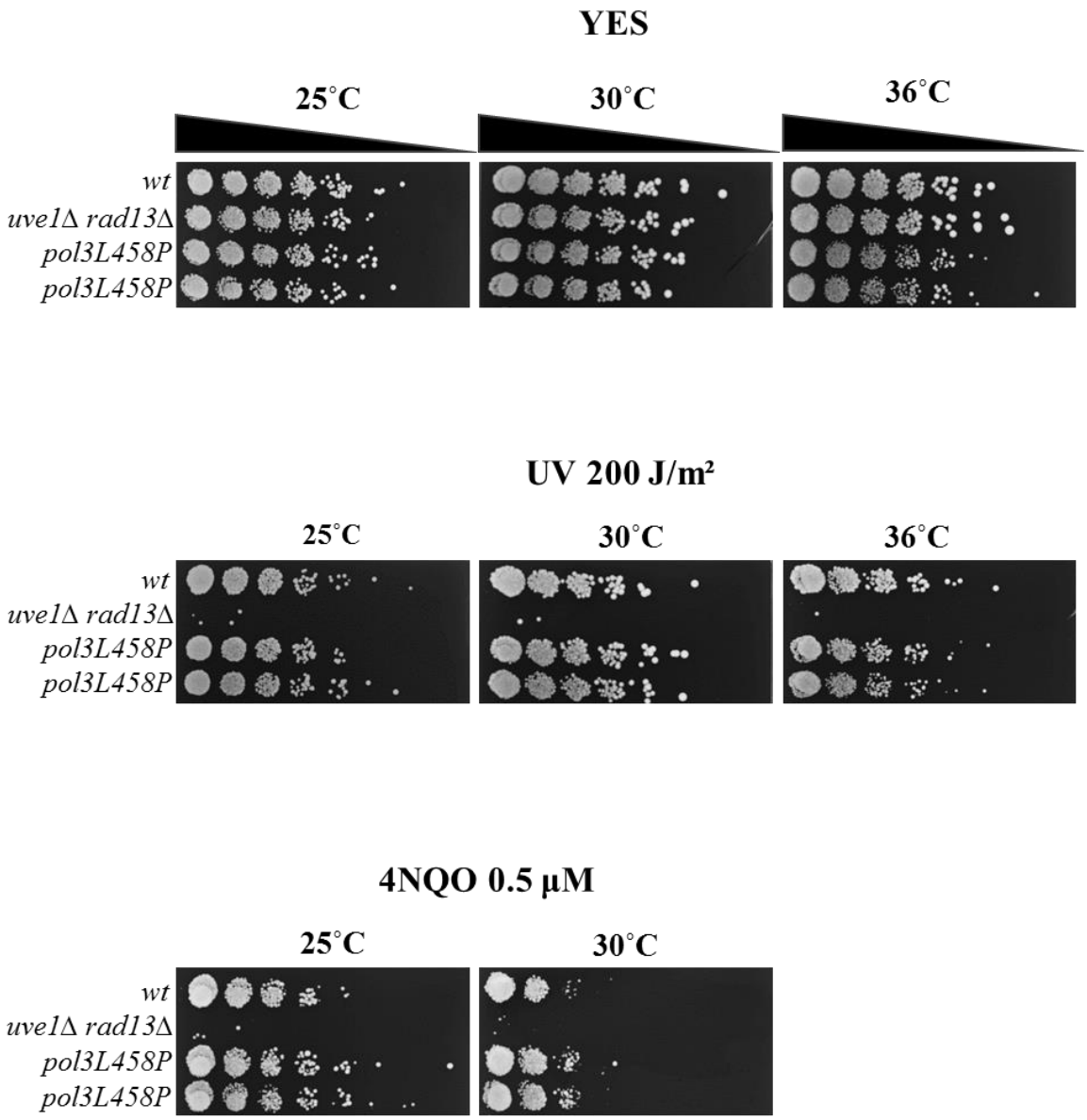


Figure 3.15: *Pol3L458P* is not sensitive to UV and 4NQO DNA damage. Spot-dilution assay of *pol3L458P* mutant strain. Strains were serially diluted five-fold and challenged with UV and 4NQO at the indicated exposure/concentration and temperatures. Wt (3500) and *uve1*Δ *rad13*Δ (1918) strains were negative and positive controls, respectively. Two biological replicate strains were used for *pol3L458P*: 3943 and 3944.

Figure 3.16

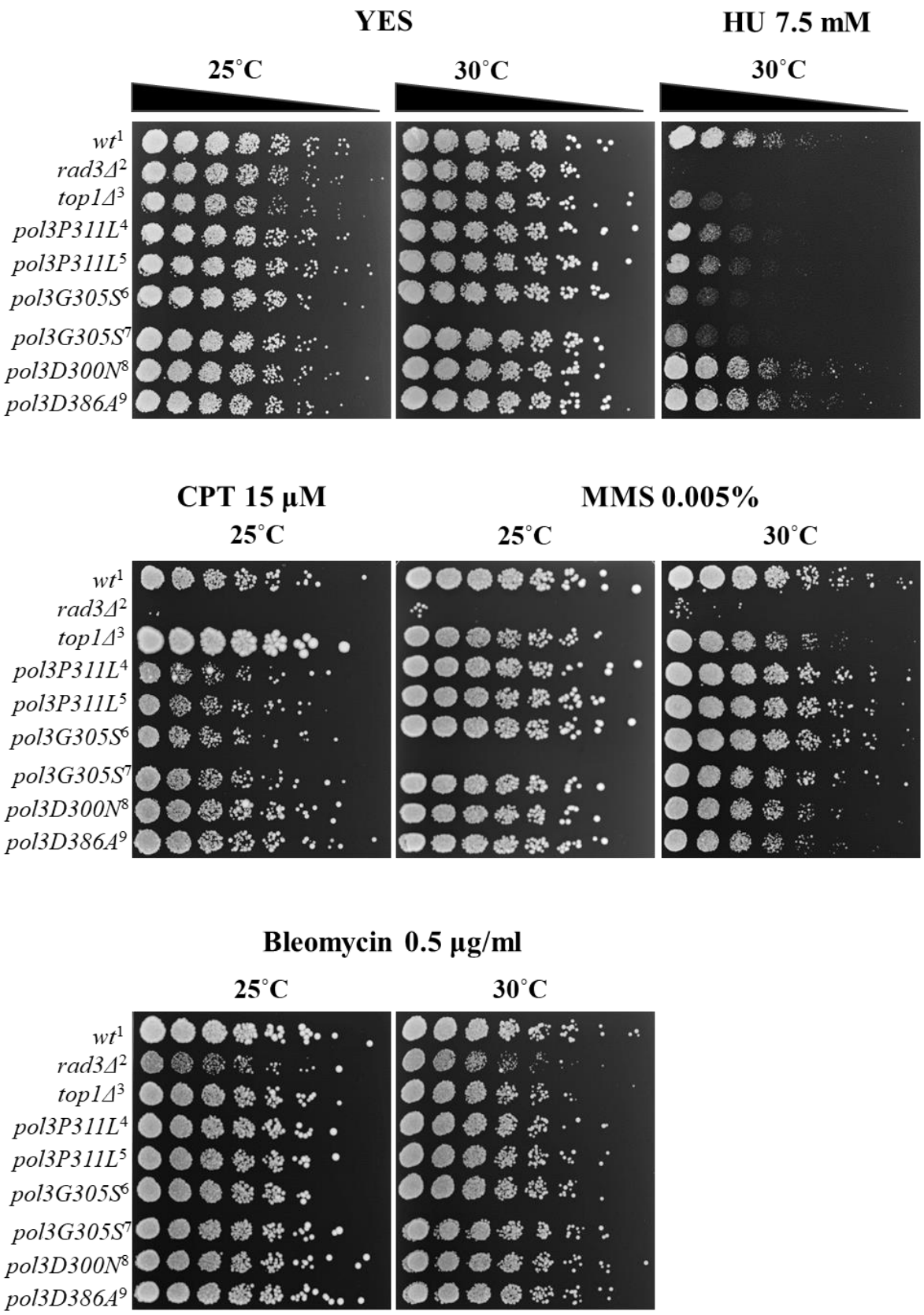

YES
HU 7.5 mM
25˚C
30˚C
30˚C
wt1
rad3Δ2
top1Δ3
pol3P311L4
pol3P311L5
pol3G305S6
pol3G305S7
pol3D300N8
pol3D386A9
CPT 15 µM
MMS 0.005%
25˚C
25˚C
30˚C
wt1
rad3Δ2
top1Δ3
pol3P311L4
pol3P311L5
pol3G305S6
pol3G305S7
pol3D300N8
pol3D386A9
Bleomycin 0.5 µg/ml
25˚C
30˚C
wt1
rad3Δ2
top1Δ3
pol3P311L4
pol3P311L5
pol3G305S6
pol3G305S7
pol3D300N8
pol3D386A9

Figure 3.16: *Pol3P311L* and *pol3G305S* mutants confer sensitivity to HU. Spot-dilution (five-fold serial dilution) of *pol3P311L*, *G305S*, *D300N* and *D386A* mutants on YE3S, HU, CPT, MMS and bleomycin at the indicated concentrations and temperatures. 3500[1] (Wt), 1617[2] (*rad3*Δ) and 3251[3] (*top1*Δ) strains acted as controls. Two biological replicates were used for the *P311L* and *G305S* variants. The rest of the strains used were: 3354[4], 3355[5], 3941[6], 3942[7], 3945[8] and 3273[9]. YES, MMS and bleomycin plates were incubated at 25˚C and 30˚C. Note that nothing grew on HU plate at 25˚C and the same was true for CPT plate at 30˚C. Most of the DNA damaging agents were not compatible with temperatures above 32˚C.

Figure 3.17

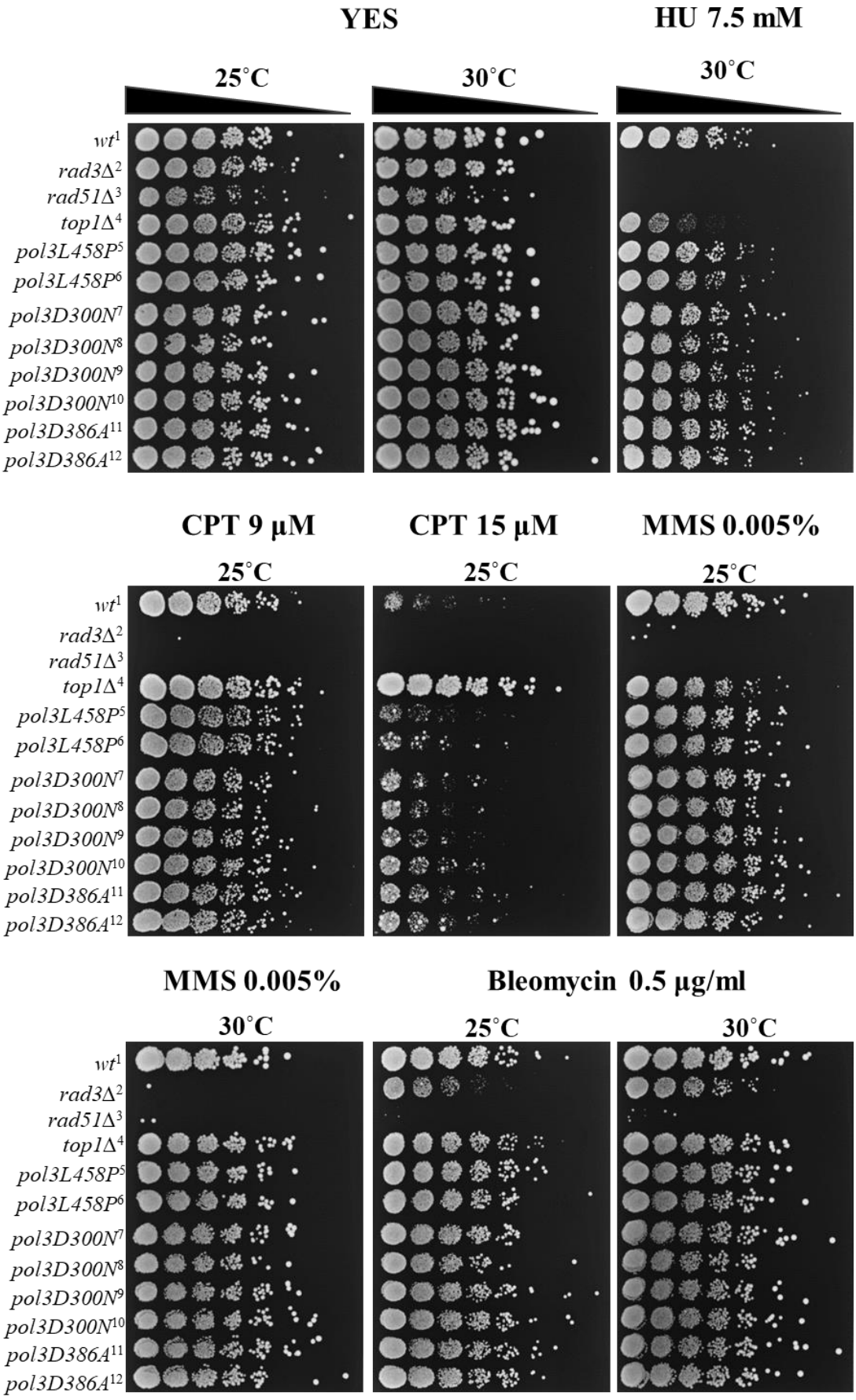

YES
HU 7.5 mM
25˚C
30˚C
30˚C
wt1
rad3Δ2
rad51Δ3
top1Δ4
pol3L458P5
pol3L458P6
pol3D300N7
pol3D300N8
pol3D300N9
pol3D300N10
pol3D386A11
pol3D386A12
CPT 9 µM
CPT 15 µM
MMS 0.005%
25˚C
25˚C
25˚C
MMS 0.005%
Bleomycin 0.5 µg/ml
30˚C
25˚C
30˚C

Figure 3.17: *Pol3L458P, D300N and D386A* mutants are not sensitive to DNA damaging agents. Spot-dilution (five-fold serial dilution) of *pol3L458P*, *D300N* and *D386A* (exo-null *pol3*) mutants on YES, HU, CPT, MMS and bleomycin at the indicated concentrations and temperatures. 3500[1] (Wt), 1617[2] (*rad3Δ*), TH 1846[3] (*rad51*Δ) and 3251[4] (*top1Δ*) strains were controls. Two biological replicates were used for all strains. The remainder of the strains used were: 3943[5], 3944[6], 3945[7,9], 3946[8,10], 3273[11] and 3421[12].

3.3 DISCUSSION

3.3.1 Pol δ mutant orthologues in humans and in yeasts

Table 3.2 lists the human cancer-associated Pol δ variants and their equivalent *S. pombe* and *S. cerevisiae* mutations.

Table 3.2: *POLD1* EDM orthologues

Human *POLD1*	***S. pombe* *Pol3***	***S. cerevisiae* *Pol3***
P327L	*P311L*	*P332L*
G321S	*G305S*	*G326S*
L474P	*L458P*	*L479P*
D316N	*D300N*	*D321N*
D402A	*D386A*	*D407A*
P327R	*P311R*	*P332R*

Note that *POLD1* D402A and P327R (in red) are not clinically-found mutations in humans. Sp. *pol3D386A* is a positive control strain with 0% proofreading ability. *POLD1* P327R is the equivalent Pol δ mutation to the hypermutating somatic Pol ε mutation, *POLE* P286R. The rest of the *POLD1* variants (in black) are clinically relevant mutations. See text for further details.

3.3.2 Summary of results

Human *POLD1* EDMs are suspected to cause a genetic predisposition to colorectal cancer and in order to investigate this, I modelled the equivalent mutations in *S. pombe* and assessed their mutation rates and sensitivity to DNA-damaging agents.

The main findings are:

- The Sp. *pol3P311L* and *pol3G305S* strains, expressing mutations equivalent to the human germline mutations *POLD1* P327L and *POLD1* G321S, respectively, do not have strong mutator phenotypes.

- Sp. *pol3L458P*, expressing the polymerase variant equivalent to the human germline mutation *POLD1* L474P, shows a slight increase in mutation rate, suggesting it retains some proofreading activity but it is not entirely deficient.

- Sp. *pol3D300N*, equivalent to the human somatic *POLD1* D316N EDM, has a strong mutator phenotype which is comparable to that of a yeast strain that lacks proofreading activity in Pol δ.

- The orthologous hypermutating Hs. *POLE* P286R mutation in fission yeast (Sp. *pol2(e)P287R*) has a much higher mutation rate than that of the Sp. *pol3(d)P311R* variant. This indicates that the equivalent missense mutation in Pol ε has a more dramatic effect on mutagenesis and genome instability in the cell than in Pol δ.

- None of the *S. pombe pol3* EDMs show an increased frameshift mutation rate when replicating GT dinucleotide repeats, nor do they have any significant growth defects under physiological conditions.

- The *pol3P311L* and *pol3G305S* Sp. strains confer sensitivity to hydroxyurea (HU) at 30°C, suggesting that they do not cope well when placed under some form of replicative stress.

3.3.3 Overview of the pathogenicity of *pol3* EDMs

Originally, it was predicted that the human *POLD1* P327L (Sp. *pol3P311L*) mutation would be pathogenic because it is a germline heterozygous mutation that was found in a 70-year-old patient with several colorectal adenomas and it is located in a highly conserved region of the POLD1 exonuclease domain (Palles et al., 2013). Moreover, it is at the equivalent residue to the hypermutating somatic *POLE* P286R mutation suggesting that it, too, would produce a

strong mutator phenotype (Palles et al., 2013; Church et al., 2013). Structural mapping of *POLD1* P327L and *POLE* P286R mutations onto a hybrid structure of yeast DNA polymerase and T4 polymerase show that they are situated adjacent to the DNA binding pocket next to the exonuclease catalytic site (Palles et al., 2013; Briggs and Tomlinson, 2013). Thus, a mutation at this site might alter the conformational structure of the DNA binding pocket, however, it is possible that a conservative amino acid change, such as proline (hydrophobic with a cyclic side chain) to leucine (hydrophobic), is not as deleterious to the polymerase's structure and function as a non-conservative amino acid substitution, such as proline to arginine (basic, polar). The cancer-associated *POLE* P286R mutation proved to be as highly mutagenic in yeast and bacteria (Reha-Krantz, 1988; Kane and Shcherbakova, 2014), as it is in humans (Shinbrot et al., 2014). In contrast to the initial hypothesis, the data presented in this study proves that the *S. pombe* equivalent to the germline *POLD1* P327L mutation, *pol3P311L*, does not have a strong mutator phenotype, but it appears to display growth defects under HU-induced depletion of dNTP pools, which will be discussed later.

The *pol3G305S* fission yeast strain (Hs *POLD1* G321S) equally had a low mutation rate like the yeast strain *pol3P311L*. This was expected because it was identified in a middle-aged patient with suspected Lynch Syndrome and currently lacks in vitro evidence of pathogenicity from either yeast mutation rate assays or biochemical assays of exonuclease function (Jansen et al., 2016; Palles et al., 2018). The *POLD1* G321S mutation affects a highly conserved residue in yeast and it has a low Polyphen score (data not shown), implying that the G321S variant has low functional impact on the holoenzyme. It is important to mention that PolyPhen is an in silico algorithm used to analyse the potential functional disruption in regard to protein function (Adzhubei et al., 2010). Whether this is a true reflection of the phenotype of the G321S variant in human colorectal cancer is not yet known. However, the HU sensitivity of the equivalent

yeast mutation, *pol3G305S*, would suggest that this missense genetic variant might be pathogenic under conditions of replication stress, similarly to the *pol3P311L* missense variant.

The *S. pombe pol3P311L* and *G305S* mutants are sensitive to hydroxyurea (HU). The main question here is why should a mutation in the exonuclease domain of Pol δ affect sensitivity to HU? Since HU reduces dNTP pools (Tyrsted, 1982), a mutation in the exonuclease or polymerase domains of Pol δ may be more prone to stalling or may have reduced synthesis rates under these conditions, respectively (Pai and Kearsey, 2017). If the polymerase is moving more slowly with the fork, effected by HU-mediated RNR inhibition, then perhaps with the HU-sensitive EDMs, the 3' terminus of the newly synthesised strand is more likely to flip to the (presumably active) exonuclease site but remains stuck there for some reason, leading to fork stalling (Reha-Krantz, 2010; Ganai et al., 2014). In vitro studies would be a useful way of extending this work by measuring directly the polymerase and exonuclease activities and the misincorporation rate of these EDMs.

Human *POLD1* D316N (Sp. *pol3D300N*) was predicted to have a high functional impact because the mutation affects a highly conserved aspartate catalytic residue situated in the Exo I motif of the exonuclease active site (Prindle and Loeb, 2012). The *pol3D300N* variant displayed a mutator phenotype in the yeast fluctuation assays, which is consistent with the findings of the budding yeast studies conducted by Jin et al (2001), Shevelev and Hübscher (2002), and Murphy et al (2006). Moreover, the strong mutator phenotype of this variant is in concordance with the fact that the human homologous mutation, *POLD1* D316N, is a somatic proofreading domain mutation (The Cancer Genome Atlas Network, 2014). Additionally, it was expected that the *pol3D300N* strain would have a similarly high mutation rate to the non-clinical exonuclease devoid version of Pol δ, *pol3D386A*: they both affect key catalytic residues pivotal to exonuclease activity (Murphy et al., 2006), and the equivalent mutations of yeast *pol3D386A*

in mice and in purified human Pol δ displayed a complete lack of proofreading activity and increase in base-substitution rates in addition to cancer manifestation in mice (Goldsby et al., 2002; Schmitt et al., 2009).

It is important to mention that the Can^r mutation rates of the *pol3D300N* and *D386A* variants were 20-40 fold higher than Wt, whereas the Pol ε EDM that is devoid of any proofreading capabilities, *pol2D276A/E278A* (Henninger and Pursell, 2014), had a mutation rate up to seven-fold higher than Wt. This emphasises the limited understanding that we have regarding the differential roles and functions of Pol ε versus Pol δ (Miyabe et al., 2011; Daigaku et al., 2015; Johnson et al., 2015; Miyabe et al., 2015). Furthermore, it is important to add that there are not as many identifiable cancer-related somatic Pol δ mutations as there are Pol ε mutations (Palles et al., 2013; Church et al., 2013). One interpretation of this finding is that in vivo, errors on the lagging strand can be more easily rectified due to dissociation of Pol δ after misincorporation, and proceeded by proofreading by another enzyme. On the other hand, switching to mutagenic TLS polymerases may be more efficient on the leading strand.

Evidence from co-segregation in families, the highly conserved location of the variant in the exonuclease domain, in silico analysis of the variant's functional impact, and yeast fluctuation assays all provide credence to the likely pathogenicity of the *POLD1* L474P mutation in human cancers (Valle et al., 2014; Bellido et al., 2016; Murphy et al., 2006). Mutation of the equivalent position but to a different amino acid in *S. cerevisiae* (*pol3-L479S*), was shown to cause a strong mutator phenotype like the DNA polymerase δs with amino acid substitutions in the Exo I and II motifs; for example, the *pol3D300N* (Sc. *pol3-D321N*) and *pol3D386A* (Sc. *pol3-D407A*) mutations (Murphy et al., 2006). A moderate mutator phenotype was observed for the fission yeast strain expressing the equivalent variant to *POLD1* L474P, *pol3L458P*, which was about three-fold less than the mutation rates observed for the *pol3D00N/D386A* strains combined.

Therefore, residue L458 seems to be important for replication fidelity in *S. pombe* (this study), *S. cerevisiae* (Murphy et al., 2006) and phage DNA polymerases (Sattar et al., 1996). This predicts that the *POLD1* L474P germline variant is pathogenic, consistent with the finding of this variant in two independent hereditary nonpolyposis families, predominantly associated with CRC or EC (Valle et al., 2014; Bellido et al., 2016).

It is possible that *pol3L458P* would have a moderate mutator phenotype because the equivalent human *POLD1* L474P mutation is paralogous to the recurrent germline *POLE* mutation encoding an L424V variant, although the mutations encode different amino acids. *POLE* L424V predisposes to multiple colorectal adenomas and carcinomas in affected individuals with dominant inheritance and high penetrance (Palles et al., 2013). Furthermore, *POLE* L424V has been shown to have reduced but not absent exonuclease activity (Shinbrot et al., 2014). Modelling EDMs on T4 bacteriophage polymerase complex revealed that *POLE* L424 amino acid residue maps to a helix and packs against another helix, forming part of the base of the exonuclease active site in Pol ε (Palles et al., 2013). Therefore, alterations to the equivalent leucine residue in Pol δ may disrupt the packing of helices and distort the active site (Palles et al., 2013). It is also possible that the L474P mutation distorts the polymerase active site: in crystal structures of editing complexes of the T4-like RB69 DNA polymerase, L290, which corresponds to L479 in yeast DNA polymerase δ, and L287 in the T4 DNA polymerase, in conjunction with another amino acid residue, W216, appear to have a role in movement of the nascent DNA terminus between the polymerising and proofreading active sites (Hogg et al., 2004; Murphy et al., 2006). Overall, the evidence suggests that the mechanism of tumourigenesis caused by the *POLD1* L474P mutation is decreased fidelity of polymerase δ proofreading leading to mutagenesis.

None of the *pol3* exonuclease domain mutations (EDMs) displayed increased frameshifts with the $(GT)_8$ repetitive tract compared to wild type. Briefly, accurate DNA replication is a product of the synergy that exists between base selectivity by the DNA polymerase, exonucleolytic proofreading, and post-replicative DNA mismatch repair (MMR) (Schaaper, 1993). DNA polymerase slippage events are defined by frameshifts within simple repetitive DNA sequences (microsatellites) or deletions between direct repeats (Kokoska et al., 2000). Therefore, the low mutagenicity of wild type cells is likely to reflect the high level of processivity of replicative DNA polymerases and the efficiency of MMR (Kokoska et al., 2000). Thus, one might expect that mutator alleles of the lagging strand DNA Pol δ, that affect proofreading activity, are likely to encounter slippage events at homopolymeric or microsatellite sequences, increasing subsequent frameshift and/or deletion mutations. The latter was true for a particular temperature-sensitive (ts) missense mutation located in the *POL3* gene of *S. cerevisiae*: *pol3-ts1* (*D396N*) mutation is located in the Exo II motif of the exonuclease domain (Kokoska et al., 2000). *Pol3-ts1* elevated the frequency of poly-(GT) tract instability two-fold and largely increased the number of deletion of sequences flanked by short direct repeats (Kokoska et al., 2000; Liu et al., 1999). Mutant alleles in yeast affecting the exonuclease catalytic site of DNA polymerases δ and ε, *pol3-01* and *pol2-4* mutants, respectively, largely elevated the frequency of base pair substitutions but had a moderate effect on the stability of long microsatellites (Morrison and Sugino, 1994; Strand et al., 1993; Tran et al., 1999a). Note that the *pol3-01* variant in budding yeast comprises two mutations affecting key catalytic residues in the exonuclease active site, *D321A* and *E323A* (Morrison et al., 1993; Jin et al., 2005; Prindle and Loeb, 2012); moreover, the D321 amino acid is situated equivalently to the Sp. *pol3D300* and Hs. *POLD1* D316 residues. On the other hand, mutations that attenuated or inactivated MMR elevated both single-base-pair substitutions and frameshifts, but the increase observed for frameshifts was much greater (Sia et al., 1997). Though Kokoska et al (2000) has shown that

the *pol3-01* mutant increases the rate of frameshifts, followed by deletions, at long dinucleotide repeat sequences, the consensus is that MMR is the predominant independent pathway responsible for rectifying frameshift and indel mutations at repetitive sequences (Strand et al., 1993, 1995; Tran et al., 1997; Kunkel and Erie, 2015), and this appears to be evident in the *pol3* mutant strains examined in this study.

Future work into the rates or efficiencies of polymerisation and proofreading of these EDM polymerases in vitro would illuminate to what extent these mutations affect these activities. Primer extension assays can be used to measure polymerisation fidelity and the ability of the mutant polymerases to extend a primer with a mismatched 3' terminus (Ganai et al., 2014). Such experiments typically involve digested ssDNA, the primer-template mix, dNTPs and the mutant Pol δ enzyme. The primer is labelled in order to track the activity of the enzyme. The primer can either be a complementary match to the template or it can consist of a mismatch at the 3' end. Similarly, the exonuclease activity of the *pol3* EDMs can be assessed in vitro by examining the ability of the mutant polymerases to degrade a 5'-end-labelled oligonucleotide template-primer substrate in the absence of dNTPs (Fortune et al., 2005). One would expect the 3'-5' exonuclease of wild type yeast or human Pol δ to degrade the primer in the absence of dNTPs. On the contrary, one would predict an exonuclease-deficient Pol δ to leave the template-primer strand intact, i.e. no degradation products observed on polyacrylamide gel (Fortune et al., 2005). Secondly, single molecular analysis, for example, DNA molecular combing, would directly measure the fork rates of these EDM polymerases in vivo (Kaykov et al., 2016). Lastly, it would be very useful to identify the mutational pattern of single base substitutions that accumulate in the Sp. *pol3* mutants to understand whether this corresponds to the mutational signatures found in human cancers associated with *POLE*/*POLD1* EDMs (Alexandrov et al., 2020).

3.3.4 *Pol2P287R* and *pol3P311R* are homologous mutations affecting two separate eukaryotic polymerases but have different mutator phenotypes

In this project, the importance of the Pol δ P311 residue was addressed by constructing the *P311R* missense mutation in *S. pombe pol3* to see if this particular mutation would have a hypermutator phenotype such as that observed for the homologous *P287R* mutation in the *pol2* gene. Interestingly, my work revealed that the *pol3P311R* mutant has a relatively low mutation rate. Therefore, this result shows that the Pro (P) to Arg (R) mutation has a marked effect on Pol ε, not on Pol δ, in fission yeast. There are a number of possible reasons for this observation. One possibility for the hypermutator phenotype of *pol2P287R* is due to stalling of Pol ε on the leading strand and polymerase switching to Pol δ. Leading-strand synthesis by Pol δ after fork stalling is known to be mutagenic (Miyabe et al., 2015). Furthermore, stalling on the lagging strand may have a lesser effect as reinitation of another Okazaki fragment can occur downstream of the stall, thus allowing continuation of Pol δ synthesis. Another possibility is that eukaryotic Pol ε is evolutionarily unique from the other polymerases of the B family and the mutation affects it differently compared to Pol δ: it possesses a very large C-terminal domain (of the catalytic subunit) that functions in the initiation of replication and is essential for viability (Dua et al., 1998, 1999; Kesti et al., 1999). Furthermore, Pol ε is involved in chromatin remodelling based on the structure of its accessory subunits (Iida and Araki, 2004). Therefore, key structural and biological differences between Pols ε and δ might potentially determine the level of pathogenicity certain substitution mutations have in the exonuclease catalytic domain. Two other studies in yeast have reported the *pol2P287R* variant to be highly mutagenic (Kane and Shcherbakova, 2014; Soriano et al., 2021). In the same context, tumours with P286R changes were characterised by hypermutation and elicited a strong immune response (Church et al., 2013, 2015; Van Gool et al., 2015; Domingo et al., 2016). Further work is required to establish how and why the P to R mutation differentially affects the functions of Pols ε and δ.

The mutator phenotypes observed for some of the *pol3* variants (e.g. *pol3L458P* and *pol3D300N*) can be explained by either partial or complete loss of exonuclease function, however, this was not the case for the *pol2(e)* variant, P287R. The *pol2P287R* strain had a mutation rate that exceeded that of the exonuclease devoid Pol ε, implying that the high mutagenicity that this mutation displays can only be partially explained by proofreading deficiency. This was the opposite for the *pol3P311R* strain which had a mutation rate approximately 15 times lower than that of the proofreading-defective Pol δ (*pol3D386A*). One interpretation of this observation is that the proline to arginine mutation in the conserved exo I motif of the leading-strand replicase Pol ε may cause reduced processivity of the polymerase, resulting in polymerase disassociation and replication fork stalling, as previously discussed. This can ultimately be more mutagenic than the lack of proofreading activity per se.

When replication is blocked by a lesion, the Rad6-Rad18 E2-E3 ligase complex binds to ssDNA-RNA complexes and mono-ubiquitylates PCNA to recruit error-prone translesion synthesis (TLS) polymerases, such as Pols κ (Sp. Kpa1) and ζ (Sp. Rev3/Rev7), to continue DNA replication in both budding and fission yeast, and in humans (Davies et al., 2008; Niimi et al., 2008; Daigaku et al., 2017). Yeast Pol ζ accounts for more than half of the spontaneous mutations generated in the genome (Northam et al., 2006; Pavlov et al., 2006b), and Pol κ contributed greatly to the mutator phenotype of a yeast strain expressing deficient Pol α (Kai and Wang, 2003). Strains with defective replicative polymerases may show enhanced TLS-dependent mutagenesis in response to polymerase switching at stalled or collapsed replication forks (Soriano et al., 2021). Most notably, deletion of the *kpa1* gene, and to a lesser extent deletion of *eso1*, in *S. pombe* largely suppressed *pol2P287R* hypermutation (Soriano et al., 2021). Therefore, it is possible that TLS polymerases are recruited to the leading strand in *pol2P287R*, to restart DNA synthesis at the cost of an increased mutation rate, but perhaps not to the lagging strand in the *pol3P311R* strain. It would be interesting to see if the EDM

polymerases characterised in this study show synthetic interactions with TLS polymerases, such as Rev7 and Rev3 (Pol ζ combined), Kpa1 (Pol κ) and Eso1 (Pol η).

The varying mutator phenotypes of similar mutations affecting two different eukaryotic polymerases are not fully understood. Also, the equivalent mutation to *pol2P287L* in *S. cerevisiae*, *pol2P301L*, had a hypermutator phenotype which strongly supports the concept that these EDMs affect Pol ε and Pol δ in completely different ways (Hamzaoui et al., 2020). Since the mutation rates are measured in vivo in MMR proficient cells, it is unclear whether the difference in the mutation rates of the *pol2P287R* and *pol3P311R* mutants is due to a direct effect on the polymerase per se, or some difference in the efficiency of post-replication repair on leading and lagging strands. It has been shown that MMR corrects errors made by Pols δ and ε with different efficiencies, thus a mutation could affect Pols δ and ε in identical ways but the in vivo phenotype would be different, for example: Lujan et al (2013) suggested that ribonucleotide incorporation functions as an alternative strand-discrimination signal for MMR, and ribonucleoside monophosphate (rNMP) incorporation is much higher in Pol ε than Pol δ (McElhinny et al., 2010b). For those reasons, MMR might not be as accurate in correcting mismatches made by Pol δ on the leading strand. On the contrary, evidence in yeast conveys that MMR efficiency is two-fold higher for lagging- than leading-strand errors (reviewed in Kunkel and Erie, 2015). The data in this study showed that the proline equivalent to P286 in Pol δ does not cause hypermutation, and Rayner et al (2016) reported significantly fewer somatic Pol δ EDMs compared to Pol ε. This implies that efficient MMR uses the 5' termini of Okazaki fragments rather than ribonucleotides for old/new strand discrimination (Pavlov et al., 2003; McElhinny et al., 2010a), preventing hypermutation in Pol δ EDMs. Although, it is fair to say that it is unlikely that the differences in mutagenicity between *pol2P287R* and *pol3P311R* can be accounted for by differences in MMR efficiency alone. The in vitro studies described earlier would be a useful way of extending this work.

Chapter 4 Characterisation of the hydroxyurea sensitivity observed with some of the *pol3* variants

4.1 INTRODUCTION

In the last chapter, it was discovered that the *pol3P311L* and *G305S* variants are hydroxyurea (HU)-sensitive on solid rich media. Strikingly, these particular *pol3* mutations are not typically mutagenic. Firstly, to understand the phenotype of these *pol3* mutations when DNA replication is compromised, I explored the HU sensitivity further through various experiments, in comparison with the non-HU sensitive mutagenic *pol3* strains, to gain some insight to what extent and why the *pol3P311L* and *G305S* variants are sensitive to HU. This will be discussed in more detail later on in the chapter.

Secondly, several control mechanisms that preserve the order of cell cycle events are called checkpoints (Hartwell and Weinert, 1989). Since the DNA damage checkpoint involving Sp. Rad3/ Hs. ATR protein, is important for many aspects of the DNA damage response (DDR), I determined whether the *pol3* variants in this study activate the sensor protein kinase, Rad3. Rad3 in *S. pombe*, also known as ataxia telangiectasia and Rad3-related protein (ATR) in humans, is important in detecting DNA damage or S phase problems and activating the DNA damage and/or replication checkpoint pathways, leading to cell cycle arrest and DNA repair (Bentley et al., 1996; Sancar et al., 2004). If the *pol3* mutant cells are inviable or sick when Rad3 is inactivated then this would suggest that the cells are experiencing some kind of DNA damage or S phase stress that requires the checkpoint to be activated in order to maintain cell viability. In other words, Rad3 activation would essentially keep the *pol3* mutant cells alive.

Thirdly, the possibility of the HU sensitivities of *pol3G305S* and *pol3P311L* variants being the result of increased replication fork stalling and collapse was explored by deleting the *mus81*$^{+}$

gene. The endonuclease Mus81 cleaves blocked and unstable forks to form DSBs and instigates homologous recombination (HR) repair of these forks in order to resume DNA replication (Doe et al., 2002; Kai and Wang, 2003). Hence, in theory, *mus81*Δ should reduce replication fork collapse in these *pol3* mutants, particularly upon HU-induced replicative stress. By generating *pol3, mus81*Δ double mutants, the HU sensitivity phenotype might be rescued.

In order to fully comprehend the results of Chapter 4, the following sections in this introduction provide a brief introduction to the functions of the DNA integrity checkpoints, including Rad3, and Mus81 in *S. pombe*.

Finally, to further elucidate the effects of HU on *pol3* EDMs, particularly *pol3P311L* and *pol3G305S*, the *pol3* mutants were crossed with a strain that has a mutation in the larger subunit of the ribonucleotide reductase (RNR) complex, *cdc22-D57N*, which alleviates allosteric feedback inhibition leading to an elevated dNTP pool (Fleck et al., 2013). Apart from the active catalytic site, there are two nucleotide-binding allosteric sites located in the Cdc22 subunit that regulate overall RNR activity: the allosteric specificity site and the allosteric activity site. The allosteric specificity site selects the appropriate substrate for reduction to maintain a balanced nucleotide pool (Fleck et al., 2013). The allosteric activity site regulates overall RNR activity via negative feedback control: binding of dATP reduces the activity of the enzyme, whereas ATP stimulates catalysis (Reichard et al., 2000; Williams et al., 2015). Substitution of a highly conserved aspartic acid at position 57 for asparagine (D57N) in the allosteric activity site of yeast and mammalian RNR leads to eradication of dATP feedback inhibition, and increased nucleotide levels (Caras and Martin JR, 1988; Reichard et al., 2000; Chabes et al., 2003; Fleck et al., 2013). Since HU works by reducing dNTP pools via inhibition of RNR activity, then perhaps by creating *pol3, cdc22-D57N* double mutations this will alleviate the HU sensitivity phenotypes of the *pol3P311L* and *G305S* variants by increasing dNTP levels. Additionally, it

will be interesting to see if an elevated nucleotide pool will have an effect on the replicative fitness of the other *pol3* variants that are not HU-sensitive, such as *pol3L458P* and *pol3D386A*, because in *S. cerevisiae*, high dNTP levels delayed S phase entry and resulted in DNA damage sensitivity due to inhibition of the DNA damage checkpoint response (Chabes and Stillman, 2007). Also, high dNTP pools can be mutagenic because of the tendency of wild-type DNA polymerase to extend a damaged or mismatched primer-template, and decreased proofreading efficiency at high nucleotide levels (Pai and Kearsey, 2017).

4.1.1 The DNA damage response (DDR)

Mammalian cells have developed an intricate network of pathways to detect DNA damage, signal its presence, and trigger repair (Harper and Elledge, 2007; Rouse and Jackson, 2002). A plethora of well-defined mechanisms employed in response to DNA lesions fall under the term "DNA damage response" (DDR), such as: cell cycle arrest, transcription, DNA repair, apoptosis, autophagy, replication, RNA metabolism, and chromatin remodelling (Ljungman, 2010; Jackson and Bartek, 2009). Different types of DNA lesions require a number of distinct repair pathways within the cell, each one dealing with a specific type of lesion (Christmann et al., 2003). Howbeit, in order to mobilise the DDR, initiation of the signal cascade is required, and in mammalian cells this is mainly coordinated by two major phosphatidylinositol 3-kinase-like kinases (PI3KK): Ataxia-Telangiectasia Mutated (ATM) and ATM and Rad3-related (ATR) (Lee and Paull, 2004; Abraham, 2001; Bentley et al., 1996). A faulty DDR can lead to many different human diseases, such as: cancers, neurodegenerative disorders (e.g. Alzheimer's, Huntington's and Parkinson's diseases), and immune deficiencies (e.g. B- and T-cell immune deficiency) (Jackson and Bartek, 2009). The high evolutionary conservation of the DDR in various orthologues illustrates the significance of the DDR in maintaining genome stability and cell survival (Jackson and Bartek, 2009).

4.1.2 DNA integrity checkpoints

The DNA repair pathways described above function collaboratively with cell cycle checkpoints to safeguard genome stability. The DNA integrity checkpoints ensure completion of DNA replication and DNA repair before entry into mitosis and, also, at different cell cycle transitions (O'Connell et al., 2000). They enhance efficient repair not only by sensing DNA lesions, but also by stimulation of appropriate cellular responses: for example, arresting the cell cycle to provide time for repair, regulation of dNTP levels and transcription, chromatin remodelling, and initiating cell senescence or apoptosis in metazoan cells (Hartwell and Weinert, 1989; Su, 2006). There are two classes of DNA checkpoints: the DNA damage checkpoint that detects and responds to DNA damage, and the replication checkpoint that responds to problems in DNA replication. The DNA damage and replication checkpoints (Hs. ATR and ATM, respectively), collectively termed the DNA integrity checkpoints, prevent aberrant chromosomal segregation due to incomplete or inefficient DNA replication and repair (O'Connell et al., 2000). In fission yeast, the DNA damage or replication checkpoint responses are executed by the serine/threonine kinases, Chk1 or Cds1, respectively (**Figure 4.1**) (Humphrey, 2000).

Similar to the DDR, the checkpoint machinery is evolutionarily conserved from yeast to humans, and the disruption of checkpoint genes augments genomic instability, which can result in loss of viability or abnormal growth, and lead to tumours in multicellular organisms; hence, checkpoint genes are considered tumour suppressors (Zhou and Elledge, 2000). Checkpoint pathways that recognise the presence of damaged DNA or replication fork barriers can block progression at different stages of the cell cycle cell (namely, G1/S, S and G2/M checkpoints) (Sancar et al., 2004; Harrison and Haber, 2006). In both fission and budding yeasts, the ATM homologue is Tel1 (Sanchez et al., 1996; Zhao et al., 2003), and the corresponding ATR homologues are Rad3 (Sp) and Mec1 (Sc). However, unlike in humans and *S. cerevisiae*

(Shiloh, 2003; Morrow et al., 1995; Sanchez et al., 1996), Tel1 in *S. pombe* plays a minor role in the checkpoint response to replication stress. Also, in mammals, ATR activation in response to DSBs requires ATM, which is not seen in yeasts (Myers and Cortez, 2006). Furthermore, the ATR and Mec1 proteins are essential for the viability of mammalian and budding yeast cells, respectively (Brown and Baltimore, 2000; Zhao and Rothstein, 2002), whereas Rad3 in fission yeast is not essential.

DNA damage, including nicks, gaps and double-strand breaks (DSBs), stem from many causes such as radiation, reactive oxygen species (ROS) and replication across nicked DNA. The types of sensor proteins that associate with a particular DNA lesion may serve as recognition complexes to recruit specific target proteins for that type of lesion. The pathway for checkpoint activation involves these three major groups of proteins and other checkpoint factors that transduce the signal of damaged DNA or incomplete replication into the response of cell cycle arrest and repair (Humphrey, 2000) (see **Figure 4.1**). Evolutionary conserved checkpoint proteins have been categorised into three groups as follows: first, the sensor proteins, which include the ATR-ATRIP kinase complex (Sp. Rad3-Rad26), the RFC- and PCNA-like complexes (Rad1, Rad9, Hus1 and Rad17), and the MRN complex (Rad32/Mre11, Rad50 and Nbs1); second, the mediator proteins (Crb2 and Mrc1); third, the effector kinases (Chk1 and Cds1) (Furuya and Carr, 2003).

4.1.2.1 Sensing the damage

In *S. pombe*, the Rad3-Rad26 (Hs. ATR-ATRIP) complex phosphorylates many of the other checkpoint proteins which are paramount to the checkpoint response (Furuya and Carr, 2003). Therefore, Rad3-dependent Chk1 and Cds1 phosphorylation is indispensable for checkpoint activation and cell cycle inhibition (Rhind and Russell, 2000a). The phosphatidylinositol-3 kinase (PI3K), Rad3, is recruited to sites of DNA damage or replication stress by Rad26. The

prolonged presence of replication protein A (RPA) bound to single-stranded DNA (ssDNA), which is prevalent at stalled replication forks and sites of single-strand breaks (SSBs) and double-strand breaks (DSBs) (Brown and Baltimore, 2003; Boye et al., 2009), activates Rad3 via interaction with Rad26 (Cortez et al., 2001; Edwards et al., 1999; Namiki and Zou, 2006; Zou and Elledge, 2003). ATR activation in humans works similarly to the above. In humans, specifically, the sensor proteins involved in the recruitment and activation of the second major PI3K, Hs. ATM, are Mre11, Rad50 and Nbs1, known as the MRN complex. In fission yeast, the MRN complex further modulates the checkpoint response via phosphorylation of downstream targets, including Cds1, the yeast homologue of human Chk2, and Chk1 (D'Amours and Jackson, 2001; Grenon et al., 2001; Uziel et al., 2003). ATR phosphorylates Chk1 in response to replication blocks and UV-irradiation (Shiloh, 2003). Therefore, ATM and ATR phosphorylate many of the same downstream substrates in vivo and the two pathways overlap (Zhou and Elledge, 2000).

The 9-1-1 complex is a heterotrimeric ring structurally related to PCNA but containing Rad9-Rad1-Hus1 in both humans and *S. pombe,* and Ddc1-Rad17-Mec3 in *S. cerevisiae* (Caspari et al., 2000; Volkmer and Karnitz, 1999). The PCNA-like Rad1-Hus1-Rad9 (9-1-1) complex detects replication perturbation and DNA damage via replication factor-C-like (RFC-like) proteins, namely the clamp loader Rad17-RFC (Caspari and Carr, 2002; Kemp and Sancar, 2009; Zou et al., 2002). This complex may connect Rad3-Rad26 to the mediator complexes, Crb2 and Mrc1, which in turn recruit Chk1 and Cds1, respectively, to be phosphorylated and, thus, activated by Rad3 (Furuya and Carr, 2003; Mochida et al., 2004; Qu et al., 2012; Xu et al., 2006).

The multifunctional Mre11-Rad50-Nbs1 (MRN) complex efficiently recognises DSBs, especially during S phase (reviewed in Stracker and Petrini, 2011). Once MRN associates with

the DSB, it activates ATM in metazoans to initiate checkpoint signalling to provide cells time to repair and restart (Falck et al., 2005; You et al., 2005). Additionally, MRN and ATM are required to initiate DSB resection in order to generate RPA-coated ssDNA which is the essential structure intermediate for DNA repair and ATR-dependent signalling (You et al., 2002; Jazayeri et al., 2006; Myers and Cortez, 2006). The MRN complex, together with RPA and Rad3/ATR, is equally important for replication fork protection, remodelling and restart, as well as HR rescue of collapsed forks in yeasts and direct checkpoint signalling in response to damage (Bressan et al., 1999; Chahwan et al., 2003; Porter-Goff and Rhind, 2009; Syed and Tainer, 2018).

RPA protects ssDNA from nucleases and prevents hairpin formation at the replication fork that would disrupt DNA replication (Heyer et al., 1990; Szüts et al., 2003). It also cooperates with other replication factors to stimulate the activity of both Pols α and δ during the initiation stage of DNA replication. Apart from its function in DNA replication, RPA plays a crucial role in damage signalling, in conjunction with several checkpoint proteins, to stabilise replication forks and support DNA repair during S phase (Zou and Elledge, 2003; Namiki and Zou, 2006; Zou et al., 2006). Note that RPA from both human and yeast cells is regulated in a cell-cycle-dependent manner: it becomes phosphorylated at the G1/S cell cycle transition and dephosphorylation takes place at mitosis (Din et al., 1990).

4.1.2.2 Signal transduction

Post DNA damage detection and initiation of the checkpoint response by Rad3 in fission yeast, the checkpoint signal is transduced and amplified by the recruitment of effector kinases, Chk1 and/or Cds1, and this recruitment is mediated by Crb2 or Mrc1 depending on the initial type of genotoxic stress, explained below (also refer to **Figure 4.1**).

Figure 4.1

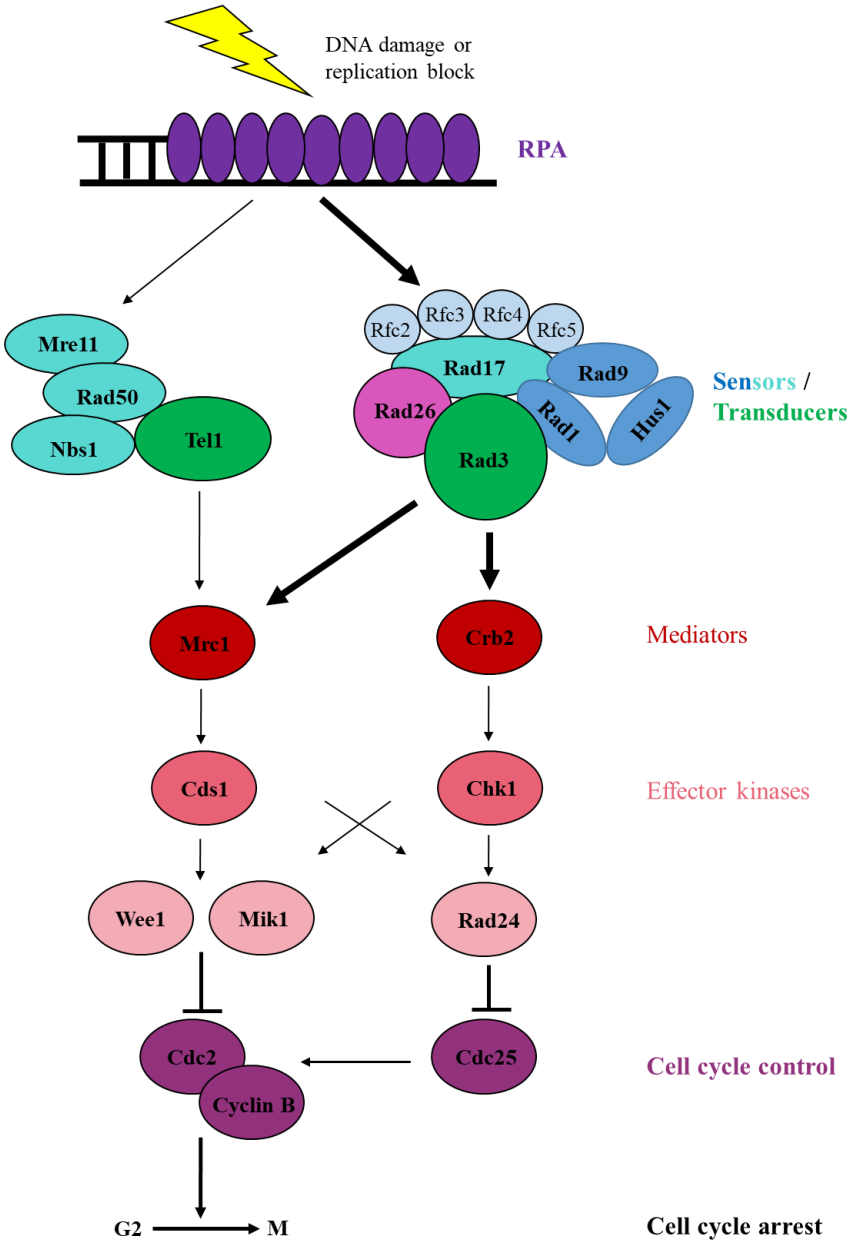


Figure 4.1: Components involved in the *S. pombe* checkpoint response. Upon detection of damaged DNA or replication block, checkpoints initiate a phosphorylation cascade to arrest cell cycle and promote DNA repair. DSBs or SSBs are recognised by the sensors MRN (Mre11-Rad50-Nbs1) complex or by the PCNA-like 9-1-1 (Rad9-Rad1-Hus1) complex which is loaded by the replication factor C (RFC)-like clamp-loader complex Rad17-Rfc2-Rfc3-Rfc4-Rfc5. Upstream signalling involves the activation of the Rad3-Rad26 complex, as indicated by the fatter arrows. Signal transduction is relayed by either Mrc1 or Crb2, depending on the type of genotoxic stress. The aforementioned mediator proteins allow the activated Rad3-Rad26 complex to phosphorylate the effector kinases Cds1 and/or Chk1 which, in turn, both phosphorylate Wee1, Mik1 and Rad24. This subsequently leads to cell cycle arrest in G2/M by inhibition of the Cdc2-CyclinB complex and phosphatase Cdc25. See text for further details. Figure and legend adapted and modified from Kasparek (2013) and Pai (2009).

Different mediator complexes function in S phase and G2 phase: in S phase, Mrc1 (Hs. Claspin) mediates Cds1-dependent checkpoint signalling and in G2 phase, Crb2 (Hs. 53BP1) mediates Chk1-dependent checkpoint signalling (Alcasabas et al., 2001; Chini and Chen, 2003; Saka et al., 1997). In fission yeast, Chk1 (Hs. Chk1) phosphorylation is involved in the DNA damage checkpoint pathway, and Cds1 (Hs. Chk2) phosphorylation is specifically required for the replication checkpoint pathway (Rhind and Russell, 2000b). Moreover, it has been reported that the Mus81-Eme1 endonuclease complex directly interacts with Cds1 via Mrc1 during S phase in order to stabilise stalled forks (Boddy et al., 2000). Therefore, in fission yeast, the Mrc1-Cds1 interplay has an accessory role in the S phase response to replication perturbation by inhibiting homologous recombination (HR), and inappropriate fork cleavage by Mus81 (Kai et al., 2005), and by preventing late-firing replication origins (Furuya and Carr, 2003). Additionally, Rad3 activation followed by Chk1 phosphorylation in G2 is believed to indirectly upregulate dNTP synthesis for DNA repair via Spd1 degradation - Spd1 is degraded by the ubiquitin ligase complex, $CRL4^{Cdt2}$ (Liu et al., 2003; Holmberg et al., 2005; Moss et al., 2010; Salguero et al., 2012). Spd1 is an inhibitor of ribonucleotide reductase (RNR) which is degraded in unperturbed S phase in a checkpoint-independent fashion, and after DNA damage in a checkpoint-dependent manner (Liu et al., 2003; Salguero et al., 2012).

4.1.2.3 Arresting the cell cycle

S. pombe cells spend most of their time in the G2 phase of the cell cycle, and since the G2/M transition is the major control point in the fission yeast cell cycle, both the DNA damage and replication checkpoints mediate cell cycle arrest at the G2-M cell cycle interface (Humphrey, 2000).

Following Cds1 and Chk1 phosphorylation, Wee1, Mik1, and the 14-3-3 protein Rad24 are activated to induce cell cycle arrest (Rhind and Russell, 2000b). The G2-M transition is

regulated via a number of interconnected pathways: firstly, by inhibitory phosphorylation of the cyclin-dependent kinase (CDK), Cdc2, by Wee1 and Mik1 kinases (Rhind et al., 1997; Rhind and Russell, 2001). Cdc2 works together with Cyclin B to drive mitosis. Secondly, following checkpoint activation, the Cdc2 phosphatase Cdc25, a mitotic inducer, is inactivated two-fold. Chk1 and Cds1 kinases inactivate Cdc25 via direct inhibitory phosphorylation, and subsequent binding to Rad24 (a member of the 14-3-3 protein complex) mediates the nuclear export of Cdc25 (Furnari et al., 1997, 1999; Zeng et al., 1998; Lopez-Girona et al., 1999; Zeng and Piwnica-Worms, 1999).

To summarise, cell cycle arrest in G2 is directly induced via the inhibition of Cdc2-CyclinB complex and indirectly induced via the inhibition of Cdc25. Comparable mechanisms of checkpoint control exist in both yeast and humans (Niida and Nakanishi, 2006).

4.1.3 An overview of the role of Mus81 in eukaryotes

The faithful and fulfilled replication of chromosomes is essential to limit the accumulation of mutations and maintain genetic stability. Exogenous- or endogenous-induced replication stress can result in stalled and cleaved replication forks during S phase, for example, DNA secondary structures, unrepaired DNA damage and agents like hydroxyurea (HU) and aphidicolin that block fork progression (Petermann and Helleday, 2010). A stalled replication fork is arrested but can resume replication (known as replication fork restart) once the inhibition is removed or rectified, whereas a collapsed/cleaved fork has become inactivated (known as replication fork collapse) via the dissociation of the replication machinery and DSB formation (Petermann and Helleday, 2010). In eukaryotic cells, fork cleavage is carried out by the structure specific endonuclease – methyl methanesulfonate (MMS) and ultraviolet sensitive 81 – Mus81 (Hanada et al., 2007) (see **Figure 4.2** for further details). The role of Mus81 in cells, particularly in yeast,

has been extensively reviewed in Hollingsworth and Brill (2004), Osman and Whitby (2007), Kim and Forsburg (2018), and briefly discussed here.

Replication fork recovery or restart can be mediated via Holliday junction (HJ), or DSB formation, depending on the type of block (Michel et al., 2004). For example, short-term exposure to HU (up to 12 hours) will stabilise the stalled replication fork until the block is removed and DNA synthesis can be resumed. Members of the RecQ family of DNA helicases, including Sgs1 and Rqh1 in budding and fission yeast, respectively, and Bloom syndrome helicase (BLM) and Werner syndrome ATP-dependent helicase (WRN) in humans, also play critical roles in preventing fork disassociation by recombination intermediates (Ahn et al., 2005; Hickson, 2003; Sidorova et al., 2008). RecQ helicases have been reported to rescue stalled replication forks by branch migrating Holliday junctions that are formed when nascent strands anneal to each other (Ahn et al., 2005; Doe et al., 2000, 2002; Constantinou et al., 2000). This activity is believed to inhibit inappropriate recombination and DSB formation at stalled forks as well as to avert replication fork collapse by the endonucleases, Mus81-Eme1 (Ira et al., 2003; Wu and Hickson, 2003; Doe et al., 2002; Kaliraman et al., 2001). The mechanisms of replication fork-restart have been reviewed in Yeeles et al (2013) and Petermann and Helleday (2010).

If exposure to HU extends to 24 hours, then the stalled replication forks take the DSB-mediated restart pathway, which requires Mus81 to cleave stalled and unresolved replication forks (Doe et al., 2002; Hanada et al., 2007; Kaliraman et al., 2001) (**Figure 4.2**). DSB formation promotes the Rad51-dependent homologous recombination (HR) repair of collapsed forks (Petermann et al., 2010; Petermann and Helleday, 2010). Moreover, it has been demonstrated that in replication checkpoint-deficient yeast cells, under some form of replicative stress, DNA upstream of the collapsed fork is resected by the MRN helicase complex and Exo1 and this

genome degradation is prevented largely by checkpoint activation, and subsequent coordination of recombination factors associated at collapsed forks (Cotta-Ramusino et al., 2005; Sogo et al., 2002; Tsang et al., 2014). It has also been reported that both Rqh1 and Mus81-Eme1 complex (Eme1 is a Holliday junction resolvase) promote the repair of collapsed forks and fork restart (Doe et al., 2002; Yokoyama et al., 2007; Franchitto et al., 2008; Shimura et al., 2008). In human cells, after long hydroxyurea treatments, replication restarts by the firing of new origins, followed by DSBR of collapsed forks (Petermann et al., 2010). However, the cell has to be circumspect about its use of recombination on broken forks because it can result in genome instability, via gene deletion and/or chromosomal translocation, one of the hallmarks of cancer (Ahn et al., 2005; Lambert et al., 2005, 2010; Negrini et al., 2010).

4.1.4 Aims of Chapter 4

The main aim and objectives of Chapter 4 are to:

- Elucidate the HU sensitivity phenotype of some of the *pol3* variants by:
    - Measuring the physiological levels of Pol3 protein in the mutants.
    - Observing the mitotic effects of HU on the cells after 6 hours treatment under the microscope and quantifying any abnormalities.
    - Assessing the survival of the *pol3* mutant cells in the presence of HU during a time-course using colony formation assay.
    - Evaluating S phase recovery after cell cycle block and release.
- Verify Rad3 activation in the *pol3* mutant strains.
- Study the effects of *mus81*Δ in the *pol3* mutants, particularly the HU-sensitive strains expressing *pol3P311L* and *pol3G305S*.

- Decipher whether elevated dNTP levels, via allosteric inhibition of ribonucleotide reductase (RNR), rescue the HU sensitivities attributed to the *pol3P311L* and *pol3G305S* mutations.

Figure 4.2

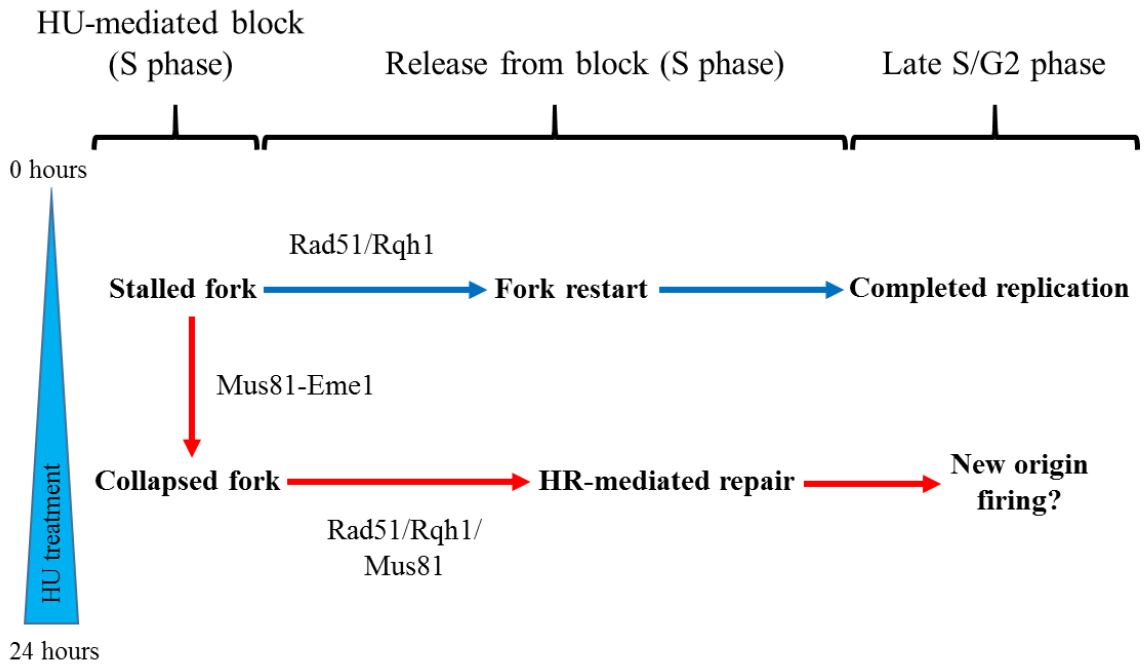


Figure 4.2: Mus81 cleaves stalled and unresolved replication forks. A simplified depiction of Mus81/Eme1-dependent cleavage of stalled forks in yeast and mammalian cells. Most replication forks resume progression after release from short (2-4 hours) hydroxyurea (HU)-induced S phase blocks. Early replication fork restart is promoted by the recombinase, Rad51, and the DNA helicase, Rqh1 via Holliday junction-mediated restart (Doe et al., 2000, 2002; West, 2003; Willis and Rhind, 2009; Petermann et al., 2010). Stalled forks become unstable and collapse during long (24 hour) HU treatments/prolonged exposure to DNA damage. Fork collapse correlates with the accumulation of double strand breaks (DSBs) that are predominantly dependent on the endonuclease, Mus81 (Boddy et al., 2000; Chen et al., 2001; Ciccia et al., 2003; Froget et al., 2008; Fugger et al., 2013). Replication fork collapse is followed by DSB-mediated restart in mice and human cell lines: DSB formation is believed to promote replication restart and the Rad51-dependent, homologous recombination (HR) repair of forks (Hanada et al., 2007; Shimura et al., 2008). Similarly, HR-dependent fork restart occurs in *S. pombe* (Lambert et al., 2010). Other evidence implies that DSB generation does not play a role in fork restart in human cancer cell lines after prolonged HU treatments and, additionally, Mus81 depletion does not ameliorate fork restart after long HU exposure (Petermann et al., 2010; Franchitto et al., 2008). Overall, Rqh1 and namely, Mus81 are believed to promote double-strand break repair (DSBR) once forks have collapsed (Murray et al., 1997; Doe et al., 2002; Hanada et al., 2007; Roseaulin et al., 2008; Shimura et al., 2008; Petermann et al., 2010). After release from long HU treatments, global replication restart is achieved by the firing of new origins in mammalian cells, followed by DSBR of collapsed forks (Petermann et al., 2010). It is not yet known if this applies to *S. pombe*. Figure and legend adapted and modified from Petermann and Helleday (2010).

4.2 RESULTS

4.2.1 Pol3 levels in the *pol3* EDMs

It was important to firstly establish whether the hydroxyurea (HU) sensitivity observed with some of the *pol3* variants was due to depleted levels of the Pol3 protein compared to the wild type as it is possible that the amino-acid changes associated with the variants might destabilise the protein. In response to this question, the *pol3* variants were reconstructed to possess a FLAG tag marked by antibiotic resistance, other than $G418^R$, and a western blot was subsequently carried out with the FLAG-tagged strains.

4.2.1.1 Construction of FLAG-tagged pol3 variants

The scheme for tagging existing *pol3* strains with the epitope tag, 5FLAG, is outlined in **Figure 4.3** and explained in detail in Noguchi et al (2008). The first step was to design the primers for FLAG-tagging the *pol3* variants: the forward primer, #1350 (see **Table 2.2**), was designed so that it is complementary to part of the Pol3 reading frame sequence and to part of the *pFA6a-5FLAG-hphMX6* plasmid sequence (F2 primer – **Figure 4.3**). Thus, the DNA sequence of primer 1350 is long, consisting of 100 bp of the Pol3 sequence, upstream of the STOP codon, and 20 bp of the pFA6a tagged plasmid sequence. Note that the Pol3 reading frame has to be in frame with the FLAG tag, so the STOP codon to the Pol3 open reading frame was not included in the design of the forward primer (see **Figure 4.3**). The reverse primer (R2), #736 (**Table 2.2**), is a universal primer complementary to the pFA6a-MX6 vector and, since it gives more than 200 bp shared homology, there was no need for the primer sequence to be long.

Using primers 736 and 1350, colony PCR was carried out with *pFA6a-5FLAG-hphMX6* vector (Plasmid 997 – **Table 2.3**) as template in order to amplify the tagged vector for yeast transformation. The PCR fragment was purified, the yield checked (380 ng/µl) and a small

aliquot was run on agarose gel to ensure the fragment size was correct (2175 bp). The purified and amplified *pFA6a-5FLAG-hphMX6* plasmid was separately transformed into wild-type *pol3* and *pol3* EDM strains that possess G418 resistance (KanMX6 cassette) (**Figure 4.3**). Colonies were selected for both hygromycin resistance (hphMX6 cassette) and G418 sensitivity. Yeast transformants were also screened via colony PCR using the primer pair 1183 and 1088 to identify which transformants had successfully incorporated the FLAG tag at the correct position of the genome. If the vector was correctly integrated at the *pol3* locus, a fragment size of 3103 bp was produced on agarose gel (**Figure 4.4**). This created the following *pol3*-FLAG tagged wild-type and mutant strains: 3960 – 3971 (**Table 2.1**).

4.2.1.2 The pol3 variants all have physiological levels of Pol3

Following TCA extraction and western blotting of the *pol3*-tagged strains (see **Section 2.3** for methods), it was ascertained that all of the *pol3* variants in question have approximately the same levels of the Pol3 protein as Wt (**Figure 4.5**). Therefore, any increase in the rate of mutations or other phenotypes observed in these *pol3* strains is not a reflection of the abnormal protein levels but due to the sequence change in these mutant polymerases (Kokoska et al., 2000).

Figure 4.3

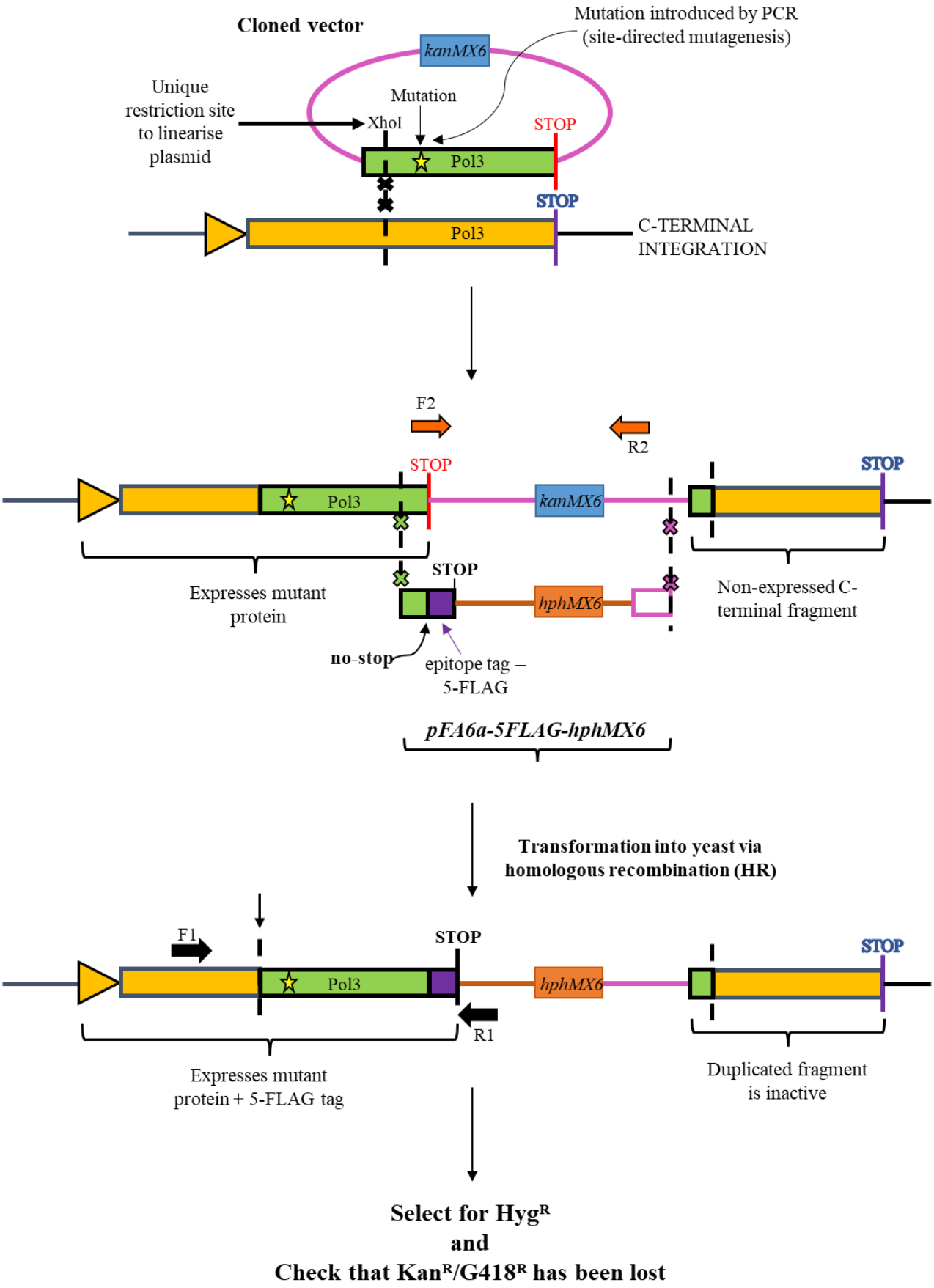

Cloned vector
Mutation introduced by PCR
(site-directed mutagenesis)
kanMX6
Unique
restriction site
to linearise
plasmid
XhoI
Mutation
STOP
Pol3
STOP
Pol3
C-TERMINAL
INTEGRATION
F2
R2
STOP
Pol3
kanMX6
STOP
STOP
Expresses mutant
protein
hphMX6
Non-expressed C-
terminal fragment
no-stop
epitope tag –
5-FLAG
pFA6a-5FLAG-hphMX6
Transformation into yeast via
homologous recombination (HR)
F1
STOP
STOP
Pol3
hphMX6
R1
Expresses mutant
protein + 5-FLAG tag
Duplicated fragment
is inactive
Select for Hyg^R
and
Check that Kan^R/G418^R has been lost

Figure 4.3: A schematic outlining the construction of Pol3-tagged EDMs. Upper panel: A reminder of how the germline EDMs were constructed initially, as described in Figure 3.3B. Since the *pol3* mutants were constructed by transforming a *pFA6a-kanMX6* vector consisting of the desired *pol3* mutation into the yeast genome, an epitope tag on the same pFA6a-MX6 system, with a different antibiotic resistance marker, can be successfully transformed into *the pol3* strains whilst maintaining the *pol3* mutation in the genome. **Middle and lower panels:** Transformation of the *pFA6a-5FLAG-hphMX6* plasmid into the Wt and *pol3* mutant strains. The PCR'd plasmid integrates with part of the Pol3 reading frame (green) from the *pol3* mutant strain, forming a Pol3 coding domain, with the desired *pol3* mutation (yellow star) intact, that is now tagged with the 5FLAG epitope (purple) and hphMX6 cassette (orange), conferring hygromycin resistance (Hyg^R). The other duplicated Pol3 fragment remains inactive and is not expressed. The F2 and R2 primers represent primers 1350 and 736, respectively, and were used to set up colony PCR with the *pFA6a-5FLAG-hphMX6* template prior to yeast transformation. Note that the Pol3 reading frame has to be in frame with the FLAG tag, therefore, the stop codon to the Pol3 reading frame was not included in the design of the F2 primer and instead, was introduced at the end of the FLAG tag. The yeast colonies carrying the desired tag are selected on hygromycin-containing plates and are checked for the loss of kanamycin (G418) resistance (Kan^R /$G418^R$). The F1 and R1 primers represent 1183 and 1088 primers respectively and they check that the plasmid has been correctly integrated in the yeast genome, via colony PCR.

Figure 4.4

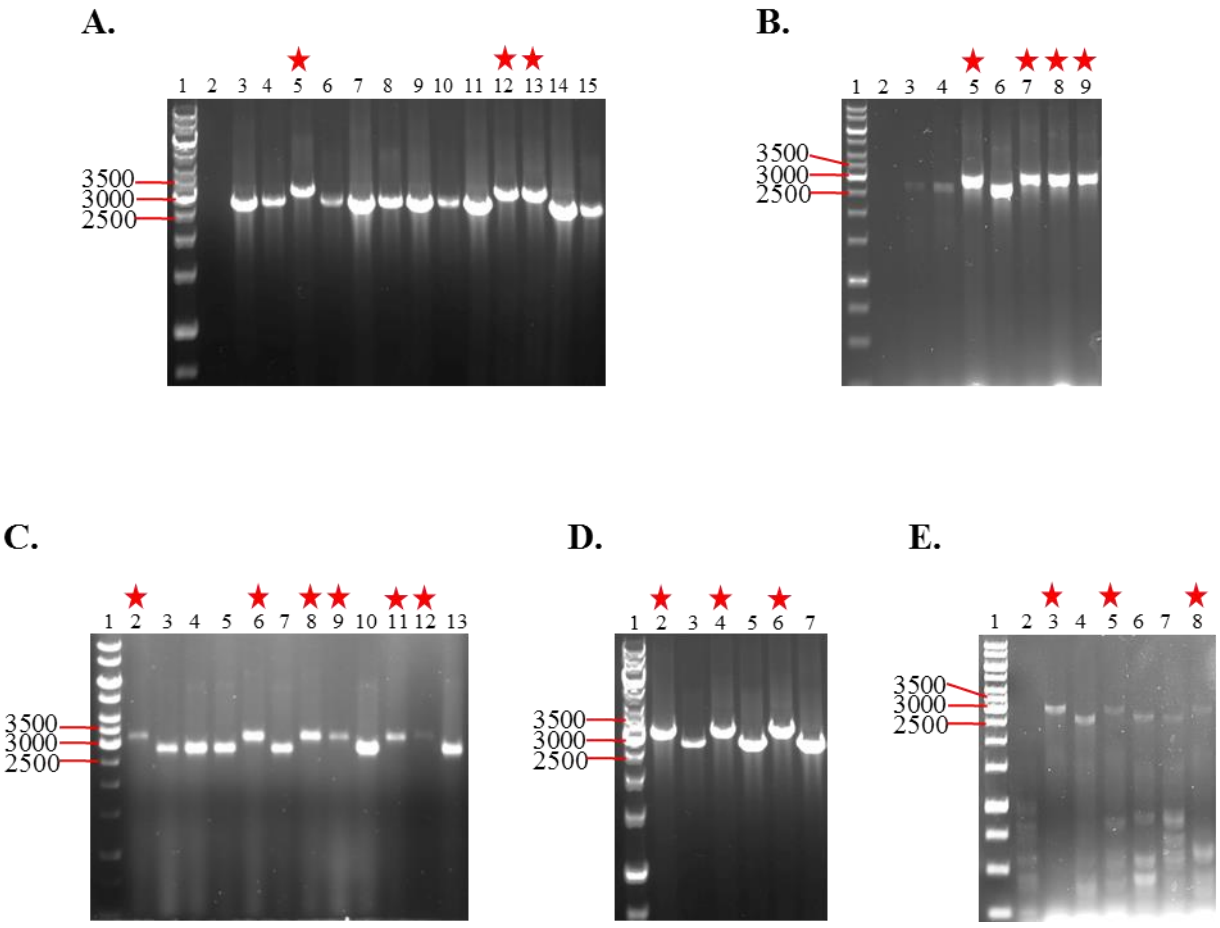


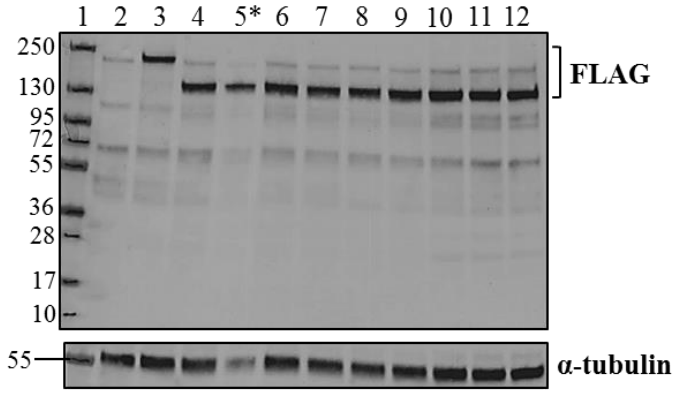
Figure 4.4: Characterisation of *pol3*-tagged yeast transformants' genotype via colony PCR. Colony PCR of yeast transformant single colonies using the primer pair 1183 and 1088. Correct integration of the *pFA6a-5FLAG-hphMX6* plasmid into the Wt and various *pol3* mutant strains, yields a 3.1 kbp band on agarose gel. If the FLAG-hphMX6 tag has not been correctly integrated in the genome then the band size remains 2.8 kbp. Positive transformants are marked with a red star above the lane numbers. For all gels, Lane 1 is the 1 kb DNA molecular marker. **(A)** Yeast transformants of *pol3G305S* were run on agarose gel post-colony PCR. Lane 2 is a 'no DNA' control. Lanes 3 and 4 are the *pol3G305S* strains (untagged, negative controls). Lanes 5, 12 and 13 are successful transformant strains: *pol3G305S-5FLAG-hphMX6*. **(B)** Yeast transformants of *pol3D300N* were run on agarose gel post-colony PCR. Lane 2 is a 'no DNA' control. Lanes 3 and 4 are the *pol3D300N* strains (untagged, negative controls). Lanes 5, 7, 8 and 9 are positive yeast transformants: *pol3D300N-5FLAG-hphMX6*. **(C)** Yeast transformants of wild-type *pol3* and *pol3L458P* were run on agarose gel post-colony PCR. Lanes 2, 6, 8 and 9 are successful transformant Wt-tagged strains: *pol3-5FLAG-hphMX6*. Lanes 11 and 12 are positively pol3*L458P*-tagged transformant strains: *pol3L458P-5FLAG-hphMX6* **(D)** Yeast transformants of *pol3D386A* (exo-null) were run on agarose gel post-colony PCR. Lanes 2, 4 and 6 are positively tagged strains: *pol3D386A-5FLAG-hphMX6*. **(E)** Yeast transformants of *pol3P311L* were run on agarose gel post-colony PCR. Lane 2 is a 'no DNA' control. Lanes 3, 5 and 8 are positively tagged yeast strains: *pol3P311L-5FLAG-hphMX6*.

Figure 4.5

A.

1. MW marker – protein ladder (kDa)
2. Untagged *wt* strain
3. *pol1 – 5-FLAG* tagged control
4. *pol3 – 5-FLAG_1* (*wt*-tagged)
5. *pol3 – 5-FLAG_2** (*wt*-tagged)
6. *pol3D386A – 5-FLAG_1*
7. *pol3D386A – 5-FLAG_2*
8. *pol3D300N – 5-FLAG_1*
9. *pol3D300N – 5-FLAG_2*
10. *pol3G305S – 5-FLAG_1*
11. *pol3G305S – 5-FLAG_2*
12. *pol3L458P – 5-FLAG_1*

*Broken well: sample leaked out into buffer



B.

1. MW marker – protein ladder (kDa)
2. *pol3 – 5-FLAG* (wt-tagged)
3. *pol3L458P – 5-FLAG_2*
4. *pol3P311L – 5-FLAG_1*
5. *pol3P311L – 5-FLAG_2*

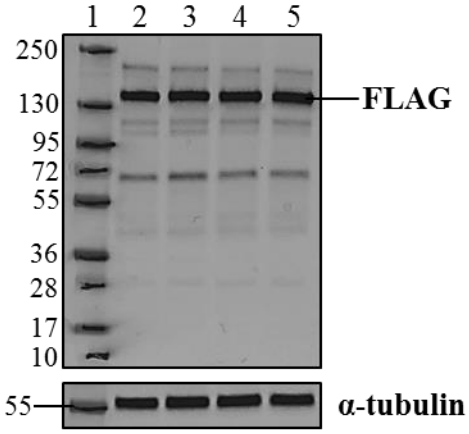


Figure 4.5: *Pol3* EDMs have physiologically normal levels of the Pol3 protein. (A & B) Western blot of FLAG-tagged *pol3* mutants showing the levels of the Pol3 protein. Two biological replicate strains were used for each genotype. **(A)** The strains used in Western Blot A were: [2]3500, [3]2067 (5-FLAG-tagged positive control), [4]3960, [5]3961, [6]3970, [7]3971, [8]3968, [9]3969, [10]3964, [11]3965, and [12]3966. An untagged Wt strain (#3500) and *pol1(α)-5FLAG* strain (#2067) were used as negative and positive controls, respectively. Note that Well 5 broke and the sample leaked into the buffer. **(B)** The strains used in Western Blot B were: [2]3960, [3]3967, [4]3962, and [5]3963.

4.2.2 *Pol3P311L* cells appear to have defective checkpoint arrest, whereas *pol3G305S* cells have overactive checkpoint arrest

In order to investigate possible defects in cell cycle checkpoints, the strains were treated with hydroxyurea (HU). HU is a drug that reduces the levels of dNTPs via ribonucleotide reductase (RNR) inhibition, consequently giving rise to replication fork stalling (Petermann et al., 2010). In wild type cells, this leads to activation of the replication checkpoint which blocks the cells in early S phase and prevents them from mitotic catastrophe as a result of incomplete DNA replication (**Figure 4.7A**) (Furuya and Carr, 2003; Slater, 1973; Timson, 1975). An important function of the S phase checkpoint is to stabilise stalled replication forks and prevent fork collapse upon HU arrest, so that cells maintain the ability to resume DNA synthesis when the stress is removed (Paulsen and Cimprich, 2007). When the checkpoint is activated, checkpoint-proficient cells elongate because the cells continue to grow without dividing (Enoch and Nurse, 1990). Checkpoint-deficient cells, such as *rad3*Δ, undergo cell division without completing a full round of replication (Enoch et al., 1992; Lieberman et al., 1996; Rowley et al., 1992; Xu et al., 2016). These cells typically exhibit the *'cut'* (cell untimely torn) phenotype, observable by DAPI-staining of the DNA (**Figure 4.6**) (Enoch et al., 1992; Hirano et al., 1986; Saka and Yanagida, 1993; Samejima et al., 1993).

Wild-type, *pol3P311L*, *G305S* and *D386A* asynchronous cells were grown to mid-logarithmic phase and challenged with 10 mM HU for 6 hours at 30˚C in liquid YES and then stained with DAPI for genomic DNA and calcofluor for the septum, as described in **Chapter 2.1.7**. The stained cells were examined under a fluorescence microscope before and after the addition of HU (**Figure 4.7B**). A *rad3*Δ strain was used as a positive control as it has been well-documented that these cells extensively undergo aberrant mitosis (forming *'cut'* cells) in the presence of DNA damaging or replication blocking agents (**Figures 4.7B** & **C**) (Al-khodairy and Carr, 1992; Enoch et al., 1992; Xu et al., 2016). The proportion of cells (out of 250 cells per strain

+/- HU) that appeared abnormal, as per defined in **Figure 4.6** and in the legend of **Figure 4.7**, was scored. *Pol3P311L* cells exhibited nine times more septated or abnormal-looking cells compared to Wt in the presence of HU which was significant (**Figure 4.7C**). This suggests that *pol3P311L* has leaky checkpoint arrest because approximately 10% of these cells experienced mitotic catastrophe under conditions of low dNTP levels, and this may explain the HU sensitivity phenotype displayed by the *P311L* variant on HU-containing plates. The other *pol3* variants, *pol3G305S*, *pol3L458P* and *pol3D386A*, did not have a significantly increased amount of mitotic abnormalities in the presence of HU (**Figure 4.7C**), which implies proficient checkpoint arrest in response to DNA damage or replication stress. Still, this does not explain the HU sensitivity observed in *pol3G305S* cells on solid media.

After 6 hours of incubation in HU, all the *pol3* mutant cells were noticeably elongated (**Figures 4.7B** & **D**). Conversely, checkpoint mutants, such as *rad3*Δ, do not elongate at all in HU because cell cycle progression is not delayed (Enoch et al., 1992) (**Figures 4.7B** & **D**). *Pol3G305S* and *pol3D386A* cells were elongated in the presence of HU but did not septate, unlike *pol3P311L* cells, meaning that the checkpoint is activated and effectively maintained in response to 6 hours of DNA replication inhibition. Also, it was observed that the *pol3G305S* cells had a significantly elongated phenotype without the addition of HU: the average cell length of *G305S* cells was significantly longer than that of Wt cells (**Figure 4.7D**). This implies that cells expressing *pol3G305S* cells activate the checkpoint under unperturbed conditions, possibly contributing to the high sensitivity to HU.

Figure 4.6

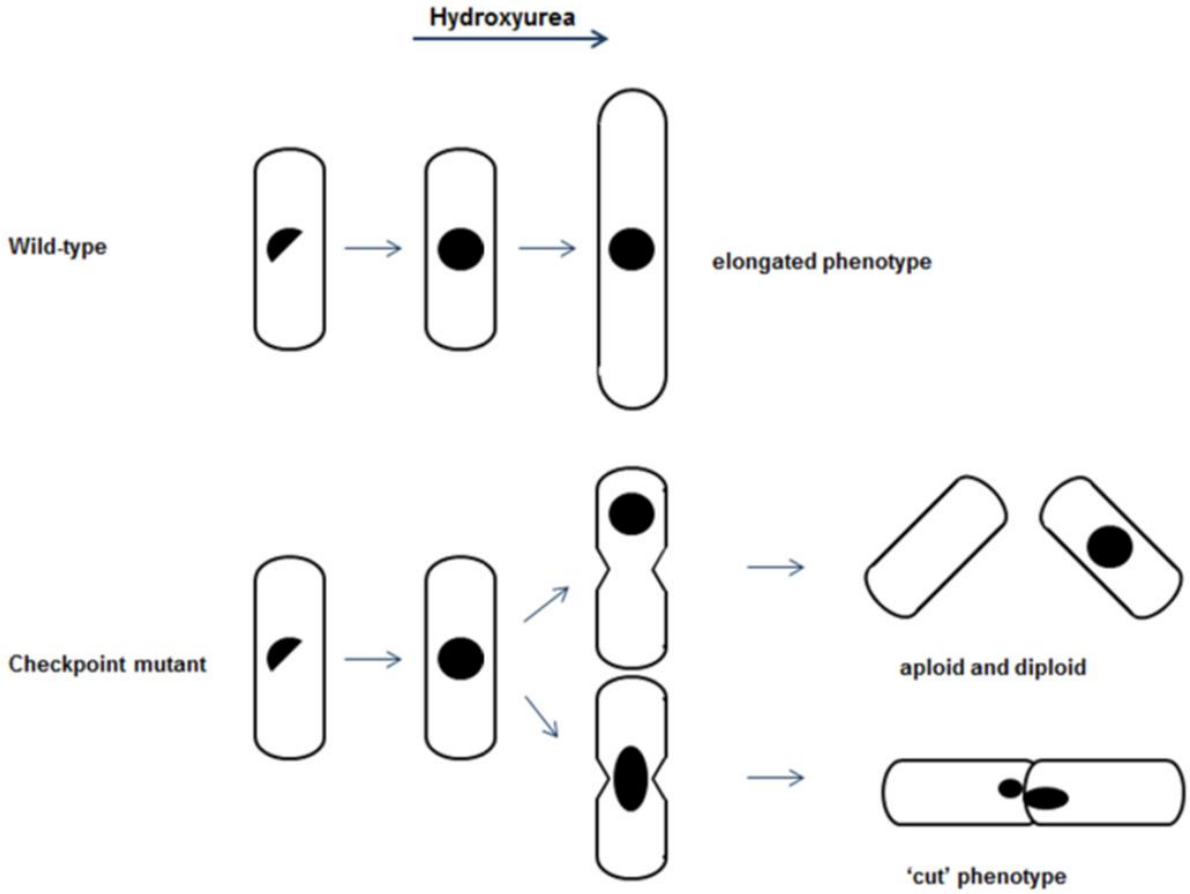
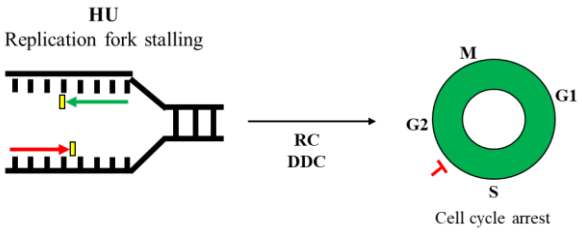


Figure 4.6: Diagram of the *'cut'* phenotype assay. Cells are treated with HU which reduces dNTP levels which, in turn, activates the S-phase checkpoint. In wild-type cells, cell cycle arrest is characterised by an elongated cell phenotype after 6 hours of HU treatment. Strains with deficient checkpoint control enter mitosis without completing a full round of DNA replication. This causes aploid and diploid cell pairs, the *'cut'* phenotype, as well as binucleation and micronuclei formation (latter not shown). Visualisation is achieved by DAPI stain and microscopy. Figure and legend adapted from Kasparek (2013).

Figure 4.7

A.


HU
Replication fork stalling
RC
DDC
M
G1
G2
S
Cell cycle arrest

B.

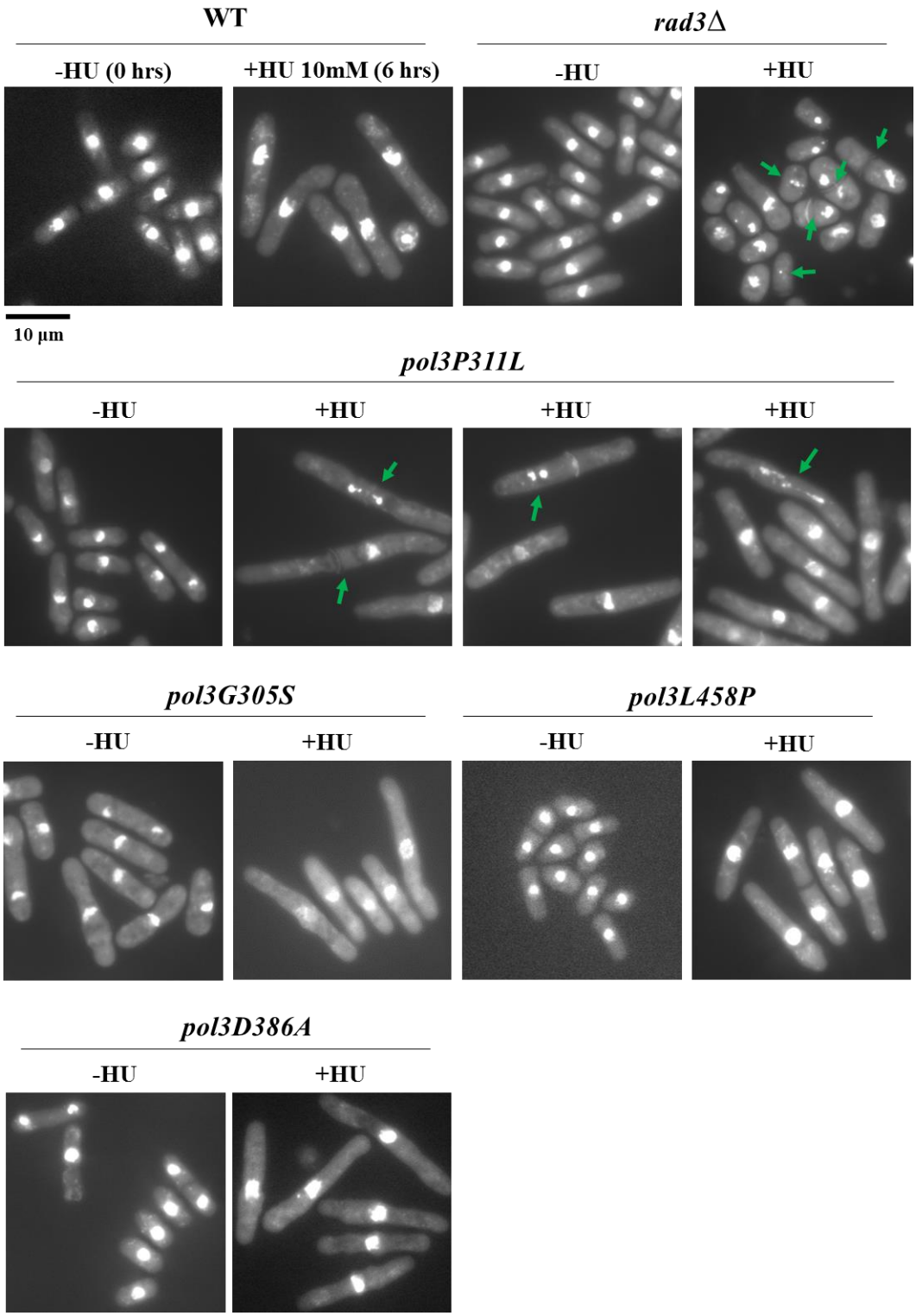
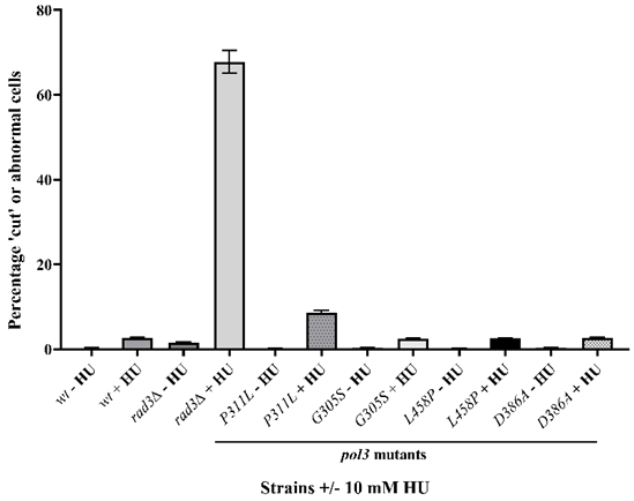

WT
rad3Δ
-HU (0 hrs)
+HU 10mM (6 hrs)
-HU
+HU
10 µm
pol3P311L
-HU
+HU
+HU
+HU
pol3G305S
pol3L458P
-HU
+HU
-HU
+HU
pol3D386A
-HU
+HU

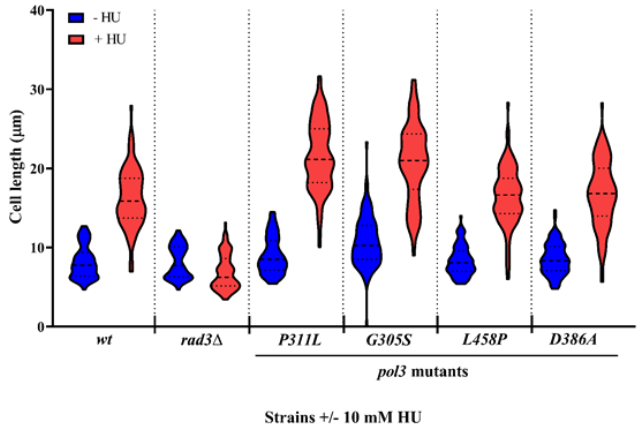
Figure 4.7

C.



Wild-type vs Strain 'X', + HU	P-value using Unpaired Student t-test with Welch's correction (two-tailed)
wt vs *pol3P311L*	0.0002***
wt vs *pol3G305S*	0.4^{NS}
wt vs *pol3L458P*	0.8^{NS}
wt vs *pol3D386A*	0.5^{NS}

D.



Wild-type vs Strain 'X'	P-value using the Mann Whitney test (two-tailed)	
	-HU	+HU
wt vs *pol3P311L*	0.013*	<0.0001****
wt vs *pol3G305S*	<0.0001****	<0.0001****
wt vs *pol3L458P*	0.4^{NS}	0.5^{NS}
wt vs *pol3D386A*	0.1^{NS}	0.3^{NS}

Figure 4.7: A significant proportion of *pol3P311L* cells show a *'cut'* phenotype in HU and the length of *pol3G305S* cells is significantly greater than wild type under normal conditions. (A) Schematic showing that hydroxyurea (HU) leads to replication fork stalling and cell activation of the replication checkpoint (RC) and DNA damage checkpoint (DDC), resulting in cell cycle arrest in S phase. This increases the number of cells stuck in G1. **(B)** Microscopy images (100x; Phase/DAPI) of Wt (3500), *rad3*Δ (1617), *pol3P311L* (3354), *pol3G305S* (3941), *pol3L458P* (3943) and *pol3D386A* (3273) variants before and after 6 hours of treatment with 10mM HU at 30°C. Strain numbers are in brackets above. *Rad3*Δ, the positive control, is DNA damage and replication checkpoint-defective and displays the typical *'cut'* phenotype in HU (see green arrows). Cells with *'cut'*, anucleate, binucleate, pyknotic nuclei, micronuclei and/or other abnormal-looking phenotypes, were scored out of 250 cells. Examples of such cells are highlighted with green arrows. **(C)** Quantitation of (B). Data are shown as mean ±SD (n=3). The P values are displayed adjacent to the graph. **(D)** A violin plot showing the median cell length for each strain out of 100 cells (n=3), +/- HU. The cell lengths were appropriately scaled and measured using NIH image software (ImageJ). The P values are also adjacent to the graph. P values: ^{NS} $p > 0.05$, * $p < 0.05$, *** $p < 0.001$, and **** $p < 0.0001$. NS = Not Significant.

4.2.3 The viability of *pol3P311L* and *pol3G305S* mutants is dependent on Rad3 activation

Checkpoint-defective cells are very sick under conditions of DNA damage: when Rad3, the DNA damage/replication checkpoint sensor, is not effectively activated in response to DNA damage or replication problems then the cells are liable to mitotic catastrophe which threatens the genomic stability and survival of the cells (Brown and Baltimore, 2003). Checkpoint activation and signalling is covered in **Chapter 4.1.2**. Accordingly, in this study, it was established whether Rad3-dependent checkpoint pathway activation is required for cell viability in the *pol3* mutant strains. Since the *pol3G305S* and *pol3P311L* cells were remarkably longer than Wt cells under normal circumstances in **Figure 4.7D**, this suggests that Rad3 is activated in these cells in response to DNA damage or replicative stress attributable to the *pol3* mutation (Enoch and Nurse, 1990).

4.2.3.1 Construction of pol3 mutations in a rad3ts background strain

The *pol3* mutant plasmids: 983, 1012, 1013 and 1014 (**Table 2.3**), were linearised using the restriction enzyme XhoI and transformed into a *rad3ts* background strain (2839 – **Table 2.1**), which possesses a temperature-sensitive *rad3* allele (*rad3ts*). Colony PCR and restriction digestion diagnostics for the *pol3*, *rad3ts* double mutants were the same as for the *pol3* variants in the wild-type background strain (see **Chapter 2.1.4**). *Pol3P311L*, *pol3G305S*, *pol3L458P* and *pol3D300N* (ex *rad3ts*) strains were thus characterised and selected to provide the following strains: 3416, 3957, 3958 and 3959 (see **Table 2.1**). *Pol3D386A* (exo-null) ex *rad3ts* strain was constructed prior to, and used in this study (#3292).

4.2.3.2 Spot tests

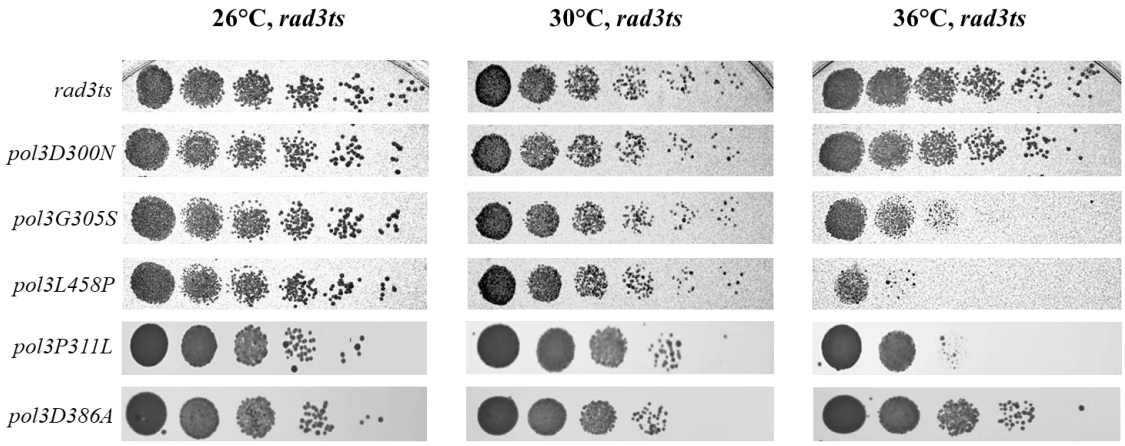
To test whether the *pol3* mutations are synthetically lethal/sick with *rad3* inactivation, the growth of the *pol3*, *rad3ts* double mutant strains were analysed on YES plates at 26°C

(permissive temperature, i.e. Rad3 active), 30°C (semi-permissive temperature, i.e. partially Rad3 active) and 36°C (restrictive temperature, i.e. Rad3 inactive) (**Figure 4.8A**). Decreased growth rates of any of the *pol3* mutant strains possessing a *rad3ts* allele on YES at 36°C suggests that the cells require the checkpoint to be activated in order to survive.

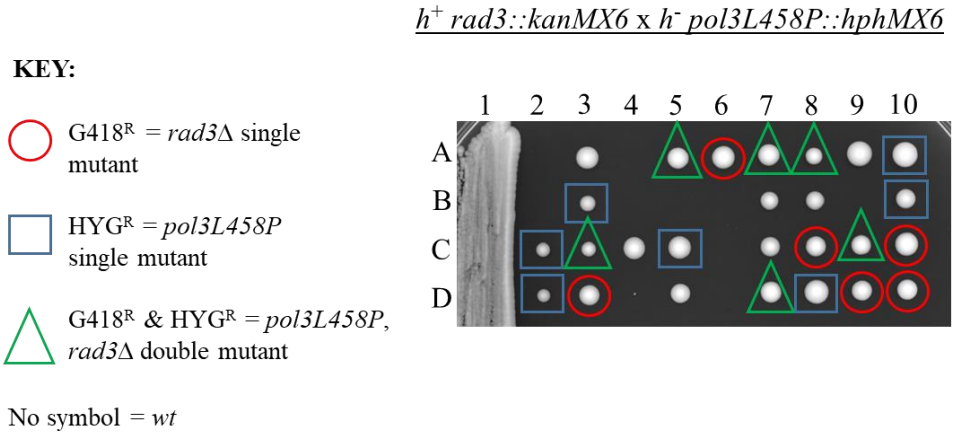
At the restrictive temperature, the *pol3P311L* and *pol3G305S, rad3ts* double mutants were much less viable compared to the *rad3ts* control strain (**Figure 4.8A**). Therefore, the fission yeast mutants equivalent to the human germline *POLD1* P327L and *POLD1* G321S variants, located in conserved regions of the exonuclease domain (other than the exonuclease catalytic site), are synthetically sick upon inactivation of Rad3, a key sensor and initiator of the checkpoint signalling cascade. This further implies that Rad3 is partially activated, indicating that DNA damage or stress has occurred, and is vital for the viability of cells expressing the *pol3P311L* or *G305S* mutations. The results from **Figure 4.7D** support the previous statement: the mean cell length of *pol3P311L* ($p < 0.05$) and *G305S* ($p < 0.0001$) cells are significantly longer than Wt cells under normal conditions (i.e. – HU), and this is particularly true for cells expressing *pol3G305S*. Conversely, the exonuclease-dead *pol3* variants (*pol3D386A* and *pol3D300N*, ex *rad3ts*), expressing mutations in the exonuclease active site, are not synthetically lethal with *rad3* inactivation (**Figure 4.8A**). *Pol3L458P* also appears to be sick when Rad3 function is impaired, however, this is discussed in more detail in the forthcoming section.

Figure 4.8

A.



B.



C.

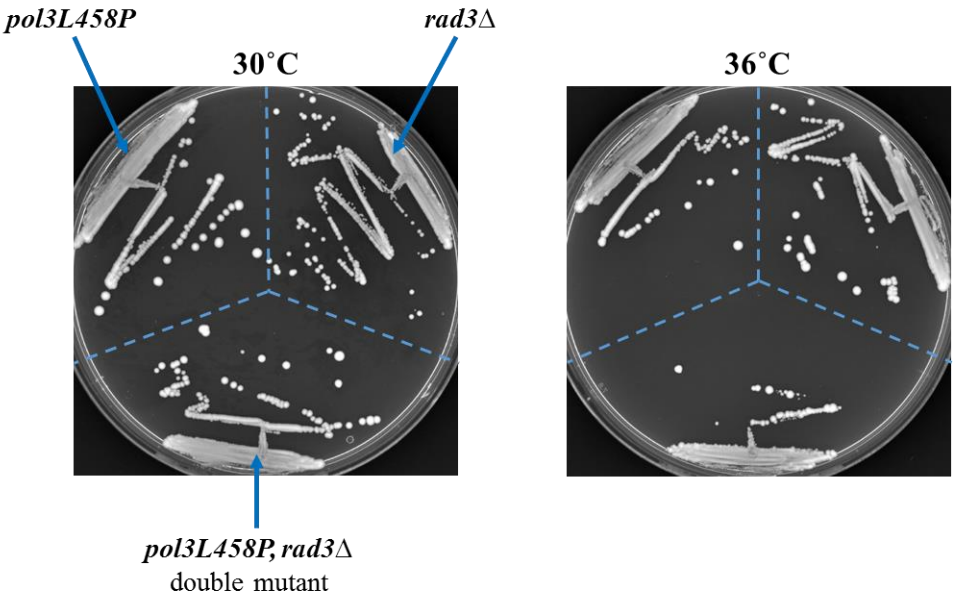


Figure 4.8: The *pol3P311L* and *pol3G305S* mutations are synthetically sick upon *rad3* inactivation. The *pol3L458P* strain is temperature-sensitive (ts). (A) Spot tests of *pol3* EDMs ex *rad3ts* on YE3S at 26°C (permissive temperature, i.e. fully Rad3 active), 30°C (semi-permissive temperature, i.e. partially Rad3 active) and 36°C (restrictive temperature, i.e. Rad3 inactive). The strains spotted were 2839, 3292, 3416, 3957, 3958 and 3959. **(B)** *Pol3L458P* is not synthetically lethal/sick with *rad3*Δ at 30°C. Tetrad dissection of a cross grown at 30˚C between *rad3*Δ (Strain U2-54-D-08 from the Bioneer deletion library), marked with G418 resistance ($G418^R$), and *pol3L458P* (Strain #3982), marked with hygromycin resistance (Hyg^R). For each ascus, four tetrads/spores are positioned individually in a column from 2A-D, 3A-D, 4A-D, etc. Single colonies that were replica-plated and grew on both G418-and HYG-plates are double mutants (marked by a green triangle). Note that not all four tetrads per ascus successfully germinate and grow. **(C)** The parental and double mutant strains from (B) were single colony-streaked on YES at 30˚C and 36˚C, separately. Note that the strains labelled at 30˚C are exactly the same at 36˚C. The double mutant strain used was 3985.

4.2.3.3 The synthetic interaction between pol3L458P and rad3 genes

It appeared that the *pol3L458P* EDM had an increased dependence on *rad3* activation for viability (**Figure 4.8A**), however, it has been shown that this variant is slightly temperature-sensitive (ts) in **Figure 3.15** (at 36˚C). Hence, in order to address whether the synthetic lethality observed is largely due to the dependence of the *pol3L458P* cells on *rad3* activation for survival, or whether it is largely due to the ts nature of the *pol3L458P* cells, tetrad dissection was conducted on a mating cross between *pol3L458P* and *rad3*Δ strains at 30˚C (**Figure 4.8B**).

*4.2.3.3.1 Construction of pol3L458P, rad3*Δ *double mutant strains*

Since the h^+ *rad3*Δ strain was from the haploid Bioneer deletion library (U2-54-D-08 – **Table 2.1**), hence marked with the kanMX6 cassette (conferring $G418^R$), the kanMX6 marker of the original *pol3L458P* strain constructed in Chapter 3 had to be replaced with another antibiotic resistance marker, such as the hphMX6 cassette (conferring Hyg^R), in order to select for the double mutants. Firstly, in furtherance of the replacement of the kanMX6 with the hphMX6 cassette, the *pFA6a-hphMX6* plasmid (p116 – **Table 2.3**) had to have its hygromycin cassette amplified via colony PCR using the primer pair, 512 and 513 (**Table 2.2**) (refer to **Chapter 2.2.1**). The final PCR fragment (1.7 kbp) was purified and, subsequently, transformed into the h^- *pol3L458P::kanMX6* strain (3943 – **Table 2.1**) to replace the kanMX6 cassette with the hphMX6 cassette via HR. Successful yeast transformants were selected for growth on HYG-containing plates and were confirmed for G418 sensitivity ($G418^S$). This formed the strain, h^- *pol3L458P::hphMX6* (3982 – **Table 2.1**), making it easier to identify 2:2 segregation of parental alleles via tetrad dissection when crossed with the h^+ *rad3::kanMX6* Bioneer strain.

*4.2.3.3.2 Pol3L458P is not synthetically sick/lethal with rad3*Δ

The *pol3L458P::hphMX6* strain was crossed with *rad3*Δ strain at 30˚C, and the tetrads from asci were separated onto YE6S via tetrad dissection and, subsequently, grown at 30˚C for 4 days (**Figure 4.8B**). Tetrad dissection is a remarkable tool in yeast genetics that permits the analysis of products of a single meiosis. A few tetrads can help analyse linkage, distinguish novel phenotypes associated with double mutants, or assess specific meiotic defects (Escorcia and Forsburg, 2018). For the purposes of this experiment, tetrad dissection clearly defines whether a certain mutated/deleted gene is synthetically lethal/sick with the deletion or inactivation of another gene, based on tetrad colony size: i.e. double mutants display relatively small tetrad colony sizes or no colony growth, signifying synthetic sickness or lethality, respectively, for the two independent alleles. Additionally, tetrad dissection can assess synthetic rescue, i.e. when a deleted gene rescues the phenotype of another mutated/deleted gene, defined by relatively larger tetrad colonies in size. The tetrad plates were replica plated onto separate YE6S + G418 and YE6S + HYG plates to select for single and double mutants, defined in **Figure 4.8B**. The experiment revealed that the *pol3L458P, rad3*Δ double mutant grows similarly to either of the parental strains, thus there is no synthetic interaction between *pol3L458P* and *rad3*Δ at 30°C. This suggests that the synthetic lethality observed at 36°C in **Figure 4.8A** is predominantly due to the *pol3L458P* variant's temperature sensitivity, which is magnified by *rad3* inactivation.

To determine whether the synthetic lethality observed at 36°C was mainly due to the ts nature of the *pol3L458P* single mutation (**Figure 3.15**) or due to some genetic interaction between *pol3L458P* and *rad3*Δ, the parental and double mutant strains were single-colony streaked on at least two separate YE6S plates and incubated at 30˚C and 36˚C for 3-4 days, respectively (**Figure 4.8C**). The single and double mutant strains grew normally at 30˚C, as depicted by the

healthy growth of approximately the same number and same sized colonies. However, the growth of the *pol3L458P* parental strain was slightly compromised at 36˚C compared to the alternative parental strain, *rad3*Δ, reflecting the innate temperature sensitivity (ts) of the *pol3L458P* mutation (**Figure 4.8C**). As predicted, the single colonies of the *pol3L458P, rad3*Δ double mutant strain were generally less than and smaller than either of the colonies of the single mutant strains, confirming that cells with both mutations grew poorly at 36˚C. By looking at the sparsity and relatively smaller sized colonies expressing the double mutation, this insinuates the development of suppressor mutations (Williams et al., 2013). Presumably, the ts nature of *pol3L458P* makes it more *rad3* dependent at 36˚C. Moreover, it could be possible that the ts nature of the *pol3L458P* mutation in yeast is a reflection of the pathogenic nature of the equivalent mutation (*POLD1* L474P) in human CRCs. The mutation may alter the structure of the Pol δ holoenzyme, affecting its overall function, or it may just alter the conformation of both the exonuclease and polymerase active sites (N-terminal domain), compromising these activities.

4.2.4 The viability of the *pol3G305S* mutant is compromised in hydroxyurea-induced replicative stress

Hydroxyurea (HU) sensitivity of the *pol3* variants was determined in terms of relative viability, as previously described in: Al-khodairy and Carr, (1992); Enoch et al., (1992); Lieberman, (1995); Stewart et al., (1997). The method has been described in detail in **Figure 4.9**. Briefly, wild-type, *rad3*Δ, and *pol3P311L*, *G305S*, *L458P* and *D386A* cells, were cultured to mid-logarithmic phase at 30°C and hydroxyurea added to 12 mM at time-point (t)=0, and 12 mM HU was re-added at t=1 (i.e. at 3 hours). Hydroxyurea was re-added after 3 hours of incubation because previous studies have shown that HU only blocks cell division temporarily in *S. pombe* and, thus, the drug's potency may reduce over a shorter period (i.e. under 6 hours of HU treatment) at warm temperature, e.g. 30°C (Sazer and Nurse, 1994). The fraction of the

population surviving was determined at the indicated times (0, 3, 6 and 9 hours) after HU addition, using a colony formation assay, as previously described in Lieberman (1995) and schematically detailed in **Figure 4.9**.

It was shown that the viability of the *pol3P311L*, *L458P* and *D386A* (exonuclease-dead) cells was not reduced by HU compared to the wild type (**Figure 4.10**). The observation was not expected for *pol3P311L* (**Figure 4.10B**), since it displayed inefficient checkpoint arrest and defective chromosome segregation to DNA synthesis inhibition, (**Figures 4.7B** & **C**) and conferred HU sensitivity on plates (**Figure 3.16**). Therefore, this means that even though 10% of *pol3P311L* cells undergo aberrant mitosis after 6 hours in HU at 30°C, this does not greatly affect the strain's viability to short HU treatments (i.e. up to 9 hours). The results might differ when the cells experience prolonged HU exposure, for example, up to 24 hours' treatment. The *pol3L458P* and *D386A* variants followed almost exactly the same viability trend as wild type (**Figures 4.10D** & **E**) which was not unexpected since they did not show a phenotype on HU-containing plates (**Figure 3.17**). Since the germline *pol3D300N* variant behaved similarly to the non-clinical exonuclease devoid, *pol3D386A*, variant in previous assays and they both affect key amino acids in the exonuclease active site, the *pol3D300N* mutant was not included in this experiment. It is predicted that it would follow the same viability pattern as *pol3D386A*.

On the other hand, the *pol3G305S* mutant cells had the same viability as Wt cells up to 3 hours' treatment in HU, however, after 3 hours the viability of *pol3G305S* cells began to decrease gradually (**Figure 4.10C**). This was in contrast to the trend seen with Wt and the other *pol3* variant strains: the relative viability continued to increase slowly between 3 and 6 hours, and only after 6 hours in HU did it then begin to decline. Therefore, overall, it appears that the *pol3G305S* mutant has a moderately reduced viability in HU compared to the Wt and alternative *pol3* mutant strains, albeit not as drastically attenuated as the viability of the checkpoint

defective mutant, *rad3*Δ (positive control). *Rad3*Δ is classed as an *'early cut'* mutant because a significant level of *'cut'* formation can be detected at 4 hours' incubation in HU and this greatly disrupts checkpoint control and affects the recovery function of the cells post DNA replication block (Enoch et al., 1992). It is also much less viable in HU compared to *pol3G305S* cells, as seen in **Figure 4.10A**, and it has been well documented that *'early cut'* mutant cells lose viability to a significant extent upon DNA synthesis inhibition (Enoch et al., 1992). The higher viability of the *pol3G305S* culture, in comparison to *rad3*Δ, is the result of a more efficient checkpoint as the cells do not enter mitosis, judged by few mitotic abnormalities, and they are significantly longer than Wt cells +/-HU (**Figure 4.7**). In turn, this might explain its reduced viability compared to Wt cells in HU; perhaps prolonged activation of the checkpoint in *pol3G305S* cells makes them unable to recover from the S phase block.

4.2.5 *Pol3G305S* recovers more slowly after S phase arrest compared to wild type

In order to assess the resumption of cell cycle progression post cell cycle arrest in the *pol3* EDMs, cells were blocked in early S phase by incubation with 24 mM hydroxyurea (HU) for 4 hours and released into the cell cycle by removal of HU and suspension in fresh medium. A high concentration of HU was used to arrest the cells because it has been shown previously in the laboratory, through survival rate assays, that most cells (particularly wild-type) still progress through the cell cycle and divide during the first 2 hours in 10 mM HU (Pai, 2009); presumably because of a decline in the efficacy of HU overtime in liquid media at a relatively high temperature (30ºC). It has also been shown that mammalian cells proceed through S phase synchronously after a few hours of HU treatment followed by HU removal from the medium (Sinclair, 1965). Samples were extracted and analysed for DNA content at 10 minute intervals for up to 1 hour after release from the 4-hour cell-cycle block induced by HU. Fluorescence-activated single cell sorting (FACS) analysis at each time-point shows the progress of bulk

DNA synthesis (**Figure 4.11**). In addition, a sample of asynchronous cells was analysed by FACS before the addition of HU for each culture to provide a '2C' control: 2C-DNA content in asynchronous cells means that the cells are predominantly in G2 (Knutsen et al., 2011). Similarly, a sample was collected just before the removal of HU, for each culture, and analysed via FACS to reveal 1C-DNA content profile: HU arrests the cells in early S phase so the frequency of cells with a 1C-DNA content increases relative to that of cells with 2C-DNA content (Carlson et al., 1997). Cells that have just undertaken DNA replication increase their DNA content profile from 2C- to 4C-DNA before dividing (Carlson et al., 1997), which can be seen after 60 minutes' release from the HU block for all the cultures (**Figure 4.11**).

The *pol3* variants *P311L*, *L458P*, *D300N* and *D386A* resumed the cell cycle and DNA replication similarly to Wt, after release from the S phase block (**Figure 4.11**); by 10-20 minutes after release, cell cycle progression was back to normal, indicating that these strains maintained high viability after release from HU. This was expected since all of the prior mutants did not have compromised viability in liquid HU (**Figure 4.10**). On the other hand,10-20 minutes after the removal of HU, *pol3G305S* cells had not returned to 2C-DNA content, unlike the Wt cells, meaning that *pol3G305S* has a slower S phase recovery after HU-induced cell cycle block and release. This observation coincides with the result from **Figure 4.10C**: increased death of *pol3G305S* cells in HU compared to the Wt and other *pol3* mutant strains. In other words, if the *pol3G305S* cells are slowly dying in HU then this means they are not being released efficiently from the HU-induced cell cycle block. This could be due to the increased replication fork stalling and collapse that occurs as a result of HU exposure.

Figure 4.9

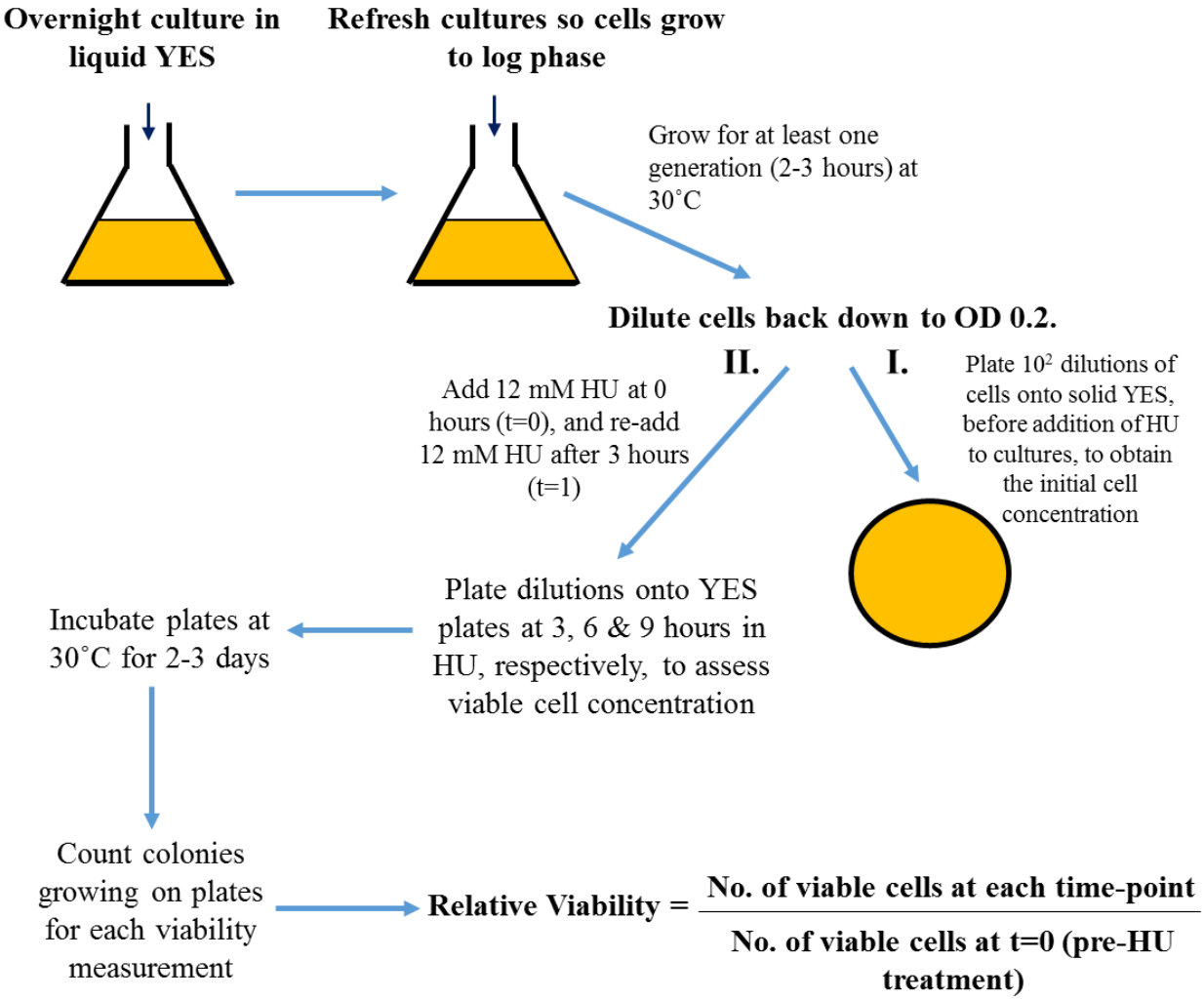


Figure 4.9: Schematic: Step-by-step flow chart of the relative viability assay method. The viability of Wt, *rad3*Δ and the *pol3* variants was assayed by colony formation at times before and after the addition of 12 mM HU to the cultures (**I** and **II**). 12 mM HU was re-added after 3 hours (final concentration 24 mM). The relative viability was calculated by dividing the number of viable cells at each time-point (**II**) by the number of viable cells before addition of HU to the culture (**I**).

Figure 4.10

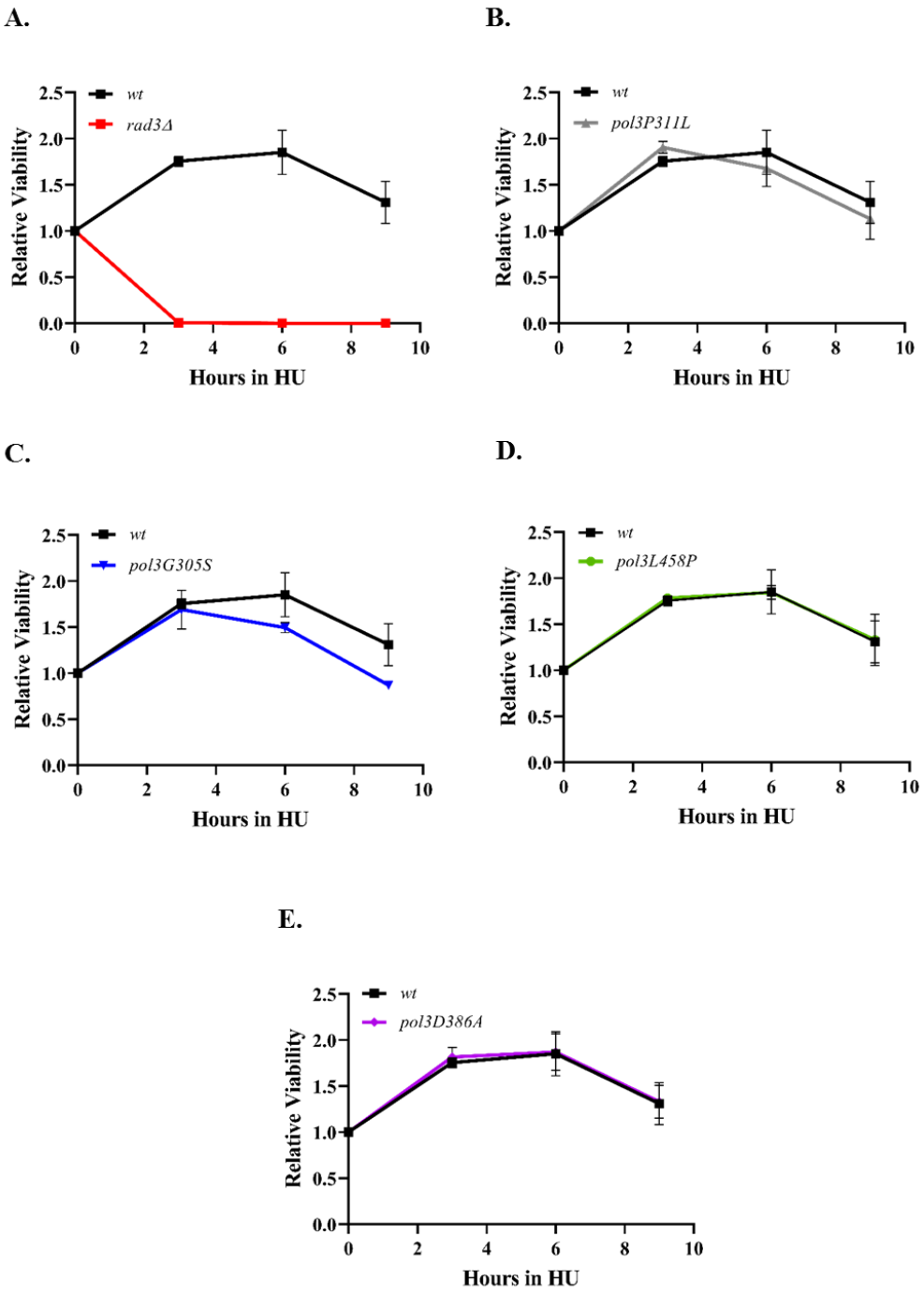


Figure 4.10: The viability of *pol3G305S* is compromised in HU. The relative viability of Wt (3500), **(A)** *rad3*Δ (1617), **(B)** *pol3P311L* (3354), **(C)** *pol3G305S* (3941), **(D)** *pol3L458P* (3943) and **(E)** *pol3D386A* (3273) cells was assayed at the indicated times before and after the addition of 12-24 mM HU, as described in **Figure 4.9**. Note that strain numbers are shown in brackets next to the aforementioned genotypes. The number of colonies growing on two plates was counted for each viability measurement and each number was expressed as a proportion of the number of viable cells for each cell type at the start of the experiment. In most cases, the starting measurement corresponded to an average of 400 cells. *Rad3*Δ cells are inviable in HU (positive control) **(A)**. Data are shown as the mean ±SEM (n=3).

Figure 4.11

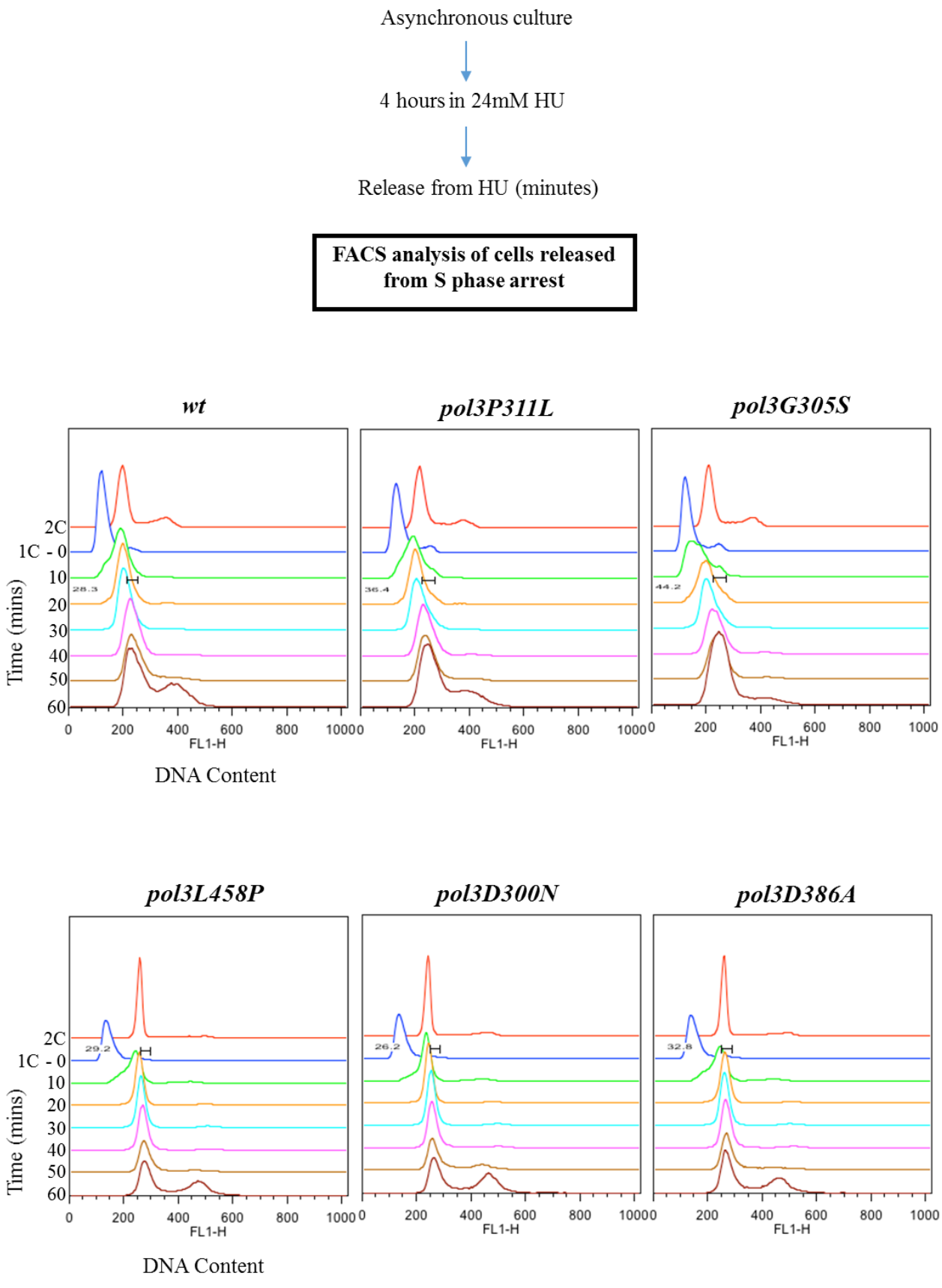

Asynchronous culture
4 hours in 24mM HU
Release from HU (minutes)
FACS analysis of cells released from S phase arrest
wt
pol3P311L
pol3G305S
Time (mins)
2C
1C - 0
10
20
30
40
50
60
28.3
36.4
44.2
0
200
400
600
800
1000
FL1-H
DNA Content
pol3L458P
pol3D300N
pol3D386A
29.2
26.2
32.8
DNA Content

Figure 4.11: FACS analysis of cells released from S phase arrest, induced by the addition of HU: *pol3G305S* has a relatively slower recovery from cell cycle block and release. 12mM HU was added to asynchronous cultures of Wt (3500), *pol3P311L* (3354), *pol3G305S* (3941), *pol3L458P* (3943), *pol3D300N* (3945) and *pol3D386A* (3273) cells growing in rich medium (YES). 12mM HU was re-added after 2 hours of cell cycle arrest (final concentration 24mM). After 4 hours in HU, the cells were washed with sterile water and transferred to rich medium without HU to grow for up to 1 hour. Samples were removed and fixed in 70% ethanol at 10 min intervals (for up to 60 minutes) after removal of HU. The ethanol-fixed cells were stained with sytox green for analysis of DNA content by FACS. Note that asynchronous cultures of fission yeast have a predominantly 2C DNA content, and cells blocked in G1/S by HU have a typical 1C DNA content peak. Strain numbers are shown in brackets next to the yeast genotypes, above.

4.2.6 The effect of Mus81 on replication fork stability in the *pol3* mutants

Pol3G305S cells exhibit S phase recovery problems after arrest, possibly due to replication-stress-induced stalled and deactivated replication forks. This may be alleviated by eliminating the endonuclease, Mus81, from the cells for the reasons given at the beginning of this chapter, in **Chapter 4.1**. The function of Mus81 in eukaryotic cells is described in **Chapter 4.1.3**.

In this study, *pol3, mus81*Δ double mutant strains were created via tetrad dissection to analyse the progeny and assess any synthetic interactions between the various *pol3* mutations and *mus81*. Subsequently, these strains were spot-diluted onto YES plates containing 2 mM HU to see if the HU sensitivity of the *pol3G305S* variant, and possibly the *pol3P311L* variant, is rescued by deleting *mus81*. The model being that the aforementioned *pol3* variants, particularly *pol3G305S*, progress through S phase slowly and even more slowly when a replication inhibitor, such as HU, is applied (as shown in **Figures 4.10** & **4.11**). HU increases replication fork stalling and, after prolonged exposure, induces fork collapse (see model in Figure 4.15) (reviewed in Singh and Xu, 2016; Petermann and Helleday, 2010). Since replication fork collapse leads to DSB formation, which can be more damaging to the cells (as outlined in **Chapter 4.1.3**), by removing Mus81, it may prevent the inappropriate cleavage of stalled replication forks and promote more fork restart in a non-recombinogenic way; thus, easing S phase progression of the *pol3* mutants.

*4.2.6.1 Construction of pol3, mus81*Δ *double mutant strains*

The *S. pombe* equivalent polymerase mutants constructed in **Chapter 3.2.1** are all marked by G418 resistance ($G418^R$). The original *mus81*Δ strain in the lab is also marked by $G418^R$ (TH 1483 – **Table 2.1**). To cross these two strains together to form double mutants, they both have to be marked with different antibiotic resistance markers and be of opposite mating types.

Therefore, the kanMX6 marker gene of *mus81* was swapped with the hphMX6 marker gene, via colony PCR amplification of the *pFa6a-hphMX6* plasmid, followed by yeast transformation, as described in **Chapter 4.2.3.3.1**. Successful transformants were selected for growth on HYG-containing plates and were confirmed for G418 sensitivity ($G418^S$). This formed the strain, h^+ *mus81::hphMX6* (3972 – **Table 2.1**). This strain was then crossed separately with h^- *pol3P311L*, *G305S*, *L458P*, *D300N* and *D386A* strains (which are all $G418^R$) and, subsequently, the double mutants were obtained via tetrad dissection after selection for growth on YES plates containing HYG and G418. The following *pol3, mus81*Δ double mutant strains were made and are recorded in **Table 2.1**: 3973-3976.

4.2.6.2 The exonuclease active site variants, pol3D300N and pol3D386A, are synthetically sick upon the deletion of the mus81 gene

Pictures of the tetrad dissected plates were taken and, consequently, replica-plated onto YES plates containing either HYG or G418 200 μg/ml in order to characterise the genotype of the tetrad colonies as follows: Wt (no antibiotic resistance marker), *pol3* single mutant ($G418^R$, Hyg^S), *mus81*Δ single mutant (Hyg^R, $G418^S$) and *pol3, mus81*Δ double mutant ($G418^R$ and Hyg^R) (**Figure 4.12A**). The size of the double mutant tetrad colonies is a clear indication of the type synthetic interaction that is occurring: the smaller the colony means that the genes in question depend on one another to function for cell survival. If the double mutant does not grow at all then this means that 'Gene X' is synthetically lethal with 'Gene Y'. Alternatively, if the size of the double mutant colonies is bigger than either of the parental strains then this suggests that 'Gene X' synthetically rescues the phenotype or growth defect of 'Gene Y'.

All of the *pol3, mus81*Δ double mutants exhibited significantly reduced growth compared to the *pol3* single mutant strains (**Figure 4.12**). Moreover, the tetrad dissected plates showed that the *pol3D300N/pol3D386A, mus81*Δ double mutant colonies appeared modestly sicker than either of the parental strains (**Figure 4.12A IV** & **V**). It was difficult to decipher by eye whether

the *pol3P311L/G305S/L458P, mus81*Δ double mutant colonies were less viable than the *mus81*Δ single mutant colonies. To determine this, the diameters of the colonies in each cross were arbitrarily but relatively measured using the same scale in ImageJ, and the average diameters were plotted in **Figure 4.12B**. On all the graphs, there was no difference in the size of the tetrad colonies between the wild type and *pol3* single mutant strains. The *mus81*Δ single mutant colonies consistently had an average diameter of approximately 0.3 cm which was significantly less than that of Wt (**Figure 4.12B: I** – **V**). This means that the *mus81*Δ strain struggles to grow and divide. The EDMs that are located in the exonuclease active site of Pol3, such as *pol3D300N* (a clinical mutation) and *pol3D386A* (non-clinical mutation – positive control), when combined with *mus81*Δ to make the double mutant, showed a significantly reduced tetrad colony size in comparison to the *mus81*Δ single mutant (**Figure 4.12B: IV** & **V**). This suggests that *pol3* mutations that are within the exonuclease active site exacerbate the phenotype of *mus81*Δ and vice versa.

Conversely, the *pol3P311L/G305S/L458P, mus81*Δ double mutant colonies did not display a difference in colony size compared to the *mus81*Δ single mutant colonies ($p > 0.05$, **Figure 4.12B: I, II** & **III**). Additionally, these EDMs are situated in conserved exo motifs of Pol3, not including the exonuclease catalytic site.

In conclusion, most of the EDM variants do not have a negative interaction with *mus81*Δ with the exception of *pol3D300N* and *D386A*. Hence, this observation may depend on the location of these mutations along the exonuclease domain.

4.2.6.3 The growth of the pol3, mus81Δ double mutant strains is further attenuated by HU compared to mus81Δ

In **Figure 4.12**, the effect of *mus81Δ* on the *pol3* exonuclease domain mutations (EDMs) was very subtle in terms of synergy, probably due to the fact that *mus81Δ* itself has poor cell growth

(Dovey et al., 2009; Fadden et al., 2013; Sanyal et al., 2018). Since *mus81Δ* in *S. pombe* has been shown to cause hyper-sensitivity to HU and other genotoxins (Yokoyama et al., 2007; Dovey et al., 2009; Fadden et al., 2013), the HU effects on *pol3, mus81Δ* double mutants were examined to see if they were more sensitive than the respective single mutants.

In response to the above, spot assays were carried out: exponentially growing cell cultures were serially diluted four-fold and aliquots of each dilution were spotted onto YE6S plates and YE6S plates containing 2 mM HU. The plates were incubated for 3-4 days at 30ºC or 36ºC and then photographed. Note that 2 mM of HU was used in solid media because *mus81Δ* cells did not grow in 5 mM and 7.5 mM HU (see **Appendix I**). **Figure 4.13** presents the spot assays comparing the HU sensitivity of Wt, *mus81Δ*, *pol3P311L*, *pol3G305S*, *pol3L458P* and *pol3D386A* single and double mutant strains. The *pol3D300N* single and double mutant strains were not included in the spot assay since the *pol3D300N* mutation, thus far, has behaved phenotypically similar to the *pol3D386A* mutation, as expected for two mutations that are situated in the Exo I catalytic motif of Pol δ. *Mus81Δ* grew more slowly than wild type (Wt) at both 30 and 36ºC in **Figure 4.13**, which has been observed in several past studies owing to its poor cell fitness (Yokoyama et al., 2007; Dovey et al., 2009; Fadden et al., 2013; Sanyal et al., 2018). The *pol3, mus81Δ* double mutant cells grew similarly to *mus81Δ* single mutant cells without HU, thus the slow growth affiliated with all these double mutant strains is largely due to the innate sick phenotype of *mus81Δ*. Bear in mind that the *pol3L458P, mus81Δ* strain barely grew at 36ºC because the *pol3L458P* mutation is slightly temperature-sensitive (ts), as previously shown in **Figure 3.15** and **Figure 4.8**. This is probably because the L458P mutant polymerase is more dependent on Mus81 for replication fork processing and restart at the restrictive temperature. Strikingly, all of the *pol3, mus81Δ* double mutants grew slightly worse than *mus81Δ* in the presence of 2 mM HU at 30ºC, in particular the *pol3P311L*/*G305S*/*L458P* and *mus81Δ* double mutations, while growth of the single *pol3* variants was hardly affected

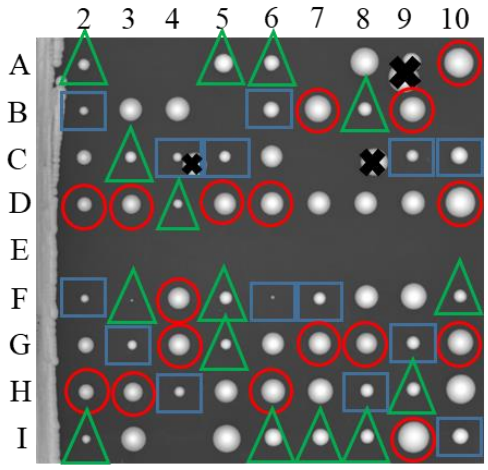
(**Figure 4.13**). This means that the *pol3* mutations have a mild additive effect to the *mus81Δ* hyper-sensitivity to HU. Secondly, at 36ºC, the two strains that clearly grew worse than the *mus81Δ* parental strain were *pol3G305S, mus81Δ* and *pol3L458P, mus81Δ* (**Figure 4.13**). The *pol3G305S, mus81Δ* double mutation was particularly sick at a higher temperature suggesting that Mus81 may help in the restarting of collapsed forks by promoting fork cleavage and recombination-mediated fork restart. This leads to the proposed model in **Figure 4.15:** *pol3G305S* has slower moving replication forks (due to increased replication fork stalling) that arrest more frequently when exposed to an environment of low dNTP levels resulting in fork collapse and recombination-mediated fork restart. The process relies heavily on efficient fork cleavage by Mus81 to convert terminally blocked or damaged forks into structures that are more amenable to homologous recombinational repair and break-induced replication (BIR) (Kai et al., 2005; Hanada et al., 2007). Finally, even though the *pol3D386A/D300N, mus81Δ* double mutant tetrads were significantly smaller (p-values) than the *mus81Δ* single mutant tetrads (**Figure 4.12**), the cell growth of the *pol3D386A, mus81Δ* strain was similar to *mus81Δ* at both temperatures +/- HU (**Figure 4.13**).

In conclusion, evidence from tetrad analysis and cell growth spot assays disproved the original hypothesis that eliminating Mus81 activity would prevent the replisome components from destabilising, thus forks would be more readily re-started via non-recombinational and non-mutagenic mechanisms. Consequently, the results confirm the requirement of Mus81 in the double-strand break repair (DSBR) of permanently deactivated forks in all genotypes studied, even wild type. Although the main caveat of this experiment was the HU hyper-sensitivity attributed to *mus81Δ* cells, the data illuminated the subtle changes that the *pol3* EDMs have on cells with deficient Mus81 function and the need to measure the fork movement rate of these mutant polymerases via DNA molecular combing.

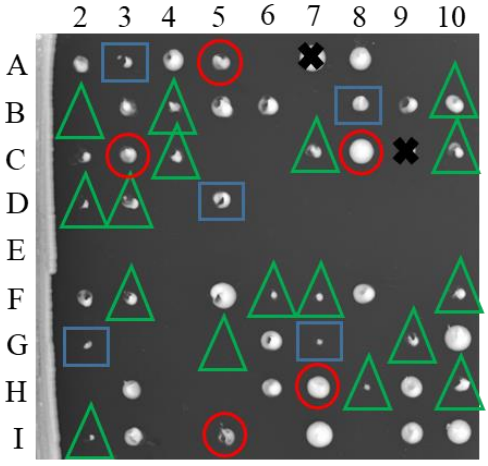
Figure 4.12

A.

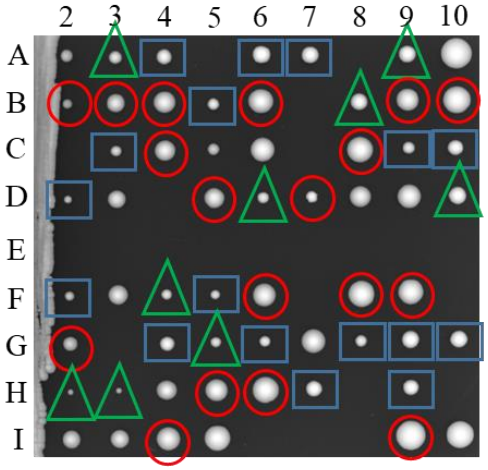
I. *pol3P311L* x *mus81*Δ



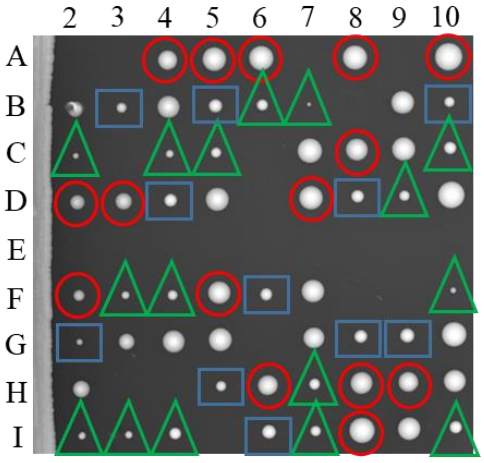
II. *pol3G305S* x *mus81*Δ



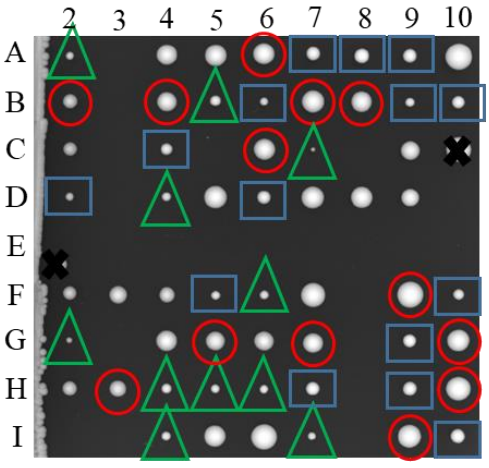
III. *pol3L458P* x *mus81*Δ



IV. *pol3D300N* x *mus81*Δ



V. *pol3D386A* x *mus81*Δ



KEY:

HYG^R - *mus81*Δ single mutant

G418^R - *pol3* single mutant

HYG^R & G418^R - *pol3, mus81*Δ double mutant

Ignore

No symbol = revertant *wt*

Figure 4.12

B.

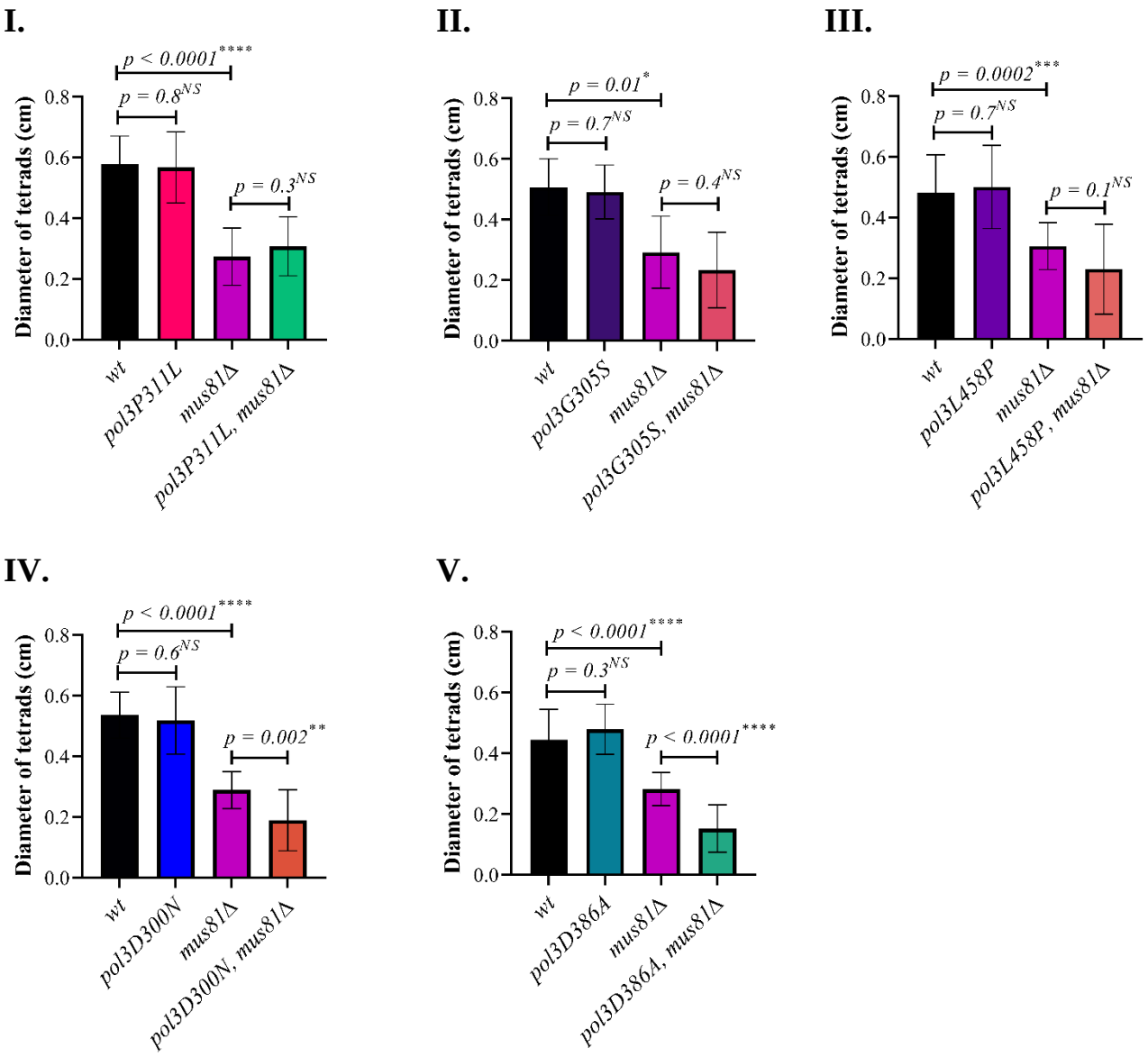


Figure 4.12: The *pol3D300N* and *pol3D386A* mutations are synthetically sick with *mus81*Δ. (A) Tetrad dissection of genetic crosses between *mus81Δ* (3972) and the *pol3* mutant strains *P311L* (3354), *G305S* (3941), *L458P* (3943), *D300N* (3945) and *D386A* (3273), respectively. Strain numbers are in brackets. Representative spores from four asci (not all tetrads successfully germinated) are shown for each cross (**I – V**). For each ascus, four tetrads/spores are positioned individually in a column from 2A-D, 3A-D, 2F-I, 3F-I, etc. Single colonies are replica-plated onto YES plates containing either HYG or G418 to select for single and double mutants, and scored accordingly (see key). Single mutants are either $G418^R$ or HYG^R, and double mutants are both $G418^R$ and HYG^R. Note that any unmarked tetrads are wild type as a result of the cross. Incorrectly positioned tetrads are marked with a black cross ('X'). **(B)** The diameters of the individual tetrad colonies were measured with a ruler relatively and uniformly using ImageJ. The mean diameters of the tetrads (in centimetres) were plotted for each *pol3* variant and *mus81*Δ mating cross, clearly outlined in **I – V**. Error bars represent SD. P-values were calculated using the two-tailed unpaired t test with Welch's correction: ^{NS} $p > 0.05$, * $p < 0.05$, ** $p < 0.01$, *** $p < 0.001$, and **** $p < 0.0001$. NS = Not Significant.

Figure 4.13

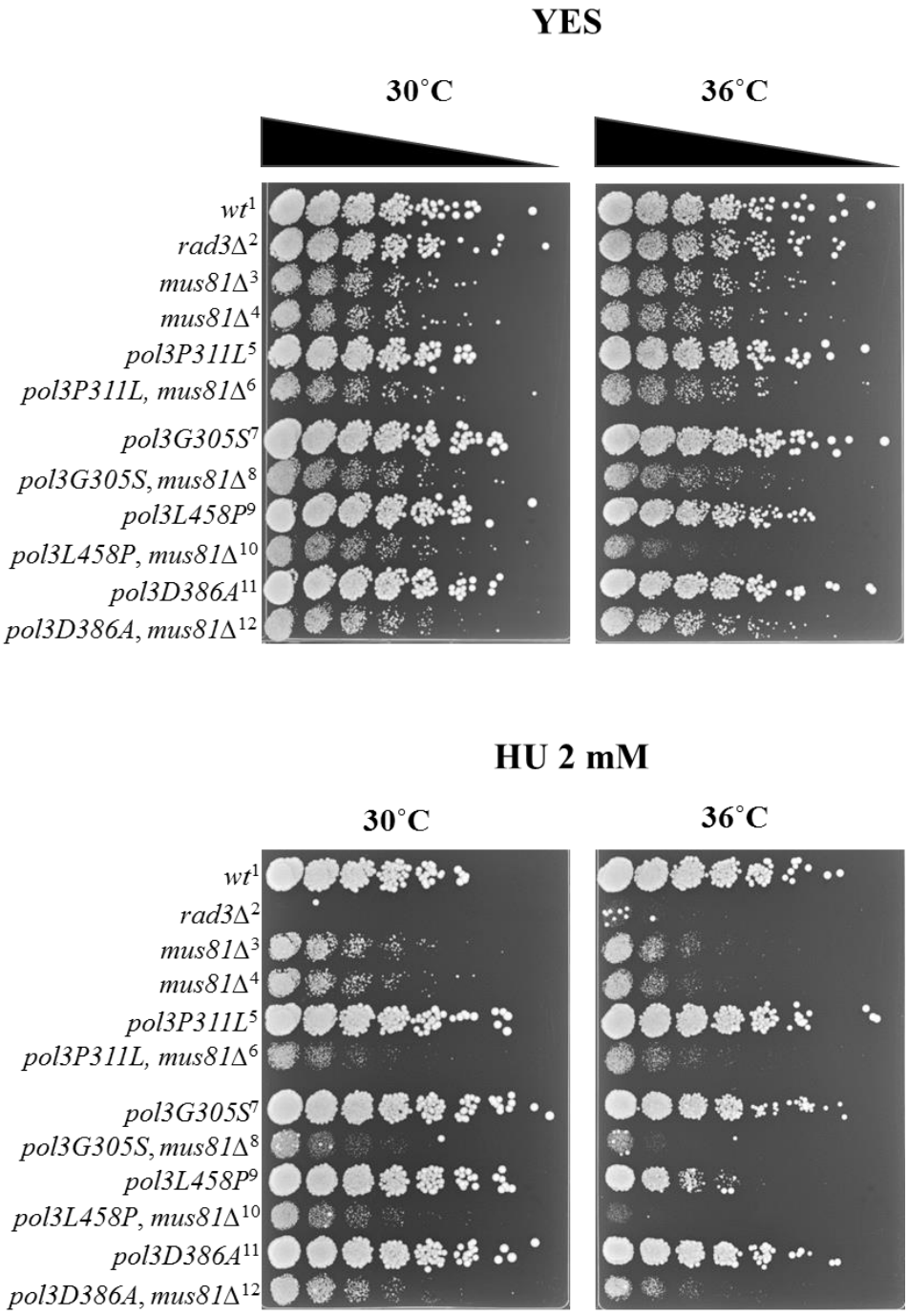


Figure 4.13: The *pol3, mus81*Δ double mutants grow modestly worse than *mus81*Δ in the presence of hydroxyurea. Four-fold serial spot-dilution of the *pol3* mutations and *mus81*Δ, single and double mutant strains on YE6S +/- HU 7.5 mM at 30˚C and 36˚C. 3500[1] and 1617[2] strains were negative and positive controls, respectively. The remaining strains utilised in this experiment were: TH 1483[3], 3972[4], 3354[5], 3973[6], 3941[7], 3974[8], 3943[9], 3975[10], 3273[11] and 3976[12]. Note that HU is incompatible for use in solid agar at 25˚C.

4.2.7 The implications of increased dNTP pools on exonuclease *pol3* variants

The *pol3P311L* and *G305S* variants are sensitive to HU, indicating that they have decreased cell fitness when the levels of dNTPs are reduced. Therefore, by increasing dNTP pools in these cells, this would theoretically rescue the HU-sensitive phenotype of the *pol3P311L* and *pol3G305S* mutants. To test this hypothesis, a cell growth spot assay +/- 7.5 mM HU was carried out on YE6S plates with the *pol3* and *cdc22-D57N* single and double mutant strains; *cdc22-D57N* has much higher dNTP levels than Wt due to the *D57N* mutation deactivating the allosteric negative feedback control of RNR (Chabes et al., 2003; Chabes and Stillman, 2007; Fleck et al., 2013).

4.2.7.1 Construction of pol3, cdc22-D57N double mutant strains

The first step was to cross the h^+ *cdc22-D57N* strain (3285) with the h^- *pol3P311L* (3354), *pol3G305S* (3941), *pol3L458P* (3943) and *pol3D386A* (3273) strains, respectively, on SPAS. It is important to add that the *pol3L458P* and *D386A* variants behaved as controls in the spot assay since these single *pol3* mutations were not sensitive to HU in the original spot assay (**Figure 3.17**). The spores of the *pol3* mutant genotypes were isolated using random spore analysis and selected for $G418^R$ (see **Chapter 2.1.2.1**). Since the *cdc22-D57N* strain does not have a selective marker attached to it, colony PCR using primers 989 and 997, and subsequent digestion of PCR products was carried out on several $G418^R$ single colonies isolated from each cross in order to identify the *cdc22-D57N* mutation. If the mutation was present, the PCR product (~ 0.8 kbp) was cleaved once by DdeI enzyme to produce two fragment sizes of 0.5 and 0.3 kbp on agarose gel. This created the following *pol3, cdc22-D57N* double mutant strains: 3977 – 3981 (**Table 2.1**).

4.2.7.2 Raised dNTP levels do not fully rescue the HU sensitivity phenotype of the low-mutator pol3 variants

Spot assays were conducted with the *pol3, cdc22-D57N* single and double mutant strains on YE6S agar +/- 7.5 mM HU, incubated at 30ºC and 36°C separately. All the *pol3, cdc22-D57N* double mutants grew comparably to wild type and to the two parental strains at both temperatures on YE6S, except for the *pol3L458P, cdc22-D57N* double mutant, which was clearly sicker than the slightly temperature-sensitive (ts) *pol3L458P* variant at 36ºC (**Figure 4.14**). In the presence of HU, the *pol3P311L* and *pol3G305S* mutants were sensitive confirming the results in **Figure 3.16**, and it appears that the *cdc22-D57N* mutation improved cell fitness but did not completely rescue the HU sensitivities of *pol3P311L* and *G305S* in the double mutants at both temperatures (**Figure 4.14**). This means that by elevating the dNTP pools in these variants by approximately 6-12 fold (Fleck et al., 2013), it partially rescues the HU sensitivity phenotypes.

Interestingly, the *pol3L458P, cdc22-D57N* double mutant strain was sick when exposed to HU at the semi-permissive temperature (30ºC), indicating that increased RNR activity, via inactivated allosteric feedback inhibition, and subsequent elevated dNTP levels, are potentially lethal to cells expressing *pol3L458P* under HU-induced replication stress. It has been shown in budding yeast that raised dNTP levels increase mutagenesis in cells with replication or repair defects (Datta et al., 2000; Davidson et al., 2012; Williams et al., 2015; Mertz et al., 2015), and compromise DNA replication fidelity (Chabes et al., 2003; Fleck et al., 2013). The contradiction here is that the *pol3L458P cdc22-D57N* double mutant strains grew relatively well under normal conditions at the permissive temperature. The double mutation was unsurprisingly sick at 36ºC because it has already been shown that *pol3L458P* is slightly ts. Thus, when the DNA damage checkpoint is impaired (see **Figure 4.8**), or nucleotide levels are altered (**Figure 4.14**), at the restrictive temperature, the replicative fitness of *pol3L458P* is significantly exacerbated.

Unexpectedly, the *cdc22-D57N* mutation alone is slightly HU-sensitive at 30ºC and 36ºC and this might be because HU has been shown to have an additional mode of action other than RNR inhibition (Davies et al., 2009; Singh and Xu, 2016).

Figure 4.14

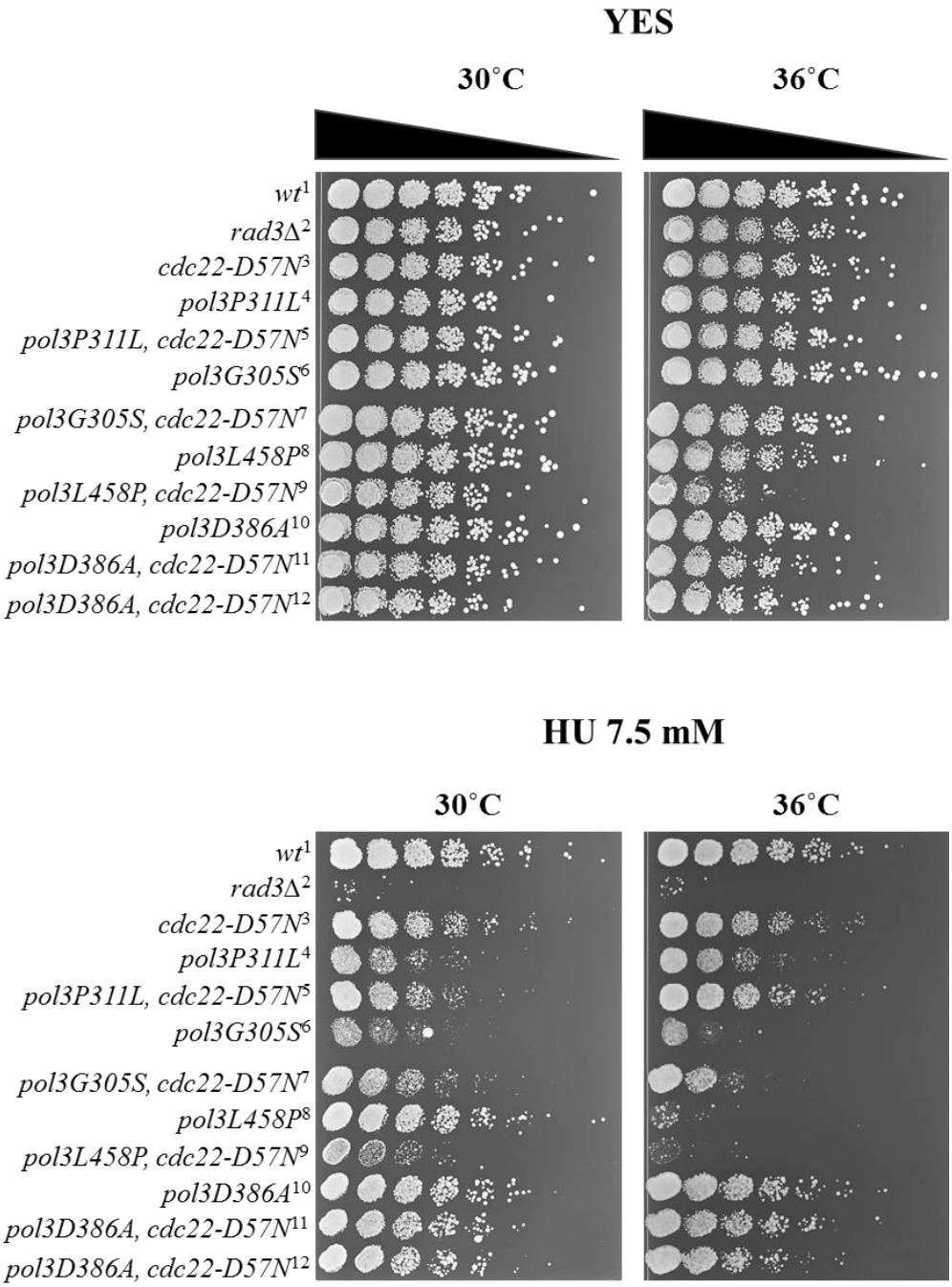


Figure 4.14: Increased RNR activity, followed by elevated dNTP pools, partially rescues the HU sensitivities of the *pol3P311L* and *pol3G305S* strains. Five-fold serial spot-dilution of the *pol3* mutations and *cdc22-D57N* single and double mutant strains on YE6S +/- HU 7.5 mM at 30˚C and 36˚C. 3500[1] and 1617[2] strains were negative and positive controls, respectively. The rest of the strains used in the assay were: 3285[3], 3354[4], 3977[5], 3941[6], 3978[7], 3943[8], 3979[9], 3273[10], 3980[11] and 3981[12].

4.3 DISCUSSION

4.3.1 Summary of key findings

In an attempt to explore and understand the mechanism behind the HU sensitivity phenotypes of the low-mutator *pol3* mutants, *P311L* and *G305S*, the main results acquired from Chapter 4 are:

- The *pol3* variants, *P311L* and *G305S*, are HU-sensitive but not due to reduced levels of endogenous Pol3. All the *pol3* exonuclease domain mutants (EDMs) in this study had normal levels of the Pol δ protein.
- *Pol3P311L* cells are sensitive to extended HU treatment because of displaying leaky checkpoint arrest and the aberrant *'cut'* cell phenotype, causing cellular lethality.
- *Pol3G305S* cells are sensitive to HU exposure and show defective recovery from HU arrest.
- Both *pol3P311L* and *G305S* mutants are Rad3-dependent for viability.
- The *pol3L458P*, *D300N* and *D386A* variants are not HU-sensitive and do not have a synthetic interaction with *rad3*.
- The *pol3L458P* mutant shows synthetic lethality in conjunction with *rad3* or *cdc22-D57N* mutations at the restrictive temperature.
- There is not a notable negative synthetic interaction between the various *pol3* mutations and *mus81*, perhaps reflecting the importance of Mus81 in replication fork restart.
- Increasing RNR activity and, hence, elevated dNTP production, partially rescues the HU sensitivity conferred by the *pol3P311L* and *pol3G305S* variants, respectively.
- Paradoxically, upregulated RNR activity is deleterious to the growth of *pol3L458P* cells under exogenous HU application.

4.3.2 The *pol3D300N* and *pol3D386A* exonuclease-null mutant strains are not sensitive to hydroxyurea-induced replicative stress and are not dependent upon Rad3 activation for viability in unperturbed DNA replication

Western analysis of the Pol3 protein demonstrated that all the mutant Pol3 proteins are expressed at levels comparable to wild-type Pol3 protein, and this is partly supported by a similar observation in human hTERT fibroblast cell lines expressing wild-type *POLD1* and *POLD1* D316H, respectively (Zhang et al., 2020). Note that *POLD1* D316H (Sp. *pol3D300H*) is a highly penetrant germline mutation affecting one of the catalytic carboxylates of the exonuclease domain that was found to be malignant in 4 of 4 carriers either presenting with colonic adenomas or polyps, or CRC. In addition, budding yeast fluctuation analysis revealed that the equivalent mutation has a strong mutator phenotype (Bellido et al., 2016; Murphy et al., 2006). It has been previously shown that reduction of the levels of Pol δ in yeast cells increased sensitivity to DNA-damaging agents and, additionally, depletion in the level of wild-type DNA polymerase resulted in a similar mutator phenotype to polymerase mutants (Kokoska et al., 2000). In this study, at least, it can be said that the hypermutator phenotype of the *pol3D300N* mutant is not due to altered physiological levels of the Pol3 protein.

In dissonance with the key findings in Zhang et al (2020), it was revealed in my work that the homologous *S. pombe* mutation to human *POLD1* D316H/N, *pol3D300N*, was not sensitive at all to the effects of HU. Additionally, the non-clinical exonuclease null mutant, *pol3D386A*, was not sensitive to the effects of replication inhibition. Since these *pol3* variants are highly mutagenic, this indicates that perhaps the effects of these exonuclease catalytic mutations escape checkpoint detection and activation (Chabes and Stillman, 2007). This is in accordance with a Pol ε proofreading-deficient mutation, *pol2-4*, in *S. cerevisiae* which shows no significant checkpoint activation and has the same dNTP concentrations as wild type, despite having a mutator phenotype (three-fold increase in mutation rate over Wt) (Williams et al.,

2015). On the contrary, reports in budding yeast have shown that the mutagenic phenotype of a Pol δ proofreading exonuclease-defective mutation, *pol3-01*, is dependent on the activation of the S phase checkpoint and the downstream phosphorylation of the Dun1 effector kinase (Datta et al., 2000; Herr et al., 2014). Dun1 plays a part in modulating dNTP pools by regulating negative regulators of ribonucleotide reductase (RNR) activity, assembly and transcription (Rouse and Jackson, 2002). Moreover, some polymerase mutants that are defective in base selectivity, rather than defective in exonuclease activity, generate mutagenesis in cells by checkpoint-dependent augmentation of intracellular dNTP pools (Mertz et al., 2015; Williams et al., 2015). This rise in nucleotide levels further accrued Pol ε/δ errors in the genome, creating a vicious cycle. However, there is no evidence that this situation applies to the *pol3D300N* and *pol3D386A* strains.

To recapitulate, the *pol3* exonuclease null mutants *D300N* and *D386A*, most likely increase mutation rates due to a lack of proofreading and appear to evade the checkpoint response despite their hypermutator phenotypes; taking into account that these mutant cells are viable upon checkpoint inactivation. The Rad3/ATR checkpoint pathway could still be activated in cells with replicative polymerases lacking exonuclease activity but, in this case, it is not essential for the cells' survival. Extensive exploration into the processes that coordinate mutagenesis in these variants is absolutely required. Alternatively, it is possible that misincorporation may not occur often enough within the cell population being analysed, complicating the detection of checkpoint activation during experiments (Sohl et al., 2015). It would be necessary to measure the dNTP levels and to detect activation of the checkpoint via Chk1/Cds1 phosphorylation in order to elucidate the mechanism of mutagenesis in these mutants; not only in yeast, but also in mice and human cell lines.

4.3.3 The *pol3P311L* and *pol3G305S* mutant strains are sensitive to hydroxyurea and require Rad3 for viability

Firstly, the HU sensitivity conferred by the *pol3P311L* and *pol3G305S* variant alleles was definitively not due to compromised levels of the Pol3 protein. Both *pol3* mutant cells are non-mutagenic under normal conditions, but they do not cope well during long periods of replication stress.

Though *pol3P311L* cells expressed HU sensitivity on solid media, they did not die readily in the presence of liquid YE3S containing up to 24 mM HU for 9 hours. Moreover, the *pol3P311L* mutant cells recovered similarly to wild type in response to S phase block and release, thus this implies that replication fork collapse does not occur in these cells. This might mean that any replication problems the *pol3P311L* cells are experiencing can be rectified if the cells are not exposed to the stress for prolonged periods. What was observed was a small, yet significant, fraction of *P311L* cells exhibiting faulty or weak checkpoint arrest, followed by detrimental mitotic effects, in response to replication stress. Initially, this did not affect cell growth too negatively based on the liquid viability assays, however, the increase in the number of *'cut'* cells probably accounts for the slow growth of pol3*P311L* seen on HU plates after multiple generations (i.e. five days of growth in incubation).

In this study, the exo-null *pol3D386A* mutant had an average 30 fold increase in mutation rate over wild type, yet it seems not to be Rad3 dependent for survival, whereas *pol3P311L* and *pol3G305S* mutants have a mutation rate similar to wild type and both require Rad3 for cell viability. One interpretation of this finding is that during unstressed conditions the *pol3P311L* and *G305S* variants may experience increased replication fork stalling (not replication fork collapse per se), which, in turn, activates the Rad3 checkpoint pathway in response to increased RPA on the lagging strand (see **Figure 4.15**). In order to activate the Rad3 checkpoint pathway

in response to various types of DNA damage (including DSBs and UV crosslinks) or replication stresses (e.g. fork stalling), it is believed that the length of ssDNA and chromatin-bound RPA are typically involved in initiating the checkpoint response (Zou and Elledge, 2003). RPA bound to ssDNA is generated by the uncoupling of replicative helicase and polymerases during replication fork stalling and this appears necessary for S phase checkpoint activation (Zou and Elledge, 2003; Byun et al., 2005). The removal of checkpoint proteins during replication stress results in fork collapse and chromosomal rearrangements (Friedel et al., 2009). Furthermore, mutations affecting yeast RPA cause checkpoint defects (Longhese et al., 1996; Kim and Brill, 2001). Therefore, I hypothesise that the *pol3P311L* and *G305S* mutant polymerases have a higher tendency to stall during DNA replication under normal conditions; this partially activates the replication checkpoint kinase, Cds1, through Rad3 activation in order to slow S phase progression and stabilise the stalled forks, so that DNA synthesis can resume once the stress is removed (**Figure 4.15**). In budding yeast, the Mec1/ATR pathway stabilises stalled forks by preventing dissociation of the replisome from the stalled fork (Cobb et al., 2003, 2005). There are a number of proteins required to prevent fork collapse upon HU-induced S phase arrest (reviewed in Paulsen and Cimprich, 2007). One would expect an increased number of *'cut'* cells in the *pol3P311L* or *G305S* and *rad3*Δ double mutants because of the dependency these *pol3* mutants have on Rad3 to survive.

In corroboration with the above results, it appears that *pol3P311L* might partially activate the S phase checkpoint under normal circumstances based on the cells being slightly longer than Wt. Similarly, *pol3G305S* showed synthetic sickness upon *rad3* inactivation and had significantly elongated cells during unperturbed DNA replication. Cells expressing *pol3G305S* gradually started dying during 9 hours of HU treatment and struggled to recover from temporary HU arrest, indicating that these cells experience replication fork collapse upon exogenous stress. Strikingly, these results demonstrate that once the checkpoint is fully

activated in response to exogenous replicative stress, e.g. HU, a proportion of *pol3G305S* cells die, possibly due to replication fork collapse and failure to restart (**Figure 4.15**). Thus, HU exacerbates the phenotype of *G305S* cells by further increasing fork stalling and collapse. Furthermore, the *pol3G305S* mutant did not display the typical *'cut'* phenotype after HU treatment meaning that cells were successfully blocked in S phase and prevented entry to mitosis. The *pol3P311L* strain exhibited leaky checkpoint arrest and mitotic abnormalities. Therefore, it seems that *pol3G305S* has a greater tendency to activate Rad3 at a larger extent or stronger affinity than *pol3P311L*. In support of this theory, it was shown in *Xenopus* egg extracts that the amount of ssDNA coated with RPA at replication forks directly correlated with the extent of Chk1 activation (Byun et al., 2005). RPA-ssDNA association is a common intermediate that activates ATR signalling in response to all types of genotoxic lesions (reviewed in Cortez, 2005). In fission yeast, the biochemical basis of this response could be the amount of Rad3-Rad26 and/or 9–1–1 loaded onto the RPA–ssDNA. Bearing all of this in mind, it appears that replication forks generally stall more, generating more ssDNA-RPA chromatin-bound complexes and a stronger checkpoint response, in *pol3G305S* cells than in *pol3P311L* cells, under physiological conditions. This phenotype was worsened, particularly for *pol3G305S*, when perturbed replication occurred (by adding HU) causing cell death, as previously described. It is likely that full checkpoint activation in *G305S* cells involves the participation of both the DNA damage checkpoint (Chk1) and the replication checkpoint effector proteins (Cds1), especially if there is more fork collapse and the formation of DSBs. On the other hand, *pol3P311L* shows some evidence for loss of viability on 7.5 mM HU-containing plates but it is not a big effect: the increase in *P311L 'cuts'* in HU is not consistent with little loss of viability after 9 hours' treatment with high concentration HU. To summarise, it is believed that the *P311L* cells have attenuated growth after chronic exposure to HU because checkpoint activation and cell cycle arrest are not fully maintained, leading to aberrant mitosis.

Figure 4.15

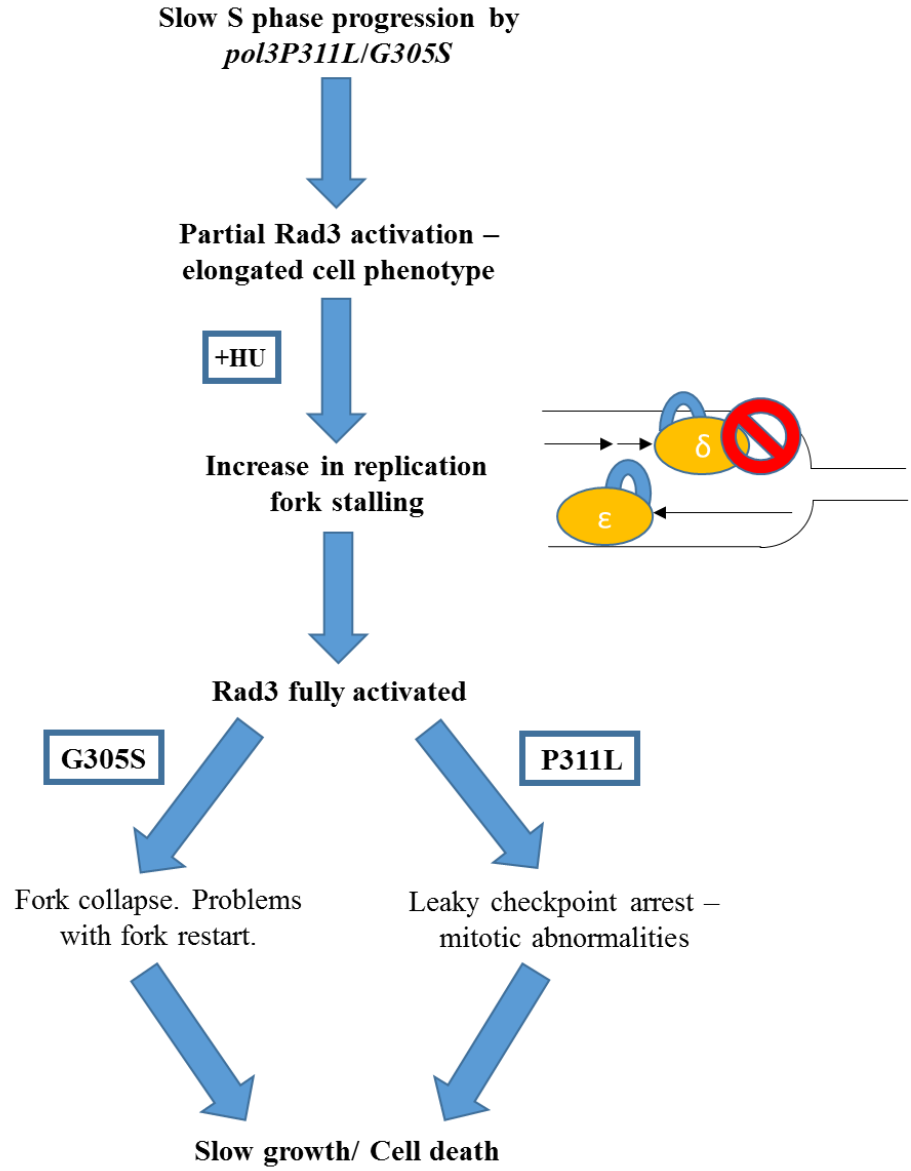


Figure 4.15: A proposed model to explain the HU sensitivities of the *pol3P311L* and *G305S* EDMs. The *pol3P311L/G305S* mutations cause inherently slow S phase progression due to replication fork stalling. Extended ssDNA coated with RPA is generated by the uncoupling of the MCM helicase and polymerase at replisomes during replication fork stalling. RPA-ssDNA triggers the activity of the replication checkpoint protein, Cds1, via Rad3 partial activation, thus leading to stabilisation of replisomes and preventing replisome dissociation from stalled forks, as well as premature entry to mitosis. DNA replication can recover from replication stalling when replication stresses are resolved. Upon HU application, depletion of dNTP pools causes increased fork stalling in both mutants, followed by an accumulation of RPA deposition on elongated ssDNA. This then leads to full activation of the Rad3 checkpoint-mediated response and, presumably, subsequent phosphorylation of the replication (Cds1) and/or DNA damage (Chk1) checkpoint proteins. However, *pol3G305S* has the ability to activate Rad3 at a greater affinity or extent than *pol3P311L*. Exposure to HU in *pol3G305S* cells causes irreversible fork collapse and gradual cell death. Hydroxyurea (HU)-induced checkpoint arrest is not fully maintained in *pol3P311L* cells resulting in deleterious mitosis and attenuated growth. See text for further details.

Evidence supporting fork stalling in the *pol3P311L* and *G305S* variants under physiological conditions comes from the observation that the *mus81*Δ allele did not have a strong negative interaction with these *pol3* mutations in the absence of HU. This might signify that fork collapse is not taking place in *pol3P311L/G305S* mutant cells, only fork stalling. The drug spot assay, however, showed that the double *pol3P311L*/*G305S*, *mus81Δ* mutants are sicker than the single mutants in the presence of low HU. Since Mus81 is implicated in replication fork cleavage and restart (Pepe and West, 2014), this supports the notion that increased fork stalling and collapse is occurring in these strains, at least in the presence of HU. The fact that *pol3G305S* cells had the slowest recovery from HU arrest implies that there is a greater incidence of fork collapse in *polG305S* cells compared to *P311L* cells during perturbed DNA replication.

It is not known what exactly triggers cell death in *pol3G305S* versus *pol3P311L* cells, in HU. Moreover, I still do not know what exactly activates the Rad3 checkpoint protein in *pol3G305S* and *P311L* cells and why it is activated, at least partially, during unchallenged DNA replication. For future work, it would be important to confirm Rad3 activation in these mutants by assessing phosphorylation of the downstream kinases, Chk1 and Cds1. Uncoupling between the CMG helicase and polymerase, or perhaps stalling of Pol δ on the lagging strand, could result in the formation of RPA-coated ssDNA at the replisome, followed by checkpoint activation (Sogo et al., 2002; Lambert et al., 2007; Pai and Kearsey, 2017). Therefore, the number of RPA (Sp. Rad11) foci can be examined for future work in order to shed light on what kind of DNA damage or replication problems are causing activation of Rad3 in these *pol3* mutants. To test fork stalling, it is important to measure the length of unperturbed S phase in the *pol3* EDMs. Nitrogen starvation, sometimes combined with M-factor pheromone, has been traditionally used to arrest the cell cycle in G1/S for synchronising passage of cells through S phase (Egel, 1971; Nurse, 1975; Nielsen, 2016). Conclusively, the implications for the treatment of *POLD1* P327L/G321S-driven tumours (Sp. *pol3P311L/G305S*, respectively) in the future might include

a combination of HU or gemcitabine with an ATR or Chk1 inhibitor (Aye et al., 2015; Peasland et al., 2011; Oo et al., 2019; Montano et al., 2012, 2013).

4.3.4 The augmentation of nucleotide levels in the *pol3P311L* and *pol3G305S* cells partially rescues their hydroxyurea sensitivities

The *pol3P311L* and *G305S* variants were HU-sensitive on rich agar and, during HU treatment, the *cdc22-D57N* mutation improved cell growth of *pol3P311L* and *G305S* in the double mutants, consistent with the notion that they are sensitive to low levels of dNTPs. The *cdc22-D57N* mutation did not completely restore growth of these *pol3* mutations in HU when compared to the controls, but this may simply reflect the fact that dNTP levels are still not high enough, although it cannot be ruled out that HU could have targets other than RNR (Davies et al., 2009). To investigate this further, it would be of interest to make triple mutant strains comprising *pol3P311L* or *pol3G305S* with *cdc22-D57N* and *spd1*Δ mutations, since Spd1 deletion should further enhance dNTP levels (Fleck et al., 2013).

Comprehending the repercussions of low dNTP pools is paramount not least as RNR-inhibiting drugs, such as HU and gemcitabine, are used as anti-proliferative agents for the treatment of chronic myeloid leukaemia, melanoma, as well as cervical, bladder, ovarian and breast cancers (reviewed in Aye et al., 2015; Pai and Kearsey, 2017). The activities of these drugs are not always selectively toxic to cells that possess DNA repair or checkpoint deficiencies and they may also exacerbate oncogene-induced stress in healthy cells due to compromised nucleotide pools (Palles et al., 2013; Pai and Kearsey, 2017). Therefore, the selectivity and efficiency of these therapies can be ameliorated by identifying tumours that are sensitive to dNTP deprivation (Pai and Kearsey, 2017), namely *POLD1* P327L (Sp. *pol3P311L*)- and *POLD1* G305S (Sp. *pol3G305S*)- driven tumours.

4.3.5 The augmentation of nucleotide levels in *pol3L458P* mutant cells causes synthetic lethality

Remarkably, *pol3L458P*, like the *pol3D300N* and *pol3D386A* mutants, was not HU-sensitive in solid nor liquid media and did not have a synthetic interaction with *rad3* at the physiological temperature for yeast, yet it had a modest mutator phenotype: it was ten times more mutagenic than wild type. Paradoxically, in this study, the double *pol3L458P cdc22-D57N* mutant showed reduced growth at both 30°C and 36°C in the presence of HU. The double mutant's growth alone was unaffected at normal temperatures. High dNTP levels can increase base mis-insertions, elevating mutation rates in cells (Williams et al., 2015). Hence, a synergistic increase in mutation rate, together with attenuated proofreading, can lead to cell death by error-induced catastrophe (Herr et al., 2014). Specifically, in Mertz et al (2015), a Pol δ mutation affecting DNA polymerase nucleotide selectivity induced a checkpoint-dependent increase of dNTP levels in budding yeast and the resultant elevation of substrates caused Pol δ errors to accumulate. A similar mechanism was responsible for the mutator phenotype of *pol2-M644G*, encoding altered Pol ε base selectivity (Williams et al., 2015). Furthermore, high dNTP levels compromise the fidelity of DNA replication in bacteria, yeast and mammalian cells (reviewed in Pai and Kearsey, 2017).

The human analogous mutation to Sp. *pol3L458P*, *POLD1* L474P, has recently been identified as a pathogenic germline mutation in at least two non-polyposis, microsatellite stable (MSS) CRC/EC families (Valle et al., 2014; Bellido et al., 2016). Therefore, *POLD1* L474P is a recurring Pol δ EDM found in human cancers compared to the rest of the Pol δ variants discussed in this study. The mutation displays a moderate mutator phenotype in *S. pombe* and does not appear to have any obvious growth defects or drug sensitivities, with the exception of the reduced cell growth observed for the double *pol3L458P cdc22-D57N* mutant under HU exposure, which is not understood, or at high temperatures. Therefore, in order, to try and

understand how this Pol δ variant might cause oncogenesis and to unveil potential drug targets for the treatment of *POLD1* L474P carriers with cancer, in the next chapter, genome-wide epistasis analysis will be carried out with the fission yeast homologous mutation, *pol3L458P* (Roguev et al., 2007, 2008; Kim et al., 2010). Moreover, this type of analysis might help us acquire a deeper understanding of what genes are relevant to the function of Pol δ in the cell.

Chapter 5 High-throughput genetic interaction mapping in the fission yeast *S. pombe* expressing *pol3L458P*

5.1 INTRODUCTION

This chapter describes a systematic genome-wide study to detect synthetic lethal interactions between one of the Pol δ variants, *pol3(d)L458P*, and thousands of non-essential genes in the *S. pombe* deletion collection. Epistasis analysis reports on the extent to which the viability of a mutant depends on the presence or function of a second gene and is a powerful tool for studying the functional organisation of the cell (Roguev et al., 2007). This might identify genes that exacerbate the phenotype of *pol3L458P* and could be relevant to how this germline Pol δ variant causes cancer predisposition. Moreover, in this study, we will be looking for synthetically sick/lethal (SSL) (negative/aggravating) genetic interactions between *pol3L458P* and the deletion haploid library; something that has not been carried out yet in the literature. Note that SSL interactions with potential clinical utility in cancer therapy were initially discovered via genetic screens in model organisms such as yeast (Hartwell et al., 1997). Additionally, we did not seek positive genetic interactions or phenotypic suppression because the query strain assessed for genetic interactions (GIs) in this chapter did not have growth defects, and it is not easy to set up an assay to see if the mutator phenotype is suppressed. Fission yeast has an easily manipulatable genome and, notably, for several biological processes, *S. pombe* is more similar to metazoans than is *S. cerevisiae*. Thus, analysis of genetic interaction networks in *S. pombe* will provide information that cannot be obtained from studies performed with *S. cerevisiae*.

Briefly, the first step to setting up the Bioneer cross was to initially construct the PEM-2 version of the *pol3L458P* strain, so to be able to cross the Pol δ mutant with the whole of the Bioneer library: PEM-2 allows haploid double mutants to be selected for (i.e. *pol3L458P*, *geneXΔ*),

while selecting against parental haploid and diploid parents (Roguev et al., 2007). The PEM-2 system is compatible with the high-throughput pinning robotic platforms available for automated plate-based selection of double mutants (Roguev et al., 2018a; c). Moreover, a screen using the PEM-2 strategy only requires 9 days, making it a good choice for conducting genome-wide screens in *S. pombe* (Roguev et al., 2018a). The mass-automated cross using the PEM-2 system can be carried out in a couple of weeks due to the introduction of the ROTOR HDA Colony Replicating Robot (Singer Instruments) (Roguev et al., 2018c).

The *pol3L458P* variant was selected for high-throughput double mutant screening because this exonuclease domain mutation (EDM) causes a moderate mutator phenotype and is well characterised as a clinical variant. The analogous human mutation, *POLD1* L474P, is a recurrent germline mutation that causes CRC or EC in carriers of the mutation (Bellido et al., 2016; Valle et al., 2014). Hence, in my opinion, it was a suitable candidate in acquiring a deeper understanding of what genes are relevant to the function of Pol δ in the cell.

5.1.1 Aims of Chapter 5

The aims and objectives are the following:

- Construction of the PEM-2 system in the *pol3L458P* strain.
- Cross *pol3L458P* with the entire Bioneer collection and explore interesting SSL interactions.
- Follow up on a selection of SSL hits by repeating these crosses manually via tetrad dissection to confirm any phenotypes.

5.2 RESULTS

5.2.1 Genetic Interaction Mapping in *S. pombe* using the Pombe Epistasis Mapper-2 (PEM-2) System

The PEM system is configured to expedite high-throughput generation of haploid double mutants in *S. pombe* (**Figure 5.1**). Haploid double mutants are created on agar plates through mating and multiple selection with the aid of the ROTOR HDA Colony Replicating Robot (Singer Instruments) (Roguev et al., 2018a; c). Firstly, heterozygous diploids are generated by mating a query strain, containing a particular gene deletion or mutation, with a library of haploid gene deletion strains. Secondly, meiosis and sporulation result in a cell mixture of unmated parental cells, non-sporulated diploids, and haploid meiotic products consisting of wild type, single and double mutants (Roguev et al., 2018a). Therefore, it is paramount to remove all parental and diploid cells when assessing the phenotype of double mutants. Three key selections are implemented in the PEM system: anti-diploid selection (ADS), mating-type selection (MTS) and double-mutant selection (DMS) (Roguev et al., 2007, 2018a).

The selectable markers for ADS and MTS are introduced on the query side of the genetic cross, hence making the PEM system independent of the genetic background of the library (**Figure 5.1**) (Roguev et al., 2018a). ADS is achieved through the use of the protein synthesis inhibitor, cycloheximide, and a recessive mutation (P56Q) in a large ribosomal subunit protein L36/L42 encoded by *rpl42* (SPAC15E1.03, Pombase) (Roguev et al., 2018a). The wild-type allele of *rpl42* (*rpl42*$^{+}$) confers cycloheximide sensitivity, whereas the mutant allele (*rpl42-P56Q*) confers cycloheximide resistance, in a haploid setting (Roguev et al., 2007). In the PEM-2 system, for example, the *h*$^{-}$ query strain is engineered to contain a cycloheximide-sensitive (*cyh*^{S}) allele in the *h*$^{-}$ mating-type locus (MTL) (*mat1*) carrying the *smt-0* mutation, and a cycloheximide-resistance (*cyh*^{R}) allele at the endogenous *rpl42* locus. This design mimics a

heterozygous *cyh*^{R}-*cyh*^{S} diploid, where the *cyh*^{S} allele is dominant, and is therefore sensitive to cycloheximide (Roguev et al., 2007). Note that the *smt-0* mutation prevents the loss of the selectable marker by abolishing mating-type switching, thus making the PEM-2 system more robust (Styrkársdóttir et al., 1993). MTS relies on introducing a copy of *rpl42*$^{+}$ in the *h*$^{-}$ MTL of the query strain to counter-select this mating type (Roguev et al., 2018a). Therefore, following mating and sporulation, growth in the presence of cycloheximide acts as both ADS and MTS since it selects for solely meiotic *h*$^{+}$ haploid species while eradicating any surviving diploids and unmated parent cells, as well as preventing remating (Roguev et al., 2007). DMS selects against wild-type and single-mutant haploid products while selecting for haploid double mutants. DMS is usually achieved using two dominant antibiotic resistance markers, KanMX6 and HphMX6, which confer resistance to geneticin (G418) and hygromycin (HYG), respectively (Roguev et al., 2018a). The PEM system is schematically depicted in **Figure 5.1** and explained in much detail in Roguev et al (2007).

In this study, 'your favourite gene' (YFG) is the *pol3L458P* mutation, therefore it was integrated in the PEM-2 genetic background (**Figure 5.2A**).

5.2.1.1 Construction of the PEM-2 strategy in the pol3L458P strain

The step-by-step construction of *pol3L458P* ex PEM-2 is outlined in **Figure 5.2B**. Firstly, the original *pol3L458P* mutation made was marked by kanMX6 (G418) resistance. Since each strain in the deletion library carries a deletion cassette with the same resistance marker as YFG, the KanMX6 cassette had to be exchanged for another resistance marker, such as HphMX6 (hygromycin). This was carried out via yeast transformation of the PCR amplified *pFA6a-hphMX6* plasmid into the *h*$^{-}$ *pol3L458P::kanMX6* strain (#3943 – **Table 2.1**). Yeast transformants were selected against G418 resistance, and selected for hygromycin resistance,

and the *pol3L48P* mutation was confirmed via colony PCR, with primers 1148 and 1088, and subsequent digestion with BsmI. This created the strain, *h⁻ pol3L458P::hphMX6* (#3982).

Secondly, the transformed yeast strain had to be converted from h^- to h^+ mating type in order to mate with the *h⁻ PEM-2* strain (TH 3181 in strain table) at the final stage. Therefore, strain 3982 was crossed with h^+ wild-type (TH 2093) in order to generate haploid h^+ strains with the *pol3L458P::hphMX6* genotype. All crosses were conducted via tetrad dissection. Meiotic products were selected for Hyg^R and the mating type was tested via colony PCR using primers 738, 739 and 740 (**Table 2.2**). As a result, *h⁺ pol3L458P::hphMX6* (#3983) was identified, isolated and stored.

Finally, strain 3983 was crossed with the *h⁻ PEM-2* parental strain (TH 3181). The meiotic recombinants were selected for Hyg^R and the presence of the cyh^S and cyh^R alleles was confirmed by colony PCR using the primer pairs 304 & 305 and 306 & 307, respectively. This produced the following strain, *h⁻ pol3L458P::hphMX6* ex PEM-2 (#3984).

5.2.2 The Bioneer deletion library

The Version 2, Version 2-Upgrade and Version 2-Replacement *S. pombe* Bioneer deletion libraries consist of over 5500 haploid strains with single deletions, marked by $G418^R$, and flanked by unique up- and down-tags for identification purposes (Kim et al., 2010). The library represents 95.3% of the non-essential genome of fission yeast (Roguev et al., 2018a) (http://us.bioneer.com/). It is important to add that the strains in the Version 2-Upgrade and Version 2-Replacement Bioneer libraries are newer versions of the strains in the Version 2 (V2) library because many of the original strains in the V2 library are either sick or contaminated.

Figure 5.1

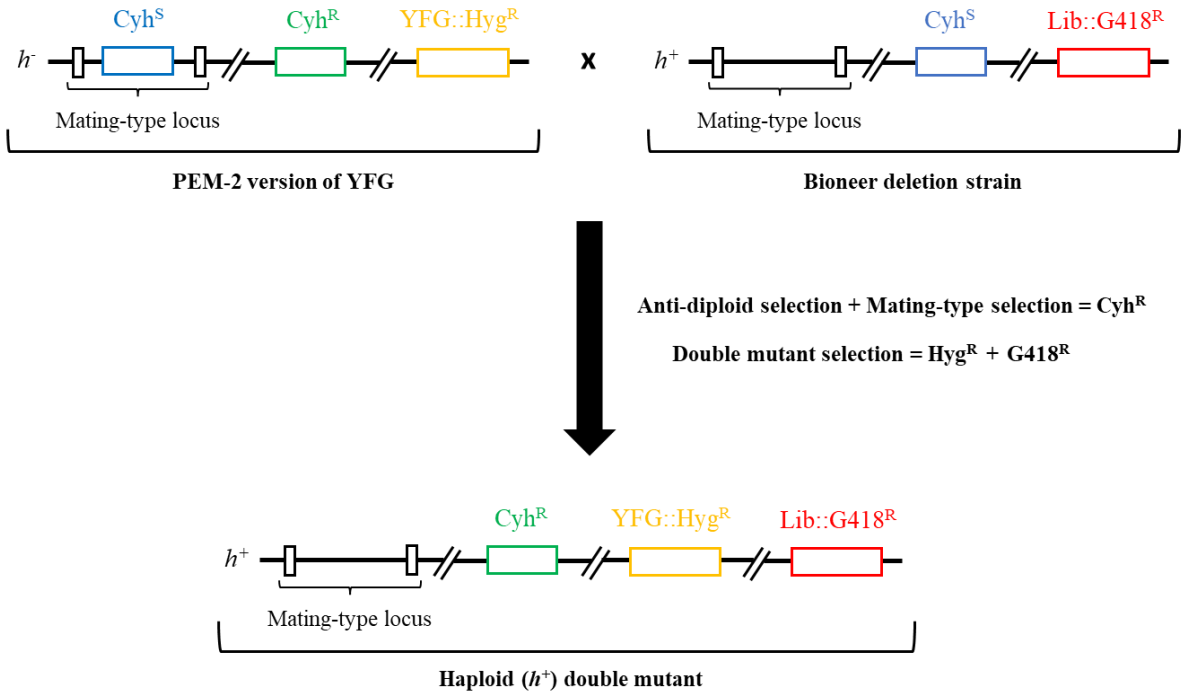


Figure 5.1: A schematic representation of a genetic cross using the PEM-2 system. In the PEM-2 genetic background, a *cyh*^{S} allele is expressed from within the mating type locus of *h*$^-$ cells while a *cyh*^{R} allele is expressed from the endogenous locus, creating a genotype that mimics a heterozygous diploid. After meiosis, the only cells able to survive on medium containing cycloheximide are haploids from the opposite mating type (*h*$^+$). *Cyh*^{S} and *cyh*^{R} are cycloheximide-sensitive (Cyh^S) (*rpl42*$^+$) and cycloheximide-resistant (Cyh^R) (*rpl42-P56Q*) alleles, respectively. YFG::Hyg and Lib::G418 are the query strain and library deletion strain, respectively. YFG, your favourite gene; Lib, library. See text for further details. Image and legend adapted from Roguev et al (2018a).

Figure 5.2

A.

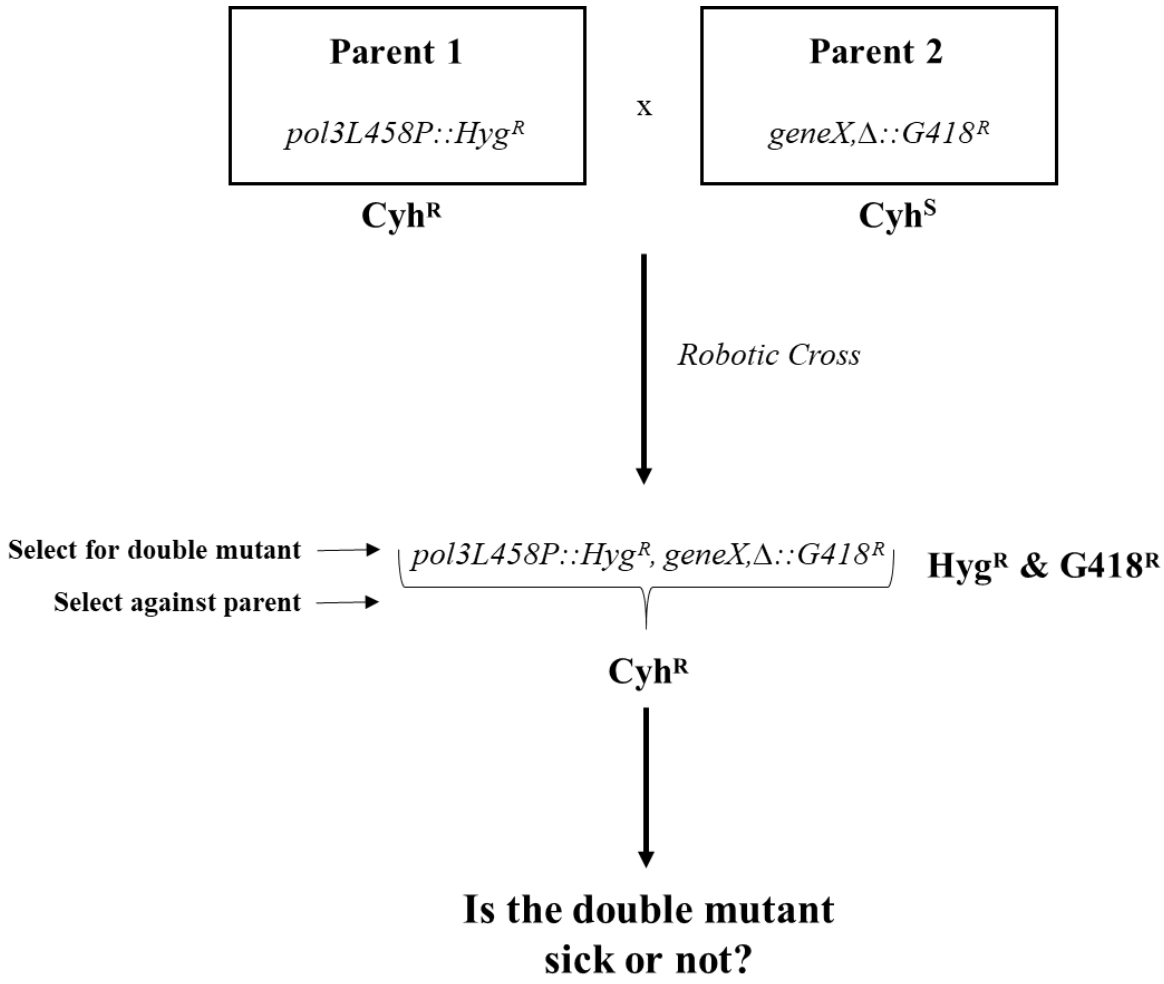
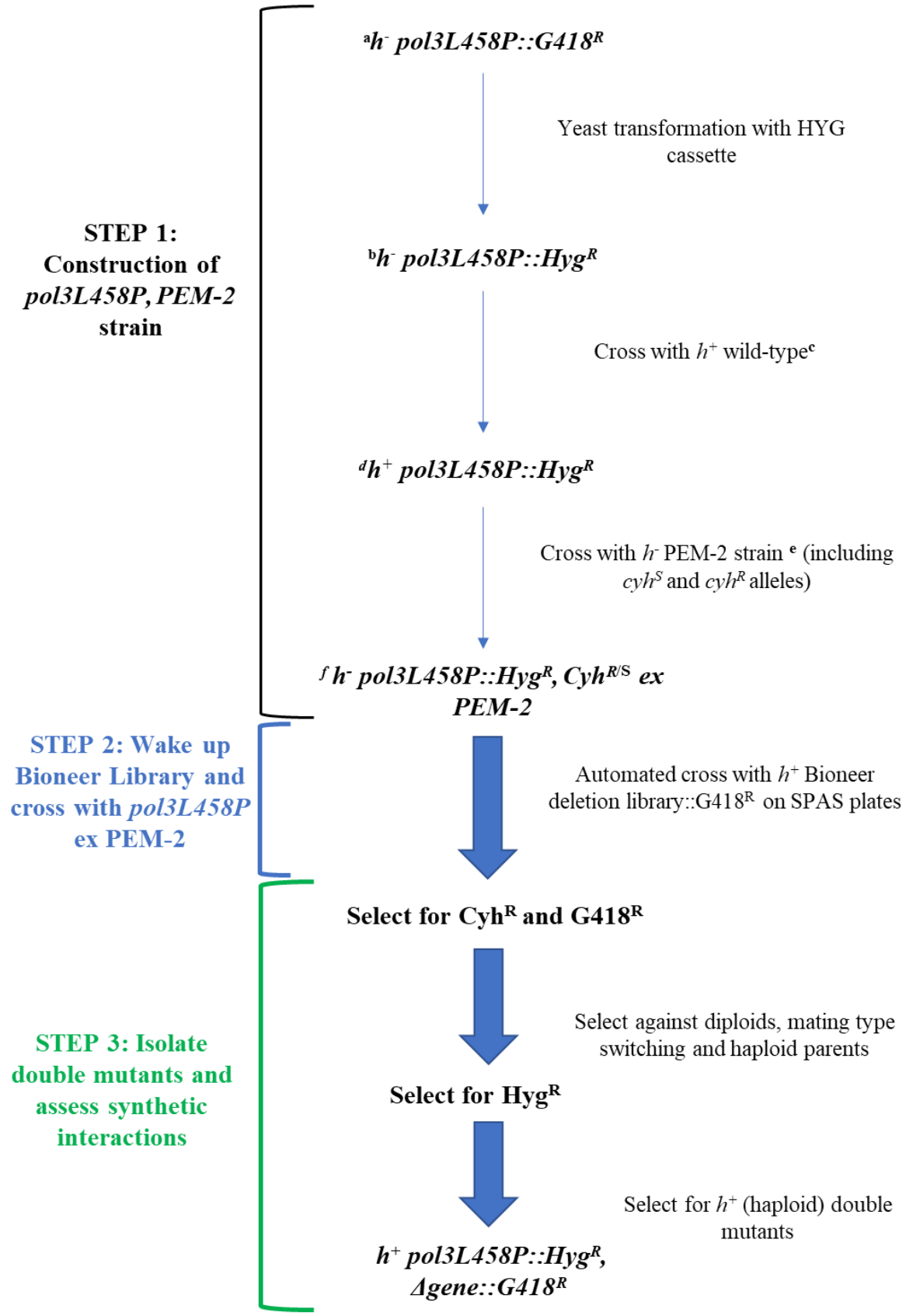


Figure 5.2: Simplified step-by-step diagrams depicting the construction of the PEM-2 system in the query strain and subsequent systematic genetic interaction mapping. (A) Parent 1 is the *pol3L458P* mutation (YFG) expressed in the *PEM-2* genetic background which is cycloheximide-resistant (Cyh^R) and hygromycin-resistant (Hyg^R). Parent 2 is the gene deleted strain (*gene X,Δ*) from the Bioneer deletion library which is cycloheximide-sensitive (Cyh^S) and geneticin-resistant ($G418^R$). The two strains are crossed using the Singer Instruments Robot. Meiotic progeny are selected against diploidy (Cyh^R) and the parental strains (Hyg^S/$G418^S$), and are selected for the double mutation (Hyg^R & $G418^R$). Synthetically sick/lethal (SSL) interactions are assessed by no or little growth of the double mutant on selective media. **(B)** A more detailed flow chart showing systematic double mutant construction using the PEM-2 strategy. The following strains represented are: [a]3943, [b]3982, [c]TH 2093 [d]3983, [e]TH 3181 and [f]3984. YFG, your favourite gene. In this study, YFG is the *pol3L458P* mutation.

Figure 5.2

B.


[a] h- pol3L458P::G418R
Yeast transformation with HYG cassette
[b] h- pol3L458P::HygR
Cross with h+ wild-type[c]
[d] h+ pol3L458P::HygR
Cross with h- PEM-2 strain [e] (including cyhS and cyhR alleles)
[f] h- pol3L458P::HygR, CyhR/S ex PEM-2
STEP 1: Construction of pol3L458P, PEM-2 strain
STEP 2: Wake up Bioneer Library and cross with pol3L458P ex PEM-2
Automated cross with h+ Bioneer deletion library::G418R on SPAS plates
Select for CyhR and G418R
Select against diploids, mating type switching and haploid parents
Select for HygR
Select for h+ (haploid) double mutants
h+ pol3L458P::HygR, Δgene::G418R
STEP 3: Isolate double mutants and assess synthetic interactions

5.2.3 High-throughput genetic interaction mapping using the colony replicating robot ROTOR HDA

High-throughput GI mapping via the experimental platform – synthetic genetic array (SGA) – is performed by colony arrays on agar plates using array replicating robotics (Roguev et al., 2018a). For instance, the ROTOR HDA colony replicating robot (Singer Instruments) was used for high-throughput pinning of yeast strains in an array format, and this method of genetic interaction mapping using the robot has been described in Roguev et al (2018c). The same strategy was adopted for the purposes of this study. The Bioneer library of strains ($G418^R$) were woken up onto non-selective plates in a 384 array format, and crossed with the PEM-2 strain on SPAS mating media. The *S. pombe* 'YFG' in this study was the *pol3L458P* mutation (marked by Hyg^R) in the PEM-2 genetic background (#3984 – **Table 2.1**). Colonies were finally pinned onto plates selective for both the PEM-2 and the library strains' deletion markers (e.g. YE6S + CYC + G418 + HYG).

5.2.4 Bioneer screen results and identification of SSL hits

Growth rate as a factor for fitness is widely used to evaluate genetic interactions (GIs) presenting themselves as strong qualitative differences in growth rates between the observed and expected phenotype of the double mutant given the phenotypes of the two single mutants. GIs report on functional relationships between genes in the same or separate biological pathways. In this study, synthetic sickness/lethality (SSL) is observed when two mutations or two deletions do not cause severe growth defects by themselves but, when combined, result in reduced cell fitness or death. SSL, or negative GIs, may result from two genes acting in independent but complementary parallel pathways (Hartman IV et al., 2001). High-throughput GI mapping via classical SGA utilises a binary scoring scheme for phenotypic strength (growth

versus no growth) and captures only the extreme cases within a much broader spectrum of interactions (Tong et al., 2001; Roguev et al., 2018a).

All the YE6S non-selective and selective plates were photographed and analysed by eye (see **Figure 5.3**). Since the plates were pinned in a 384-array format, each cross was repeated three times (pairwise crosses) to form a square of four colonies (i.e. one array). Thus, "positive" SSL hits were scored when at least three colonies that grew in one array on double selective media (ADS and MTS), i.e. YE6S + CYC + G418 plates, did not grow on triple selective media (DMS), i.e. YE6S + CYC + G418 + HYG plates. "Maybe" SSL hits were scored when one to two colonies that grew on double selective plates did not grow at all on triple selective plates. **Figures 5.3: A-D**, are examples of Bioneer plates photographed and analysed, as described above. The original, untouched images of the respective plates are in **Appendix II**. Photographs of the YE6S, followed by YE6S + G418, plates were studied by eye to assess the state of viability of the original haploid library deletion strains in an attempt to exclude any false positive results. Plates 1-33 of the Version 2 (V2) Bioneer library and Plates 43-56 of the Version 2 Replacement (V2R), upgraded Bioneer library were crossed systematically with the *pol3L458P PEM-2* strain. After careful analyses of the photographed plates from the automated Bioneer screen, a total of 565 negative GIs were identified and are listed with their respective gene ontology (GO) terms in a long table in **Appendix III**.

5.2.5 Criteria for selection of SSL hits

The number of potential SSL interactions extracted from the Bioneer screen was 565. Gene ontology (GO) slim terms from Pombase (https://www.pombase.org/) describing the biological process(es) were assigned to each genetic hit (**Appendix III**): most genes had more than one GO term and there was a plethora of unexpected hits based on the relation of the genes' biological process(es) to DNA replication. The number of synthetic lethal interactions for a

particular gene is generally small: similar systematic studies of gene interaction in yeast discovered no more than eight SSL interactions (Hartman IV et al., 2001). Moreover, examination of the synthetic lethal relationships reported in the Yeast Proteome Database (for *S. cerevisiae*) revealed that a defect in a single gene is usually synthetically lethal with at most 26 other genes (Hartman IV et al., 2001; Hodges et al., 1998). Considering the overwhelming number of negative epistatic interactions identified in this systematic study and, thus, the increased likelihood of false positive results (Hartman IV et al., 2001), interesting/likely hits were highlighted (see **Appendix III**) according to at least one of the following rationale being met:

I. GO terms relevant or related to the function of Pol3

Firstly, the majority of synthetic lethal relationships occur among genes acting in a single biological process but some occur between genes situated in biochemically distinct yet functionally related pathways; for example, DNA repair pathways compensate for defects in DNA replication (Friedberg et al., 1995). Therefore, genes from the "hits" list associated with GO slim terms such as "DNA replication", "DNA repair", "Mitotic cell cycle phase transition", "Checkpoint signalling" and "Chromatin organisation" were brought to the foreground based on their biological/functional link to DNA replication and genomic integrity as a whole. For example, cell cycle regulatory genes and chromatin silencing are functionally linked to the DNA damage response and/or repair (Lee et al., 2004).

II. Physical or genetic interaction with the subunits of the three main replicative polymerases

The genes that emerged from the high-throughput screen, which were previously reported to have a physical or genetic synthetic interaction with any of the subunits of

Pols δ, ε or α, were also emphasised as likely SSL hits. This information was obtained from Pombase which extracts its information from the literature. Pols δ and ε are tetrameric protein complexes. The genes expressing the four subunits of Pol δ are *cdc6* (catalytic subunit), *cdc27*, *cdc1*, and *cdm1*, and the genes expressing the four subunits of Pol ε are *cdc20* (main catalytic subunit), *dpb2*, *dpb3* and *dpb4*. *Pol1* expresses the largest DNA Pol α catalytic subunit, which binds to the Pol α accessory factor, Mcl1 (*mcl1* gene). Mcl1 is needed for the propagation of centromere chromatin structures during DNA replication and is important for the S phase DNA damage response pathway and Okazaki fragment processing on the lagging strand (Tsutsui et al., 2005; Williams and McIntosh, 2005; Natsume et al., 2008).

III. Repeated SSL hit

Thirdly, any SSL GIs observed in the V2 Bioneer library that were also observed in the V2R Bioneer library were selected as probable bona fide synthetic interactions. Repeated observations of GIs on some duplicated V2 Bioneer plates were also taken into consideration.

On the other hand, it was possible to narrow down the list of SSL hits by selecting against the following criteria:

I. Genes closely linked to the *cdc6* locus

The fundamental principle of genetic linkage is that for any two loci on the same chromosome, the closer they are to each other, the less likely it is that they will undertake recombination (Cantor, 2019). An example of two linked genes in *S. pombe* are *leu1* and *his7* (Forsburg, 2003) which are located on Chromosome II, approximately 66,000 bp apart from each other, according to Pombase. Here, the cut-off limit for linkage used was 140,000 bp distance between two genetic loci on the same

chromosome, based on the weak linkage between the *leu1* and *mat1-M* loci. In the laboratory, it is feasible to obtain a few tetratype (TT) zygotic asci via tetrad dissection even though the occurrence of parental ditype (PD) asci is considerably higher in a mating cross between *leu1* and *mat1-M* strains (Ekwall and Thon, 2017b). The arbitrary limit of 140,000 bp was selected for linkage analysis between *pol3L458P* and the gene hits produced from the synthetic lethal screen because failure to obtain the double mutants could simply reflect the low probability of recombination events between two closely linked genes (Ekwall and Thon, 2017a). Furthermore, spontaneously-occurring suppressor mutations reversing true mutant phenotypes may arise from the automated screen which can be problematic when they outgrow a mutant population (Osman et al., 2005; Ekwall and Thon, 2017a). Note that random sporulation is the preferred mating technique to isolate recombinants between tightly-linked loci because of the exceedingly large numbers of spores generated which supports the detection of rare meiotic products (Ekwall and Thon, 2017a).

To conclude, any genetic loci less than 140,000 bp away from *cdc6*, expressing the largest catalytic subunit of Pol δ, were classed as false positive results. Tightly-linked loci to the *rpl42* locus were also excluded.

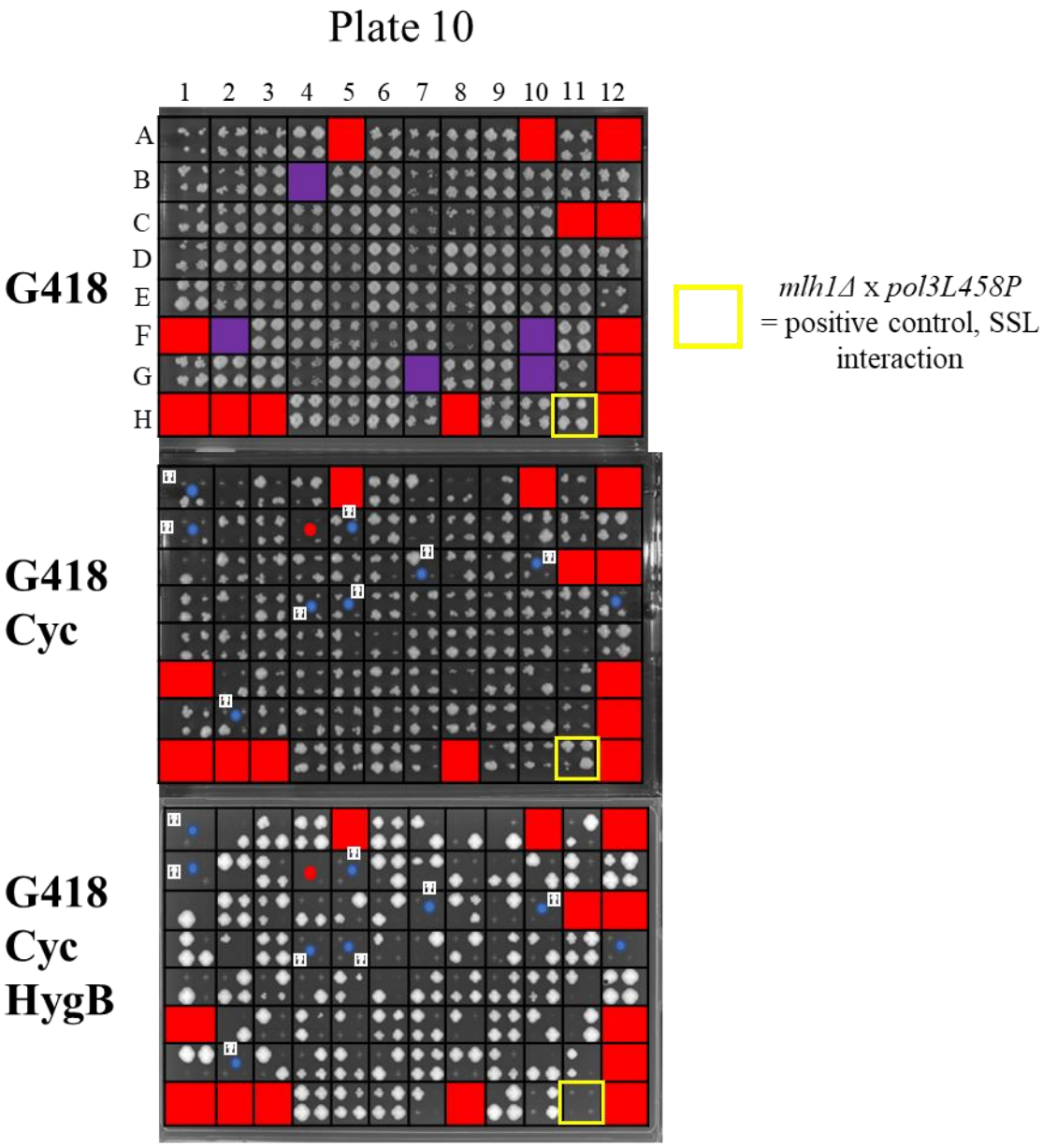
II. Slow-growing Bioneer library deletion strains

The parental Bioneer strains were checked for viable growth on the original YE6S and YE6S G418 plates. Those that were sick were ruled off the list because of inadequate cells for efficient meiosis between haploid strains.

Figure 5.4 summarises the criteria used to select for plausible negative synthetic interactions and to select against false-positive synthetic interactions from a very long list of GIs.

Figure 5.3

A.

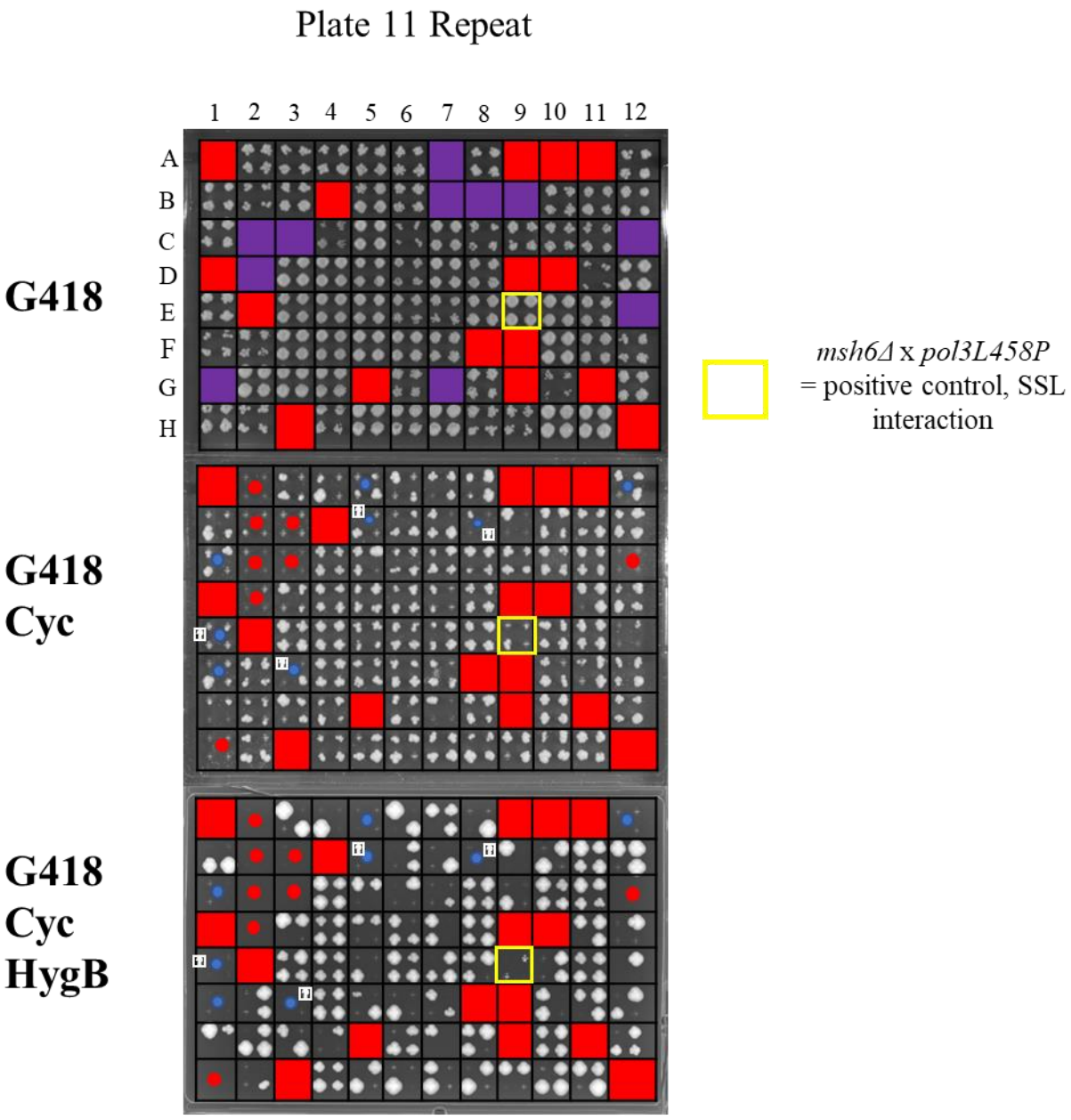


Synthetically lethal double mutants:

- P10-A-01 ? = cbf11 transcription factor
- P10-B-01 ? = tsn1 translin
- P10-B-05 ? = gpd1, glycerol-3-phosphate dehydrogenase
- P10-C-07 ? = sst1, ER membrane calcium transmembrane transporter
- P10-C-10 ? = top1, DNA topoisomerase I
- P10-D-04 ? = nto1, histone acetyltransferase complex subunit
- P10-D-05 ? = hip4, histone promoter control protein Hip4
- P10-D-12 = inp53, inositol polyphosphate phosphatase
- P10-G-02 ? = nbr1, cargo receptor for selective autophagy pathway
- **P10-H-11 = mlh1, MutL family protein – KNOWN SSL INTERACTION**

Figure 5.3

B.

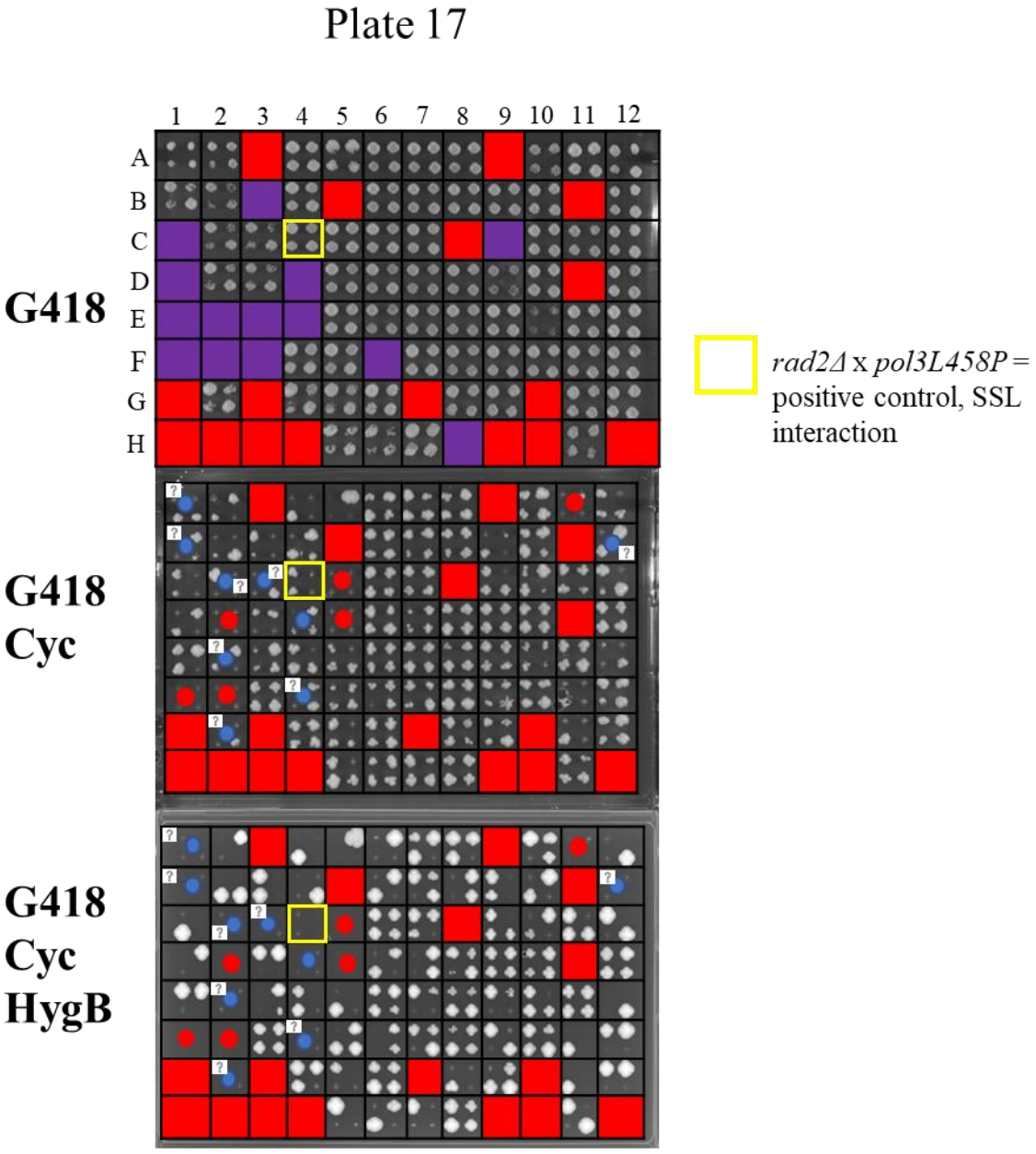


Synthetically lethal double mutants (blue dots):

- P11R-A-05 = alpha/beta hydrolase fold, SO
- P11R-A-12 = rho2, Rho family GTPase Rho2
- P11R-B-05 ? = ssm4, dynactin microtubule-binding subunit, p150-Glued
- P11R-B-08 ? = trt1, telomerase reverse transcriptase 1 protein Trt1 - SICK
- P11R-C-01 = hydrolase, implicated in cellular detoxification (predicted)
- P11R-E-01 ? = ligE3 ubiquitin-protein ligase E3, implicated in DNA repair
- **P11R-E-09 = msh6, MutS protein homolog – KNOWN SSL INTERACTION**
- P11R-F-01 = haloacid dehalogenase-like hydrolase, pseudouridine-5'-phosphatase
- P11R-F-03 ? = swd2, Set1C/COMPASS complex subunit Swd2

Figure 5.3

C.

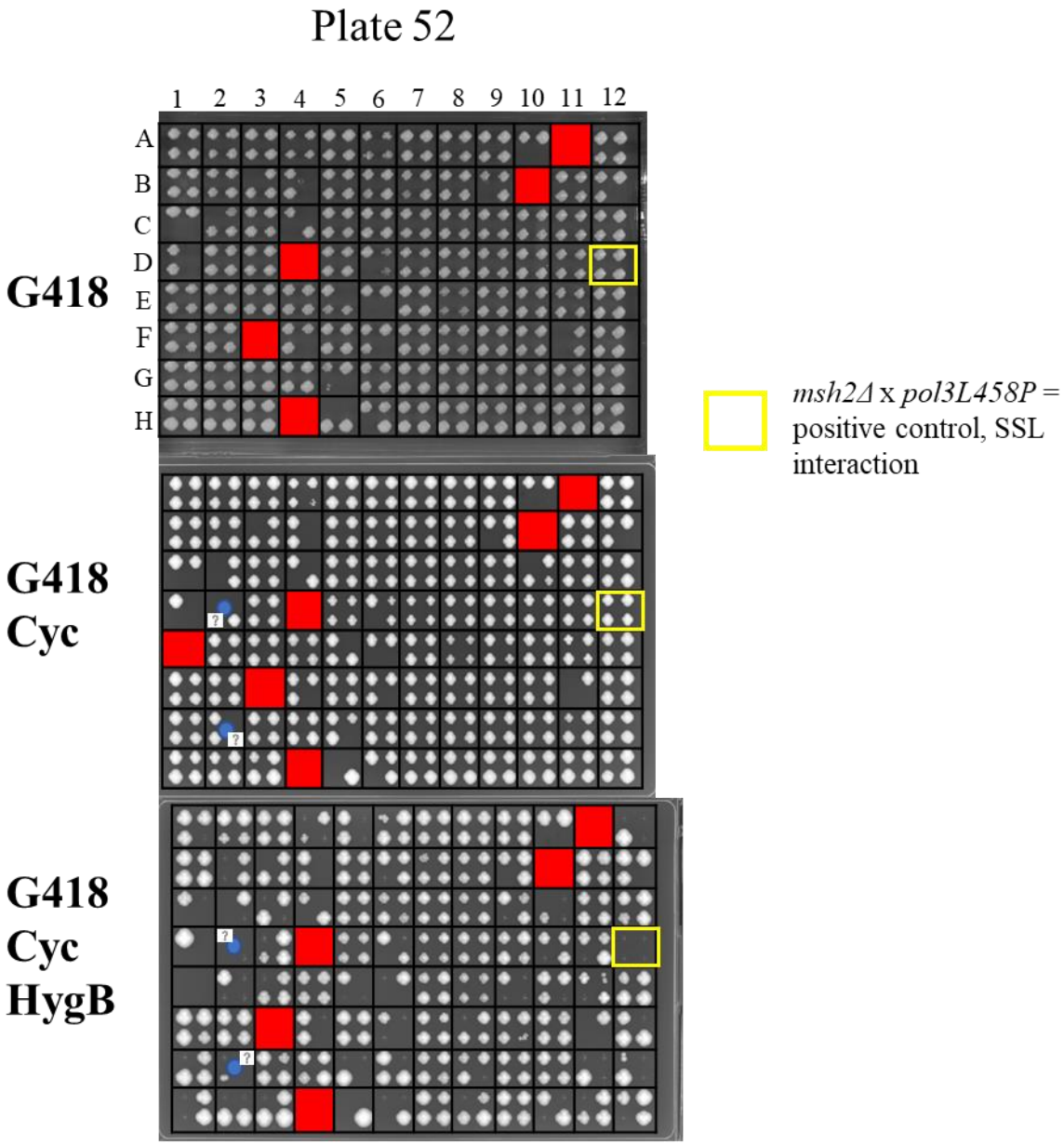


Synthetically lethal double mutants (blue dots):

- P17-A-01 ? = pfl9, cell surface glycoprotein, flocculin Pfl9, DIPSY family
- P17-B-01 ? = ure2, nickel-dependent urease Ure2
- P17-B-12 ? = thp1, uracil DNA N-glycosylase Thp1
- P17-C-02 ? = iwr1, RNA polymerase II nuclear import protein Iwr1 (predicted)
- P17-C-03 ? = plasma membrane basic amino acid transmembrane transporter (predicted), G-protein coupled receptor
- **P17-C-04 = rad2, FEN-1 endonuclease – KNOWN SSL INTERACTION**
- P17-D-04 = hsr1, transcription factor Hsr1 (sick)
- P17-E-02 ? = phospho-2-dehydro-3-deoxyheptonate aldolase (sick)
- P17-F-04 ? = dli1, meiotic dynein intermediate light chain Dli1/Dil1
- P17-G-02 ? = mug105, K48-linkage specific deubiquitinase

Figure 5.3

D.



Synthetically lethal double mutants:

- P52-D-02 ? = dis1, TOG/XMAP215 microtubule plus end tracking polymerase Dis1
- **P52-D-12 = msh2, MutS protein homolog 2 – KNOWN SSL INTERACTION**
- P52-G-02 ? = dihydroxy-acid dehydratase (predicted)

Figure 5.3

E.

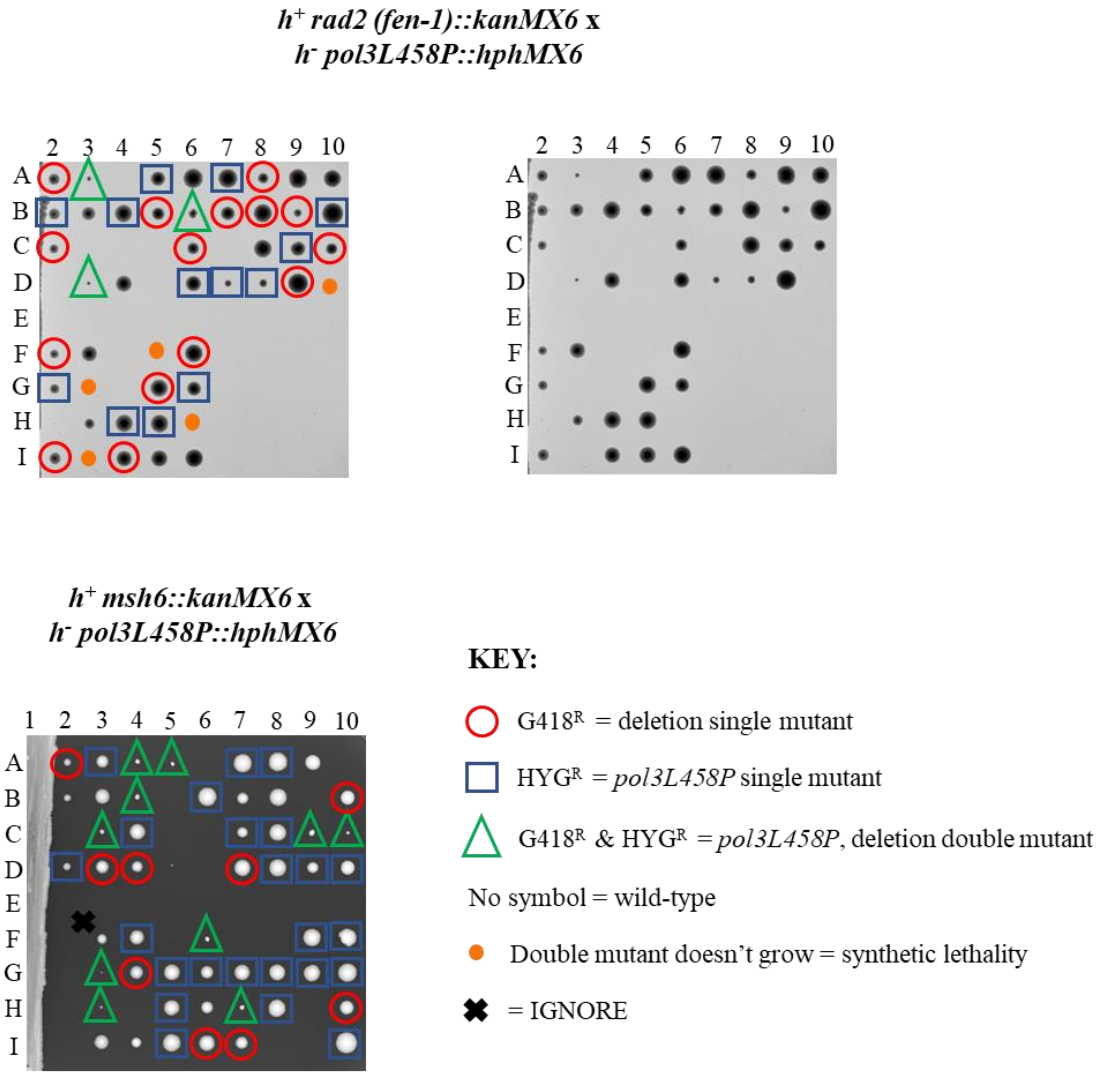


Figure 5.3: Examples of epistatic analysis and confirmation of two renowned synthetic interactions via tetrad analysis. (A - D): Examples of how the plates from the automated Bioneer screen were analysed and how negative genetic interactions were identified. MMR genes, such as *msh6*, *msh2* & *mlh1*, and the endonuclease *rad2* (*fen1*), are known to be synthetically lethal/sick (SSL) with *pol3* (yellow squares). See text for further details. Note that: red squares represent Bioneer strains that never grew; purple squares represent slow-growing/sick Bioneer strains from the library; red circles represent crossed strains that never grew on double and triple selective media; blue circles represent crossed strains that grew on double but not on triple selective media; question marks were used to annotate possible SSL double mutants. **(E)** Confirmation of two well-known SSL interactions via tetrad analysis. Representative meiotic progeny are shown for both indicated crosses. Note that the original, non-annotated image of the *rad2Δ* x *pol3L458P* cross is also provided. For each ascus, four tetrads/spores are positioned individually in a column, for example from 2A-D, 3A-D, 2F-I, 3F-I, etc. Tetrads were replica-plated onto YES plates containing either HYG or G418 to establish single and double haploid mutants, and scored accordingly (see key). Single mutants are either $G418^R$ or HYG^R, and double mutants are both $G418^R$ and HYG^R. Note that any unmarked tetrads are wild type as a result of the cross. Incorrectly positioned tetrads are marked with a black cross ('X'). Naturally, not all spores successfully germinate.

Figure 5.4

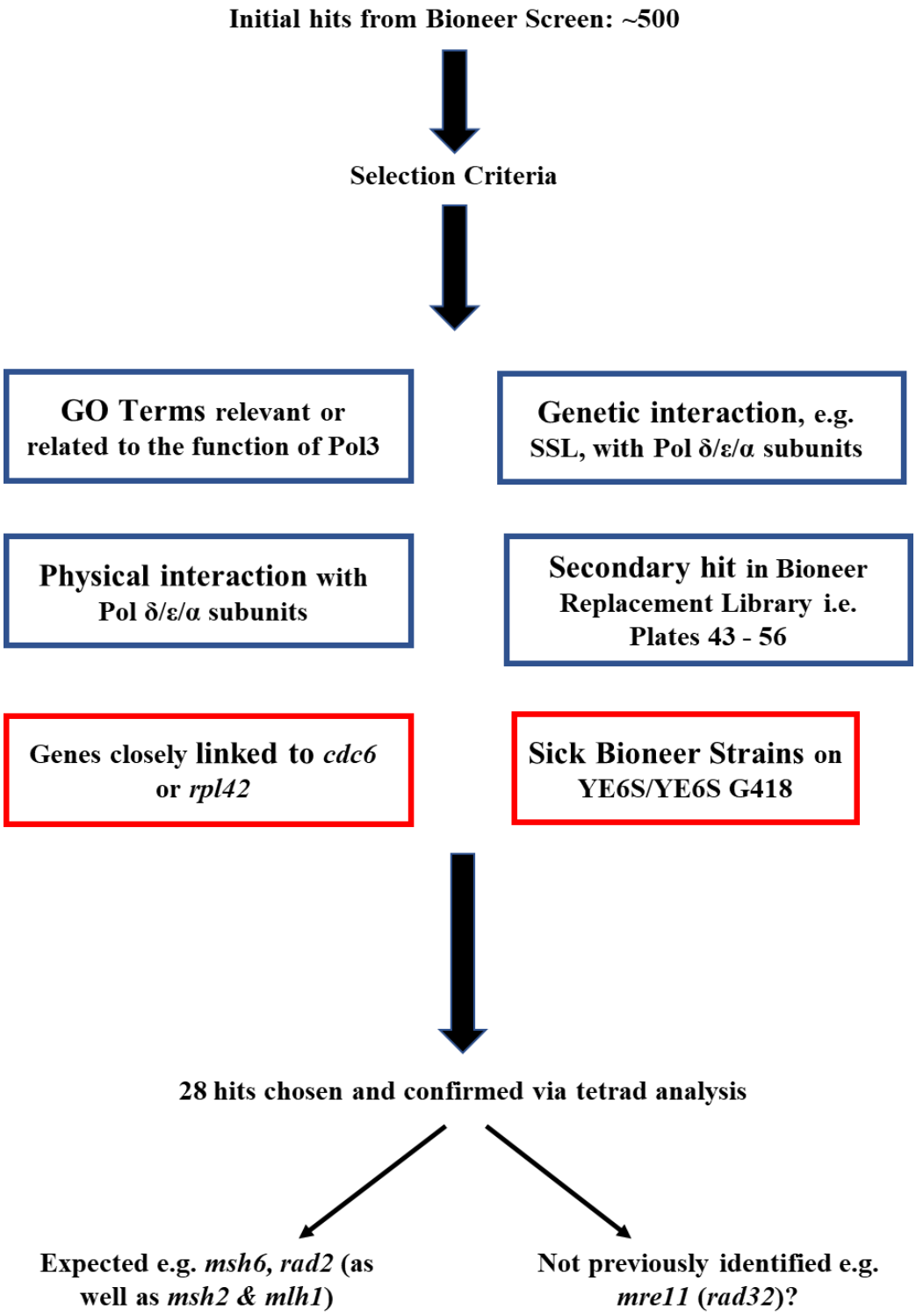


Figure 5.4: Flow chart illustrating the selection criteria for synthetically sick/lethal (SSL) interactions and the identification of known and novel genetic interactions with *pol3*. Criteria highlighted in blue boxes were selected for the identification of potential SSL hits. Criteria highlighted in red boxes were selected against SSL hits. See text for further details.

5.2.6 SSL hits confirmed via tetrad analysis

Twenty-eight hits were subjectively chosen from the compressed list of credible GIs to be validated by tetrad dissection: two of which were positive controls, namely *msh6* and *rad2* (*fen1*) (**Figure 5.3E**). The latter genes are known in the literature to be synthetically lethal with replicative polymerase mutantions which will be discussed later. The remaining twenty-six GIs are defined in **Table 5.1**, along with each gene's respective protein, GO term(s), human homologous gene, and reason(s) for selection based on the aforementioned criteria:

Table 5.1: Twenty-six potential SSL interactions that were validated by tetrad analysis

Strain	Gene/ Gene Product	Protein	GO (Slim) Term(s)	Human homologue	Reason for selection
SPCC736.11	*ago1*	Argonaute	Transcription, DNA-templated; Protein-containing complex assembly; Chromatin organisation	*PIWIL, 1-4*	GO term
SPAC140.03	*arb1*	Argonaute inhibitor protein 1	Transcription, DNA-templated; Chromatin organisation	N/A	GO term; Second hit in the Replacement library
SPBC21D10.10	*bdc1*	Bromodomain protein Bdc1	Chromatin organisation	*BRD8*	GO term: SSL interaction with Pol α subunit
SPCC736.08	*cbf11*	DNA-binding transcription factor, CBF1/Su(H)/LAG-1 family Cbf11	Lipid metabolic process; Transcription, DNA-templated	*RBPJ*	Physical interaction with Cdc6 (catalytic Pol δ subunit)
SPAC17H9.19c	*cdt2*	WD repeat protein Cdt2	DNA repair; Protein catabolic process	*DTL*	GO term; SSL interaction with Pol α subunit
SPAC4G9.11c	*cmb1*	Cytosine-mismatch binding protein 1	DNA repair	*HMGB, 1-4*	GO term

SPBC902.02c	*ctf18*	Ctf18 RFC-like complex subunit Ctf18	DNA replication	*CHTF18*	GO term; SSL interaction with Pol α subunit
SPBC3D6.09	*dpb4*	DNA polymerase epsilon subunit Dpb4	Transcription, DNA-templated; DNA replication; Protein-containing complex assembly; Chromatin organisation	*POLE3*	GO terms; SSL interactions with Pols ε & α subunits. Physical interaction with Pol ε subunits.
SPAC13C5.02	*dre4*	Splicing associated factor Dre4	mRNA metabolic process	*PRPF40A/B*	Defect in REplication
SPBC29A10.05	*exo1*	Exonuclease I Exo1	DNA recombination; DNA repair; DNA replication; Telomere organisation	*EXO1*	GO terms
SPBC947.08c	*hip4*	Histone promoter control protein Hip4	Protein-containing complex assembly; Chromatin organisation	*UBN1*	GO term; SSL interaction with Pol α subunit
SPBC2G2.01c	*liz1*	Plasma membrane pantothenate transmembrane transporter Liz1	Transmembrane transport	*SLC17A, 1-8*	Second hit in the Replacement library
SPBC146.09c	*lsd1*	Histone demethylase SWIRM1	DNA replication; Chromatin organisation	*KDM1B*	GO terms
SPAC1071.02	*mms19*	CIA machinery protein Mms19	Protein maturation; Iron-sulphur cluster assembly; Sulphur compound metabolic process	*MMS19*	Physical interaction with Cdc20 (catalytic Pol ε subunit); SSL interaction with Pol α subunit
SPBC651.10	*nse5*	Smc5-6 complex non-SMC subunit Nse5	DNA replication; DNA recombination; DNA repair	*SLF1*	GO terms. Second hit in the Replacement library
SPAC23C11.15	*pst2*	Clr6 histone deacetylase complex subunit Pst2	Transcription, DNA-templated; Chromatin organisation	*SIN3A/B*	GO term
SPAC1952.07	*rad1*	Checkpoint clamp complex protein Rad1	Mitotic cell cycle phase transition; Signalling; DNA repair; Telomere organisation	*RAD1*	GO terms; SSL interactions with Pols δ, ε & α subunits

SPAC30D11.10	*rad22* (*rad52*)	DNA recombination protein, Rad51 mediator Rad52 (previously Rad22)	DNA replication; DNA recombination; DNA repair; Telomere organisation; Protein-containing complex assembly	*RAD52*	GO terms
SPAC13C5.07	*rad32* (*mre11*)	Mre11 nuclease	DNA recombination; DNA repair; Meiotic nuclear division; Telomere organisation; Mitotic cell cycle phase transition; Signalling	*MRE11*	GO terms; SSL interaction with Pol α subunit
SPCC970.07c	*raf2*	CLRC ubiquitin ligase complex subunit Raf2	Transcription, DNA-templated; Telomere organisation; Protein-containing complex assembly; Chromatin organisation	*DNMT1*	GO term; Physical interaction with Cdc20 (catalytic Pol ε subunit); SSL interaction with Pol α subunit; Second hit in the Replacement library
SPBC1734.06	*rhp18*	Rad18 homolog ubiquitin protein ligase E3, Rhp18	Protein modification (ubiquitination); DNA repair	*RAD18*	GO term; SSL interaction with Pols δ & α subunits
SPCC330.02	*rhp7* (*rad7*)	Rad7 homolog Rhp7	DNA repair	N/A	GO term
SPBC23E6.02	*rrp2*	DNA translocase/ SUMO-targeted ubiquitin ligase E3	DNA replication; Protein modification; DNA repair; DNA recombination; Protein catabolic process	*HLTF*	GO terms
SPCC965.05c	*thp1*	Uracil DNA N-glycosylase Thp1	DNA repair	*TDG*	GO term
SPBC1703.14c	*top1*	DNA topoisomerase I	Mitotic sister chromatid segregation; Chromatin organisation	*TOP1*	GO term
SPCC18B5.03	*wee1*	M phase inhibitor protein kinase Wee1	Mitotic cell cycle phase transition; Signalling	*WEE1*	GO term

A list of putative SSL hits chosen for further analyses via tetrad dissection. The table includes the Strain (systematic ID), Gene, Protein, Gene Ontology (GO) term/s, and Human homologue. N/A = Not Applicable. Information obtained from Pombase.

For tetrad dissections, four spores are isolated from individual asci and positioned in a column on a YES plate, hence tetrad dissection assesses the progeny of individual meiosis, unlike random spores. Tetrad dissection is also a powerful tool when investigating synthetic genetic interactions, such as suppression or synthetic lethality (Ekwall and Thon, 2017a). With just a few tetrads, one can determine linkage, evaluate phenotypes of double mutants, or assess specific meiotic defects (Escorcia and Forsburg, 2018). Also, tetrad analysis is useful for scoring a synthetic lethal combination of mutations because the 2:2 segregation (Mendelian genetics) of individual genes allows spore genotypes to be deduced. A cross between two mutant loci produces three types of asci: non-parental ditype (NPD), tetratype (TT) and parental ditype (PD) ascus. If the genes are linked then PD > NPD, whereas for unlinked genes PD = NPD (Ekwall and Thon, 2017a). When all the tetrads possess the same genotype (i.e. the same marker resistance), then it signifies self-mating amongst the h^+ parental cell population. Finally, when the asci display non-Mendelian inheritance, for example, a 1:3 segregation pattern for a given marker, this is suggestive of gene conversion; possibly indicating meiotic defects in either the single-mutant and/or double-mutant spores (Escorcia and Forsburg, 2018). Mixed phenotypes seen in single colonies indicate post-meiotic segregation (Forsburg, 2003; Smith, 2009). Failure to create double-strand breaks in meiotic prophase produces failed spores which can be ascribed to the phenotype (Escorcia and Forsburg, 2018).

Conclusively, besides the abundance of information tetrads provide, it was important to confirm via tetrad dissection the synthetic lethalities of some of the hits processed from the Bioneer screen in order to validate the accuracy and efficiency of the high-throughput SGA approach.

5.2.7 Results overview from tetrad analyses

Two known SSL hits that were verified by tetrad dissection have been previously reported in the literature. Firstly, Msh6 is a mismatch repair (MMR) protein and studies in yeast show that

polymerase proofreading and post-replication mismatch repair (MMR) are the predominant guardians of DNA replication fidelity (Simon et al., 1991; Morrison et al., 1991, 1993; Morrison and Sugino, 1994). Replication errors that escape Pol ε or δ proofreading can be corrected by post-replication mismatch repair. Problems with either alone greatly elevates spontaneous mutation and combined defects exhibit strong synergistic interactions among proofreading and MMR processes (Morrison et al., 1993; Morrison and Sugino, 1994; Tran et al., 1999b; Albertson et al., 2009). Defective proofreading in either Pol ε or Pol δ together with entire MMR loss is synthetically lethal in budding yeast and mice (Albertson et al., 2009; Williams et al., 2013; Herr et al., 2014). Sporadic CRC tumours, consisting of polymerase-associated exonuclease domain mutations (EDMs), tend to acquire mutations in *MSH6* yet remain partially MMR proficient, i.e. microsatellite-stable (MSS) (The Cancer Genome Atlas Network, 2012, 2013; Shlien et al., 2015; Rayner et al., 2016). Additionally, in *S. cerevisiae*, *msh6Δ* displays synthetic sickness (i.e. reduced spore viability) in a *pol3-01* strain, which is completely devoid of any proofreading activity (Sokolsky and Alani, 2000; Bulock et al., 2020b). **Figure 5.3B** shows the reduced viability of the *pol3L458P, msh6Δ* double mutant on the triple selective plates and tetrad analysis corroborated this result and what was expected (**Figure 5.3E**). Generally, in human cancers, loss of MSH6 function causes a milder mutator phenotype, sometimes lacking microsatellite instability (MSI), than loss of other MMR components, such as MSH2 and MLH1 (Williams et al., 2013; Heyer et al., 1999; Rayner et al., 2016). *Msh2* or *mlh1* mutations completely impair post-replication MMR pathways (Bulock et al., 2020b). Also, in haploid budding yeast cells, *msh2Δ* and *mlhΔ* are synthetically lethal with *pol3-01* and *pol2-04* (which encodes proofreading-deficient Pol ε), separately (Williams et al., 2013; Herr et al., 2014). These SL interactions are evident from the Bioneer screen in **Figures 5.3A** and **5.3D**.

Secondly, another known SL interaction in yeast is one between Sc. *rad27*, homologue of human *FEN1*, and *pol3* mutations (Kokoska et al., 1998; Gary et al., 1999; Jin et al., 2001). The *S. pombe* orthologue is *rad2*. Rad27/Fen1 is required to process Okazaki fragments into ligatable nicks because of its ability to remove 5' ribonucleotide and 5' flaps caused by strand displacement by DNA polymerase δ (Jin et al., 2001). Flap removal is indispensable for the maturation of shorter Okazaki fragments into a continuously long DNA strand (Bambara et al., 1997; Garg and Burgers, 2005). There are various hypotheses explaining this synthetic interaction between *pol3* and *fen1* mutations: one hypothesis is that the exonuclease activity of Pol δ and the 5' flap endonuclease activity of Rad27 behave redundantly in Okazaki fragment maturation, an important process during DNA replication (Jin et al., 2001). Another possible reason is that the synthetic lethality between *pol3-01* and *rad27* mutations is not a consequence of the polymerase's lack of or reduced exonuclease activity but is a result of irreversible cell cycle arrest caused by simultaneous activation of different parts of the checkpoint pathway (Datta et al., 2000; Vallen and Cross, 1995). In consonance with the latter statement, a synthetic lethal interaction was observed between *pol3L458P* and *rad2Δ* (*fen1Δ*), both in the automated genetic screen and in the tetrad analysis (**Figure 5.3C** & **Figure 5.3E**).

The results above appear to validate the methodology of the widescreen genetic mapping using the PEM system and the robot, however, tetrad dissections on the other 26 hits designated for further analysis did not reveal any notable synthetic interactions (**Figure 5.5**). It should be noted that synthetic lethality is defined by the lack of growth of the double mutant and synthetic sickness is demonstrated by a significant difference in size (namely growth) between the tetrad colonies of the double mutants vs the parental single mutants. Where there was uncertainty with subtle effects observed by eye, colony diameters were measured and statistically analysed (**Figure 5.5**). The DNA recombination gene *rad52* (*rad22*) is known to be sick and has difficulties in spore germination and spore viability in *S. pombe* (Ostermann et al., 1993), so it

was not easy to obtain and analyse *pol3L458P, rad52Δ* double-mutant spores (**Figure 5.5**). Additionally, spontaneously occurring suppressors can occur in *rad22* mutants which can be a problem when they overtake a mutant population and conceal its true phenotype (Osman et al., 2005; Ekwall and Thon, 2017a). Surprisingly, the *pol3L458P* mutation did not have an SSL interaction with *exo1* which is in contrast to the *S. cerevisiae* orthologue, *pol3L479P* (Tran et al., 1999b) (**Figure 5.5**).

The tetrad analyses may reveal subtle phenotypic interactions between two genes, however, the purpose of this study was to unveil pronounced and novel genetic interactions (GIs), specifically synthetic lethality (inviable spores) or unambiguous synthetic sickness. It appears that the systematic synthetic genetic array (SGA) employed in *S. pombe* is far from clean and results in a saturation of false positive outcomes, thus making it difficult to infer bona fide GIs. In addition, the large-scale SGA cannot differentiate between modest vs pronounced phenotypic differences among meiotic progeny. The advantage here is that I have shown the importance of confirming GI outcomes from any high-throughput epistatic analysis using a definitive technique such as tetrad dissection.

5.2.8 The *pol3L458P* mutation is not SSL in an *mre11Δ* or a *rad50Δ* genetic background

It was initially believed that the *pol3L458P* mutant was synthetically sick with *mre11* (*rad32*) deletion based on the results from the Bioneer screen and the first tetrad dissection carried out between the two genes in **Figures 5.6A** and **B**. Mre11 associates with Nbs1 and Rad50 proteins to form a complex known as MRN (D'Amours and Jackson, 2002; Connelly and Leach, 2002). MRN is involved in many processes such as the S-phase DNA damage checkpoint, DNA recombinational repair, telomere maintenance, and the formation of meiotic double-strand breaks (DSBs) (Haber, 1998; Bressan et al., 1999; Chahwan et al., 2003; Willis and Rhind, 2010; Syed and Tainer, 2018). Importantly, Mre11 has been shown to regulate replication fork

processing and progression (Falck et al., 2002; Willis and Rhind, 2010), rendering *mre11* a strong SSL candidate with a *pol3* EDM. Alas, two repeats of the tetrad dissection, including an alternative *mre11Δ* strain (TH 5346 – **Table 2.1**), other than the Bioneer deletion strain, revealed no significant difference between the diameters of the *mre11Δ* single-mutant colonies and the double mutant colonies (**Figures 5.6C-F**). Furthermore, photographs taken of spores germinating post-dissection 1-2 days in 30ºC incubation did not demonstrate a noticeable difference in the cell shape or size between the *mre11Δ* and *mre11Δ, pol3L458P* (micro-) colonies; noted that both genotypes displayed an elongated cell phenotype compared to the wild type and *pol3L458P* (**Appendix IV**). Germination takes place within a few hours, while it takes 2-5 days to visualise colonies, depending on the incubation temperature.

Since the synthetic GI between the two genes was ambiguous, a *rad50* deletion strain, defective in another member of the MRN complex, was crossed with *pol3L458P* and the spores were dissected and analysed for synthetic sickness/lethality (SSL) (**Figure 5.7**). Analysis of the meiotic progeny exhibited equivocal results where there was much variation in the tetrad colony sizes, similarly observed in the progeny of *pol3L458P* x *mre11Δ*. Sometimes the double mutant spores grew into comparably large colonies and sometimes they appeared as small, sick colonies. The same pattern of colony growth was seen in *mre11Δ* and *rad50Δ* single-mutant colonies. Overall, since most of the tetrad outcomes showed reduced colony formation, it appears that MRN deficiency alone causes problems with sporulation and germination (Limbo et al., 2012; Bonfils et al., 2011; Tavassoli et al., 1995; Young et al., 2004). Nonetheless, no synthetic genetic interaction can be conclusively deduced between *mre11* or *rad50*, and *pol3L458P*. Tetrad dissection was not performed on a sporulating cross between *nbs1* and *pol3L458P* mutations because the two genetic loci are situated less than 100,000 base pairs apart, thus the two genes are moderately linked to each another.

In conclusion, high-throughput genetic mapping in fission yeast cannot distinguish between meiotic, sporulation or spore germination defects, and synthetic sickness/lethality, and ways of overcoming this need to be explored. In addition, very modest genetic variations between single and double mutants, particularly when the Bioneer parental strain was readily sick, were scored as synthetic lethalities on the Bioneer plates.

Figure 5.5

KEY:

○ G418^R = deletion single mutant

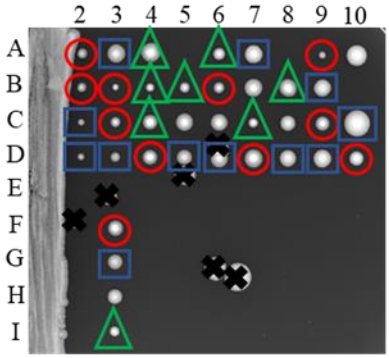
□ HYG^R = *pol3L458P* single mutant

△ G418^R/HYG^R = *pol3L458P*, deletion double mutant

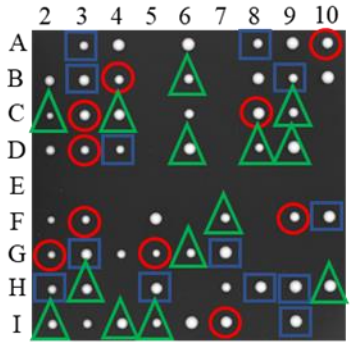
No symbol = wild-type

✖ = IGNORE

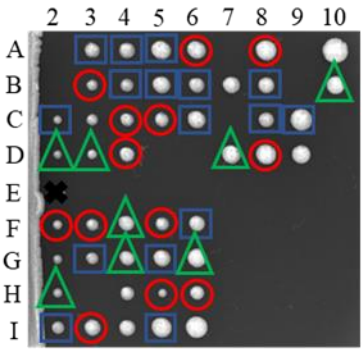
h+ pst2::kanMX6 x *h- pol3L458P::hphMX6*



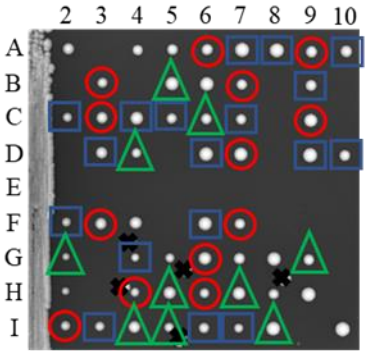
h+ dpb4::kanMX6 x *h- pol3L458P::hphMX6*



h+ ctf18::kanMX6 x *h- pol3L458P::hphMX6*



h+ top1::kanMX6 x *h- pol3L458P::hphMX6*



h+ rhp18 (rad18)::kanMX6 x *h- pol3L458P::hphMX6*

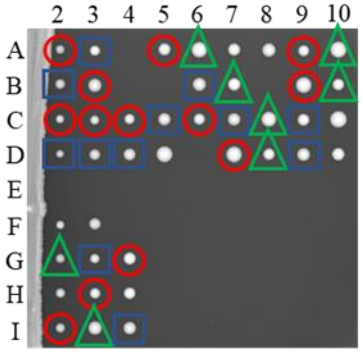
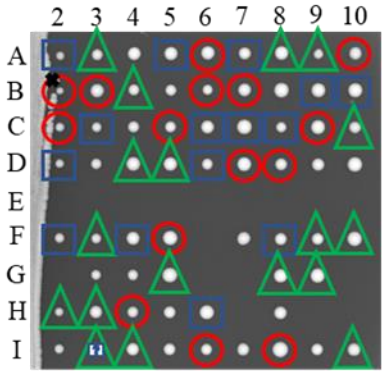


Figure 5.5

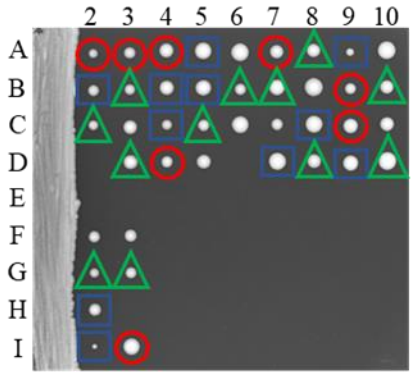
KEY:

- G418^R = deletion single mutant
- HYG^R = *pol3L458P* single mutant
- G418^R/HYG^R = *pol3L458P*, deletion double mutant
- No symbol = wild-type
- ✖ = IGNORE

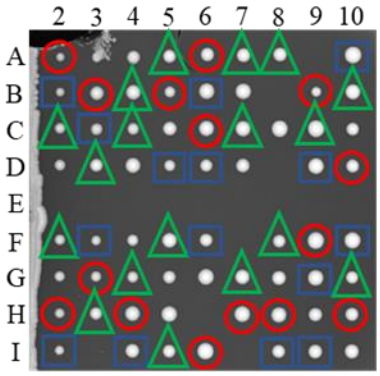
h+ liz1::kanMX6 x *h- pol3L458P::hphMX6*



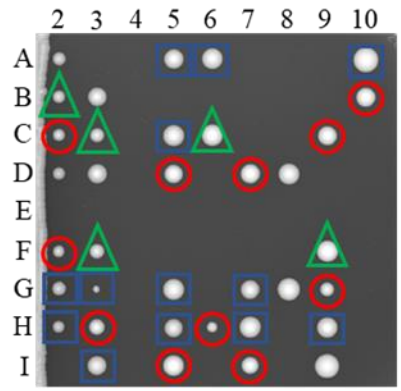
h+ cmb1::kanMX6 x h- pol3L458P::hphMX6



h+ arb1::kanMX6 x *h- pol3L458P::hphMX6*



h+ raf2::kanMX6 x *h- pol3L458P::hphMX6*



h+ thp1::kanMX6 x *h- pol3L458P::hphMX6*

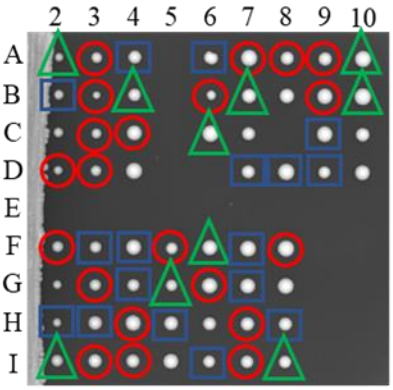
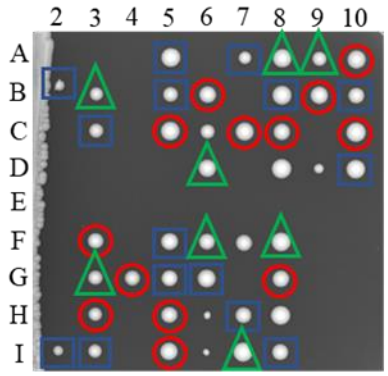


Figure 5.5

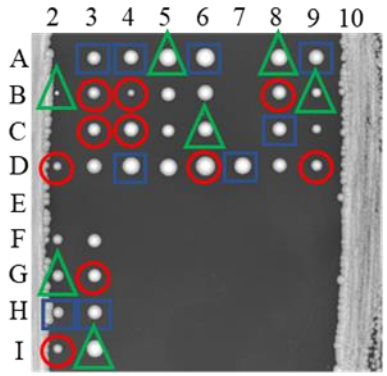
KEY:

- ○ G418^R = deletion single mutant
- □ HYG^R = *pol3L458P* single mutant
- △ G418^R/HYG^R = *pol3L458P*, deletion double mutant
- No symbol = wild-type
- ✖ = IGNORE

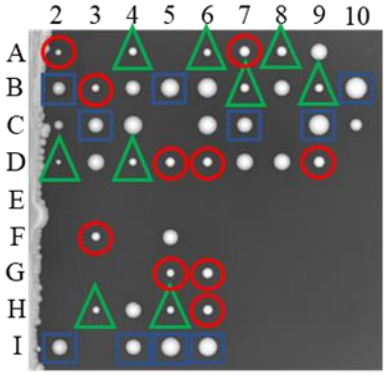
h+ bdc1::kanMX6 x *h- pol3L458P::hphMX6*



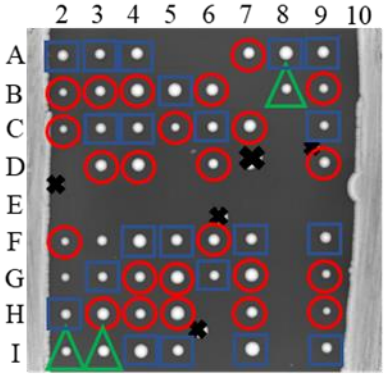
h+ hip4::kanMX6 x *h- pol3L458P::hphMX6*



h+ mms19::kanMX6 x *h- pol3L458P::hphMX6*



h+ exo1::kanMX6 x *h- pol3L458P::hphMX6*



h+ rad52 (rad22)::kanMX6 x *h- pol3L458P::hphMX6*

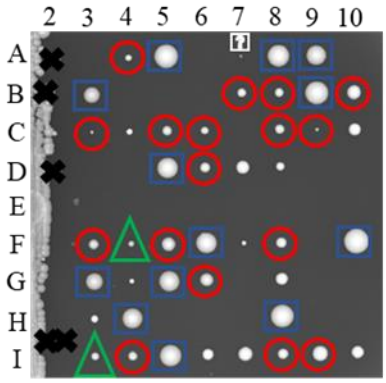


Figure 5.5

KEY:

○ G418^R = deletion single mutant

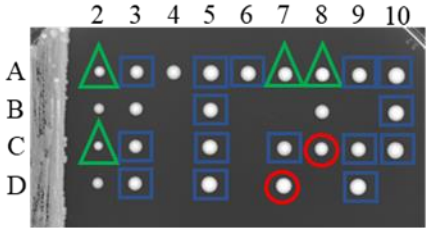
□ HYG^R = *pol3L458P* single mutant

△ G418^R/HYG^R = *pol3L458P*, deletion double mutant

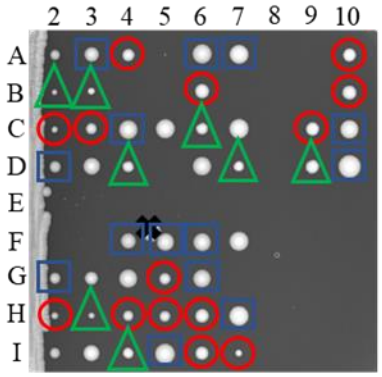
No symbol = wild-type

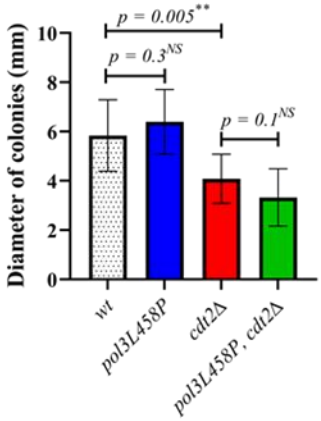
✖ = IGNORE

h+ rad1::kanMX6 x *h- pol3L458P::hphMX6*

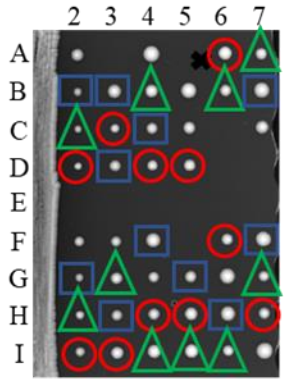


h+ cdt2::kanMX6 x *h- pol3L458P::hphMX6* - REPEAT

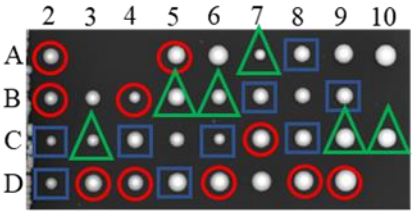




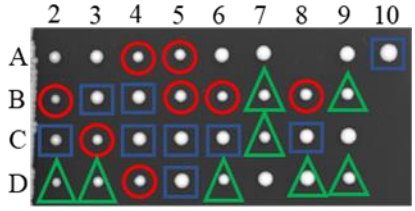
h+ ago1::kanMX6 x *h- pol3L458P::hphMX6*



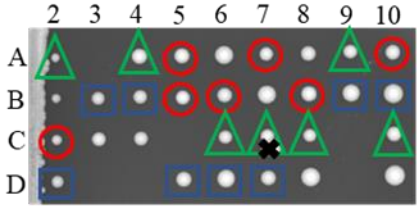
h+ nse5::kanMX6 x *h- pol3L458P::hphMX6*



h+ rhp7(rad7)::kanMX6 x *h- pol3L458P::hphMX6*



h+ cbf11::kanMX6 x *h- pol3L458P::hphMX6*



h+ rrp2::kanMX6 x *h- pol3L458P::hphMX6*

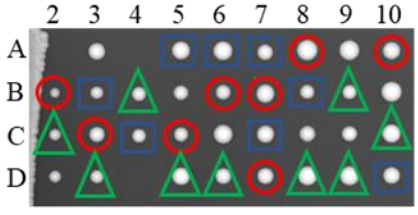


Figure 5.5

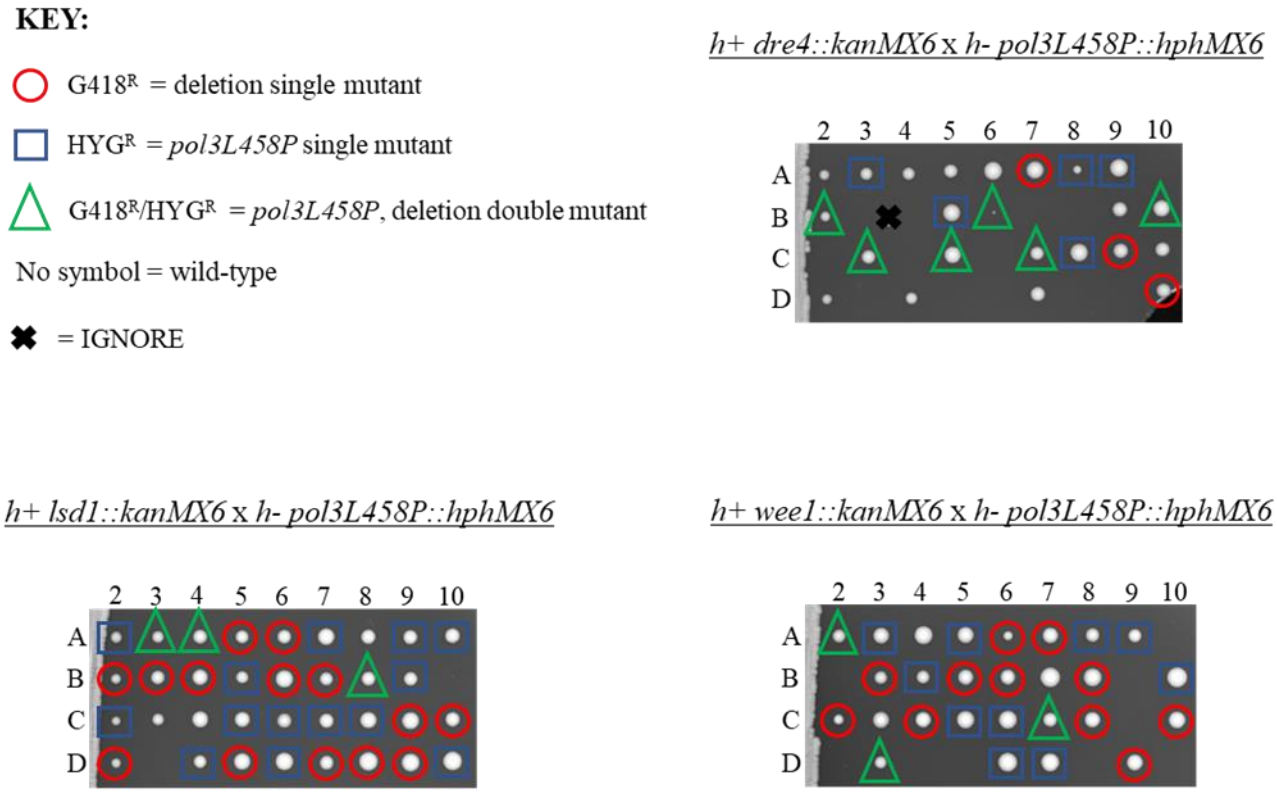
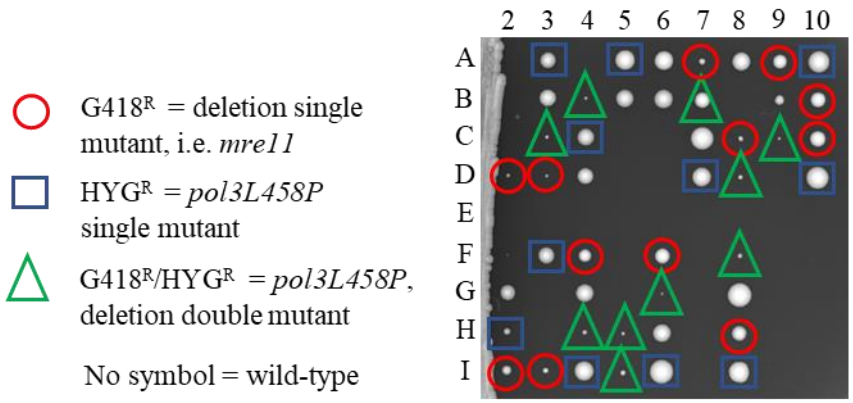


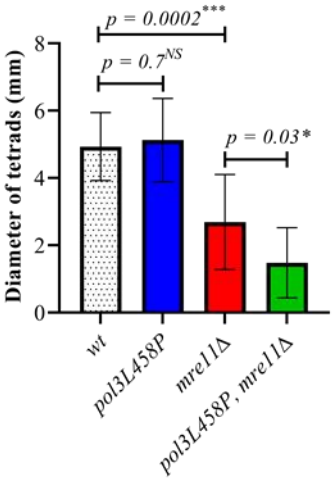
Figure 5.5: Tetrad analyses to confirm a selection of hits from the high-throughput screen. Tetrad dissections of genetic crosses between *h⁻ pol3L458P::hphMX6* (Strain 3982) and the *h⁺* Bioneer strains (see Table 2.1), separately. For each ascus, four tetrads/spores are positioned individually in a column, for example from 2A-D, 3A-D, 4A-D, etc. Colonies were replica-plated onto YES plates containing either HYG or G418 to select for double mutants and scored according to genotype (see key). Single mutants are either $G418^R/HYG^S$ or $HYG^R/G418^S$, depending on their genotype, and double mutants are both $G418^R$ and HYG^R. Note that any unmarked tetrads are wild type as a result of the cross, and some spores do not always germinate, hence there are gaps with no colony growth. Incorrectly positioned tetrads/random colonies are marked with a black cross ('X'). Relative quantification of the diameters of colonies/tetrads from the meiotic progeny of *h⁻ pol3L458P::hphMX6* x *h⁺ cdt2::kanMX6* genetic cross, were measured using ImageJ. The mean diameters of the colonies (in millimetres) were plotted for the wild type, parental strains and double mutants. Error bars represent SD. P-values were calculated using the two-tailed unpaired t-test with Welch's correction: ^{NS} $p > 0.05$ and ** $p < 0.01$. NS = Not Significant.

Figure 5.6

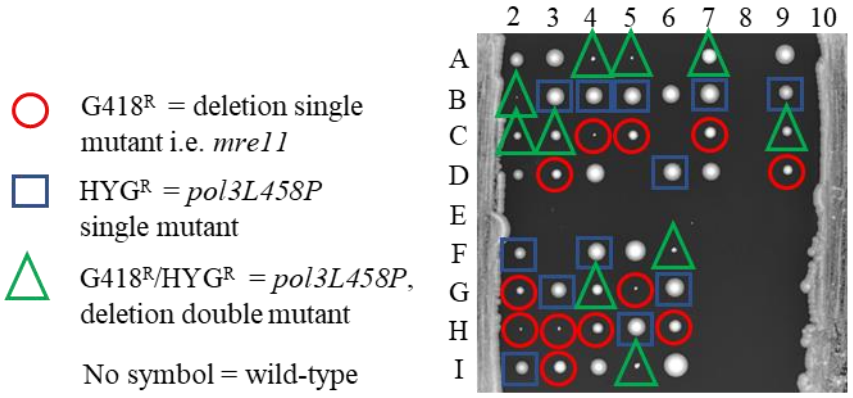
A.



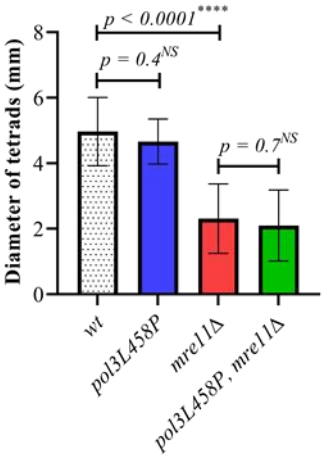
B.



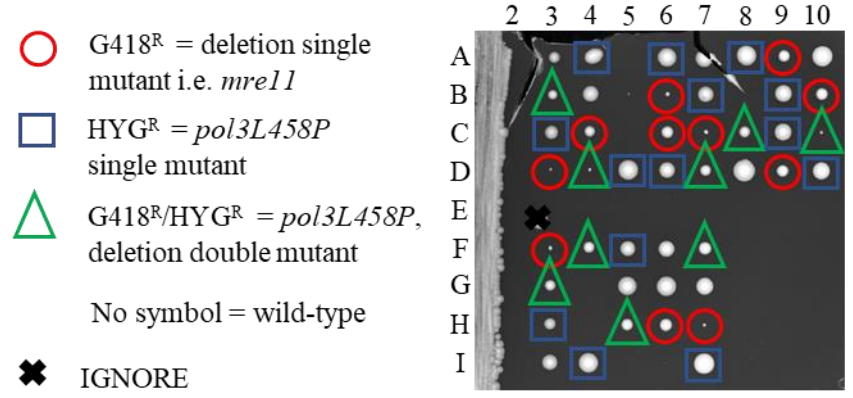
C.



D.



E.



F.

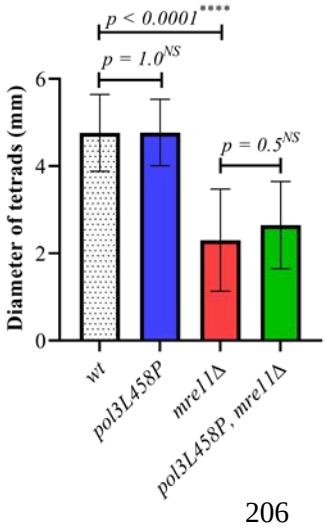
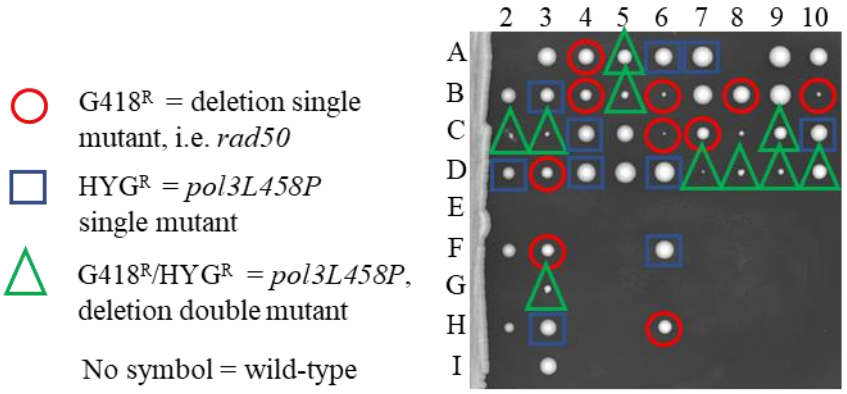


Figure 5.6: There is no clear negative synthetic interaction between *pol3L458P* and *mre11*. **(A), (C)** and **(E)** Tetrad dissection of a genetic cross between h^- *pol3L458P::hphMX6* (Strain 3982) and h^+ *mre11::kanMX6*. For each ascus, four tetrads/spores are positioned individually in a column, for example from 2A-D, 3A-D, 2F-I, 3F-I, etc. Colonies were replica-plated onto YES plates containing either HYG or G418 to select for double mutants, and scored accordingly (see key). Single mutants are either $G418^R/HYG^S$ or $HYG^R/G418^S$, depending on their genotype, and double mutants are both $G418^R$ and HYG^R. Note that any unmarked tetrads are wild type as a result of the cross and not all spores successfully germinate and grow. Incorrectly positioned tetrads are marked with a black cross ('X'). The *mre11Δ* parental strains used in (A) and (C) were from the Bioneer library (V2R-44-C-04). The *mre11Δ* parental strain used in (E) was from the TH strain collection (TH 5346). (**B), (D)** and **(F)** are the relative quantification of the diameters of individual colonies/tetrads from (A), (C) and (E), respectively, measured using ImageJ. The mean diameters of the colonies (in millimetres) were plotted for wild type, parental strains and double mutants. Error bars represent SD. P-values were calculated using the two-tailed unpaired t test with Welch's correction: ^{NS} $p > 0.05$, * $p < 0.05$, *** $p < 0.001$, and **** $p < 0.0001$. NS = Not Significant.

Figure 5.7

A.



B.

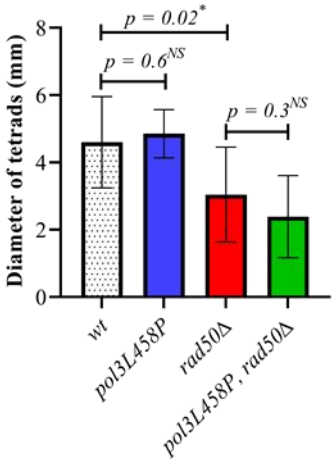


Figure 5.7: *Pol3L458P* does not have an SSL interaction with *rad50*, part of the MRN complex. (A) Tetrad dissection of a genetic cross between *h⁻ pol3L458P::hphMX6* (3982) and *h⁺ rad50::kanMX6* (V4R-46-C-05, Bioneer). Strain numbers are shown in brackets. For each ascus, four tetrads/spores are positioned individually in a column, for example from 2A-D, 3A-D, 4A-D, etc. Colonies were replica-plated onto YES plates containing either HYG or G418 to select for double mutants, and scored accordingly (see key). Single mutants are either $G418^R$ or HYG^R, and double mutants are both $G418^R$ and HYG^R. Note that any unmarked tetrads are wild type as a result of the cross. **(B)** Relative quantification of the diameters of colonies/tetrads from (A) were measured using ImageJ. The mean diameters of the colonies (in millimetres) were plotted for wild type, parental strains and double mutants. Error bars represent SD. P-values were calculated using the two-tailed unpaired t test with Welch's correction: ^{NS} $p > 0.05$ and * $p < 0.05$. NS = Not Significant.

5.3 DISCUSSION

5.3.1 Summary of results

In this chapter, the PEM-2 system was introduced into the *pol3L458P* mutant, marked by hygromycin (HYG) resistance. The *pol3L458P, PEM-2* strain was then systematically crossed against a library of more than 5000 strains, each carrying a unique genetic modification marked with a gene for kanamycin (Kan/G418) resistance. The plates were photographed and analysed for potentially SSL genes (i.e. growth vs no group upon triple selection). The result of the mass screen was 565 "SSL" hits, each grouped by their GO terms to understand their biological pathways. Despite the noisy data and random genes generated by the screen, hits that had GO terms involved in or in relation biochemically or functionally to DNA replication, were highlighted as probable true SSL GIs. Further to this, a set of genes (28 to be precise) was rationally selected from the exhaustive list to confirm synthetic interactions via tetrad analysis. Two of these genes were already known SSL interactions and other renown negative GIs were yielded from the Bioneer screen analysis, such as MMR genes (e.g. *msh6*, *mlh1*, *msh2*) and Okazaki fragment processing gene, *rad2* (*fen1*). The rest of the tetrad dissections did not reveal any apparent SSL interactions, questioning the validity of the Bioneer screen.

5.3.2 General discussion

The Bioneer screen, with *pol3L458P* mutation as the gene of choice, unfortunately generated many false positive results; evidently from the negative results obtained from tetrad analyses of twenty-six SSL candidates. One could say that the selection criteria were too arbitrary and subjective and require reformulation. On the other hand, the high-throughput GI screen created 565 "SSL" hits which is unusual because generally, in yeast studies, the number of synthetic lethal interactions for a particular gene is small, for example, not more than 30 synthetic lethal

interactions (Hardy, 1996; York et al., 1999; Hartman IV et al., 2001). The small number of synthetic lethal interactions for any gene indicates the low threshold for tolerability of genetic variation and redundancy in a population (Hartman IV et al., 2001). That being said, it seems more likely that there is much technical error involved in the robotic technique. Firstly, the pinning effect of the robot was not always accurate, especially if the plates were not entirely flat. This meant that some cells were not being successfully picked up and transferred to the next plate, hence the very high number of "SSL hits" resulting from the yeast screen. Repeat pinning on plates was carried out to try to minimise this problem, where possible. In future, a plate pouring machine (also made by Singer Instruments) would be more accurate in preparing horizontal plates for a mass genetic screen than pouring plates manually, though there was no such equipment in the laboratory at the time. Secondly, the actual pinning approach of the robot, together with the very fine pins used to transfer the cells, meant that very few cells were being picked up from one plate and deposited on the following plate. This was particularly noticeable when the original Bioneer strains grew poorly on YES + G418 plates. Not all the strains, however, that were in the V2 library were replaced or upgraded in the newer Bioneer libraries which may have partly resulted in the incidence of false positives.

The purpose of conducting the large-scale epistasis mapping in a 384-array format rather than a 96-array format was to ensure that every strain and respective meiotic products were present in quadruple spots to increase the number of technical repeats. This was used as a scoring tool when analysing SSL candidate hits through a reduction in colony size among the quadruple spots on the triple drug plate. Nonetheless, mild negative genetic interactions were deemed as SSL hits by the Bioneer screen (see tetrad dissection plates) making this type of GI mapping using the PEM-2 system and the robotic machine not 100% reliable. Another limiting factor is growth rate of the individual strain: what was commonly observed was that double mutant strains appeared sick or dead if the respective Bioneer single-mutant strain was also challenged

in growth. Tetrad analysis on over a dozen hits corroborates the former statement. Moreover, since the SGA method depends on bulk transfer of double-mutant progeny, mutations that negatively affect germination efficiency may have incorrectly scored as inviable (Tong et al., 2001).

From the further analysis undertaken on a relatively small selection (5%) of potential SSL candidates from the total hits generated, no definitive synthetic interactions were identified. This, again, emphasises the inaccuracy of the screen. Admittedly, the selection criteria devised were rather arbitrary and subject to bias and were based on the nature of known SSL interactions and the literature (acquired from Pombase) which may not be entirely accurate. In retrospect, in silico analysis may have been useful in creating a spectrum of GIs, both positive and negative, assigned with quantitative scores, each of which may be laborious to interpret in isolation (Roguev et al., 2007). Heat maps created by hierarchical clustering are typically used to analyse GIs based on a set of GI scores associated with that mutant, taking into account its relationship biochemically or functionally with another mutant/s (Roguev et al., 2007, 2008). This creates a complex and diverse "genetic interaction profile" of a mutant which, in hindsight, could have facilitated the identification of potential novel synthetic interactions in this study. The methodology of computational analysis of genetic screens is described in Roguev et al (2018b), including the calculation of the genetic interaction score (S-score) using the epistatic mini-array profile (E-MAP) approach. The E-MAP strategy uses the SGA platform for high-throughput generation of double mutants and a continuous GI score (S-score) (Collins et al., 2006, 2010; Roguev et al., 2018a; b). The caveat to carrying out an E-MAP in this setting is that it would form incorrect clustering predicated on predominantly noisy, false positive data. Hence, a Venn diagram and/or a gene ontology (GO) network of GIs was not composed due to the absurdly high number of so-called SSL hits resulting from the screen (Kasparek, 2013).

Following this, it seemed reasonable at the time to narrow down the list according to what was believed to be the logical and acceptable rationale proposed in the results of this chapter. Taking time constraints into consideration, only a relatively small number of hits could be investigated by tetrad dissection. First, the purpose of this study, like many other SGA methods, was not to identify the buffering relationships between genes, but, rather, was to pinpoint new genes that function in the same or a related pathway (Hartman IV et al., 2001). Currently, SGA analysis yields a substantial number of false positives; however, these can be reduced by repeated screening or withdrawn through confirmation of the interactions by tetrad dissection (Tong et al., 2001), which requires mating the selected strains from scratch. Although an unbiased search was conducted, i.e. by crossing the query strain with the entire Bioneer deletion library, the considerably high number of false positives consequently meant that only selected genes within the inclusion criteria were tested for SSL interactions, for example, by candidate crosses. Additionally, it is difficult to assess false negatives. However, for the query mutation reported here, SGA analysis identified almost all previously known negative GIs (e.g. MMR genes and the endonuclease *fen1*).

In summary, there is evidence to strongly suggest that the robotic pinning effect on unevenly distributed media, together with the unpredictable nature of genetic instability and growth variability in certain deletion mutants, are the two main caveats of this type of GI mapping technique. The positive aspect is that I have brought to the forefront the requirement to perform tetrad analysis on as many SSL genes as possible that are yielded from these types of large-scale screens in order to convincingly define these synthetic interactions, which was reinforced in Tong et al (2001, 2004). The fact that previously known synthetic interactions were positive outcomes from the Bioneer screen validates the experiment to some degree, regardless of the noisy output. Not to mention that large-scale genetic mapping using the PEM system is a well-published protocol and is widely used (Roguev et al., 2007, 2008; Ryan et al., 2012; Roguev et

al., 2018a; b; c). Furthermore, this is the first study to undertake mass epistasis analysis in *S. pombe* on a Pol δ exonuclease domain mutation (EDM) that has human cancer implications. Importantly, the groundwork has been done in terms of carrying out the high-throughput genetic study and therefore the way has been paved for follow-up work to be done on the rest of the hits generated from the Bioneer screen.

Upon re-examination of the "saturating" Bioneer screen results, it would have been more appropriate to introduce a second copy of the wild type version of the *pol3* gene, regulated by an *nmt1* promoter (Matsuyama et al., 2008), adjacent to the *pol3* locus containing the *L458P* mutation, in order to avoid recombination between two copies of the same gene. The strain would still include the *PEM-2* genotype and the experiment would still be executed in exactly the same way; the main difference here is that all the double mutants that grow on double selection will also grow on triple selection because wild-type polymerase delta function is still intact. The double mutants from the triple selective media would be replica-pinned onto EMM + thiamine plates to repress the *nmt1* promoter and, essentially, switch off the wild-type *pol3* gene. This creates a conditional growth system whereby "no growth" of haploid double mutants on EMM + thiamine would positively score as synthetic lethality, excluding linked genes. This approach would theoretically overcome the inefficient pin-plating technique of the robot and improve the accuracy of the SGA analysis in this context.

Although the main aim of this experiment was to identify novel SSL interactions, it is plausible to say that there may not be any new SSL interactions associated with the *pol3* mutation in question. Future work involving computational analysis of genetic interaction screens would not only score extreme phenotypes but it would also identify subtle phenotypes. A distinctive feature of classical SGA is that it utilises a binary scoring scheme for phenotype strength (growth vs. no growth) and captures only the extreme cases within a broader spectrum of

interactions (Roguev et al., 2018a). A comprehensive search of all gene combinations, together with measurements, allows quantitative comparison of the degree of buffering (modest phenotypes) (Hartman IV et al., 2001). The results of such a study would not only provide an archive of buffering relationships, but it might expedite the process of elimination by further compressing the list of potential SSL hits from the screen by taking into account problematic strains with high growth variability (Hartman IV et al., 2001; Roguev et al., 2018b). Additional studies examining the subtleties of GIs can be enacted by genome-wide sequencing and microarray analysis of nucleic acids and proteins (Hartman IV et al., 2001).

Chapter 6 General discussion

This study describes the efforts to characterise, for the first time, cancer-associated Pol δ proofreading domain mutations in *S. pombe*. For this purpose, the equivalent yeast mutants were constructed by classical cloning and their mutation rates, as well as GT repeat instability, were measured by fluctuation analyses against wild type (**Chapter 3**). DNA damage sensitivity assays were carried out with the following agents: MMS, bleomycin, CPT, HU, UV and 4-NQO, which are presented in **Chapter 3**. Further characterisation of the two *pol3* exonuclease domain mutations (EDMs) that displayed hypersensitivity to HU was undertaken in **Chapter 4**, namely by studying the cells in the presence of HU using fluorescence microscopy, FACS analysis post cell cycle arrest, viability assays, and undertaking genetic interaction analysis with *mus81* and *cdc22-D57N* mutations. Finally, the *S. pombe* deletion library was systematically crossed with the *pol3L458P* mutant and screened for double mutants displaying no or reduced growth on selective media (**Chapter 5**). The aim was to identify any novel genes which show synthetic sick/lethal (SSL) interactions with a Pol δ EDM. Validation of a selection of putative hits from the screen, using tetrad analysis, is also presented in **Chapter 5**. Preliminary data of Pol δ EDMs in this thesis using the fission yeast model pave the way for future research in this field, ideally using a human cell system, given that approximately 70% of *S. pombe* genes have human orthologues.

6.1 THE POL δ EDMs HAVE INDIVIDUAL PHENOTYPES

The *pol3* EDMs in this study had varying mutation rates and introduction of these mutations did not affect the steady state levels of the Pol3 protein. The somatic *POLD1* D316N (Sp. *pol3D300N*) mutation, which was identified in a highly mutated sporadic gastric cancer (The Cancer Genome Atlas Network, 2014), was predicted to have a very strong mutator phenotype

in *S. pombe*, as shown in the fluctuation analysis. It was expected that the germline variants, *POLD1* P327L, G321S and L474P, would not have hypermutator phenotypes because these germline mutations were found to be largely linked to CRC predisposition in middle-aged patients, and so are tolerated and relatively genetically stable during childhood and young adulthood in affected patients (Jansen et al., 2016; Palles et al., 2018). Interestingly, the sites of these amino acid substitutions in the exonuclease domain are highly conserved among various species. Sp. *pol3L458P* (Hs. *POLD1* L474P) had a moderate mutator phenotype consistent with the idea that the *pol3L458P* variant has impaired but not entirely deficient proofreading ability. Indeed, the less prevalent variants studied here were substantially weaker mutators, such as the *pol3P311L* (Hs. *POLD1* P327L) and *pol3G305S* (Hs. *POLD1* G321S) mutants. Therefore, these mutations appear to be non-mutagenic, particularly under normal conditions.

Data from this study and published studies in yeast confirm that the equivalent somatic *POLE* P286R (Sp. *pol2P287R*) variant, that is strongly associated with EC development (Church et al., 2013), is hypermutating (Kane and Shcherbakova, 2014; Soriano et al., 2021). The rate of mutation exceeded that of the proofreading-inactive Pol ε mutant by one order of magnitude, supporting the hypothesis that this change results in defects that are significantly worse than loss of proofreading per se. Intriguingly, mutation of the equivalent proline to arginine (P311R) in *S. pombe* Pol3/Cdc6 did not prompt a hypermutating phenotype. To reiterate, the *pol3P311L* mutant did not have a mutator phenotype, however, mutation of the analogous proline to leucine in *S. cerevisiae* Pol2 had a substantial mutagenic effect (Hamzaoui et al., 2020). This possibly reflects the unique roles of Pol ε and Pol δ at the replication fork, which is still poorly understood (Johnson et al., 2015). The results show the strikingly different mutagenic effects of the various *POLD1* EDMs using the fission yeast model organism and raise the question of whether these differences might correlate with localisation and cancer penetrance in humans. In summary, my work supports the inclusion of *POLD1* (and probably *POLE*) variants in the

genetic testing panel for familial or sporadic CRC and adenomatous polyposis, and perhaps EC (Taylor et al., 2018; Hamzaoui et al., 2020).

For a more thorough characterisation, in silico structural 3D modelling and in silico mutagenesis using yeast or human Pol δ X-ray crystal protein structure, would elucidate the structural differences and level of protein stability among the *pol3* variants, as described in Hamzaoui et al (2020). Moreover, in vitro replication assays using budding yeast Pol3 would help clarify to what extent the polymerase and proofreading activities are affected in these mutants (Pasero and Gasser, 2002).

The *pol3P311L* and *G305S* mutants had increased sensitivity to hydroxyurea (HU), suggesting that they have problems replicating the DNA when placed under an environment of low dNTP pools. They had normal growth under unstressed circumstances. The rest of the *pol3* variants studied in the thesis showed a high tolerance to various DNA damaging agents. Additionally, the *pol3P311L* and *G305S* EDMs had reduced viability with *rad3* inactivation and physiologically, had an elongated cell phenotype (compared to wild type). This implies that Rad3 is activated in these strains to ensure viability after DNA damage or replication fork problems (e.g. fork stalling) have occurred. The same is not true for the *pol3L458P*, *D300N*, and *D386A* (exonuclease null) mutants which are not Rad3 dependent for survival under normal conditions. The Rad3 checkpoint pathway could still be activated in cells with replicative polymerases lacking exonuclease activity but, in this case, it is not essential for the cells' survival. For future work, it would be interesting to look directly for activation of the Rad3 checkpoint pathway by phosphorylation of the DNA damage and/or replication checkpoint kinases, Chk1 and Cds1, respectively. Perhaps the synthetic sickness between *pol3P311L/G305S* mutations and *rad3* inactivation is correlated with the HU sensitivities observed in these variants, albeit this is not fully understood.

6.2 THE HYDROXYUREA-SENSITIVITIES OF THE *pol3P311L* AND *G305S* STRAINS

In an attempt to understand the effects of HU on the low mutator *pol3* variants, *P311L* and *G305S*, a number of experiments were carried out. Fluorescence microscopy showed that a proportion of *pol3P311L* cells undertook defective mitosis signifying leaky checkpoint arrest, whereas *pol3G305S* cells displayed strong checkpoint activation upon HU induction. Both the *pol3P311L* and, in particular, the *pol3G305S* cells were elongated without HU indicating that the Rad3 checkpoint pathway is partially activated under normal circumstances in these cells. This is in agreement with the observation that these strains were dependent on partial Rad3 activation for viability which is indicative of inherent replicative stress. The *pol3G305S* strain had slow S phase recovery post HU-induced cell cycle block and release, further implying that there is enhanced DNA replication stress, such as fork stalling and collapse, occurring in these cells. *Pol3G305S* also had reduced relative viability in liquid HU consistent with the HU-sensitivity observed on plates. The data was ambiguous for the *pol3P311L* variant: although it was sensitive to HU on solid media, the cells did not appear to die in liquid HU and *P311L* had normal S phase recovery after the release of HU. Nonetheless, a small, yet significant, number of *pol3P311L* cells exhibited aberrant mitosis, unlike the rest of the *pol3* mutants, upon HU treatment. This suggests that the *P311L* variant has slower growth after prolonged exposure to HU (i.e. many hours/days) which was not evident during acute exposure. Deletion of Mus81 did not rescue the HU sensitivities of the *pol3P311L* and *G305S* variants and, in fact, Mus81 is required to assist in fork repair after fork collapse. The results obtained from this study brought about the predicted model described in **Figure 4.15**, explaining why the *pol3P311L* and *G305S* variants are sensitive HU.

Elevation of the dNTP levels (incorporating the *cdc22-D57N* mutation) in the *pol3P311L* and *G305S* cells, partially rescued the HU sensitive phenotype of these cells, suggesting that the

predominant effect of HU in these cells is increased fork stalling caused by a depletion of dNTPs (Lopes et al., 2001). It is not understood why the *pol3L458P*, *cdc22-D57N* double mutant was sensitive to HU, considering it grew relatively well without HU at the permissive temperature. The same strain had attenuated growth at 36˚C with and without HU, partly owing to the slight temperature-sensitivity (ts) observed in *pol3L458P*. What can be inferred from these data is that an increase in dNTP pools is deleterious to the cell fitness of *pol3L458P* under certain conditions, consistent with similar observations in wild-type cells (Chabes et al., 2003; reviewed in Pai and Kearsey, 2017).

In summary, more experiments need to be carried out in order to understand the full biological aspects contributing to the HU sensitivities of the *pol3P311L* and *G305S* variants. There is scope for using HU, alone or with a combination of other drugs, for the treatment of *POLD1* P327L/G321S-driven tumours (Sp. *pol3P311L*/*G305S*, respectively) in the future, however, this is a very preliminary observation that requires much investigation, particularly in human cells.

DNA combing, a single-molecule technique, would be an informative way of studying replication kinetics in the *pol3* EDMs (Iyer et al., 2018). The same technique can be modified to measure fork stalling in vivo (Iyer and Rhind, 2017) Secondly, it would be useful to investigate different aspects of genome stability in the *pol3* EDMs, for example, with the use of the minichromosome, Ch^{16}, a 530 kb chromosome derivative of ChIII, to determine the rate of chromosome loss associated with a variety of misrepair events (Niwa et al., 1986; Antequera and Humphrey, 2017). The frequency of half-sectored colonies (red/white), based on adenine auxotrophy or prototrophy, provides a reasonable estimation of spontaneous-induced minichromosome loss per mitotic cell division which leads to genome/chromosomal instability (Niwa, 2016). This study can be extended to assess the efficiency of double-strand break repair

(DSBR) and homologous recombination (HR) in *S. pombe* by conducting a DSBR assay (Antequera and Humphrey, 2017). This assay, described in Pai et al (2018), can be used to evaluate and quantify a range of repair, misrepair or failed repair outcomes, including gross chromosomal rearrangements (GCR), resulting from a site-specific DSB-induced event generated in the background of the nonessential chromosome, Ch^{16}. Therefore, these techniques provide insight into the mechanism(s) of DSBR in these *pol3* EDM genetic backgrounds for the purposes of biological and medical interests.

6.3 GENOME-WIDE EPISTASIS ANALYSIS SCREENS IN *S. pombe*

For many years, yeast deletion-library screens have been used to comprehend the complex biology underlying sub-cellular systems in the form of temperature-sensitive, synthetic genetic interaction (positive or negative) or over-expression screens (Roguev et al., 2008; Li et al., 2011; Douglas et al., 2012; Guenole et al., 2013). The study presented here made efforts to further extend the cohort of known genes related to the function of or involved in the biological pathways of Pol δ by studying synthetic lethality. Differential synthetic lethal interactions may serve a purpose in the ‘‘synthetic-lethal’’ approach to cancer therapy (Jackson and Bartek, 2009). *Pol3 L458P* was crossed with the Bioneer deletion library because the human equivalent mutation, *POLD1* L474P, has high-penetrance in tumours and is one of the most common cancer-associated *POLD1* germline variants found to date (Valle, 2014; Bellido et al., 2016; Rayner et al., 2016). Unfortunately, the aim of the study was not achieved mainly because the screen was limited by a number of factors and, so, it was not entirely exhaustive. However, two known synthetic lethal interactions were identified from the screen and confirmed by tetrad analysis, namely *fen-1* and *msh6*, as well as *mlh1* and *msh2*, providing some validity to using this well-documented approach (Roguev et al., 2007, 2018c). Furthermore, the disadvantage of

working with the deletion library is that only non-essential genes were assessed, excluding all potential players in DNA replication and repair with essential functions for cell survival.

Follow-up work would include confirming more hits via tetrad dissection and improving methods, for example, by using computer analysis or repeating some of the Bioneer crosses to narrow down the list of SSL hits yielded from the Bioneer screen since they are mostly false positive results.

Overall, the results of this study illustrate the complexity of Pol δ EDMs and their unique responses to DNA damage and replication stress, justifying the efforts of this and similar studies.

References

Abraham, R.T. 2001. Cell cycle checkpoint signaling through the ATR and ATM kinases. *Genes Dev.* 15:2177–2196.

Adzhubei, I.A., S. Schmidt, L. Peshkin, V.E. Ramensky, A. Gerasimova, P. Bork, A.S. Kondrashov, and S.R. Sunyaev. 2010. A method and server for predicting damaging missense mutations. *Nat. Methods*. 7:248–249.

Ahn, J.S., F. Osman, and M.C. Whitby. 2005. Replication fork blockage by RTS1 at an ectopic site promotes recombination in fission yeast. *EMBO J.* 24:2011–2023.

Aksenova, A., K. Volkov, J. Maceluch, Z.F. Pursell, I.B. Rogozin, T.A. Kunkel, Y.I. Pavlov, and E. Johansson. 2010. Mismatch repair-independent increase in spontaneous mutagenesis in yeast lacking non-essential subunits of DNA polymerase ε. *PLoS Genet.* 6:1–11.

Al-khodairy, F., and A.M. Carr. 1992. DNA repair mutants defining G2 checkpoint pathways in Schizosaccharomyces pombe. *EMBO J.* 11:1343–1350.

Albertson, T.M., M. Ogawa, J.M. Bugni, L.E. Hays, C. Yang, Y. Wang, P.M. Treuting, J.A. Heddle, R.E. Goldsby, and B.D. Preston. 2009. DNA polymerase ε and δ proofreading suppress discrete mutator and cancer phenotypes in mice. *Proc. Natl. Acad. Sci. U. S. A.* 106:17101–17104.

Alcasabas, A.A., A.J. Osborn, J. Bachant, F. Hu, P.J.H. Werler, K. Bousset, K. Furuya, J.F.X. Diffley, A.M. Carr, and S.J. Elledge. 2001. Mrc1 transduces signals of DNA replication stress to activate Rad53. *Nat. Cell Biol.* 3:958–965.

Alexandrov, L.B., J. Kim, N.J. Haradhvala, M.N. Huang, A.W. Tian Ng, Y. Wu, A. Boot, K.R. Covington, D.A. Gordenin, E.N. Bergstrom, S.A. Islam, N. Lopez-Bigas, L.J. Klimczak, J.R. McPherson, S. Morganella, R. Sabarinathan, D.A. Wheeler, V. Mustonen, G. Getz, S.G. Rozen, and M.R. Stratton. 2020. The repertoire of mutational signatures in human cancer. *Nature*. 578:94–101.

Antequera, F., and T.C. Humphrey. 2017. Analysis of DNA metabolism in fission yeast. *Cold Spring Harb. Protoc.* July:239–244.

Arroyo, M.P., K.M. Downey, A.G. So, and T.S. Wangt. 1996. Schizosaccharomyces pombe proliferating cell nuclear antigen mutations affect DNA polymerase δ processivity. *J. Biol. Chem.* 271:15971–15980.

Aye, Y., M. Li, M. Long, and R. Weiss. 2015. Ribonucleotide reductase and cancer: biological mechanisms and targeted therapies. *Oncogene*. 34:2011–2021.

Bahler, J., J.-Q. Wu, M.S. Longtine, N.G. Shah, A. McKenzie III, A.B. Steever, A. Wach, P. Philippsen, and J.R. Pringle. 1998. Heterologous modules for efficient and versatile PCR-based gene targeting in Schizosaccharomyces pombe. *Yeast*. 14:943–951.

Bailleul, B., S. Galiégue, and M.-H. Loucheux-Lefebvre. 1981. Adducts from the reaction of O,O'-diacetyl or O-acetyl derivatives of the carcinogen 4-hydroxyaminoquinoline 1-oxide with purine nucleosides. *Cancer Res.* 41:4559–4565.

Bambara, R.A., R.S. Murante, and L.A. Henricksen. 1997. Enzymes and reactions at the eukaryotic DNA replication fork. *J. Biol. Chem.* 272:4647–4650.

Barbari, S.R., D.P. Kane, E.A. Moore, and P. V Shcherbakova. 2018. Functional analysis of cancer-associated DNA polymerase ε variants in Saccharomyces cerevisiae. *Genes, Genomes, Genet.* 8:1019–1029.

Barbari, S.R., and P. V Shcherbakova. 2017. Replicative DNA polymerase defects in human cancers:

Consequences, mechanisms, and implications for therapy. *DNA Repair (Amst)*. 56:16–25.

Bebenek, K., and T.A. Kunkel. 2004. Functions of DNA polymerases. *In* Advances in Protein Chemistry. Elsevier Ltd. 137–165.

Bellido, F., M. Pineda, G. Aiza, R. Valdés-Mas, M. Navarro, D.A. Puente, T. Pons, S. González, S. Iglesias, E. Darder, V. Piñol, J.L. Soto, A. Valencia, I. Blanco, M. Urioste, J. Brunet, C. Lázaro, G. Capellá, X.S. Puente, and L. Valle. 2016. POLE and POLD1 mutations in 529 kindred with familial colorectal cancer and/or polyposis: review of reported cases and recommendations for genetic testing and surveillance. *Genet. Med.* 18:325–332.

Bentley, N.J., D.A. Holtzman, G. Flaggs, K.S. Keegan, A. Demaggio, J.C. Ford, M. Hoekstra, and A.M. Carr. 1996. The Schizosaccharomyces pombe rad3 checkpoint gene. *EMBO J.* 15:6641–6651.

Bernad, A., L. Blanco, J.M. Lázaro, G. Martín, and M. Salas. 1989. A conserved 3′→5′ exonuclease active site in prokaryotic and eukaryotic DNA polymerases. *Cell*. 59:219–228.

Bianchi, V., E. Pontis, and P. Reichard. 1986. Changes of deoxyribonucleoside triphosphate pools induced by hydroxyurea and their relation to DNA synthesis. *J. Biol. Chem.* 261:16037–16042.

Billingsley, C.C., D.E. Cohn, D.G. Mutch, J.A. Stephens, A.A. Suarez, and P.J. Goodfellow. 2014. Polymerase ε (POLE) mutations in endometrial cancer: Clinical outcomes and implications for Lynch syndrome testing. *Cancer*. 121:386–394.

Blank, A., B. Kim, and L.A. Loeb. 1994. DNA polymerase δ is required for base excision repair of DNA methylation damage in Saccharomyces cerevisiae. *Proc. Natl. Acad. Sci. U. S. A.* 91:9047–9051.

Boddy, M.N., A. Lopez-Girona, P. Shanahan, H. Interthal, W.-D. Heyer, and P. Russell. 2000. Damage tolerance protein Mus81 associates with the FHA1 domain of checkpoint kinase Cds1. *Mol. Cell. Biol.* 20:8758–8766.

Bonfils, S., A.E. Rozalén, G.R. Smith, S. Moreno, and C. Martín-Castellanos. 2011. Functional interactions of Rec24, the fission yeast ortholog of mouse Mei4, with the meiotic recombination-initiation complex. *J. Cell Sci.* 124:1328–1338.

Boye, E., H.C. Skjolberg, and B. Grallert. 2009. Methods in molecular biology, DNA replication. Chapter 4: Checkpoint regulation of DNA replication. S. Vengrova and J.Z. Dalgaard, editors. Humana Press, a part of Springer Science + Business Media. 55–70 pp.

Bressan, D.A., B.K. Baxter, and J.H. Petrini. 1999. The Mre11-Rad50-Xrs2 protein complex facilitates homologous recombination-based double-strand break repair in Saccharomyces cerevisiae. *Mol. Cell. Biol.* 19:7681–7687.

Briggs, S., and I. Tomlinson. 2013. Germline and somatic polymerase ε and δ mutations define a new class of hypermutated colorectal and endometrial cancers. *J. Pathol.* 230:148–53.

Brown, E., and D. Baltimore. 2003. Essential and dispensable roles of ATR in cell cycle arrest and genome maintenance. *Genes Dev.* 17:615–628.

Brown, E.J., and D. Baltimore. 2000. ATR disruption leads to chromosomal fragmentation and early embryonic lethality. *Genes Dev.* 14:397–402.

Bulock, C.R., X. Xing, and P. V Shcherbakova. 2020a. DNA polymerase δ proofreads errors made by DNA polymerase ϵ. *Proc. Natl. Acad. Sci. U. S. A.* 117:6035–6041.

Bulock, C.R., X. Xing, and P. V Shcherbakova. 2020b. Mismatch repair and DNA polymerase δ proofreading prevent catastrophic accumulation of leading strand errors in cells expressing a cancer-associated DNA polymerase ϵ variant. *Nucleic Acids Res.* 48:9124–9134.

Burgers, P.M. 1991. Saccharomyces cerevisiae replication factor C. II. Formation and activity of complexes with the proliferating cell nuclear antigen and with DNA polymerases δ and ε. *J. Biol.*

Chem. 266:22698–22706.

Byun, T.S., M. Pacek, M. Yee, J.C. Walter, and K.A. Cimprich. 2005. Functional uncoupling of MCM helicase and DNA polymerase activities activates the ATR-dependent checkpoint. *Genes Dev.* 19:1040–1052.

Cantor, R.M. 2019. Analysis of genetic linkage. *In* Emery and Rimoin's Principles and Practice of Medical Genetics and Genomics: Foundations. R.E. Pyeritz, B.R. Korf, and W.W. Grody, editors. Elsevier Inc. 227–236.

Caras, I.W., and D.W. Martin JR. 1988. Molecular cloning of the cDNA for a mutant mouse ribonucleotide reductase M1 that produces a dominant mutator phenotype in mammalian cells. *Mol. Cell. Biol.* 8:2698–2704.

Carlson, C.R., B. Grallert, R. Bernander, T. Stokke, and E. Boye. 1997. Measurement of nuclear DNA content in fission yeast by flow cytometry. *Yeast*. 1335:1329–1335.

Caspari, T., and A.M. Carr. 2002. Checkpoints: How to flag up double-strand breaks. *Curr. Biol.* 12:105–107.

Caspari, T., M. Dahlen, G. Kanter-Smoler, H.D. Lindsay, K. Hofmann, K. Papadimitriou, P. Sunnerhagen, and A.M. Carr. 2000. Characterization of Schizosaccharomyces pombe Hus1: a PCNA-related protein that associates with Rad1 and Rad9. *Mol. Cell. Biol.* 74:1254–1262.

Chabes, A., B. Georgieva, V. Domkin, X. Zhao, R. Rothstein, and L. Thelander. 2003. Survival of DNA damage in yeast directly depends on increased dNTP levels allowed by relaxed feedback inhibition of ribonucleotide reductase. *Cell*. 112:391–401.

Chabes, A., and B. Stillman. 2007. Constitutively high dNTP concentration inhibits cell cycle progression and the DNA damage checkpoint in yeast Saccharomyces cerevisiae. *Proc. Natl. Acad. Sci. U. S. A.* 104:1183–1188.

Chahwan, C., T.M. Nakamura, S. Sivakumar, P. Russell, and N. Rhind. 2003. The fission yeast Rad32 (Mre11)-Rad50-Nbs1 complex is required for the S-phase DNA damage checkpoint. *Mol. Cell. Biol.* 23:6564–6573.

Chen, J., and J.A. Stubbe. 2005. Bleomycins: Towards better therapeutics. *Nat. Rev. Cancer*. 5:102–112.

Chen, X.-B., R. Melchionna, C.-M. Denis, P.-H.L. Gaillard, A. Blasina, I. Van De Weyer, M.N. Boddy, P. Russell, J. Vialard, and C.H. McGowan. 2001. Human Mus81-associated endonuclease cleaves holliday junctions in vitro. *Mol. Cell*. 8:1117–1127.

Chini, C.C., and J. Chen. 2003. Human claspin is required for replication checkpoint control. *J. Biol. Chem.* 278:30057–30062.

Christmann, M., M.T. Tomicic, W.P. Roos, and B. Kaina. 2003. Mechanisms of human DNA repair: an update. *Toxicology*. 193:3–34.

Chubb, D., P. Broderick, M. Frampton, B. Kinnersley, A. Sherborne, S. Penegar, A. Lloyd, Y.P. Ma, S.E. Dobbins, and R.S. Houlston. 2015. Genetic diagnosis of high-penetrance susceptibility for colorectal cancer (CRC) is achievable for a high proportion of familial CRC by exome sequencing. *J. Clin. Oncol.* 33:426–432.

Church, D.N., S.E.W. Briggs, C. Palles, E. Domingo, S.J. Kearsey, J.M. Grimes, M. Gorman, L. Martin, K.M. Howarth, S. V Hodgson, K. Kaur, J. Taylor, and I.P.M. Tomlinson. 2013. DNA polymerase ε and δ exonuclease domain mutations in endometrial cancer. *Hum. Mol. Genet.* 22:2820–8.

Church, D.N., E. Stelloo, R.A. Nout, N. Valtcheva, J. Depreeuw, N. Ter Haar, A. Noske, F. Amant, I.P.M. Tomlinson, P.J. Wild, D. Lambrechts, I.M. Jürgenliemk-Schulz, J.J. Jobsen, V.T.H.B.M. Smit, C.L. Creutzberg, and T. Bosse. 2015. Prognostic significance of POLE proofreading

mutations in endometrial cancer. *J. Natl. Cancer Inst.* 107:1–8.

Ciccia, A., A. Constantinou, and S.C. West. 2003. Identification and characterization of the human Mus81-Eme1 endonuclease. *J. Biol. Chem.* 278:25172–25178.

Cobb, J.A., L. Bjergbaek, K. Shimada, C. Frei, and S.M. Gasser. 2003. DNA polymerase stabilization at stalled replication forks requires Mec1 and the RecQ helicase Sgs1. *EMBO J.* 22:4325–4336.

Cobb, J.A., T. Schleker, V. Rojas, L. Bjergbaek, J.A. Tercero, and S.M. Gasser. 2005. Replisome instability, fork collapse, and gross chromosomal rearrangements arise synergistically from Mec1 kinase and RecQ helicase mutations. *Genes Dev.* 19:3055–3069.

Collins, S.R., A. Roguev, and N.J. Krogan. 2010. Quantitative genetic interaction mapping using the E-MAP approach. *Methods Enzymol.* 470:205–231.

Collins, S.R., M. Schuldiner, N.J. Krogan, and J.S. Weissman. 2006. A strategy for extracting and analyzing large-scale quantitative epistatic interaction data. *Genome Biol.* 7:1–14.

Connelly, J.C., and D.R. Leach. 2002. Tethering on the brink: the evolutionarily conserved Mre11-Rad50 complex. *Trends Biochem. Sci.* 27:410–418.

Constantinou, A., M. Tarsounas, J.K. Karow, R.M. Brosh, V.A. Bohr, I.D. Hickson, and S.C. West. 2000. Werner's syndrome protein (WRN) migrates Holliday junctions and co-localizes with RPA upon replication arrest. *EMBO Rep.* 1:80–84.

Cortez, D. 2005. Unwind and slow down: checkpoint activation by helicase and polymerase uncoupling. *Genes Dev.* 19:1007–1012.

Cortez, D., S. Guntuku, J. Qin, and S.J. Elledge. 2001. ATR and ATRIP: Partners in checkpoint signaling. *Science.* 294:1713–1716.

Costantino, L., S.K. Sotiriou, J.K. Rantala, S. Magin, E. Mladenov, T. Helleday, J.E. Haber, G. Iliakis, O.P. Kallioniemi, and T.D. Halazonetis. 2014. Break-induced replication repair of damaged forks induces genomic duplications in human cells. *Science.* 343:88–91.

Cotta-Ramusino, C., D. Fachinetti, C. Lucca, Y. Doksani, M. Lopes, J. Sogo, and M. Foiani. 2005. Exo1 processes stalled replication forks and counteracts fork reversal in checkpoint-defective cells. *Mol. Cell*. 17:153–159.

Cotterill, S., and S. Kearsey. 2009. Eukaryotic DNA polymerases. *Encycl. Life Sci.* 1–8.

D'Amours, D., and S.P. Jackson. 2001. The yeast Xrs2 complex functions in S phase checkpoint regulation. *Genes Dev.* 15:2238–2249.

D'Amours, D., and S.P. Jackson. 2002. The Mre11 complex: At the crossroads of DNA repair and checkpoint signalling. *Nat. Rev. Mol. Cell Biol.* 3:317–327.

Daigaku, Y., T.J. Etheridge, Y. Nakazawa, M. Nakayama, A.T. Watson, I. Miyabe, T. Ogi, M.A. Osborne, A.M. Carr, and A.M. Carr. 2017. PCNA ubiquitylation ensures timely completion of unperturbed DNA replication in fission yeast. *PLoS Genet.* 13:1–21.

Daigaku, Y., A. Keszthelyi, C.A. Müller, I. Miyabe, T. Brooks, R. Retkute, M. Hubank, C.A. Nieduszynski, and A.M. Carr. 2015. A global profile of replicative polymerase usage. *Nat. Struct. Mol. Biol.* 22:192–198.

Datta, A., J.L. Schmeits, N.S. Amin, P.J. Lau, K. Myung, and R.D. Kolodner. 2000. Checkpoint-dependent activation of mutagenic repair in Saccharomyces cerevisiae pol3-01 mutants. *Mol. Cell*. 6:593–603.

Davidson, M.B., Y. Katou, A. Keszthelyi, T.L. Sing, T. Xia, J. Ou, J.A. Vaisica, N. Thevakumaran, L. Marjavaara, C.L. Myers, A. Chabes, K. Shirahige, and G.W. Brown. 2012. Endogenous DNA

replication stress results in expansion of dNTP pools and a mutator phenotype. *EMBO J.* 31:895–907.

Davies, A.A., D. Huttner, Y. Daigaku, S. Chen, and H.D. Ulrich. 2008. Activation of ubiquitin-dependent DNA damage bypass is mediated by Replication Protein A. *Mol. Cell*. 29:625–636.

Davies, B.W., M.A. Kohanski, L.A. Simmons, J.A. Winkler, J.J. Collins, and G.C. Walker. 2009. Hydroxyurea induces hydroxyl radical-mediated cell death in Escherichia coli. *Mol. Cell*. 36:845–860.

De la Chapelle, A. 2004. Genetic predisposition to colorectal cancer. *Nat. Rev. Cancer*. 4:769–80.

Deegan, T.D., J.T. Yeeles, and J.F. Diffley. 2016. Phosphopeptide binding by Sld3 links Dbf4-dependent kinase to MCM replicative helicase activation. *EMBO J.* 35:961–973.

Diffley, J.F. 2011. Quality control in the initiation of eukaryotic DNA replication. *Philos. Trans. R. Soc. B Biol. Sci.* 366:3545–3553.

Din, S., S.J. Brill, M.P. Fairman, and B. Stillman. 1990. Cell-cycle-regulated phosphorylation of DNA replication factor A from human and yeast cells. *Genes Dev.* 4:968–977.

Doe, C.L., J.S. Ahn, J. Dixon, and M.C. Whitby. 2002. Mus81-Eme1 and Rqh1 involvement in processing stalled and collapsed replication forks. *J. Biol. Chem.* 277:32753–32759.

Doe, C.L., J. Dixon, F. Osman, and M.C. Whitby. 2000. Partial suppression of the fission yeast rqh1-phenotype by expression of a bacterial Holliday junction resolvase. *EMBO J.* 19:2751–2762.

Domingo, E., L. Freeman-Mills, E. Rayner, M. Glaire, S. Briggs, L. Vermeulen, E. Fessler, J.P. Medema, A. Boot, H. Morreau, T. van Wezel, G.J. Liefers, R.A. Lothe, S.A. Danielsen, A. Sveen, A. Nesbakken, I. Zlobec, A. Lugli, V.H. Koelzer, M.D. Berger, S. Castellví-Bel, J. Muñoz, M. de Bruyn, H.W. Nijman, M. Novelli, K. Lawson, D. Oukrif, E. Frangou, P. Dutton, S. Tejpar, M. Delorenzi, R. Kerr, D. Kerr, I. Tomlinson, and D.N. Church. 2016. Somatic POLE proofreading domain mutation, immune response, and prognosis in colorectal cancer: a retrospective, pooled biomarker study. *Lancet Gastroenterol. Hepatol.* 1:207–216.

Donehower, L. a, C.J. Creighton, N. Schultz, E. Shinbrot, K. Chang, P.H. Gunaratne, D. Muzny, C. Sander, S.R. Hamilton, R. a Gibbs, and D. Wheeler. 2013. MLH1-silenced and non-silenced subgroups of hypermutated colorectal carcinomas have distinct mutational landscapes. *J. Pathol.* 229:99–110.

Douglas, A.C., A.M. Smith, S. Sharifpoor, Z. Yan, T. Durbic, L.E. Heisler, A.Y. Lee, O. Ryan, H. Göttert, A. Surendra, D. Van Dyk, G. Giaever, C. Boone, C. Nislow, and B.J. Andrews. 2012. Functional analysis with a barcoder yeast gene overexpression system. *Genes, Genomes, Genet.* 2:1279–1289.

Dovey, C.L., A. Aslanian, S. Sofueva, J.R. Yates III, and P. Russell. 2009. Mms1-Mms22 complex protects genome integrity in Schizosaccharomyces pombe. *DNA Repair (Amst).* 8:1390–1399.

Dua, R., D.L. Levy, and J.L. Campbell. 1998. Role of the putative zinc finger domain of Saccharomyces cerevisiae DNA polymerase in DNA replication and the S/M checkpoint pathway. *J. Biol. Chem.* 273:30046–30055.

Dua, R., D.L. Levy, and J.L. Campbell. 1999. Analysis of the essential functions of the C-terminal protein/protein interaction domain of Saccharomyces cerevisiae pol ε and its unexpected ability to support growth in the absence of the DNA polymerase domain. *J. Biol. Chem.* 274:22283–22288.

Edwards, R.J., N.J. Bentley, and A.M. Carr. 1999. A Rad3-Rad26 complex responds to DNA damage independently of other checkpoint proteins. *Nat. Cell Biol.* 1:393–398.

Egel, R. 1971. Physiological aspects of conjugation in fission yeast. *Planta*. 98:89–96.

Ekwall, K., and G. Thon. 2017a. Genetic analysis of Schizosaccharomyces pombe. *Cold Spring Harb. Protoc.* 593–605.

Ekwall, K., and G. Thon. 2017b. Spore analysis and tetrad dissection of Schizosaccharomyces pombe. *Cold Spring Harb. Protoc.* 541–544.

Elsayed, F.A., C.M. Kets, D. Ruano, B. Van Den Akker, A.R. Mensenkamp, M. Schrumpf, M. Nielsen, J.T. Wijnen, C.M. Tops, M.J. Ligtenberg, H.F.A. Vasen, F.J. Hes, H. Morreau, and T. Van Wezel. 2015. Germline variants in POLE are associated with early onset mismatch repair deficient colorectal cancer. *Eur. J. Hum. Genet.* 23:1080–1084.

Enoch, T., A.M. Carr, and P. Nurse. 1992. Fission yeast genes involved in coupling mitosis to completion of DNA replication. *Genes Dev.* 6:2035–2046.

Enoch, T., and P. Nurse. 1990. Mutation of fission yeast cell cycle control genes abolishes dependence of mitosis on DNA replication. *Cell*. 60:665–673.

Escorcia, W., and S.L. Forsburg. 2018. Tetrad dissection in fission yeast. *In* Schizosaccharomyces pombe. Methods in Molecular Biology. T.L. Singleton, editor. Humana Press, New York. 179–187.

Fadden, A.J., S. Schalbetter, M. Bowles, R. Harris, J. Lally, A.M. Carr, and N.Q. McDonald. 2013. A winged helix domain in human MUS81 binds DNA and modulates the endonuclease activity of MUS81 complexes. *Nucleic Acids Res.* 41:9741–9752.

Falck, J., J. Coates, and S.P. Jackson. 2005. Conserved modes of recruitment of ATM, ATR and DNA-PKcs to sites of DNA damage. *Nature*. 434:605–611.

Falck, J., J.H. Petrini, B.R. Williams, J. Lukas, and J. Bartek. 2002. The DNA damage-dependent intra-S phase checkpoint is regulated by parallel pathways. *Nat. Genet.* 30:290–294.

Fantes, P., and J. Creanor. 1984. Canavanine resistance and the mechanism of arginine uptake in the fission yeast Schizosaccharomyces pombe. *J. Gen. Microbiol.* 130:3265–3273.

Fei, L., R. Martienssen, and W.Z. Cande. 2012. Coordination of DNA replication and histone modification by Rik1-Dos2 complex. *Nature*. 475:244–248.

Ferlay, J., H.-R. Shin, F. Bray, D. Forman, C. Mathers, and D.M. Parkin. 2010. Estimates of worldwide burden of cancer in 2008: GLOBOCAN 2008. *Int. J. Cancer*. 127:2893–917.

Fishel, R., M.K. Lescoe, M.R.S. Rao, N.G. Copeland, N.A. Jenkins, J. Garber, M. Kane, and R. Kolodner. 1993. The human mutator gene homolog MSH2 and its association with hereditary nonpolyposis colon cancer. *Cell*. 75:1027–1038.

Fleck, O., R. Vejrup-Hansen, A. Watson, A.M. Carr, O. Nielsen, and C. Holmberg. 2013. Spd1 accumulation causes genome instability independently of ribonucleotide reductase activity but functions to protect the genome when deoxynucleotide pools are elevated. *J. Cell Sci.* 126:4985–4994.

Flood, C.L., G.P. Rodriguez, G. Bao, A.H. Shockley, Y.W. Kow, and G.F. Crouse. 2015. Replicative DNA polymerase δ but not ε proofreads errors in cis and in trans. *PLoS Genet.* 11:1–32.

Forsburg, S.L. 2003. Growth and manipulation of S. pombe. *Curr. Protoc. Mol. Biol.* 64:1–17.

Fortune, J.M., Y.I. Pavlov, C.M. Welch, E. Johansson, P.M.J. Burgers, and T.A. Kunkel. 2005. Saccharomyces cerevisiae DNA Polymerase δ: High fidelity for base substitutions but lower fidelity for single-and multi-base deletions. *J. Biol. Chem.* 280:29980–29987.

Foster, P.L. 2006. Methods for determining spontaneous mutation rates. *Methods Enzymol.* 409:195–213.

Franchitto, A., L.M. Pirzio, E. Prosperi, S. Orazio, M. Bignami, and P. Pichierri. 2008. Replication fork stalling in WRN-deficient cells is overcome by prompt activation of a MUS81-dependent pathway. *J. Cell Biol.* 183:241–252.

Friedberg, E., G. Walker, and W. Siede. 1995. DNA Repair and Mutagenesis. ASM Press, Washington DC.

Friedel, A.M., B.L. Pike, and S.M. Gasser. 2009. ATR/Mec1: coordinating fork stability and repair. *Curr. Opin. Cell Biol.* 21:237–244.

Froget, B., S. Lambert, and G. Baldacci. 2008. Cleavage of stalled forks by fission yeast Mus81/Eme1 in absence of DNA replication checkpoint. *Mol. Biol. Cell*. 19:445–456.

Fugger, K., W.K. Chu, P. Haahr, A.N. Kousholt, H. Beck, M.J. Payne, K. Hanada, I.D. Hickson, and C.S. Sørensen. 2013. FBH1 co-operates with MUS81 in inducing DNA double-strand breaks and cell death following replication stress. *Nat. Commun.* 4:1–8.

Fukui, K. 2010. DNA mismatch repair in eukaryotes and bacteria. *J. Nucleic Acids*. 2010:1–16.

Furnari, B., A. Blasina, M.N. Boddy, C.H. McGowan, and P. Russell. 1999. Cdc25 inhibited in vivo and in vitro by checkpoint kinases Cds1 and Chk1. *Mol. Biol. Cell*. 10:833–845.

Furnari, B., N. Rhind, and P. Russell. 1997. Cdc25 mitotic inducer targeted by Chk1 DNA damage checkpoint kinase. *Science*. 277:1495–1497.

Furuya, K., and A.M. Carr. 2003. DNA checkpoints in fission yeast. *J. Cell Sci.* 116:3847–3848.

Gan, G.N., J.P. Wittschieben, B. Wittschieben, and R.D. Wood. 2008. DNA polymerase zeta (pol) in higher eukaryotes. *Cell Res.* 18:174–183.

Ganai, R.A., G.O. Bylund, and E. Johansson. 2014. Switching between polymerase and exonuclease sites in DNA polymerase ε. *Nucleic Acids Res.* 1–11.

Ganai, R.A., and E. Johansson. 2016. DNA replication - A matter of fidelity. *Mol. Cell*. 62:745–755.

Garbacz, M., H. Araki, K. Flis, A. Bebenek, A.E. Zawada, P. Jonczyk, K. Makiela-Dzbenska, and I.J. Fijalkowska. 2015. Fidelity consequences of the impaired interaction between DNA polymerase epsilon and the GINS complex. *DNA Repair (Amst).* 29:23–35.

Garg, P., and P.M. Burgers. 2005. DNA polymerases that propagate the eukaryotic DNA replication fork. *Crit. Rev. Biochem. Mol. Biol.* 40:115–28.

Garg, P., C.M. Stith, N. Sabouri, E. Johansson, and P.M. Burgers. 2004. Idling by DNA polymerase delta maintains a ligatable nick during lagging-strand DNA replication. *Genes Dev.* 18:2764–73.

Gary, R., M.S. Park, J.P. Nolan, H.L. Cornelius, O.G. Kozyreva, H.T. Tran, K.S. Lobachev, M.A. Resnick, and D.A. Gordenin. 1999. A novel role in DNA metabolism for the binding of Fen1/Rad27 to PCNA and implications for genetic risk. *Mol. Cell. Biol.* 19:5373–5382.

Georgescu, R.E., G.D. Schauer, N.Y. Yao, L.D. Langston, O. Yurieva, D. Zhang, J. Finkelstein, and M.E. O'Donnell. 2015. Reconstitution of a eukaryotic replisome reveals suppression mechanisms that define leading/lagging strand operation. *Elife*. 2015:1–20.

Goldsby, R.E., L.E. Hays, X. Chen, E.A. Olmsted, W.B. Slayton, G.J. Spangrude, and B.D. Preston. 2002. High incidence of epithelial cancers in mice deficient for DNA polymerase δ proofreading. *Proc. Natl. Acad. Sci. U. S. A.* 99:15560–15565.

Goldsby, R.E., N.A. Lawrence, L.E. Hays, E.A. Olmsted, X. Chen, M. Singh, and B.D. Preston. 2001. Defective DNA polymerase-δ proofreading causes cancer. *Nat. Med.* 7:638–639.

Gong, J., C. Wang, P.P. Lee, P. Chu, and M. Fakih. 2017. Response to PD-1 blockade in microsatellite stable metastatic colorectal cancer harboring a POLE mutation. *J. Natl. Compr. Cancer Netw.*

15:142–147.

Greene, C.N., and S. Jinks-Robertson. 1997. Frameshift intermediates in homopolymer runs are removed efficiently by yeast mismatch repair proteins. *Mol. Cell. Biol.* 17:2844–2850.

Grenon, M., C. Gilbert, and N.F. Lowndes. 2001. Checkpoint activation in response to double-strand breaks requires the Mre11/Rad50/Xrs2 complex. *Nat. Cell Biol.* 3:844–847.

Guenole, A., R. Srivas, K. Vreeken, Z.Z. Wang, S. Wang, N.J. Krogan, T. Ideker, and H. Van Attikum. 2013. Dissection of DNA damage responses using multiconditional genetic interaction maps. *Mol. Cell*. 49:346–358.

Haber, J.E. 1998. The many interfaces of Mre11. *Cell*. 95:583–586.

Hamada, H., M.G. Petrino, and T. Kakunaga. 1982. A novel repeated element with Z-DNA-forming potential is widely found in evolutionarily diverse eukaryotic genomes. *Proc. Natl. Acad. Sci. U. S. A.* 79:6465–6469.

Hamatake, R.K., H. Hasegawa, A.B. Clark, K. Bebenek, T.A. Kunkel, and A. Sugino. 1990. Purification and characterization of DNA polymerase II from the yeast Saccharomyces cerevisiae. Identification of the catalytic core and a possible holoenzyme form of the enzyme. *J. Biol. Chem.* 265:4072–4083.

Hamzaoui, N., F. Alarcon, N. Leulliot, R. Guimbaud, B. Buecher, C. Colas, C. Corsini, G. Nuel, B. Terris, P. Laurent-Puig, S. Chaussade, M. Dhooge, C. Madru, and E. Clauser. 2020. Genetic, structural, and functional characterization of POLE polymerase proofreading variants allows cancer risk prediction. *Genet. Med.* 22:1533–1541.

Hanada, K., M. Budzowska, S.L. Davies, E. Van Drunen, H. Onizawa, H.B. Beverloo, A. Maas, J. Essers, I.D. Hickson, and R. Kanaar. 2007. The structure-specific endonuclease Mus81 contributes to replication restart by generating double-strand DNA breaks. *Nat. Struct. Mol. Biol.* 14:1096–1104.

Hanahan, D., and R.A. Weinberg. 2000. The hallmarks of cancer. *Cell*. 100:57–70.

Hanahan, D., and R.A. Weinberg. 2011. Hallmarks of cancer: the next generation. *Cell*. 144:646–74.

Hannah, J., and P. Zhou. 2009. Regulation of DNA damage response pathways by the cullin-RING ubiquitin ligases. *DNA Repair (Amst).* 8:536–543.

Hardy, C.F. 1996. Characterization of an essential Orc2p-associated factor that plays a role in DNA replication. *Mol. Cell. Biol.* 16:1832–1841.

Harfe, B.D., and S. Jinks-Robertson. 2000. Sequence composition and context effects on the generation and repair of frameshift intermediates in mononucleotide runs in Saccharomyces cerevisiae. *Genet. Soc. Am.* 156:571–578.

Harper, J.W., and S.J. Elledge. 2007. The DNA damage response: Ten years after. *Mol. Cell*. 28:739–745.

Harrison, J.C., and J.E. Haber. 2006. Surviving the breakup: The DNA damage checkpoint. *Annu. Rev. Genet.* 40:209–235.

Hartman IV, J.L., B. Garvik, and L. Hartwell. 2001. Principles for the buffering of genetic variation. *Science.* 291:1001–1004.

Hartwell, L.H., P. Szankasi, C.J. Roberts, A.W. Murray, and S.H. Friend. 1997. Integrating genetic approaches into the discovery of anticancer drugs. *Science*. 278:1064–1068.

Hartwell, L.H., and T.A. Weinert. 1989. Checkpoints: controls that ensure the order of cell cycle events. *Science.* 246:629–634.

Hayles, J., and P. Nurse. 2016. Introduction to fission yeast as a model system. *In* Fission Yeast: A Laboratory Manual. A.M. Carr, A. Grallert, I. Hagan, and P. Nurse, editors. Cold Spring Harbor Laboratory Press, New York.

Heitzer, E., and I. Tomlinson. 2014. Replicative DNA polymerase mutations in cancer. *Curr. Opin. Genet. Dev.* 24:107–13.

Henninger, E.E., and Z.F. Pursell. 2014. DNA polymerase ε and its roles in genome stability. *IUBMB Life*. 66:339–351.

Herr, A.J., S.R. Kennedy, G.M. Knowels, E.M. Schultz, and B.D. Preston. 2014. DNA replication error-induced extinction of diploid yeast. *Genetics*. 196:677–691.

Herr, A.J., M. Ogawa, N.A. Lawrence, L.N. Williams, J.M. Eggington, M. Singh, R.A. Smith, and B.D. Preston. 2011. Mutator suppression and escape from replication error-induced extinction in yeast. *PLoS Genet.* 7:1–16.

Heyer, J., K. Yang, M. Lipkin, W. Edelmann, and R. Kucherlapati. 1999. Mouse models for colorectal cancer. *Oncogene*. 18:5325–5333.

Heyer, W.-D., M.R. Rao, L.F.E. Erdile, T.J. Kelly, and R.D. Kolodner. 1990. An essential Saccharomyces cerevisiae single-stranded DNA binding protein is homologous to the large subunit of human RP-A. *EMBO J.* 9:2321–2329.

Hickson, I.D. 2003. RecQ helicases: Caretakers of the genome. *Nat. Rev. Cancer*. 3:169–178.

Hirano, T., S. Funahashi, T. Uemura, and M. Yanagida. 1986. Isolation and characterization of Schizosaccharomyces pombe cut mutants that block nuclear division but not cytokinesis. *EMBO J.* 5:2973–2979.

Hodges, P.E., W.E. Payne, and J.I. Garrels. 1998. The yeast protein database (YPD): a curated proteome database for Saccharomyces cerevisiae. *Nucleic Acids Res.* 26:68–72.

Hogg, M., P. Osterman, G.O. Bylund, R. a Ganai, E.-B. Lundström, a E. Sauer-Eriksson, and E. Johansson. 2014. Structural basis for processive DNA synthesis by yeast DNA polymerase ε. *Nat. Struct. Mol. Biol.* 21:49–55.

Hogg, M., S.S. Wallace, and S. Doublie. 2004. Crystallographic snapshots of a replicative DNA polymerase encountering an abasic site. *EMBO J.* 23:1483–1493.

Hollingsworth, N.M., and S.J. Brill. 2004. The Mus81 solution to resolution: generating meiotic crossovers without Holliday junctions. *Genes Dev.* 18:117–125.

Holmberg, C., O. Fleck, H.A. Hansen, C. Liu, R. Slaaby, A.M. Carr, and O. Nielsen. 2005. Ddb1 controls genome stability and meiosis in fission yeast. *Genes Dev.* 19:853–862.

Howitt, B.E., S.A. Shukla, L.M. Sholl, L.L. Ritterhouse, J.C. Watkins, S. Rodig, E. Stover, K.C. Strickland, A.D. D'Andrea, C.J. Wu, U.A. Matulonis, and P.A. Konstantinopoulos. 2015. Association of polymerase e-mutated and microsatellite-instable endometrial cancers with neoantigen load, number of tumor-infiltrating lymphocytes, and expression of PD-1 and PD-L1. *JAMA Oncol.* 1:1319–1323.

Huberman, J.A., and A.D. Riggs. 1968. On the mechanism of DNA replication in mammalian chromosomes. *J. Mol. Biol.* 32:327–341.

Hubscher, U., G. Maga, and S. Spadari. 2002. Eukaryotic DNA polymerases. *Annu. Rev. Biochem.* 71:133–63.

Hübscher, U., H.P. Nasheuer, and J.E. Syväoja. 2000. Eukaryotic DNA polymerases, a growing family. *Trends Biochem. Sci.* 25:143–147.

Humphrey, T. 2000. DNA damage and cell cycle control in Schizosaccharomyces pombe. *Mutat. Res. - Fundam. Mol. Mech. Mutagen.* 451:211–226.

Iida, T., and H. Araki. 2004. Noncompetitive counteractions of DNA polymerase ε and ISW2/yCHRAC for epigenetic inheritance of telomere position effect in Saccharomyces cerevisiae. *Mol. Cell. Biol.* 24:217–227.

Ira, G., A. Malkova, G. Liberi, M. Foiani, and J.E. Haber. 2003. Srs2 and Sgs1 – Top3 suppress crossovers during double-strand break repair in yeast. *Cell*. 115:401–411.

Iyer, D.R., S. Das, and N. Rhind. 2018. Analysis of DNA replication in fission yeast by combing. *Cold Spring Harb. Protoc.* 199–207.

Iyer, D.R., and N. Rhind. 2017. Replication fork slowing and stalling are distinct, checkpoint-independent consequences of replicating damaged DNA. *PLoS Genet.* 13:1–32.

Jackson, S.P., and J. Bartek. 2009. The DNA-damage response in human biology and disease. *Nature*. 461:1071–1078.

Jain, R., K.R. Rajashankar, A. Buku, R.E. Johnson, L. Prakash, S. Prakash, and A.K. Aggarwal. 2014. Crystal structure of yeast DNA polymerase ε catalytic domain. *PLoS One*. 9:1–6.

Janner, F., F. Flury, and U. Leupold. 1979. Reversion of nonsense mutants induced by 4-nitroquinoline-1-oxide in Schizosaccharomyces pombe. *Mutat. Res.* 63:11–19.

Jansen, A.M.L., T. Van Wezel, B.E.W.M. Van Den Akker, M.V. Garcia, D. Ruano, C.M.J. Tops, A. Wagner, T.G.W. Letteboer, E.B. Gómez-garcía, P. Devilee, J.T. Wijnen, F.J. Hes, and H. Morreau. 2016. Combined mismatch repair and POLE/POLD1 defects explain unresolved suspected Lynch syndrome cancers. *Eur. J. Hum. Genet.* 24:1089–1092.

Jazayeri, A., J. Falck, C. Lukas, J. Bartek, G.C.M. Smith, J. Lukas, and S.P. Jackson. 2006. ATM- and cell cycle-dependent regulation of ATR in response to DNA double-strand breaks. *Nat. Cell Biol.* 8:37–45.

Jin, Y.H., P. Garg, C.M.W. Stith, H. Al-refai, J.F. Sterling, L.J.W. Murray, T.A. Kunkel, M.A. Resnick, P.M. Burgers, and D.A. Gordenin. 2005. The multiple biological roles of the 3'-5' exonuclease of Saccharomyces cerevisiae DNA polymerase delta require switching between the polymerase and exonuclease domains. *Mol. Cell. Biol.* 25:461–471.

Jin, Y.H., R. Obert, P.M. Burgers, T.A. Kunkel, M.A. Resnick, and D.A. Gordenin. 2001. The 3′→5′ exonuclease of DNA polymerase δ can substitute for the 5′ flap endonuclease Rad27/Fen1 in processing Okazaki fragments and preventing genome instability. *Proc. Natl. Acad. Sci. U. S. A.* 98:5122–5127.

Johansson, E., and S. a Macneill. 2010. The eukaryotic replicative DNA polymerases take shape. *Trends Biochem. Sci.* 35:339–47.

Johnson, R.E., R. Klassen, L. Prakash, and S. Prakash. 2015. A major role of DNA polymerase δ in replication of both the leading and lagging DNA strands. *Mol. Cell*. 59:163–175.

Kadyrova, L.Y., and F.A. Kadyrov. 2016. Endonuclease activities of MutLα and its homologs in DNA mismatch repair. *DNA Repair*. 38:42–49.

Kai, M., M.N. Boddy, P. Russell, and T.S. Wang. 2005. Replication checkpoint kinase Cds1 regulates Mus81 to preserve genome integrity during replication stress. *Genes Dev. Dev.* 19:919–932.

Kai, M., and T.S. Wang. 2003. Checkpoint responses to replication stalling: inducing tolerance and preventing mutagenesis. *Mutat. Res. Mol. Mech. Mutagen.* 532:59–73.

Kaliraman, V., J.R. Mullen, W.M. Fricke, S.A. Bastin-Shanower, and S.J. Brill. 2001. Functional overlap between Sgs1 – Top3 and the Mms4 – Mus81 endonuclease. *Genes Dev.* 15:2730–2740.

Kane, D.P., and P. V Shcherbakova. 2014. A common cancer-associated DNA polymerase ε mutation causes an exceptionally strong mutator phenotype, indicating fidelity defects distinct from loss of proofreading. *Cancer Res.* 74:1895–1902.

Kang, Y.H., W.C. Galal, A. Farina, I. Tappin, and J. Hurwitz. 2012. Properties of the human Cdc45/Mcm2-7/GINS helicase complex and its action with DNA polymerase ε in rolling circle DNA synthesis. *Proc. Natl. Acad. Sci. U. S. A.* 109:6042–6047.

Kasparek, T. 2013. Identification and characterisation of determinants of genome stability in response to a double-strand break. University of Oxford. 1–238 pp.

Kaykov, A., T. Taillefumier, A. Bensimon, and P. Nurse. 2016. Molecular combing of single DNA molecules on the 10 megabase scale. *Sci. Rep.* 6:1–9.

Kearsey, S.E., and S. Cotterill. 2003. Enigmatic variations: Divergent modes of regulating eukaryotic DNA replication. *Mol. Cell.* 12:1067–1075.

Kemp, M., and A. Sancar. 2009. DNA Distress: Just ring 9-1-1. *Curr. Biol.* 19:733–734.

Kesti, T., K. Flick, S. Keränen, J. Syväoja, and C. Wittenberg. 1999. DNA polymerase ε catalytic domains are dispensable for DNA replication, DNA repair, and cell viability. *Mol. Cell.* 3:679–685.

Kim, D.-U., J. Hayles, D. Kim, V. Wood, H.-O. Park, M. Won, H.-S. Yoo, T. Duhig, M. Nam, G. Palmer, S. Han, L. Jeffery, S.-T. Baek, H. Lee, Y.S. Shim, M. Lee, L. Kim, K.-S. Heo, E.J. Noh, A.-R. Lee, Y.-J. Jang, K.-S. Chung, S.-J. Choi, J.-Y. Park, Y. Park, H.M. Kim, S.-K. Park, H.-J. Park, E.-J. Kang, H.B. Kim, H.-S. Kang, H.-M. Park, K. Kim, K. Song, K. Bin Song, P. Nurse, and K.-L. Hoe. 2010. Analysis of a genome-wide set of gene deletions in the fission yeast Schizosaccharomyces pombe. *Nat. Biotechnol.* 28:617–623.

Kim, H., and S.J. Brill. 2001. Rfc4 interacts with Rpa1 and is required for both DNA replication and DNA damage checkpoints in Saccharomyces cerevisiae. *Mol. Cell. Biol.* 21:3725–3737.

Kim, S.M., and S.L. Forsburg. 2018. Regulation of structure-specific endonucleases in replication stress. *Genes (Basel).* 9:1–21.

Kim, T.-M., P.W. Laird, and P.J. Park. 2013. The landscape of microsatellite instability in colorectal and endometrial cancer genomes. *Cell.* 155:858–868.

Knutsen, J.H.J., I.D. Rein, C. Rothe, T. Stokke, B. Grallert, and E. Boye. 2011. Cell-cycle analysis of fission yeast cells by flow cytometry. *PLoS One.* 6:1–8.

Kokoska, R.J., L. Stefanovic, J. DeMai, and T.D. Petes. 2000. Increased rates of genomic deletions generated by mutations in the yeast gene encoding DNA Polymerase δ or by decreases in the cellular levels of DNA Polymerase δ. *Mol. Cell. Biol.* 20:7490–7504.

Kokoska, R.J., L. Stefanovic, H.T. Tran, M.A. Resnick, D.A. Gordenin, and T.D. Petes. 1998. Destabilization of yeast micro- and minisatellite DNA sequences by mutations affecting a nuclease involved in Okazaki fragment processing (rad27) and DNA polymerase δ (pol3-t). *Mol. Cell. Biol.* 18:2779–2788.

Krakoff, I.H., N.C. Brown, and P. Reichard. 1968. Inhibition of ribonucleoside diphosphate reductase by hydroxyurea. *Cancer Res.* 28:1559–1565.

Kunkel, T., J.D. Roberts, and R.A. Zakour. 1985. Rapid and efficient site-specific mutagenesis without phenotypic selection. *Methods Enzymol.* 154:367–382.

Kunkel, T.A. 2004. DNA Replication Fidelity. *J. Biol. Chem.* 279:16895–16898.

Kunkel, T.A., and K. Bebenek. 1988. Recent studies of the fidelity of DNA synthesis. *BBA - Gene Struct. Expr.* 951:1–15.

Kunkel, T.A., and P.M. Burgers. 2008. Dividing the workload at a eukaryotic replication fork. *Trends Cell Biol.* 18:521–527.

Kunkel, T.A., and D.A. Erie. 2005. DNA mismatch repair. *Annu. Rev. Biochem.* 74:681–710.

Kunkel, T.A., and D.A. Erie. 2015. Eukaryotic mismatch repair in relation to DNA replication. *Annu. Rev. Genet.* 49:291–313.

Lambert, S., B. Froget, and A.M. Carr. 2007. Arrested replication fork processing: Interplay between checkpoints and recombination. *DNA Repair (Amst).* 6:1042–1061.

Lambert, S., K. Mizuno, J. Blaisonneau, S. Martineau, R. Chanet, K. Fréon, J.M. Murray, A.M. Carr, and G. Baldacci. 2010. Homologous recombination restarts blocked replication forks at the expense of genome rearrangements by template exchange. *Mol. Cell*. 39:346–359.

Lambert, S., A. Watson, D.M. Sheedy, B. Martin, and A.M. Carr. 2005. Gross chromosomal rearrangements and elevated recombination at an inducible site-specific replication fork barrier. *Cell*. 121:689–702.

Lang, G.I., and A.W. Murray. 2008. Estimating the per-base-pair mutation rate in the yeast Saccharomyces cerevisiae. *Genetics*. 178:67–82.

Lange, S.S., K.I. Takata, and R.D. Wood. 2011. DNA polymerases and cancer. *Nat. Rev. Cancer*. 11:96–110.

Lange, S.S., J.P. Wittschieben, and R.D. Wood. 2012. DNA polymerase zeta is required for proliferation of normal mammalian cells. *Nucleic Acids Res.* 40:4473–4482.

Langston, L.D., D. Zhang, O. Yurieva, R.E. Georgescu, J. Finkelstein, N.Y. Yao, C. Indiani, and M.E. O'Donnell. 2014. CMG helicase and DNA polymerase ε form a functional 15-subunit holoenzyme for eukaryotic leading-strand DNA replication. *Proc. Natl. Acad. Sci. U. S. A.* 111:15390–15395.

Larrea, A.A., S.A. Lujan, S.A.N. McElhinny, P.A. Mieczkowski, M.A. Resnick, D.A. Gordenin, and T.A. Kunkel. 2010. Genome-wide model for the normal eukaryotic DNA replication fork. *Proc. Natl. Acad. Sci. U. S. A.* 107:17674–17679.

Leach, F.S., N.C. Nicolaides, N. Papadopoulos, B. Liu, J. Jen, R. Parsons, P. Peltomäki, P. Sistonen, L.A. Aaltonen, M. Nyström-Lahti, X.Y. Guan, J. Zhang, P.S. Meltzer, J.W. Yu, F. Ten Kao, D.J. Chen, K.M. Cerosaletti, R.E.K. Fournier, S. Todd, T. Lewis, R.J. Leach, S.L. Naylor, J. Weissenbach, J.P. Mecklin, H. Järvinen, G.M. Petersen, S.R. Hamilton, J. Green, J. Jass, P. Watson, H.T. Lynch, J.M. Trent, A. de la Chapelle, K.W. Kinzler, and B. Vogelstein. 1993. Mutations of a mutS homolog in hereditary nonpolyposis colorectal cancer. *Cell*. 75:1215–1225.

Lee, I., S. V Date, A.T. Adai, and E.M. Marcotte. 2004. A probalistic functional network of yeast genes. *Science.* 306:1555–1558.

Lee, J.-H., and T.T. Paull. 2004. Direct activation of the ATM protein kinase by the Mre11/ Rad50/Nbs1 complex. *Science.* 304:93–96.

Lee, W.R., D.T. Beranek, and B.J. Byrne. 1989. Dosage-response relationships for methyl methanesulfonate in Drosophila melanogaster spermatozoa: DNA methylation per nucleotide vs. sex-linked recessive lethal frequency. *Mutat. Res. - Fundam. Mol. Mech. Mutagen.* 211:243–257.

Lee, Y.S., M.T. Gregory, and W. Yang. 2014. Human Pol ζ purified with accessory subunits is active in translesion DNA synthesis and complements Pol η in cisplatin bypass. *Proc. Natl. Acad. Sci. U. S. A.* 111:2954–2959.

Lehmann, A.R. 2011. DNA polymerases and repair synthesis in NER in human cells. *DNA Repair (Amst).* 10:730–733.

Lengauer, C., K.W. Kinzler, and B. Vogelstein. 1998. Genetic instabilities in human cancers. *Nature*.

396:643–649.

Li, L., K.M. Murphy, U. Kanevets, and L.J. Reha-Krantz. 2005. Sensitivity to phosphonoacetic acid: A new phenotype to probe DNA polymerase δ in Saccharomyces cerevisiae. *Genetics*. 170:569–580.

Li, Z., F.J. Vizeacoumar, S. Bahr, J. Li, J. Warringer, F.S. Vizeacoumar, R. Min, B. VanderSluis, J. Bellay, M. Devit, J.A. Fleming, A. Stephens, J. Haase, Z. Lin, A. Baryshnikova, H. Lu, Z. Yan, K. Jin, S. Barker, A. Datti, G. Giaever, C. Nislow, C. Bulawa, C.L. Myers, M. Costanzo, A.-C. Gingras, Z. Zhang, A. Blomberg, K. Bloom, B. Andrews, and C. Boone. 2011. Systematic exploration of essential yeast gene function with temperature-sensitive mutants. *Nat. Biotechnol.* 29:361–367.

Lieberman, H.B. 1995. Extragenic suppressors of Schizosaccharomyces pombe rad9 mutations uncouple radioresistance and hydroxyurea sensitivity from cell cycle checkpoint control. *Genetics*. 141:107–117.

Lieberman, H.B., K.M. Hopkins, M. Nass, D. Demetrick, and S. Davey. 1996. A human homolog of the Schizosaccharomyces pombe rad9+ checkpoint control gene. *Proc. Natl. Acad. Sci. U. S. A.* 93:13890–13895.

Limbo, O., D. Moiani, A. Kertokalio, C. Wyman, J.A. Tainer, and P. Russell. 2012. Mre11 ATLD17/18 mutation retains Tel1/ATM activity but blocks DNA double-strand break repair. *Nucleic Acids Res.* 40:11435–11449.

Liu, C., K.A. Powell, K. Mundt, L. Wu, A.M. Carr, and T. Caspari. 2003. Cop9/signalosome subunits and Pcu4 regulate ribonucleotide reductase by both checkpoint-dependent and -independent mechanisms. *Genes Dev.* 17:1130–1140.

Liu, V.F., D. Bhaumik, and T.S. Wang. 1999. Mutator phenotype induced by aberrant replication. *Mol. Cell. Biol.* 19:1126–1135.

Ljungman, M. 2010. The DNA damage response - repair or despair? *Environ. Mol. Mutagen.* 51:879–889.

Llor, X., E. Pons, R.M. Xicola, A. Castells, C. Alenda, V. Piñol, M. Andreu, S. Castellví-Bel, A. Payá, R. Jover, X. Bessa, A. Girós, A. Roca, and M.A. Gassull. 2005. Differential features of colorectal cancers fulfilling Amsterdam criteria without involvement of the mutator pathway. *Clin. Cancer Res.* 11:7304–7310.

Loeb, L.A. 1991. Mutator phenotype may be required for multistage carcinogenesis. *Am. Assoc. Cancer Res.* 51:3075–3079.

Loeb, L.A., and R.J. Monnat. 2008. DNA polymerases and human disease. *Nat. Rev. Genet.* 9:594–604.

Longhese, M.P., H. Neecke, V. Paciotti, G. Lucchini, and P. Plevani. 1996. The 70 kDa subunit of replication protein A is required for the G1/S and intra-S DNA damage checkpoints in budding yeast. *Nucleic Acids Res.* 24:3533–3537.

Longley, M.J., A.J. Pierce, and P. Modrich. 1997. DNA polymerase delta is required for human mismatch repair in vitro. *J. Biol. Chem.* 272:10917–10921.

Lopes, M., C. Cotta-Ramusino, A. Pellicioli, G. Liberi, P. Plevani, M. Muzi-Falconi, C.S. Newlon, and M. Foiani. 2001. The DNA replication checkpoint response stabilizes stalled replication forks. *Nature*. 412:557–561.

Lopez-Girona, A., B. Furnari, O. Mondesert, and P. Russell. 1999. Nuclear localization of Cdc25 is regulated by DNA damage and a 14-3-3 protein. *Nature*. 397:172–175.

Lujan, S. a, J.S. Williams, A.R. Clausen, A.B. Clark, and T.A. Kunkel. 2013. Ribonucleotides are signals for mismatch repair of leading-strand replication errors. *Mol. Cell*. 50:437–43.

Lujan, S.A., A.R. Clausen, A.B. Clark, H.K. MacAlpine, D.M. MacAlpine, E.P. Malc, P.A. Mieczkowski, A.B. Burkholder, D.C. Fargo, D.A. Gordenin, and T.A. Kunkel. 2014. Heterogeneous polymerase fidelity and mismatch repair bias genome variation and composition. *Genome Res.* 24:1751–1764.

Lundin, C., M. North, K. Erixon, K. Walters, D. Jenssen, A.S.H. Goldman, and T. Helleday. 2005. Methyl methanesulfonate (MMS) produces heat-labile DNA damage but no detectable in vivo DNA double-strand breaks. *Nucleic Acids Res.* 33:3799–811.

Lydeard, J.R., S. Jain, M. Yamaguchi, and J.E. Haber. 2007. Break-induced replication and telomerase-independent telomere maintenance require Pol32. *Nature*. 448:820–823.

Lynch, H.T., and A. De la Chapelle. 2003. Hereditary colorectal cancer. *N. Engl. J. Med.* 348:919–932.

Lynch, H.T., and T. Smyrk. 1996. Hereditary nonpolyposis colorectal cancer (Lynch syndrome): An updated review. *Cancer*. 78:1149–1167.

Maga, G., M. Stucki, S. Spadari, and U. Hübscher. 2000. DNA polymerase switching: I. Replication factor C displaces DNA polymerase α prior to PCNA loading. *J. Mol. Biol.* 295:791–801.

Mansour, A.A., C. Tornier, E. Lehmann, M. Darmon, and O. Fleck. 2001. Control of GT repeat stability in Schizosaccharomyces pombe by mismatch repair factors. *Genetics*. 158:77–85.

Matsuyama, A., A. Shirai, and M. Yoshida. 2008. A series of promoters for constitutive expression of heterologous genes in fission yeast. *Yeast*. 25:371–376.

McCulloch, S.D., and T.A. Kunkel. 2008. The fidelity of DNA synthesis by eukaryotic replicative and translesion synthesis polymerases. *Cell Res.* 18:148–61.

McElhinny, S.A.N., D.A. Gordenin, C.M. Stith, P.M.J. Burgers, and T.A. Kunkel. 2008. Division of labor at the eukaryotic replication fork. *Mol. Cell*. 30:137–44.

McElhinny, S.A.N., G.E. Kissling, and T.A. Kunkel. 2010a. Differential correction of lagging-strand replication errors made by DNA polymerases α and δ. *Proc. Natl. Acad. Sci. U. S. A.* 107:21070–21075.

McElhinny, S.A.N., B.E. Watts, D. Kumar, D.L. Watt, E.-B. Lundström, P.M.J. Burgers, E. Johansson, A. Chabes, and T.A. Kunkel. 2010b. Abundant ribonucleotide incorporation into DNA by yeast replicative polymerases. *Proc. Natl. Acad. Sci. U. S. A.* 107:4949–54.

Mertz, T.M., S. Sharma, A. Chabes, and P. V Shcherbakova. 2015. Colon cancer-associated mutator DNA polymerase δ variant causes expansion of dNTP pools increasing its own infidelity. *Proc. Natl. Acad. Sci. U. S. A.* 112:2467–2476.

Meselson, M., and F.W. Stahl. 1958. The replication of DNA in Escherichia coli. *PNAS*. 44:671–682.

Michel, B., G. Grompone, M.-J. Flores, and V. Bidnenko. 2004. Multiple pathways process stalled replication forks. *Proc. Natl. Acad. Sci. U. S. A.* 101:12783–12788.

Miyabe, I., T.A. Kunkel, and A.M. Carr. 2011. The major roles of DNA polymerases epsilon and delta at the eukaryotic replication fork are evolutionarily conserved. *PLoS Genet.* 7:1–11.

Miyabe, I., K. Mizuno, A. Keszthelyi, Y. Daigaku, M. Skouteri, S. Mohebi, T.A. Kunkel, J.M. Murray, and A.M. Carr. 2015. Polymerase δ replicates both strands after homologous recombination-dependent fork restart. *Nat. Struct. Mol. Biol.* 22:932–938.

Mochida, S., F. Esashi, N. Aono, K. Tamai, M.J. O'Connell, and M. Yanagida. 2004. Regulation of checkpoint kinases through dynamic interaction with Crb2. *EMBO J.* 23:418–428.

Montano, R., I. Chung, K.M. Garner, D. Parry, and A. Eastman. 2012. Preclinical development of the novel Chk1 inhibitor SCH900776 in combination with DNA-damaging agents and antimetabolites.

Mol. Cancer Ther. 11:427–438.

Montano, R., R. Thompson, I. Chung, H. Hou, N. Khan, and A. Eastman. 2013. Sensitization of human cancer cells to gemcitabine by the Chk1 inhibitor MK-8776: cell cycle perturbation and impact of administration schedule in vitro and in vivo. *BMC Cancer*. 13:1–14.

Moreno, S., A. Klar, and P. Nurse. 1991. Molecular genetic analysis of fission yeast Schizosaccharomyces pombe. *Methods Enzymol.* 194:795–823.

Morrison, A., J.B. Bell, T.A. Kunkel, and A. Sugino. 1991. Eukaryotic DNA polymerase amino acid sequence required for 3'-5' exonuclease activity. *Proc. Natl. Acad. Sci. U. S. A.* 88:9473–9477.

Morrison, A., A.L. Johnson, L.H. Johnston, and A. Sugino. 1993. Pathway correcting DNA replication errors in S. cerevisiae. *EMBO J*. 12:1467–1473.

Morrison, A., and A. Sugino. 1994. The 3′ → 5′ exonucleases of both DNA polymerases δ and ε participate in correcting errors of DNA replication in Saccharomyces cerevisiae. *Mol. Gen. Genet.* 242:289–296.

Morrow, D.M., D.A. Tagle, Y. Shiloh, F.S. Collins, and P. Hieter. 1995. TEL1, an S. cerevisiae homolog of the human gene mutated in ataxia telangiectasia, is functionally related to the yeast checkpoint gene MEC1. *Cell*. 82:831–840.

Moss, J., H. Tinline-Purvis, C.A. Walker, L.K. Folkes, M.R. Stratford, J. Hayles, K.-L. Hoe, D.-U. Kim, H.-O. Park, S.E. Kearsey, O. Fleck, C. Holmberg, O. Nielsen, and T.C. Humphrey. 2010. Break-induced ATR and Ddb1-Cul4Cdt2 ubiquitin ligase-dependent nucleotide synthesis promotes homologous recombination repair in fission yeast. *Genes Dev.* 24:2705–2716.

Mossi, R., R.C. Keller, E. Ferrari, and U. Hübscher. 2000. DNA polymerase switching: II. Replication factor C abrogates primer synthesis by DNA polymerase α at a critical length. *J. Mol. Biol.* 295:803–814.

Muramatsu, S., K. Hirai, Y.-S. Tak, Y. Kamimura, and H. Araki. 2010. CDK-dependent complex formation between replication proteins Dpb11 , Sld2 , Pol e , and GINS in budding yeast. *Genes Dev.* 24:602–612.

Murphy, K., H. Darmawan, A. Schultz, E.F. Da Silva, and L.J. Reha-Krantz. 2006. A method to select for mutator DNA polymerase δs in Saccharomyces cerevisiae. *Genome*. 49:403–410.

Murray, J.M., H.D. Lindsay, C.A. Munday, and A.M. Carr. 1997. Role of Schizosaccharomyces pombe RecQ homolog, recombination, and checkpoint genes in UV damage tolerance. *Mol. Cell. Biol.* 17:6868–6875.

Myers, J.S., and D. Cortez. 2006. Rapid activation of ATR by ionizing radiation requires ATM and Mre11. *J. Biol. Chem.* 281:9346–9350.

Namiki, Y., and L. Zou. 2006. ATRIP associates with replication protein A-coated ssDNA through multiple interactions. *Proc. Natl. Acad. Sci. U. S. A.* 103:580–585.

Natsume, T., Y. Tsutsui, T. Sutani, E.M. Dunleavy, A.L. Pidoux, H. Iwasaki, K. Shirahige, R.C. Allshire, and F. Yamao. 2008. A DNA polymerase α accessory protein, Mcl1, is required for propagation of centromere structures in fission yeast. *PLoS One*. 3:1–14.

Navas, T.A., Z. Zhou, and S.J. Elledge. 1995. DNA polymerase epsilon links the DNA replication machinery to the S phase checkpoint. *Cell*. 80:29–39.

Negrini, S., V.G. Gorgoulis, and T.D. Halazonetis. 2010. Genomic instability an evolving hallmark of cancer. *Nat. Rev. Mol. Cell Biol.* 11:220–228.

Newlon, C.S., T.D. Petes, L.M. Hereford, and W.L. Fangman. 1974. Replication of yeast chromosomal DNA. *Nature*. 247:32–35.

Nielsen, O. 2016. Synchronization of S phase in Schizosaccharomyces pombe cells by transient exposure to M-factor pheromone. *Cold Spring Harb. Protoc.* 1–5.

Niida, H., and M. Nakanishi. 2006. DNA damage checkpoints in mammals. *Mutagenesis*. 21:3–9.

Niimi, A., S. Brown, S. Sabbioneda, P.L. Kannouche, A. Scott, A. Yasui, C.M. Green, and A.R. Lehmann. 2008. Regulation of proliferating cell nuclear antigen ubiquitination in mammalian cells. *Proc. Natl. Acad. Sci. U. S. A.* 105:16125–16130.

Nishida, C., P. Reinhard, and S. Linn. 1988. DNA repair synthesis in human fibroblasts requires DNA plymerase δ. *J. Biol. Chem.* 263:501–510.

Niwa, O. 2016. Determination of the frequency of minichromosome loss to assess chromosome stability in fission yeast. *Cold Spring Harb. Protoc.* 216–218.

Niwa, O., T. Matsumoto, and M. Yanagida. 1986. Construction of a mini-chromosome by deletion and its mitotic and meiotic behaviour in fission yeast. *Mol. Gen. Genet.* 203:397–405.

Noguchi, C., M. V Garabedian, M. Malik, and E. Noguchi. 2008. A vector system for genomic FLAG epitope-tagging in Schizosaccharomyces pombe. *Biotechnol. J.* 3:1280–1285.

Northam, M.R., P. Garg, D.M. Baitin, P.M.J. Burgers, and P. V Shcherbakova. 2006. A novel function of DNA polymerase zeta regulated by PCNA. *EMBO J.* 25:4316–25.

Nurse, P. 1975. Genetic control of cell size at cell division in yeast. *Nature*. 256:547–551.

O'Connell, M.J., N.C. Walworth, and A.M. Carr. 2000. The G2-phase DNA-damage checkpoint. *Trends Cell Biol.* 10:296–303.

Ogi, T., S. Limsirichaikul, R.M. Overmeer, M. Volker, K. Takenaka, R. Cloney, Y. Nakazawa, A. Niimi, Y. Miki, N.G. Jaspers, L.H. Mullenders, S. Yamashita, M.I. Fousteri, and A.R. Lehmann. 2010. Three DNA polymerases, recruited by different mechanisms, carry out NER repair synthesis in human cells. *Mol. Cell*. 37:714–727.

Oo, Z.Y., M. Proctor, A.J. Stevenson, D. Nazareth, M. Fernando, S.M. Daignault, C. Lanagan, S. Walpole, V. Bonazzi, D. Škalamera, C. Snell, N.K. Haass, J.E. Larsen, and B. Gabrielli. 2019. Combined use of subclinical hydroxyurea and CHK1 inhibitor effectively controls melanoma and lung cancer progression, with reduced normal tissue toxicity compared to gemcitabine. *Mol. Oncol.* 13:1503–1518.

Osman, F., J. Dixon, A.R. Barr, and M.C. Whitby. 2005. The F-box DNA helicase Fbh1 prevents Rhp51-dependent recombination without mediator proteins. *Mol. Cell. Biol.* 25:8084–8096.

Osman, F., and M.C. Whitby. 2007. Exploring the roles of Mus81-Eme1/Mms4 at perturbed replication forks. *DNA Repair (Amst).* 6:1004–1017.

Ostermann, K., A. Lorentz, and H. Schmidt. 1993. The fission yeast rad22 gene, having a function in mating-type switching and repair of DNA damages, encodes a protein homolog to Rad52 of Saccharomyces cerevisiae. *Nucleic Acids Res.* 21:5940–5944.

Pai, C.-C. 2009. Analysis of GINS and other replication factors in the fission yeast cell cycle. University of Oxford. 1–274 pp.

Pai, C.-C., and S.E. Kearsey. 2017. A critical balance: dNTPs and the maintenance of genome stability. *Genes (Basel).* 8:1–14.

Pai, C.C., E. Blaikley, and T.C. Humphrey. 2018. DNA double-strand break repair assay. *Cold Spring Harb. Protoc.* 2018:289–299.

Palles, C., J.-B. Cazier, K.M. Howarth, E. Domingo, A.M. Jones, P. Broderick, Z. Kemp, S.L. Spain, E. Guarino, E. Guarino Almeida, I. Salguero, A. Sherborne, D. Chubb, L.G. Carvajal-Carmona, Y.

Ma, K. Kaur, S. Dobbins, E. Barclay, M. Gorman, L. Martin, M.B. Kovac, S. Humphray, A. Lucassen, C.C. Holmes, D. Bentley, P. Donnelly, J. Taylor, C. Petridis, R. Roylance, E.J. Sawyer, D.J. Kerr, S. Clark, J. Grimes, S.E. Kearsey, H.J.W. Thomas, G. McVean, R.S. Houlston, and I. Tomlinson. 2013. Germline mutations affecting the proofreading domains of POLE and POLD1 predispose to colorectal adenomas and carcinomas. *Nat. Genet.* 45:136–44.

Palles, C., A. Latchford, and L. Valle. 2018. Adenomatous polyposis syndromes: polymerase proofreading-asociated polyposis. *In* Hereditary colorectal cancer: genetic basis and clinical implications. L. Valle, S.B. Gruber, and G. Capella, editors. Springer. 113–134.

Park, J.G., H.F. Vasen, Y.J. Park, K.J. Park, P. Peltomaki, M. Ponzo de Leon, M.A. Rodriguez-Bigas, J. Lubinski, N.E. Beck, M.L. Bisgaard, M. Miyaki, J.T. Wijnen, S. Baba, A. Lindblom, L. Madlensky, and H.T. Lynch. 2002. Suspected HNPCC and Amsterdam criteria II: evaluation of mutation detection rate, an international collaborative study. *Int. J. Colorectal Dis.* 17:109–114.

Pasero, P., and S.M. Gasser. 2002. In vitro DNA replication assays in yeast extracts. *Methods Enzymol.* 351:184–199.

Paulsen, R.D., and K.A. Cimprich. 2007. The ATR pathway: Fine-tuning the fork. *DNA Repair (Amst).* 6:953–966.

Pavlov, Y., C. Frahm, S.N. McElhinny, A. Niimi, M. Suzuki, and T. Kunkel. 2006a. Evidence that errors made by DNA polymerase alpha are corrected by DNA polymerase delta. *Curr. Biol.* 16:202–7.

Pavlov, Y., I. Mian, and T. Kunkel. 2003. Evidence for preferential mismatch repair of lagging strand DNA replication errors in yeast. *Curr. Biol.* 13:744–748.

Pavlov, Y.I., P. V Shcherbakova, and I.B. Rogozin. 2006b. Roles of DNA polymerases in replication, repair, and recombination in eukaryotes. *Int. Rev. Cytol.* 255:41–132.

Peasland, A., L.-Z. Wang, E. Rowling, S. Kyle, T. Chen, A. Hopkins, W. Cliby, J. Sarkaria, G. Beale, R. Edmondson, and N. Curtin. 2011. Identification and evaluation of a potent novel ATR inhibitor, NU6027, in breast and ovarian cancer cell lines. *Br. J. Cancer*. 105:372–381.

Pena-Diaz, J., and L.J. Rasmussen. 2016. Approaches to diagnose DNA mismatch repair gene defects in cancer. *DNA Repair (Amst).* 38:147–154.

Pepe, A., and S.C. West. 2014. MUS81-EME2 promotes replication fork restart. *Cell Rep.* 7:1048–1055.

Perera, R.L., R. Torella, S. Klinge, M.L. Kilkenny, J.D. Maman, and L. Pellegrini. 2013. Mechanism for priming DNA synthesis by yeast DNA Polymerase α. *Elife*. 2:1–22.

Petermann, E., and T. Helleday. 2010. Pathways of mammalian replication fork restart. *Nat. Rev. Mol. Cell Biol.* 11:683–687.

Petermann, E., M.L. Orta, N. Issaeva, N. Schultz, and T. Helleday. 2010. Hydroxyurea-stalled replication forks become progressively inactivated and require two different RAD51-mediated pathways for restart and repair. *Mol. Cell*. 37:492–502.

Porter-Goff, M.E., and N. Rhind. 2009. The role of MRN in the S-phase DNA damage checkpoint is independent of its Ctp1-dependent roles in double-strand break repair and checkpoint signaling. *Mol. Biol. Cell*. 20:2096–2107.

Povirk, L.F. 1996. DNA damage and mutagenesis by radiomimetic DNA-cleaving agents: Bleomycin, neocarzinostatin and other enediynes. *Mutat. Res. - Fundam. Mol. Mech. Mutagen.* 355:71–89.

Preston, B.D., T.M. Albertson, and A.J. Herr. 2010. DNA replication fidelity and cancer. *Semin. Cancer Biol.* 20:281–293.

Prindle, M.J., and L.A. Loeb. 2012. DNA polymerase delta in DNA replication and genome maintenance. *Environ. Mol. Mutagen.* 53:666–682.

Pursell, Z.F., I. Isoz, E.-B. Lundström, E. Johansson, and T.A. Kunkel. 2007. Yeast DNA polymerase ε participates in leading-strand DNA replication. *Science.* 317:127–130.

Pursell, Z.F., and T.A. Kunkel. 2008. DNA Polymerase ε: a polymerase of unusual size (and complexity). *Prog. Nucleic Acid Res. Mol. Biol.* 82:101–145.

Qu, M., B. Yang, L. Tao, J.R. Yates III, P. Russell, M.-Q. Dong, and L.-L. Du. 2012. Phosphorylation-dependent interactions between Crb2 and Chk1 are essential for DNA damage checkpoint. *PLoS Genet.* 8:1–14.

Rayner, E., I.C. Van Gool, C. Palles, S.E. Kearsey, T. Bosse, I. Tomlinson, and D.N. Church. 2016. A panoply of errors: Polymerase proofreading domain mutations in cancer. *Nat. Rev. Cancer*. 16:71–81.

Reha-Krantz, L. 1988. Amino acid changes coded by bacteriophage T4 DNA polymerase mutator mutants: relating structure to function. *J. Mol. Biol.* 202:711–724.

Reha-Krantz, L.J. 2010. DNA polymerase proofreading: Multiple roles maintain genome stability. *Biochim. Biophys. Acta*. 1804:1049–63.

Reha-Krantz, L.J., and R.L. Nonay. 1993. Genetic and biochemical studies of bacteriophage T4 DNA polymerase 3'-5'-exonuclease activity. *J. Biol. Chem.* 268:27100–27108.

Reichard, P., R. Eliasson, R. Ingemarson, and L. Thelander. 2000. Cross-talk between the allosteric effector-binding sites in mouse ribonucleotide reductase. *J. Biol. Chem.* 275:33021–33026.

Reynolds, N., A. Watt, P. Fantes, and S. MacNeill. 1998. Cdm1, the smallest subunit of DNA polymerase d in the fission yeast Schizosaccharomyces pombe, is non-essential for growth and division. *Curr. Genet.* 27:250–258.

Rhind, N., B. Furnari, and P. Russell. 1997. Cdc2 tyrosine phosphorylation is required for the DNA damage checkpoint in fission yeast. *Genes Dev.* 11:504–511.

Rhind, N., and P. Russell. 2000a. Checkpoints: it takes more than time to heal some wounds. *Curr. Biol.* 10:908–911.

Rhind, N., and P. Russell. 2000b. Chk1 and Cds1: Linchpins of the DNA damage and replication checkpoint pathways. *J. Cell Sci.* 113:3889–3896.

Rhind, N., and P. Russell. 2001. Roles of the mitotic inhibitors Wee1 and Mik1 in the G2 DNA damage and replication checkpoints. *Mol. Cell. Biol.* 21:1499–1508.

Robertson, A., A. Klungland, T. Rognes, and I. Leiros. 2009. Base excision repair: the long and short of it. *Cell. Mol. Life Sci.* 66:981–993.

Roguev, A., S. Bandyopadhyay, M. Zofall, K. Zhang, T. Fischer, S.R. Collins, H. Qu, M. Shales, H.-O. Park, J. Hayles, K.-L. Hoe, D.-U. Kim, T. Ideker, S.I. Grewal, J.S. Weissman, and N.J. Krogan. 2008. Conservation and rewiring of functional modules revealed by an epistasis map in fission yeast. *Science.* 322:405–410.

Roguev, A., C.J. Ryan, E. Hartsuiker, and N.J. Krogan. 2018a. High-throughput quantitative genetic interaction mapping in the fission yeast Schizosaccharomyces pombe. *Cold Spring Harb. Protoc.* 75–81.

Roguev, A., C.J. Ryan, J. Xu, I. Colson, E. Hartsuiker, and N. Krogan. 2018b. Genetic interaction score (S-score) calculation, clustering, and visualization of genetic interaction profiles for yeast. *Cold Spring Harb. Protoc.* 119–122.

Roguev, A., M. Wiren, J.S. Weissman, and N.J. Krogan. 2007. High-throughput genetic interaction mapping in the fission yeast Schizosaccharomyces pombe. *Nat. Methods*. 4:861–866.

Roguev, A., J. Xu, and N. Krogan. 2018c. Genetic interaction mapping in Schizosaccharomyces pombe using the pombe epistasis mapper (PEM) system and a ROTOR HDA colony replicating robot in a 1536 array format. *Cold Spring Harb. Protoc.* 112–118.

Rosche, W.A., and P.L. Foster. 2000. Determining mutation rates in bacterial populations. *Methods*. 20:4–17.

Roseaulin, L., Y. Yamada, Y. Tsutsui, P. Russell, H. Iwasaki, and B. Arcangioli. 2008. Mus81 is essential for sister chromatid recombination at broken replication forks. *EMBO J.* 27:1378–1387.

Rothstein, R. 1983. One-step gene disruption in yeast. *Methods Enzymol.* 101:202–211.

Rouse, J., and S.P. Jackson. 2002. Interfaces between the detection, signaling, and repair of DNA damage. *Science.* 297:547–551.

Rowley, R., S. Subramani, and P.G. Young. 1992. Checkpoint controls in Schizosaccharomyces pombe: rad1. *EMBO J.* 11:1335–1342.

Ryan, C.J., A. Roguev, K. Patrick, J. Xu, H. Jahari, Z. Tong, P. Beltrao, M. Shales, H. Qu, S.R. Collins, J.I. Kliegman, L. Jiang, D. Kuo, E. Tosti, H.S. Kim, W. Edelmann, M.C. Keogh, D. Greene, C. Tang, P. Cunningham, K.M. Shokat, G. Cagney, J.P. Svensson, C. Guthrie, P.J. Espenshade, T. Ideker, and N.J. Krogan. 2012. Hierarchical Modularity and the Evolution of Genetic Interactomes across Species. *Mol. Cell*. 46:691–704.

Saka, Y., F. Esashi, T. Matsusaka, S. Mochida, and M. Yanagida. 1997. Damage and replication checkpoint control in fission yeast is ensured by interactions of Crb2, a protein with BRCT motif, with Cut5 and Chk1. *Genes Dev.* 11:3387–3400.

Saka, Y., and M. Yanagida. 1993. Fission Yeast cut5+, required for S phase onset and M phase restraint, is Identical to the radiation-damage repair gene rad4+. *Cell*. 74:383–393.

Salguero, I., E. Guarino, M.E. Shepherd, T.D. Deegan, C.G. Havens, S.A. MacNeill, J.C. Walter, and S.E. Kearsey. 2012. Ribonucleotide reductase activity is coupled to DNA synthesis via proliferating cell nuclear antigen. *Curr. Biol.* 22:720–726.

Salk, J.J., E.J. Fox, and L.A. Loeb. 2010. Mutational heterogeneity in human cancers: origin and consequences. *Annu. Rev. Pathol. Mech. Dis.* 5:51–75.

Sambrook, J., E.F. Fritsch, and T. Manniatis. 1989. Molecular cloning: a laboratory manual. 2nd ed. C. Nolan, editor. Cold spring harbor laboratory press, Cold Spring Harbor, New York.

Samejima, I., T. Matsumoto, Y. Nakaseko, D. Beach, and M. Yanagida. 1993. Identification of seven new cut genes involved in Schizosaccharomyces pombe mitosis. *J. Cell Sci.* 105:135–143.

Sancar, A., L.A. Lindsey-Boltz, K. Ünsal-Kaçmaz, and S. Linn. 2004. Molecular mechanisms of mammalian DNA repair and the DNA damage checkpoints. *Annu. Rev. Biochem.* 73:39–85.

Sanchez, Y., B.A. Desany, W.J. Jones, Q. Liu, B. Wang, and S.J. Elledge. 1996. Regulation of RAD53 by the ATM-like kinases MEC1 and TEL1 in yeast cell cycle checkpoint pathways. *Science.* 271:357–360.

Sanyal, S., L. Molnarova, J. Richterova, B. Huraiova, Z. Benko, S. Polakova, I. Cipakova, A. Sevcovicova, K. Gaplovska-Kysela, K. Mechtler, L. Cipak, and J. Gregan. 2018. Mutations that prevent methylation of cohesin render sensitivity to DNA damage in S. pombe. *J. Cell Sci.* 131:1–9.

Sarkar, S., W.T. Ma, and G.V.H. Sandri. 1992. On fluctuation analysis: a new, simple and efficient method for computing the expected number of mutants. *Genetica*. 85:173–179.

Sattar, A.A., T.C. Lin, C. Jones, and W.H. Konigsberg. 1996. Functional consequences and exonuclease kinetic parameters of point mutations in bacteriophage T4 DNA polymerase. *Biochemistry*.

35:16621–16629.

Sazer, S., and P. Nurse. 1994. A fission yeast RCC1-related protein is required for the mitosis to interphase transition. *EMBO J.* 13:606–615.

Schaaper, R.M. 1993. Base selection, proofreading, and mismatch repair during DNA replication in Escherichia coli. *J. Biol. Chem.* 268:23762–23765.

Schmitt, M.W., Y. Matsumoto, and L.A. Loeb. 2009. High fidelity and lesion bypass capability of human DNA Polymerase δ. *Biochimie*. 91:1163–1172.

Sclafani, R., and T. Holzen. 2007. Cell cycle regulation of DNA replication. *Annu. Rev. Genet.* 41:237–280.

Sengupta, S., F. Van Deursen, G. De Piccoli, and K. Labib. 2013. Dpb2 integrates the leading-strand DNA polymerase into the eukaryotic replisome. *Curr. Biol.* 23:543–552.

Seshagiri, S., E.W. Stawiski, S. Durinck, Z. Modrusan, E.E. Storm, C.B. Conboy, S. Chaudhuri, Y. Guan, V. Janakiraman, B.S. Jaiswal, J. Guillory, C. Ha, G.J.P. Dijkgraaf, J. Stinson, F. Gnad, M. a Huntley, J.D. Degenhardt, P.M. Haverty, R. Bourgon, W. Wang, H. Koeppen, R. Gentleman, T.K. Starr, Z. Zhang, D. a Largaespada, T.D. Wu, and F.J. de Sauvage. 2012. Recurrent R-spondin fusions in colon cancer. *Nature*. 488:660–4.

Shcherbakova, P. V, K. Bebenek, and T.A. Kunkel. 2003a. Functions of eukaryotic DNA polymerases. *Sci. Aging Knowl. Env.* 8:1–11.

Shcherbakova, P. V, and I. Pavlov. 1996. 3'-5' exonucleases of DNA polymerases ε and δ correct base analog induced DNA replication errors on opposite DNA strands in Saccharomyces cerevisiae. *Genetics*. 142:717–726.

Shcherbakova, P. V, Y.I. Pavlov, O. Chilkova, I.B. Rogozin, E. Johansson, and T.A. Kunkel. 2003b. Unique error signature of the four-subunit yeast DNA polymerase ε. *J. Biol. Chem.* 278:43770–43780.

Shevelev, I. V, and U. Hübscher. 2002. The 3'-5' exonucleases. *Nat. Rev. Mol. Cell Biol.* 3:364–76.

Shiloh, Y. 2003. ATM and related protein kinases: Safeguarding genome integrity. *Nat. Rev. Cancer*. 3:155–168.

Shimura, T., M.J. Torres, M.M. Martin, V.A. Rao, Y. Pommier, M. Katsura, K. Miyagawa, and M.I. Aladjem. 2008. Bloom's syndrome helicase and Mus81 are required to induce transient double-strand DNA breaks in response to DNA replication stress. *J. Mol. Biol.* 375:1152–1164.

Shinbrot, E., E.E. Henninger, N. Weinhold, K.R. Covington, A.Y. Goksenin, N. Schultz, H. Chao, H. Doddapaneni, D.M. Muzny, R.A. Gibbs, C. Sander, Z.F. Pursell, and D.A. Wheeler. 2014. Exonuclease mutations in DNA polymerase epsilon reveal replication strand specific mutation patterns and human origins of replication. *Genome Res.* 24:1740–1750.

Shivji, M.K., V.N. Podust, U. Hübscher, and R.D. Wood. 1995. Nucleotide excision repair DNA synthesis by DNA Polymerase ε in the presence of PCNA, RFC, and RPA. *Biochemistry*. 34:5011–5017.

Shlien, A., B.B. Campbell, R. De Borja, L.B. Alexandrov, D. Merico, D. Wedge, P. Van Loo, P.S. Tarpey, P. Coupland, S. Behjati, A. Pollett, T. Lipman, A. Heidari, S. Deshmukh, N. Avitzur, B. Meier, M. Gerstung, Y. Hong, D.M. Merino, M. Ramakrishna, M. Remke, R. Arnold, G.B. Panigrahi, N.P. Thakkar, K.P. Hodel, E.E. Henninger, A.Y. Göksenin, D. Bakry, G.S. Charames, H. Druker, J. Lerner-Ellis, M. Mistry, R. Dvir, R. Grant, R. Elhasid, R. Farah, G.P. Taylor, P.C. Nathan, S. Alexander, S. Ben-Shachar, S.C. Ling, S. Gallinger, S. Constantini, P. Dirks, A. Huang, S.W. Scherer, R.G. Grundy, C. Durno, M. Aronson, A. Gartner, M.S. Meyn, M.D. Taylor, Z.F. Pursell, C.E. Pearson, D. Malkin, P.A. Futreal, M.R. Stratton, E. Bouffet, C. Hawkins, P.J.

Campbell, and U. Tabori. 2015. Combined hereditary and somatic mutations of replication error repair genes result in rapid onset of ultra-hypermutated cancers. *Nat. Genet.* 47:257–262.

Sia, E.A., S. Jinks-Robertson, and T.D. Petes. 1997. Genetic control of microsatellite stability. *Mutat. Res.* 383:61–70.

Sidorova, J.M., N. Li, A. Folch, and R.J. Monnat. 2008. The RecQ helicase WRN is required for normal replication fork progression after DNA damage or replication fork arrest. *Cell Cycle*. 7:796–807.

Sieber, O.M., L. Lipton, M. Crabtree, K. Heinimann, P. Fidalgo, R.K.S. Phillips, M.-L. Bisgaard, T.F. Orntoft, L.A. Aaltonen, S. V. Hodgson, H.J.W. Thomas, and I.P.M. Tomlinson. 2003. Multiple colorectal adenomas, classic adenomatous polyposis, and germ-line mutations in MYH. *N. Engl. J. Med.* 348:791–799.

Simon, M., L. Giot, and G. Faye. 1991. The 3' to 5' exonuclease activity located in the DNA polymerase delta subunit of Saccharomyces cerevisiae is required for accurate replication. *EMBO J.* 10:2165–2170.

Sinclair, W.K. 1965. Hydroxyurea: Differential lethal effects on cultured mammalian cells during the cell cycle. *Science.* 150:1729–1731.

Singh, A., and Y.-J. Xu. 2016. The cell killing mechanisms of hydroxyurea. *Genes (Basel).* 7:1–15.

Slater, M.L. 1973. Effect of reversible inhibition of deoxyribonucleic acid synthesis on the yeast cell cycle. *J. Bacteriol.* 113:263–270.

Smith, G.R. 2009. Genetic analysis of meiotic recombination in Schizosaccharomyces pombe. *Methods Mol. Biol.* 557:65–76.

Sogo, J.M., M. Lopes, and M. Foiani. 2002. Fork reversal and ssDNA accumulation at stalled replication forks owing to checkpoint defects. *Science.* 297:599–602.

Sohl, C.D., S. Ray, and J.B. Sweasy. 2015. Pools and Pols: Mechanism of a mutator phenotype. *Proc. Natl. Acad. Sci. U. S. A.* 112:5864–5865.

Sokolsky, T., and E. Alani. 2000. EXO1 and MSH6 are high-copy suppressors of conditional mutations in the MSH2 mismatch repair gene of Saccharomyces cerevisiae. *Genetics*. 155:589–599.

Soriano, I., E. Vazquez, N. De Leon, S. Bertrand, E. Heitzer, S. Toumazou, Z. Bo, C. Palles, C.C. Pai, T.C. Humphrey, I. Tomlinson, S. Cotterill, and S.E. Kearsey. 2021. Expression of the cancer-associated DNA polymerase ϵ P286R in fission yeast leads to translesion synthesis polymerase dependent hypermutation and defective DNA replication. *PLoS Genet.* 17:1–27.

Spier, I., S. Holzapfel, J. Altmüller, B. Zhao, S. Horpaopan, S. Vogt, S. Chen, M. Morak, S. Raeder, K. Kayser, D. Stienen, R. Adam, P. Nürnberg, G. Plotz, E. Holinski-Feder, R.P. Lifton, H. Thiele, P. Hoffmann, V. Steinke, and S. Aretz. 2015. Frequency and phenotypic spectrum of germline mutations in POLE and seven other polymerase genes in 266 patients with colorectal adenomas and carcinomas. *Int. J. Cancer*. 137:320–331.

St Charles, J.A., S.E. Liberti, J.S. Williams, S.A. Lujan, and T.A. Kunkel. 2015. Quantifying the contributions of base selectivity, proofreading and mismatch repair to nuclear DNA replication in Saccharomyces cerevisiae. *DNA Repair (Amst).* 31:41–51.

Stewart, E., C.R. Chapman, F. Al-Khodairy, A.M. Carr, and T. Enoch. 1997. rqh1+, a fission yeast gene related to the Bloom's and Werner's syndrome genes, is required for reversible S phase arrest. *EMBO J.* 16:2682–2692.

Stracker, T.H., and J.H. Petrini. 2011. The MRE11 complex: starting from the ends. *Nat. Rev. Mol. Cell Biol.* 12:90–103.

Strand, M., M.C. Earley, G.F. Crouse, and T.D. Petes. 1995. Mutations in the MSH3 gene preferentially

lead to deletions within tracts of simple repetitive DNA in Saccharomyces cerevisiae. *Proc. Natl. Acad. Sci. U. S. A.* 92:10418–10421.

Strand, M., T.A. Prolla, R.M. Liskay, and T.D. Petes. 1993. Destabilization of tracts of simple repetitive DNA in yeast by mutations affecting DNA mismatch repair. *Nature*. 365:274–276.

Stucki, M., B. Pascucci, E. Parlanti, P. Fortini, S.H. Wilson, U. Hübscher, and E. Dogliotti. 1998. Mammalian base excision repair by DNA polymerases δ and ε. *Oncogene*. 17:835–843.

Styrkársdóttir, U., R. Egel, and O. Nielsen. 1993. The smt-0 mutation which abolishes mating-type switching in fission yeast is a deletion. *Curr. Genet.* 23:184–186.

Su, T.T. 2006. Cellular responses to DNA damage: one signal, multiple choices. *Annu. Rev. Genet.* 40:187–208.

Suzuki, T., K. Matsumoto, M. Honma, and T. Nohmi. 2018. Impact of DNA polymerase ζ mutations on genotoxic thresholds of oxidative mutagens. *Mutat. Res. - Genet. Toxicol. Environ. Mutagen.* 828:10–14.

Svejstrup, J.Q., K. Christiansen, I.I. Gromova, A.H. Andersen, and O. Westergaard. 1991. New technique for uncoupling the cleavage and religation reactions of eukaryotic topoisomerase I. The mode of action of camptothecin at a specific recognition site. *J. Mol. Biol.* 222:669–678.

Syed, A., and J.A. Tainer. 2018. The MRE11-RAD50-NBS1 complex conducts the orchestration of damage signaling and outcomes to stress in DNA replication and repair. *Annu. Rev. Biochem.* 87:263–294.

Szüts, D., L. Kitching, C. Christov, A. Budd, S. Peak-Chew, and T. Krude. 2003. RPA is an initiation factor for human chromosomal DNA replication. *Nucleic Acids Res.* 31:1725–1734.

Tavassoli, M., M. Shayeghi, A. Nasim, and F.Z. Watts. 1995. Cloning and characterisation of the Schizosaccharomyces pombe rad32 gene: a gene required for repair of double strand breaks and recombination. *Nucleic Acids Res.* 23:383–388.

Taylor, A., A.F. Brady, I.M. Frayling, H. Hanson, M. Tischkowitz, C. Turnbull, and L. Side. 2018. Consensus for genes to be included on cancer panel tests offered by UK genetics services: guidelines of the UK Cancer Genetics Group. *J. Med. Genet.* 55:372–377.

The Cancer Genome Atlas Network. 2012. Comprehensive molecular characterization of human colon and rectal cancer. *Nature*. 487:330–337.

The Cancer Genome Atlas Network. 2013. Integrated genomic characterization of endometrial carcinoma. *Nature*. 497:67–73.

The Cancer Genome Atlas Network. 2014. Comprehensive molecular characterization of gastric adenocarcinoma. *Nature*. 513:202–209.

Timson, J. 1975. Hydroxyurea. *Mutat. Res.* 32:115–132.

Tong, A.H.Y., M. Evangelista, A.B. Parsons, H. Xu, G.D. Bader, N. Pagé, M. Robinson, S. Raghibizadeh, C.W. Hogue, H. Bussey, B. Andrews, M. Tyers, and C. Boone. 2001. Systematic genetic analysis with ordered arrays of yeast deletion mutants. *Science.* 294:2364–2368.

Tong, A.H.Y., G. Lesage, G.D. Bader, H. Ding, H. Xu, X. Xin, J. Young, G.F. Berriz, R.L. Brost, M. Chang, Y. Chen, X. Cheng, G. Chua, H. Friesen, D.S. Goldberg, J. Haynes, C. Humphries, G. He, S. Hussein, L. Ke, N. Krogan, Z. Li, J.N. Levinson, H. Lu, P. Me, C. Munyana, A.B. Parsons, O. Ryan, R. Tonikian, T. Roberts, A. Sdicu, J. Shapiro, B. Sheikh, B. Suter, S.L. Wong, L. V Zhang, H. Zhu, C.G. Burd, S. Munro, C. Sander, J. Rine, J. Greenblatt, M. Peter, A. Bretscher, G. Bell, F.P. Roth, G.W. Brown, B. Andrews, H. Bussey, and C. Boone. 2004. Global mapping of the yeast genetic interaction network. *Science.* 303:808–813.

Tran, H.T., N.P. Degtyareva, D.A. Gordenin, and M.A. Resnick. 1999a. Genetic factors affecting the impact of DNA Polymerase δ proofreading activity on mutation avoidance in yeast. *Genetics*. 152:47–59.

Tran, H.T., D.A. Gordenin, and M.A. Resnick. 1999b. The 3'-5' exonucleases of DNA polymerases δ and ε and the 5'-3' exonuclease Exo1 have major roles in postreplication mutation avoidance in Saccharomyces cerevisiae. *Mol. Cell. Biol.* 19:2000–2007.

Tran, H.T., J.D. Keen, M. Kricker, M.A. Resnick, and D.A. Gordenin. 1997. Hypermutability of homonucleotide runs in mismatch repair and DNA polymerase proofreading yeast mutants. *Mol. Cell. Biol.* 17:2859–2865.

Tsang, E., I. Miyabe, I. Iraqui, J. Zheng, S.A. Lambert, and A.M. Carr. 2014. The extent of error-prone replication restart by homologous recombination is controlled by Exo1 and checkpoint proteins. *J. Cell Sci.* 127:2983–2994.

Tsao, Y., A. Russo, G. Nyamuswa, R. Silber, and L. Liu. 1993. Interaction between replication forks and topoisomerase I-DNA cleavable complexes: studies in a cell-free SV40 DNA replication system. *Cancer Res.* 53:5908–5914.

Tseng, S.-F., A. Gabriel, and S.-C. Teng. 2008. Proofreading activity of DNA polymerase Pol2 mediates 3'-end processing during nonhomologous end joining in yeast. *PLoS Genet.* 4:1–10.

Tsutsui, Y., T. Morishita, T. Natsume, K. Yamashita, H. Iwasaki, F. Yamao, and H. Shinagawa. 2005. Genetic and physical interactions between Schizosaccharomyces pombe Mcl1 and Rad2, Dna2 and DNA polymerase a: evidence for a multifunctional role of Mcl1 in DNA replication and repair. *Curr. Genet.* 48:34–43.

Tyrsted, G. 1982. Effect of hydroxyurea and 5-fluorodeoxy-uridine on deoxyribonucleoside triphosphate pools early in phytohemagglutinin-stimulated human lymphocytes. *Biochem. Pharmacol.* 31:3107–3113.

Umar, A., and T.A. Kunkel. 1996. DNA-replication fidelity, mismatch repair and genome instability in cancer cells. *Eur. J. Biohemistry*. 238:297–307.

Uziel, T., Y. Lerenthal, L. Moyal, Y. Andegeko, L. Mittelman, and Y. Shiloh. 2003. Requirement of the MRN complex for ATM activation by DNA damage. *EMBO J.* 22:5612–5621.

Valle, L. 2014. Genetic predisposition to colorectal cancer: where we stand and future perspectives. *World J. Gastroenterol.* 20:9828–49.

Valle, L., E. Hernández-Illán, F. Bellido, G. Aiza, A. Castillejo, M.I. Castillejo, M. Navarro, N. Seguí, G. Vargas, C. Guarinos, M. Juarez, X. Sanjuán, S. Iglesias, C. Alenda, C. Egoavil, Á. Segura, M.J. Juan, M. Rodriguez-Soler, J. Brunet, S. González, R. Jover, C. Lázaro, G. Capellá, M. Pineda, J.L. Soto, and I. Blanco. 2014. New insights into POLE and POLD1 germline mutations in familial colorectal cancer and polyposis. *Hum. Mol. Genet.* 23:3506–3512.

Vallen, E.A., and F.R. Cross. 1995. Mutations in RAD27 define a potential link between G1 cyclins and DNA replication. *Mol. Cell. Biol.* 15:4291–4302.

Van Gool, I.C., F.A. Eggink, L. Freeman-Mills, E. Stelloo, E. Marchi, M. De Bruyn, C. Palles, R.A. Nout, C.D. De Kroon, E.M. Osse, P. Klenerman, C.L. Creutzberg, I.P.M. Tomlinson, V.T.H.B.M. Smit, H.W. Nijman, T. Bosse, and D.N. Church. 2015. POLE proofreading mutations elicit an antitumor immune response in endometrial cancer. *Clin. Cancer Res.* 21:3347–3355.

Volkmer, E., and L.M. Karnitz. 1999. Human homologs of Schizosaccharomyces pombe Rad1, Hus1, and Rad9 form a DNA damage responsive protein complex. *J. Biol. Chem.* 274:567–570.

Waga, S., and B. Stillman. 1998. The DNA replication fork in eukaryotic cells. *Annu. Rev. Biochem.* 67:721–751.

Watson, J.D., and F.H.C. Crick. 1953. Molecular structure of nucleic acids: A structure for deoxyribose nucleic acid. *Nature*. 171:737–738.

Weren, R.D.A., M.J.L. Ligtenberg, C. Gilissen, E.J. Kamping, A.G. Van Kessel, N. Hoogerbrugge, and R.P. Kuiper. 2017. Heritable polyposis and colorectal cancer: expanding the genetic spectrum. Radboud University Nijmegen. 110–145 pp.

West, S.C. 2003. Molecular views of recombination proteins and their control. *Nat. Rev. Mol. Cell Biol.* 4:1–11.

Williams, D.R., and J. McIntosh. 2005. Mcl1p is a polymerase α replication accessory factor important for S-phase DNA damage survival. *Eukaryot. Cell*. 4:166–177.

Williams, L.N., A.J. Herr, and B.D. Preston. 2013. Emergence of DNA polymerase ε antimutators that escape error-induced extinction in yeast. *Genetics*. 193:751–770.

Williams, L.N., L. Marjavaara, G.M. Knowels, E.M. Schultz, E.J. Fox, A. Chabes, and A.J. Herr. 2015. dNTP pool levels modulate mutator phenotypes of error-prone DNA polymerase ε variants. *Proc. Natl. Acad. Sci. U. S. A.* 112:2457–2466.

Willis, N., and N. Rhind. 2009. Mus81, Rhp51(Rad51), and Rqh1 form an epistatic pathway required for the S-phase DNA damage checkpoint. *Mol. Biol. Cell*. 20:819–833.

Willis, N., and N. Rhind. 2010. The fission yeast Rad32(Mre11)-Rad50-Nbs1 complex acts both upstream and downstream of checkpoint signaling in the S-phase DNA damage checkpoint. *Genetics*. 184:887–897.

Wood, V., R. Gwilliam, M. Rajandream, M. Lyne, R. Lyne, A. Stewart, J. Sgouros, N. Peat, J. Hayles, S. Baker, D. Basham, S. Bowman, K. Brooks, D. Brown, S. Brown, T. Chillingworth, C. Churcher, M. Collins, R. Connor, A. Cronin, P. Davis, T. Feltwell, A. Fraser, S. Gentles, A. Goble, N. Hamlin, D. Harris, J. Hidalgo, G. Hodgson, S. Holroyd, T. Hornsby, S. Howarth, E. Huckle, S. Hunt, K. Jagels, K. James, L. Jones, M. Jones, S. Leather, S. McDonald, J. McLean, P. Mooney, S. Moule, K. Mungall, L. Murphy, D. Niblett, C. Odell, K. Oliver, S. O'Neil, D. Pearson, M. Quail, E. Rabbinowitsch, K. Rutherford, S. Rutter, D. Saunders, K. Seeger, S. Sharp, J. Skelton, M. Simmonds, R. Squares, S. Squares, K. Stevens, K. Taylor, R. Taylor, A. Tivey, S. Walsh, T. Warren, S. Whitehead, J. Woodward, G. Volckaert, R. Aert, J. Robben, B. Grymonprez, I. Weltjens, E. Vanstreels, M. Rieger, and M. Schäfer. 2002. The genome sequence of Schizosaccharomyces pombe. *Nature*. 415:871–880.

Wu, L., and I.D. Hickson. 2003. The Bloom's syndrome helicase suppresses crossing over during homologous recombination. *Nature*. 426:870–874.

Xu, Y., A. Singh, and G.M. Alter. 2016. Hydroxyurea induces cytokinesis arrest in cells expressing a mutated sterol-14a-demethylase in the ergosterol biosynthesis pathway. *Genetics*. 204:959–973.

Xu, Y.J., M. Davenport, and T.J. Kelly. 2006. Two-stage mechanism for activation of the DNA replication checkpoint kinase Cds1 in fission yeast. *Genes Dev.* 20:990–1003.

Yeeles, J.T., T.D. Deegan, A. Janska, A. Early, and J.F. Diffley. 2015. Regulated eukaryotic DNA replication origin firing with purified proteins. *Nature*. 519:431–435.

Yeeles, J.T., J. Poli, K.J. Marians, and P. Pasero. 2013. Rescuing stalled or damaged replication forks. *Cold Spring Harb. Perspect. Biol.* 5:1–16.

Yokoyama, M., H. Inoue, C. Ishii, and Y. Murakami. 2007. The novel gene mus7+ is involved in the repair of replication-associated DNA damage in fission yeast. *DNA Repair (Amst).* 6:770–780.

York, J.D., A.R. Odom, R. Murphy, E.B. Ives, and S.R. Wente. 1999. A phospholipase C-dependent inositol polyphosphate kinase pathway required for efficient messenger RNA export. *Science*. 285:96–100.

You, Z., C. Chahwan, J. Bailis, T. Hunter, and P. Russell. 2005. ATM activation and its recruitment to damaged DNA require binding to the C terminus of Nbs1. *Mol. Cell. Biol.* 25:5363–5379.

You, Z., L. Kong, and J. Newport. 2002. The role of single-stranded DNA and polymerase α in establishing the ATR, Hus1 DNA replication checkpoint. *J. Biol. Chem.* 277:27088–27093.

Young, J.A., R.W. Hyppa, and G.R. Smith. 2004. Conserved and nonconserved proteins for meiotic DNA breakage and repair in yeasts. *Genetics*. 167:593–605.

Zegerman, P. 2013. DNA replication: polymerase epsilon as a non-catalytic converter of the helicase. *Curr. Biol.* 23:R273-6.

Zegerman, P., and J.F. Diffley. 2007. Phosphorylation of Sld2 and Sld3 by cyclin-dependent kinases promotes DNA replication in budding yeast. *Nature*. 445:281–285.

Zeng, Y., K.C. Forbes, Z. Wu, S. Moreno, H. Piwnica-Worms, and T. Enoch. 1998. Replication checkpoint requires phosphorylation of the phosphatase Cdc25 by Cds1 or Chk1. *Nature*. 395:507–510.

Zeng, Y., and H. Piwnica-Worms. 1999. DNA damage and replication checkpoints in fission yeast require nuclear exclusion of the Cdc25 phosphatase via 14-3-3 binding. *Mol. Cell. Biol.* 19:7410–7419.

Zhang, J., D. Hou, J. Annis, F. Sargolzaeiaval, J. Appelbaum, E. Takahashi, G.M. Martin, A. Herr, and J. Oshima. 2020. Inactivating mutations in exonuclease and polymerase domains in DNA polymerase delta alter sensitivities to inhibitors of dNTP synthesis. *DNA Cell Biol.* 39:50–56.

Zhao, H., K. Tanaka, E. Nogochi, C. Nogochi, and P. Russell. 2003. Replication checkpoint protein Mrc1 is regulated by Rad3 and Tel1 in fission yeast. *Mol. Cell. Biol.* 23:8395–8403.

Zhao, X., and R. Rothstein. 2002. The Dun1 checkpoint kinase phosphorylates and regulates the ribonucleotide reductase inhibitor Sml1. *Proc. Natl. Acad. Sci. U. S. A.* 99:3746–3751.

Zhou, B.S., and S.J. Elledge. 2000. The DNA damage response: putting checkpoints in perspective. *Nature*. 408:433–439.

Zhu, W., C. Ukomadu, S. Jha, T. Senga, S.K. Dhar, J.A. Wohlschlegel, L.K. Nutt, S. Kornbluth, and A. Dutta. 2007. Mcm10 and And-1/CTF4 recruit DNA polymerase α to chromatin for initiation of DNA replication. *Genes Dev.* 21:2288–2299.

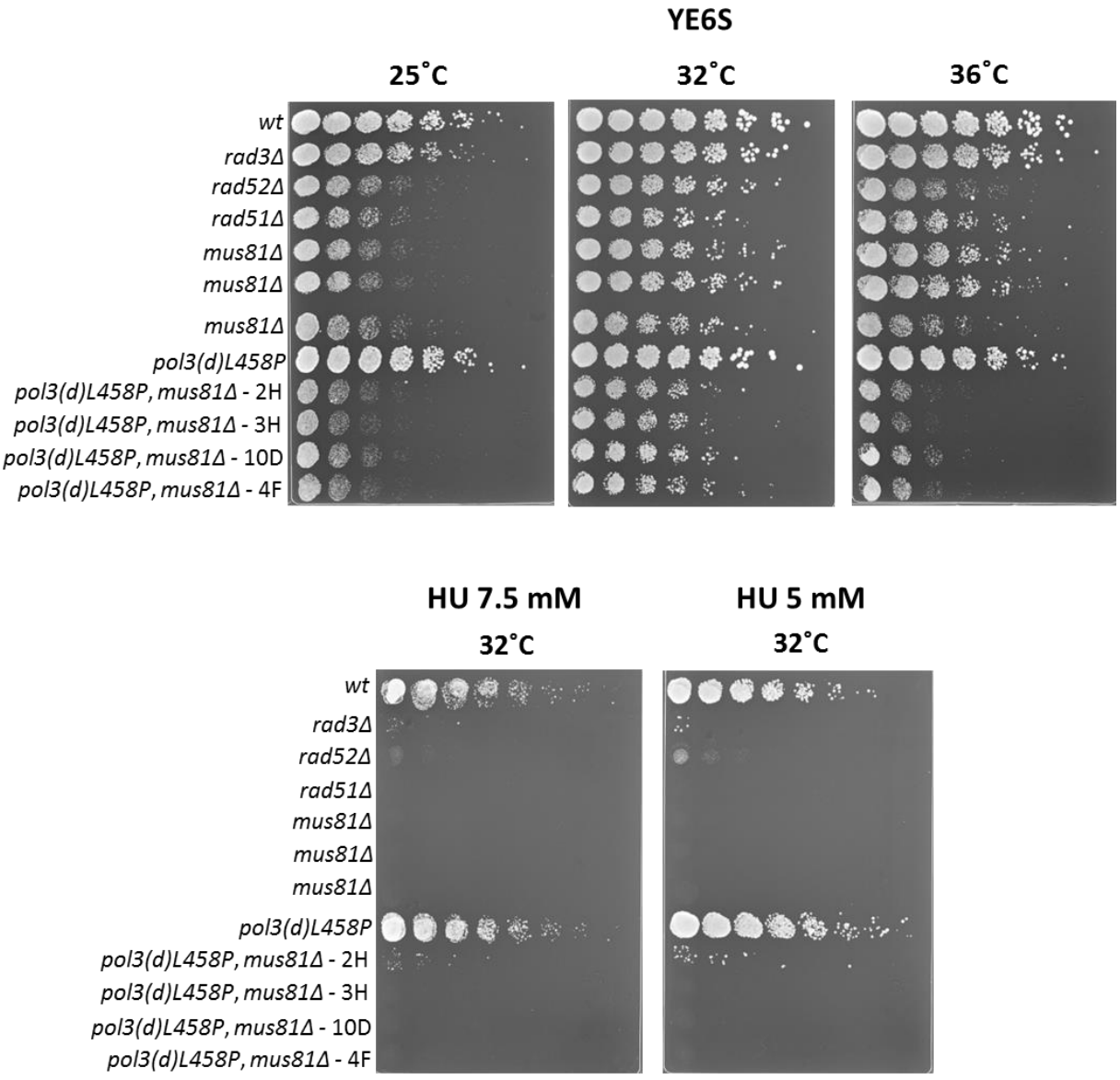
Zou, L., D. Cortez, and S.J. Elledge. 2002. Regulation of ATR substrate selection by Rad17-dependent loading of Rad9 complexes onto chromatin. *Genes Dev.* 16:198–208.

Zou, L., and S.J. Elledge. 2003. Sensing DNA damage through ATRIP recognition of RPA-ssDNA complexes. *Science*. 300:1542–1548.

Zou, Y., Y. Liu, X. Wu, and S.M. Shell. 2006. Functions of human replication protein A (RPA): from DNA replication to DNA damage and stress responses. *J. Cell. Physiol.* 208:267–273.

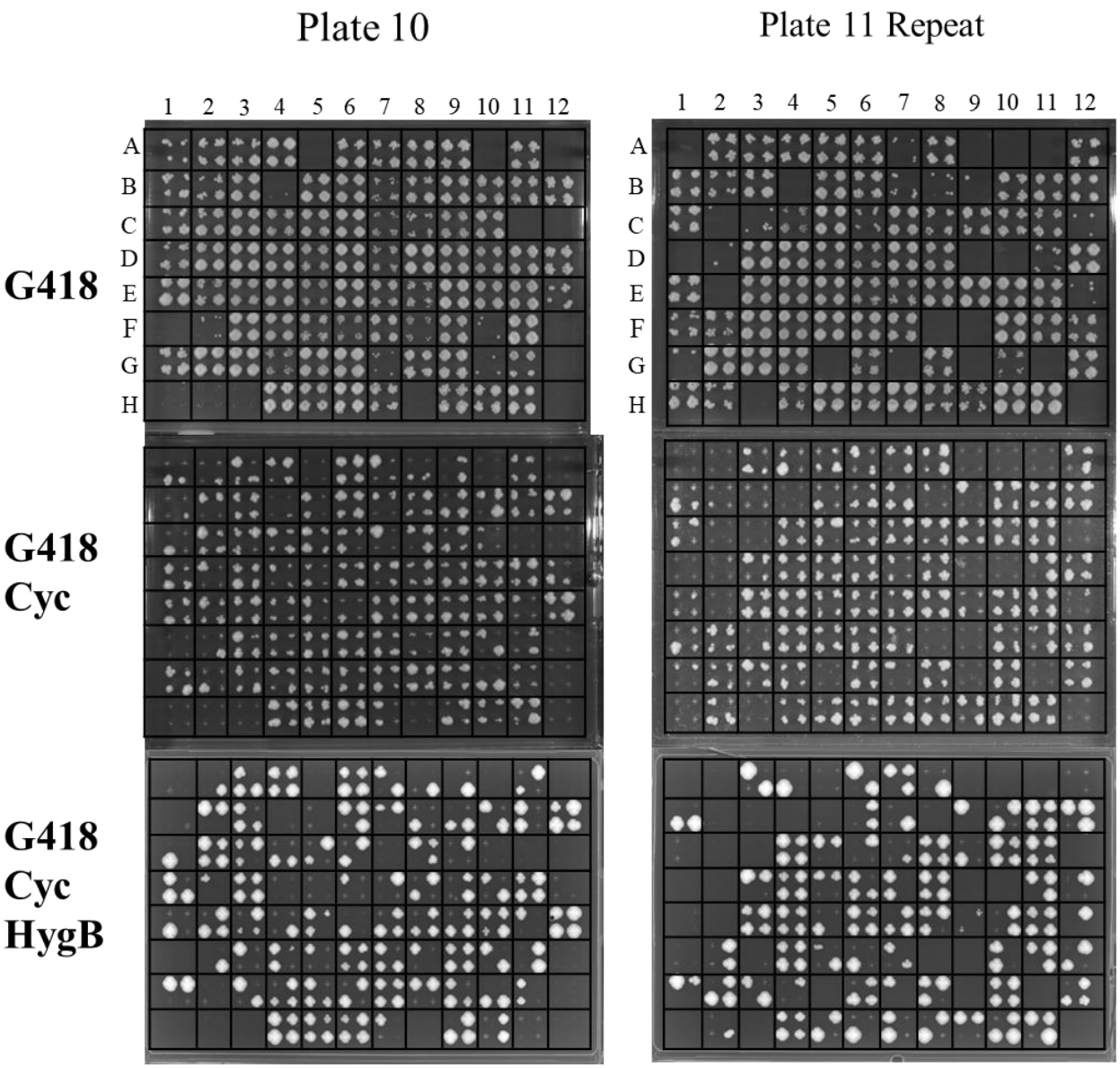
Appendices

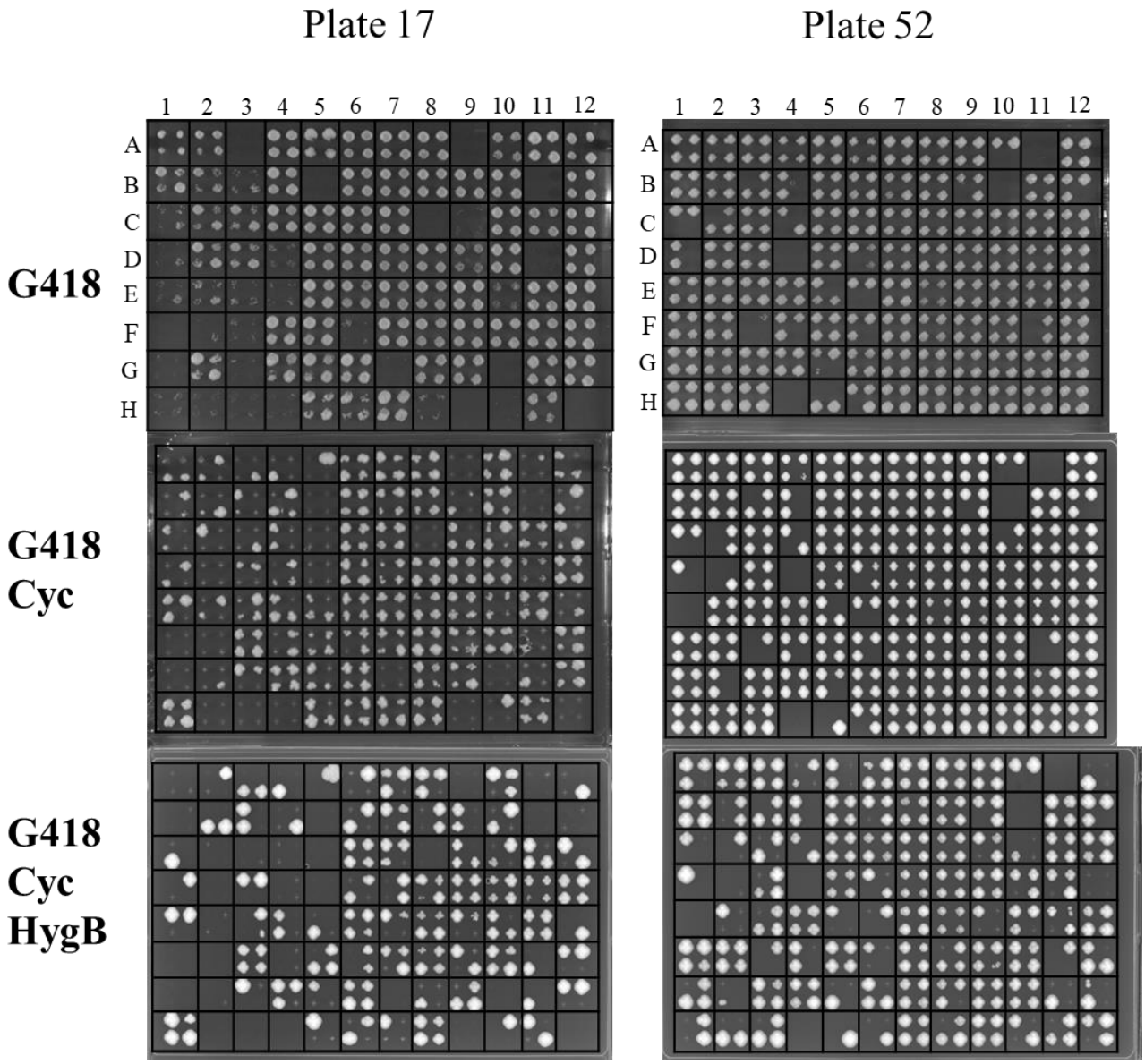
Appendix I: Serial spot-dilution of the *pol3* EDMs and *mus81*Δ single and double mutants on 5 mM and 7.5 mM HU plates



Five-fold serial spot-dilution of the *pol3* mutations and *mus81*Δ, single and double mutant strains on YE6S and HU 7.5 mM at 30˚C and 36˚C.

Appendix II: Original images of the plates from the Bioneer cross (from Figure 5.3)




Plate 17
Plate 52
1 2 3 4 5 6 7 8 9 10 11 12
A
B
C
D
E
F
G
H
G418
G418
Cyc
G418
Cyc
HygB

Appendix III: Table of Bioneer screen results

Strain	Gene/ Gene Product	GO (Slim) Term(s)
SPAC2F3.12c	*plp1*	Protein folding
SPAC17D4.01	*pex7*	Peroxisome organisation
SPAC57A10.14	*sgf11*	Chromatin organisation; Transcription, DNA-templated
SPAC212.03	Unknown	Unknown
SPAC8E11.07c	*alp31*	Protein folding; Protein-containing (e.g. tubulin) complex assembly
SPAC750.08c	NAD-dependent malic enzyme (predicted)	Cellular amino acid metabolic process
SPBC2D10.16	*mhf1*	DNA recombination; DNA replication; DNA repair; Meiotic nuclear division
SPAC105.03c	DNA-binding transcription factor (predicted)	Transcription, DNA-templated
SPBPB21E7.01c	*eno102*	Carbohydrate metabolic process
SPBC1198.11c	*reb1*	DNA replication; Transcription, DNA-templated
SPAC139.03	*toe2*	Transcription, DNA-templated
SPCC24B10.18	DUF2462 family protein	Unknown
SPAC13F5.05	*mpd1*	Protein folding
SPAC1071.02	*mms19*	Iron-sulphur cluster assembly; Sulphur compound metabolic process; Protein maturation
SPAC12B10.07	*acp1*	Actin cytoskeleton organisation; Protein-containing complex assembly; Mitotic cytokinesis
SPAC13G6.07c	*rps601*	Cytoplasmic translation; Ribosome biogenesis
SPCC320.04c	*gem1*	Mitochondrion organization
SPCC126.07c	*asr1*	Protein modification by small protein conjugation or removal; Transcription, DNA-templated
SPBC725.05c	*npp1*	Mitochondrion organisation
SPAC144.05	DNA-dependent ATPase/ ubiquitin-protein ligase E3 (predicted)	DNA repair; Protein modification (polyubiquitination)
SPCC126.11c	RNA-binding protein, rrm type	Unknown
SPCC970.07c	*raf2*	Transcription, DNA-templated; Telomere organisation; Protein-containing complex assembly; Chromatin organisation
SPCC1322.14c	*vtc4*	Autophagy; Generation of precursor metabolites and energy
SPAC23A1.07	Ubiquitin-protein ligase E3 (predicted)	Protein modification by small protein conjugation or removal
SPAC1952.07	*rad1*	Mitotic cell cycle phase transition; (Checkpoint) Signalling; DNA repair; Telomere organisation
SPAC17A2.12	*rrp1*	DNA replication; Protein modification by small protein conjugation or removal; DNA repair; DNA recombination; Chromatin organisation
SPAC22A12.14c	BSD domain protein, unknown biological role	Unknown

SPAC17A5.11	*rec12*	Meiotic nuclear division; DNA repair; DNA recombination
SPAC1B3.05	*not3*	mRNA metabolic process
SPAC23A1.04c	*mnl1*	Protein catabolic process
SPAC17G6.02c	*tco1*	Membrane organisation
SPAC1687.06c	*rpl44*	Cytoplasmic translation
SPAC1952.16	*rga9*	Signalling
SPAC20G8.08c	*fft1*	Transcription, DNA-templated; Chromatin organisation
SPAC1834.03c	*hhf1*	Protein-containing complex assembly; Chromatin organisation
SPAC23D3.03c	GTPase activating protein (predicted)	Vesicle-mediated transport
SPAC17C9.09c	tim13	Membrane organisation; Protein targeting; Mitochondrion organisation
SPAC3H1.06c	Transmembrane transporter (predicted)	Transmembrane transport
SPAC328.04	spg4	Microtubule cytoskeleton organisation
SPAC3A12.06c	Sodium/calcium exchanger (predicted)	Transmembrane transport
SPAC328.06	ubp2	Protein modification (ubiquitination); Protein catabolic process
SPAC2F7.10	*akr1*	Protein palmitoylation
SPACUNK4.13c	mitochondrial NTPase Obg family, human OLA1 ortholog, implicated in mitochondrial translation, ribosome assembly, or tRNA metabolism (predicted)	Unknown
SPAPB1A10.03	*nxt1*	Ribosome biogenesis; Nucleocytoplasmic transport
SPBC12D12.06	*srb11*	Transcription, DNA-templated
SPBC29A10.14	*rec8*	Meiotic nuclear division
SPAPB1A11.04c	*mca1*	Transcription, DNA-templated
SPAPB8E5.05	*mfm1*	Signalling
SPBC16H5.11c	*skb1*	Establishment of cell polarity; Transcription, DNA-templated; Protein-containing complex assembly; Chromatin organisation
SPBC17F3.01c	*rga5*	Carbohydrate metabolic process; Cell wall organisation; Signalling
SPAPYUK71.03c	*tcb3*	Organelle localisation by membrane tethering
SPBC1703.06	*pof10*	Protein modification; Protein-containing complex assembly; Protein catabolic process
SPBC1718.02	*hop1*	Meiotic nuclear division; Protein modification; DNA recombination
SPBC2A9.03	WD40/YVTN repeat-like protein	Unknown
SPBC19F8.04c	*lcl3*	Unknown
SPBC2A9.04c	*san1*	Protein modification; Protein catabolic process
SPBC115.02c	*afg1*	Protein catabolic process

SPBC16G5.05c	*scs2*	Membrane organisation; Autophagy; Establishment of cell polarity; Organelle localisation by membrane tethering
SPBC29A10.09c	*tri1*	Transcription, DNA-templated; mRNA metabolic process; Chromatin organisation
SPBC15C4.05	*dhx29*	Cytoplasmic translation
SPBC13E7.09	*vrp1*	Vesicle-mediated transport; Actin cytoskeleton organisation; Protein-containing complex assembly
SPBC557.04	*ppk29*	Actin cytoskeleton organisation
SPBC359.06	*mug14*	Actin cytoskeleton organisation
SPBC342.06c	*rtt109*	Protein-containing complex assembly; Transcription, DNA-templated; Chromatin organisation
SPBC651.02	*nit1*	Nucleobase-containing small molecule metabolic process
SPBC776.01	*rpl29*	Cytoplasmic translation
SPBC902.02c	*ctf18*	DNA replication
SPCC4B3.13	MatE family transmembrane transporter (predicted)	Transmembrane transport
SPCC330.02	*rhp7*	DNA repair
SPBC428.12c	Peptidyl-prolyl cis-trans isomerase E (predicted)	mRNA metabolic process
SPCC338.06c	Heat shock protein Hsp20 family (predicted)	Protein folding
SPCC1840.07c	Vacuolar endopolyphosphatase (predicted)	Generation of precursor metabolites and energy
SPCC736.11	*ago1*	Transcription, DNA-templated; Protein-containing complex assembly; Chromatin organisation
SPBC13G1.02	*mpg2*	Protein glycosylation; Nucleobase-containing small molecule metabolic process
SPAC1527.01	*mok11*	Carbohydrate metabolic process; Cell wall organisation
SPCC777.07	*omh3*	Cell wall organisation; Protein glycosylation
SPBC23E6.02	*rrp2*	DNA replication; Protein modification; DNA repair; DNA recombination; Protein catabolic process
SPAC1565.07c	*knd1*	Protein modification; Protein-containing complex assembly
SPCC63.04	*mok14*	Carbohydrate metabolic process; Cell wall organisation; Ascospore formation
SPBC1734.06	*rhp18*	Protein modification (ubiquitination); DNA repair
SPBC3B8.06	DUF2427 family conserved fungal protein	Unknown
SPBC32H8.13c	*mok12*	Carbohydrate metabolic process; Cell wall organisation; Ascospore formation
SPCC24B10.03	Unknown	Unknown
SPCC4G3.09c	*gyp3*	Vesicle-mediated transport; Actin cytoskeleton organisation

SPCC736.08	*cbf11*	Lipid metabolic process; Transcription, DNA-templated
SPAC30.03c	*tsn1*	tRNA metabolic process
SPBC215.05	*gpd1*	Carbohydrate metabolic process
SPAC521.04c	*sst1*	Metal ion homeostasis; Transmembrane transport
SPBC1703.14c	*top1*	Mitotic sister chromatid segregation; Chromatin organisation
SPBC17D11.04c	*nto1*	Protein modification; Chromatin organisation
SPBC947.08c	*hip4*	Protein-containing complex assembly; Chromatin organisation
SPAC9G1.10c	*inp53*	Carbohydrate metabolic process; Signalling; Lipid metabolic process
SPBP35G2.11c	*nbr1*	Protein targeting
SPBC1703.04	*mlh1*	DNA repair
SPAC959.06c	Alpha/beta hydrolase fold	Unknown
SPAC14C4.07	Transmembrane transporter (predicted)	Transmembrane transport
SPAC16.01	*rho2*	Actin cytoskeleton organisation; Cell wall organisation; Signalling; Carbohydrate metabolic process; Establishment of cell polarity
SPBC19F8.03c	*yap18*	Membrane organisation; Protein-containing complex assembly; Vesicle-mediated transport
SPAC27D7.13c	*ssm4*	Microtubule cytoskeleton organisation; Meiotic nuclear division; Conjugation with cellular fusion
SPAC1F8.04c	Hydrolase, implicated in cellular detoxification (predicted)	Unknown
SPAC4C5.01	pud1	Nucleobase-containing small molecule metabolic process
SPBC18H10.06c	*swd2*	Transcription, DNA-templated; Chromatin organisation
SPBC577.06c	*stt4*	Signalling; Lipid metabolic process
SPBP4H10.13	*rps2302*	Cytoplasmic translation; Nucleocytoplasmic transport; Signalling
SPAC2F3.16	Ubiquitin-protein ligase E3, implicated in DNA repair (predicted)	Protein modification (ubquitination); Protein catabolic process
SPCC285.16c	*msh6*	DNA repair
SPAPB1E7.05	*gde1*	Lipid metabolic process
SPAC22E12.11c	*set3*	Transcription, DNA-templated; Chromatin organisation; Protein modification
SPAC29A4.11	*rga3*	Signalling
SPAC22G7.11c	*cum1*	Unknown
SPCC970.02	*dcw1*	Cell wall organisation; Carbohydrate metabolic process
SPAC926.06c	Leucine-rich repeat protein, unknown role	Unknown
SPBC1198.06c	*dfg501*	Cell wall organisation; Carbohydrate metabolic process
SPAC24C9.07c	*bgs2*	Ascospore formation; Cell wall organisation; Carbohydrate metabolic process
SPBC2G2.14	*csi1*	Mitotic sister chromatid segregation

SPAC637.11	*rpm2/suv3*	Mitochondrial gene expression
SPBC1711.13	*his2*	Cellular amino acid metabolic process
SPAC29B12.14c	Plasma membrane purine transmembrane transporter (predicted)	Transmembrane transport
SPCC1183.11	*msy1*	Transmembrane transport; Metal ion homeostasis
SPAC17G6.03	Extracellular 5'-nucleotidase, human NT5E family (predicted)	Nucleobase-containing small molecule metabolic process
SPCP31B10.07	*eft202*	Cytoplasmic translation
SPBC14F5.09c	*ade8*	Nucleobase-containing small molecule metabolic process
SPAC22G7.01c	*fra1*	Transcription, DNA-templated
SPAC1805.10	Unknown	Unknown
SPCC31H12.02c	*mug73*	Unknown
SPBC365.12c	*ish1*	Unknown
SPCC4G3.05c	*mus81*	Meiotic nuclear division; Mitotic cell cycle phase transition; DNA recombination; Signalling; DNA replication; DNA repair
SPAC6F6.04c	Transmembrane transporter (predicted)	Transmembrane trannsport
SPAC30D11.05	*aps3*	Vesicle-mediated transport
SPAC1093.03	*fig4*	Signalling; Lipid metabolic process
SPCC4G3.19	*alp16*	Microtubule cytoskeleton organisation; Protein-containing complex assembly
SPBC1604.01	*egt1/mug158*	Cellular amino acid metabolic process; Sulphur compound metabolic process
SPBC19F8.06c	*meu22*	Transmembrane transport
SPBC2G5.04c	*erv41*	Vesicle-mediated transport
SPBC2G2.01c	*liz1*	Transmembrane transport
SPBC2A9.11c	*iss9*	Unknown
SPAC1F3.10c	*oct1*	Mitochondrion organisation; Metal ion homeostasis; Protein targeting; Protein maturation
SPBC27.02c	*ask1*	Meiotic nuclear division; Mitotic sister chromatid segregation; Establishment of cell polarity; Microtubule cytoskeleton organisation
SPCC4G3.08	*psk1*	Signalling
SPAC343.16	*lys2*	Cellular amino acid metabolic process
SPAC17H9.19c	*cdt2*	DNA repair; Protein catabolic process
SPAC343.15	*tit1*	tRNA metabolic process
SPAC186.01	*pfl9*	Cell adhesion
SPAC1952.11c	*ure2*	Nitrogen cycle metabolic process
SPCC965.05c	*thp1*	DNA repair
SPAC23H4.08	*iwr1*	Nucleocytoplasmic transport
SPAC2E12.03c	Plasma membrane basic amino acid transmembrane transporter (predicted)	Transmembrane transport
SPAC3G6.06c	*rad2*	DNA repair

SPAC458.04c	*dli1*	Meiotic nuclear division; Microtubule cytoskeleton organisation
SPAC25H1.04	*mug105*	Protein modification
SPAC750.06c	*S. pombe* specific DUF999 protein family 4	Unknown
SPBC405.04c	ypt7	Signalling; Vesicle-mediated transport
SPAC17A2.02c	TLC domain-containing protein	Membrane organisation
SPAC14C4.12c	*laf1*	Transcription, DNA-templated; Chromatin organisation
SPAC922.06	3-oxoacyl-[acyl-carrier-protein]reductase (predicted)	Sulphur compound metabolic process; Lipid metabolic process
SPCC1682.12c	*ubp16*	Protein catabolic process; Protein modification (deubiquination)
SPBC947.06c	Spermidine family transmembrane transporter (predicted)	Detoxification; Transmembrane transport
SPBC21D10.12	*hob1*	Protein-containing complex assembly; Actin cytoskeleton organisation; Establishment of cell polarity
SPAPB1A10.12c	*alo1*	Unknown
SPBC651.10	*nse5*	DNA replication; DNA recombination; DNA repair
SPBC543.03c	*pku80*	DNA recombination; DNA repair; Telomere organisation
SPCC622.12c	*gdh1*	Cellular amino acid metabolic process
SPCC1840.06	*atp5*	Generation of precursor metabolites and energy; Nucleobase-containing small molecule metabolic process; Transmembrane transport
SPAC1399.02	Transmembrane transporter (predicted)	Transmembrane transport
SPAC1F8.06	*pfl8*	Cell adhesion
SPAC323.05c	*mtq2*	Cytoplasmic translation
SPBC4F6.16c	*ero11*	Protein folding
SPBC405.04c	*ypt7*	Vesicle-mediated transport; Signalling
SPCC1739.08c	Short chain dehydrogenase (predicted)	Unknown
SPCC1494.09c	*tfb6*	Transcription, DNA-templated
SPAC5H10.06c	*adh4*	Generation of precursor metabolites and energy
SPAP27G11.08c	*meu32*	Unknown
SPAC3C7.09	*set8*	Unknown
SPAC589.07c	*atg1801*	Mitochondrion organisation; Protein targeting; Autophagy
SPBC31F10.10c	*mub1*	Protein catabolic process; Establishment of cell polarity
SPBP4H10.09	*rsv1*	Transcription, DNA-templated
SPBP23A10.16	*sdh4/tim18*	Mitochondrion organisation; Protein targeting; Generation of precursor metabolites and energy; Membrane organisation
SPAC869.10c	*put4*	Transmembrane transport

SPAPJ696.01c	*vps17*	Vesicle-mediated transport; Ascospore formation; Membrane organisation
SPBC1685.07c	*avt5*	Transmembrane transport
SPBC31A8.01c	*rtn1/cwl1*	Membrane organisation
SPAC20H4.06c	*gpl1*	mRNA metabolic process
SPAC23D3.04c	*gpd2*	Carbohydrate metabolic process
SPBC1198.01	*fmd2*	Detoxification
SPBC28F2.02	*mep33*	Nucleocytoplasmic transport; Cytoplasmic translation
SPAC23H3.08c	*bub3*	Mitotic cell cycle phase transition; Signalling; Mitotic sister chromatid segregation
SPBC1861.02	*abp2*	Unknown
SPBCPT2R1.01c	*S. pombe* specific DUF999 protein family 9	Unknown
SPCC613.03	Endoplasmic reticulum EF hand protein (predicted)	Unknown
SPAC4G8.10	*gos1*	Vesicle-mediated transport
SPBC609.04	*caf5*	Transmembrane transport; Detoxification
SPCC736.09c	*tfx1*	tRNA metabolic process
SPAC25B8.15c	*tyw3*	tRNA metabolic process
SPAC869.06c	*hry1*	Unknown
SPAC4H3.14c	*rng8*	Mitotic cytokinesis; Conjugation with cellular fusion; Actin cytoskeleton organisation
SPCC965.08c	*alr1*	Cellular amino acid metabolic process
SPBC1703.03c	*syo2*	Ribosome biogenesis; Nucleocytoplasmic transport
SPBC23E6.10c	*mri1*	Sulphur compound metabolic process; Cellular amino acid metabolic process
SPBC947.05c	*frp2*	Transmembrane transport; Metal ion homeostasis
SPAC13G6.02c	*rps101*	Ribosome biogenesis; Cytoplasmic translation
SPBPB10D8.07c	Transmembrane transporter (predicted)	Transmembrane transport
SPAC14C4.01c	atg43	Mitochondrion organisation; Autophagy
SPBC16G5.13	*ptf2*	Chromatin organisation
SPAC31G5.04	*lys12*	Cellular amino acid metabolic process
SPCC11E10.03	*mug1/jnm1*	Meiotic nuclear division; Microtubule cytoskeleton organisation
SPAC8F11.10c	*pvg1*	Cell wall organisation; Carbohydrate metabolic process
SPCC550.10	*atd3/meu8*	Detoxification
SPAC23G3.10c	*ssr3*	Transcription, DNA-templated; Chromatin organisation
SPCC24B10.14c	*xlf1*	DNA repair
SPAC140.04	*ctr1*	Telomere organisation
SPAC18G6.13	Unknown	Unknown
SPAC1834.09	*mug51*	Unknown
SPAC19G12.13c	*poz1*	Telomere organisation
SPBC8D2.18c	Adenosylhomocysteinase (predicted)	Sulphur compound metabolic process; Cellular amino acid metabolic process
SPBC16G5.03	*mrz1*	Protein modification; Protein catabolic process

SPAC12B10.10	*nod1*	Actin cytoskeleton organisation; Mitotic cytokinesis
SPBPB10D8.06c	Transmembrane transporter (predicted)	Transmembrane transport
SPAC1834.10c	Mitochondrial proton-transporting ATP synthase complex assembly protein (predicted)	Mitochondrion organisation; Protein-containing complex assembly
SPAC22F3.13	*tsc1*	Transmembrane transport; Signalling; Mitotic cell cycle phase transition
SPBC354.12	*gpd3*	Generation of precursor metabolites and energy; Nucleobase-containing small molecule metabolic process; Carbohydrate metabolic process
SPAC5H10.12c	*otg1*	Protein glycosylation
SPAC12B10.11	*exg2*	Cell wall organisation; Carbohydrate metabolic process; Conjugation with cellular fusion
SPCC70.10	Unknown	Unknown
SPAPB24D3.04c	*mag1*	DNA repair
SPAC23C4.07	*tht2*	Conjugation with cellular fusion
SPCC31H12.06	*mug111*	Transmembrane transport
SPAC4G9.11c	*cmb1*	DNA repair
SPCC550.08	N-acetyltransferase (predicted)	Unknown
SPBC14F5.11c	*snx41*	Vesicle-mediated transport
SPAC57A7.07c	Homocysteine methyltransferase (predicted)	Cellular amino acid metabolic process; Sulphur compound metabolic process
SPBC13E7.03c	*vts1*	mRNA metabolic process
SPAC144.01	Unknown	Unknown
SPAC11D3.03c	Aminomethyltransferase-like and DUF1989 family protein, implicated in urea metabolism	Unknown
SPCC1919.13c	*bmt5*	Ribosome biogenesis
SPBC27B12.08	*sip1*	Vesicle-mediated transport
SPAC328.03	*tps1*	Ascospore formation; Carbohydrate metabolic process
SPBC21B10.12	*rec6*	Meiotic nuclear division; DNA recombination
SPAC16E8.17c	Succinate-CoA ligase alpha subunit (predicted)	Sulphur compound metabolic process; Generation of precursor metabolites and energy; Nucleobase-containing small molecule metabolic process
SPAC17G8.14c	*pck1*	Signalling; Carbohydrate metabolic process
SPAC607.07c	Unknown	Unknown
SPBC119.03	*cmt1*	Unknown
SPBC1709.16c	Aromatic ring-opening dioxygenase (predicted)	Unknown
SPAC16E8.12c	*png3*	Chromatin organisation
SPBC1289.13c	*gmh6*	Cell wall organisation; Protein glycosylation
SPAC3A11.13	*pfd6/gim1*	Protein folding; Protein-containing complex assembly

SPAC6G9.03c	*mug183*	Protein-containing complex assembly; Chromatin organisation
SPBC15D4.12c	*mug98*	Unknown
SPBP4H10.19c	Calreticulin/calnexin homologue (predicted)	Protein folding; Protein catabolic process
SPCC1682.11c	*ctl1*	Transmembrane transport; Autophagy
SPBC2G5.01	ER protein involved in ER-nucleus signalling (predicted)	Signalling
SPAC23A1.14c	Pyridoxal phosphate-dependent transferase, unknown specificity, implicated in sulfur compound metabolism	Sulphur compound metabolic process; Cellular amino acid metabolic process
SPBC1921.06c	*pvg3*	Protein glycosylation; Carbohydrate metabolic process
SPBC2G5.03	*ctu1*	tRNA metabolic process; Protein modification by small protein conjugation or removal
SPACUNK4.15	2',3'-cyclic-nucleotide 3'-phosphodiesterase (predicted)	Nucleobase-containing small molecule metabolic process
SPAC4G9.12	*idn1*	Nucleobase-containing small molecule metabolic process; Carbohydrate metabolic process; Generation of precursor metabolites and energy
SPAC1A6.07	*sle1*	Membrane organisation
SPAPB21F2.02	*dop1*	Vesicle-mediated transport
SPAC3H5.11	NAD/NADH kinase (predicted)	Nucleobase-containing small molecule metabolic process
SPBC11G11.01	*fis1*	Membrane organisation; Mitochondrion organisation
SPBC12C2.09c	*izh2*	Metal ion homeostasis
SPCP20C8.02c	*S. pombe* specific UPF0321 family protein 1	Unknown
SPBC13E7.07	Unknown	Unknown
SPCC16A11.15c	Unknown	Unknown
SPAC7D4.05	HAD superfamily hydrolase, unknown role	Unknown
SPAC17C9.08	*pnu1*	Unknown
SPBC1271.03c	NLI interacting factor family phosphatase (predicted)	Signalling
SPBC13G1.04c	*abh1*	tRNA metabolic process
SPBC1921.04c	Unknown	Unknown
SPCC18B5.09c	Unknown	Unknown
SPAC926.03	*rlc1*	Mitotic cytokinesis; Actin cytoskeleton organisation
SPAC25B8.08	Golgi Ras-interacting protein with DIL domain, human RADIL and RASIP1 ortholog (predicted), implicated in vesicle-mediated transport	Unknown

SPAC3A11.11c	oxidoreductase, implicated in vitamin metabolism, or cellular detoxification (predicted)	Unknown
SPAC19A8.14	*pth2*	Mitochondrial gene expression
SPBC1289.06c	*ppr8*	Mitochondrial gene expression
SPCC1739.04c	*dms1*	Microtubule cytoskeleton organisation
SPAC1783.08c	*rpl1502*	Cytoplasmic translation
SPBC18H10.08c	*ubp4*	Protein modification (deubiquitination); Protein catabolic process
SPBC24C6.08c	*bhd1/ lst7*	Signalling; Vesicle-mediated transport
SPBC902.03	*spo7*	Membrane organisation; Ascospore formation; Microtubule cytoskeleton organisation
SPBC1105.13c	Unknown	Unknown
SPBC21D10.10	*bdc1*	Chromatin organisation
SPCC417.02	*dad5*	Meiotic nuclear division; Mitotic sister chromatid segregation
SPAC18G6.12c	ThiJ domain protein (predicted)	Unknown
SPAC19D5.06c	*din1*	mRNA metabolic process
SPCC1450.06c	*grx3*	Iron-sulphur cluster assembly; Protein maturation; Sulphur compound metabolic process
SPAC3H1.14	*gid4*	Protein targeting; Carbohydrate metabolic process; Protein catabolic process
SPAC3A12.13c	*tif310*	Cytoplasmic translation; Ribosome biogenesis; Protein-containing complex assembly
SPAC3H8.04	DUF4210 domain protein, human FAM214A ortholog, implicated in chromosome segregation (predicted)	Unknown
SPBC8D2.11	Unknown	Unknown
SPCC1840.08c	*pdi5*	Protein catabolic process
SPCC663.13c	*naa50*	Protein maturation
SPAC6G10.11c	*ubi3*	Cytoplasmic translation; Ribosome biogenesis; Protein modification (ubiquitination); Protein catabolic process
SPCC645.12c	Unknown	Unknown
SPBC83.16c	Protein with a role in clearing protein aggregates (predicted)	Detoxification
SPAC31A2.12	*rod1*	Vesicle-mediated transport
SPCC622.15c	Unknown	Unknown
SPAC1782.02c	Conserved fungal protein	Unknown
SPBC16C6.04	*dbl6*	Unknown
SPCC663.11	*saf1*	mRNA metabolic process
SPAC17A5.05c	Methyltransferase (predicted)	Unknown
SPAC17C9.15c	*dhm2*	Unknown
SPAC869.08	*pcm2*	Detoxification
SPBC15C4.06c	Ubiquitin-protein ligase E3 Meu34, human RNF13	Protein modification; Protein catabolic process

	family homologue, unknown biological role (predicted)	
SPBP35G2.04c	Unknown	Unknown
SPAC24C9.16c	*cox8*	Generation of precursor metabolites and energy
SPAC4D7.07c	*csi2*	Microtubule cytoskeleton organisation
SPBC17D11.03c	Carboxymuconolactone decarboxylase-like protein	Detoxification
SPBC902.05c	*idh2*	Generation of precursor metabolites and energy
SPBC1711.06	*rpl401*	Cytoplasmic translation
SPBC17G9.09	*tif213*	Cytoplasmic translation; Protein-containing complex assembly
SPBC106.01	*mph1*	Signalling; Meiotic nuclear division; Mitotic cell cycle phase transition; Mitotic sister chromatid segregation
SPAPJ691.02	Yippee-like protein	Unknown
SPAC29B12.12	*hot13*	Transmembrane transport; Protein targeting; Mitochondrion organisation
SPAC31G5.03	*rps1101*	Cytoplasmic translation; Ribosome biogenesis
SPCC622.01c	Unknown	Unknown
SPCC63.06	WD repeat protein, human WDR89 family	Unknown
SPAC56E4.07	N-acetyltransferase (predicted)	Unknown
SPBC32H8.01c	Endocytic trafficking protein (predicted)	Vesicle-mediated transport
SPAC926.05c	*dph4*	Unknown
SPAC14C4.04	ThiJ domain protein (predicted)	Unknown
SPCC965.14c	Cytosine deaminase (predicted)	Nucleobase-containing small molecule metabolic process
SPCC306.02c	*yip3*	Vesicle-mediated transport
SPCC1322.06	*kap113*	Nucleocytoplasmic transport
SPBC30D10.05c	sepiapterin reductase (predicted)	Pteridine-containing compound biosynthetic process
SPAC23C11.15	*pst2*	Chromatin organisation; Transcription, DNA-templated
SPBC3B8.04c	Phosphate (Pi) transmembrane transporter (predicted)	Transmembrane transport
SPAC5H10.07	Unknown	Unknown
SPBC19G7.03c	*rps3002*	Cytoplasmic translation; Ribosome biogenesis
SPBC29A10.16c	Cytochrome b5 (predicted)	Generation of precursor metabolites and energy; Lipid metabolic process
SPCC320.14	*sry1*	Cellular amino acid metabolic process
SPBC21C3.17c	*psg1*	Vesicle-mediated transport
SPCC1442.05c	*mic26*	Membrane organisation; Mitochondrion organisation
SPCC550.11	*nmd5*	Nucleocytoplasmic transport
SPAC1687.16c	*erg31*	Lipid metabolic process
SPBC887.18c	*hfi1*	Chromatin organisation; Transcription, DNA-templated

SPBC20F10.05	*nrl1*	Chromatin organisation
SPAC869.07c	*mel1*	Carbohydrate metabolic process; Lipid metabolic process
SPAC31A2.14	*bun107*	Protein modification
SPAPB1A11.03	Cytochrome b2 (L-lactate cytochrome-c oxidoreductase) (predicted)	Detoxification
SPAC23C11.13c	*hpt1*	Nucleobase-containing small molecule metabolic process
SPBC18H10.18c	Unknown	Unknown
SPBC1709.01	*chs2*	Mitotic cytokinesis; Cell wall organisation
SPAC1952.08c	Pyridoxamine 5'-phosphate oxidase (predicted)	Vitamin metabolic process
SPAC10F6.07c	*mug94*	Unknown
SPAC29E6.05c	*mxr1*	Sulphur compound metabolic process; Cellular amino acid metabolic process
SPAPB1A10.09	*ase1*	Signalling; Mitotic sister chromatid segregation; Meiotic nuclear division; Membrane organisation; Microtubule cytoskeleton organisation; Mitotic cell cycle phase transition
SPBC11C11.06c	Unknown	Unknown
SPAC8F11.09c	*nnt1*	Vitamin metabolic process
SPBC1198.03c	DUF4646 family conserved fungal protein	Unknown
SPBC106.04	*ada1*	Nucleobase-containing small molecule metabolic process
SPAC9E9.11	*plr1*	Vitamin metabolic process
SPAC26H5.04	*gid5*	Carbohydrate metabolic process; Protein catabolic process
SPBC29B5.01	*atf1*	Signalling; Cell wall organisation; Meiotic nuclear division; Chromatin organisation; Transcription, DNA-templated; DNA recombination
SPAC15F9.01c	*glm1*	Protein catabolic process
SPBC4B4.03	*rsc1*	Chromatin organisation; Transcription, DNA-templated
SPBC21C3.19	*rtc3*	Ribosome biogenesis
SPCC320.06	Conserved fungal protein	Unknown
SPAC23G3.04	*ies4*	Chromatin organisation; Transcription, DNA-templated; Mitotic cell cycle phase transition
SPBC2G2.10c	*mug110*	Unknown
SPBC16E9.06c	*uvi31*	Protein maturation
SPAC8E11.06	Unknown	Unknown
SPAC22F8.12c	*shf1*	Protein modification (ubiquitination); Chromatin organisation
SPBC8D2.16c	SPOUT domain containing methyltransferase (predicted)	Mitotic sister chromatid segregation
SPAC3A12.10	*rpl2001*	Cytoplasmic translation
SPBC1A4.05	*blt1*	Mitotic cell cycle phase transition
SPBC25H2.14	*mug16*	Unknown

SPAC17A2.10c	Unknown	Unknown
SPBPJ4664.05	Endomembrane system protein, FAR-17a/AIG1-like family protein, human AIG1 and ADTRP ortholog	Unknown
SPAC22F3.09c	*res2*	Transcription, DNA-templated; Mitotic cell cycle phase transition
SPBC25B2.01	*hbs1*	Signalling; mRNA metabolic process; Cytoplasmic translation
SPCC594.07c	*bqt3*	Meiotic nuclear division; Telomere organisation
SPBC1734.15	*rsc4*	Chromatin organisation; Transcription, DNA-templated
SPCC13B11.04c	*fmd3*	Generation of precursor metabolites and energy; Detoxification; Cellular amino acid metabolic process
SPBC1703.12	*ubp9*	Protein modification (deubiquitination); Protein catabolic process; Vesicle-mediated transport
SPCC777.02	DNA-binding transcription factor (predicted)	Transcription, DNA-templated
SPCC330.14c	*rpl2402*	Cytoplasmic translation; Ribosome biogenesis; Protein-containing complex assembly
SPAC19B12.12c	*yip11*	mRNA metabolic; Process protein-containing complex assembly
SPAC17H9.03c	*rdl1*	DNA repair; Meiotic nuclear division; DNA recombination
SPAC323.04	Mitochondrial ATPase (predicted)	Unknown
SPAC1687.14c	EF hand family protein, centrin-like	Unknown
SPCC1223.01	Ubiquitin-protein ligase E3 involved in rescue of stalled ribosomes (predicted)	Protein modification; Cytoplasmic translation
SPAC2E1P3.01	Dehydrogenase (predicted)	Unknown
SPBC1709.06	*dus2*	tRNA metabolic process
SPCC794.07	*lat1*	Sulphur compound metabolic process; Nucleobase-containing small molecule metabolic process
SPAC1071.07c	*rps1502*	Nucleocytoplasmic transport; Ribosome biogenesis; Cytoplasmic translation; Protein-containing complex assembly
SPAC11H11.01	*sst6*	Protein catabolic process; Protein targeting; Vesicle-mediated transport
SPAC140.03	*arb1*	Transcription, DNA-templated; Chromatin organisation
SPBP23A10.02	*pkr1*	Protein-containing complex assembly
SPBC2D10.03c	*ess1*	Unknown
SPAC30C2.08	UPF0662 family conserved fungal protein	Unknown
SPAC23C4.12	*hhp2*	Signalling; Transcription, DNA-templated; Protein catabolic process; Lipid metabolic process; Vesicle-mediated transport; Mitotic cell cycle phase transition; DNA repair; DNA

		recombination; mitotic sister chromatid segregation; meiotic nuclear division
SPAC19G12.08	*scs7*	Lipid metabolic process
SPAC17A2.11	Unknown	Unknown
SPAC4F10.08	*mug126*	Unknown
SPAC6C3.03c	Unknown	Unknown
SPBC16E9.09c	*erp5/erp6*	Vesicle-mediated transport
SPAC31F12.01	*zds1*	Signalling; Establishment of cell polarity; Ascospore formation; Mitotic cell cycle phase transition; Cell wall organisation
SPBC14C8.15	Triglyceride lipase-cholesterol esterase (predicted)	Lipid metabolic process
SPBC1198.08	*dug1*	Sulphur compound metabolic process
SPBC17G9.10	*rpl1102*	Ribosome biogenesis; Cytoplasmic translation
SPBC106.13	*gid9*	Carbohydrate metabolic process; Protein catabolic process
SPAC9G1.04	*oxa101*	Membrane organisation; Mitochondrion organisation; Protein-containing complex assembly
SPAC2F3.11	*ppxx1*	Generation of precursor metabolites and energy
SPCC622.14	GTPase activating protein (predicted)	Vesicle-mediated transport
SPAC6B12.08	*erp1 (mug185)*	Autophagy
SPBC887.11	*pus2*	tRNA metabolic process; mRNA metabolic process
SPBC660.11	*tcg1*	Telomere organisation
SPAC1071.12c	*stp1*	Signalling
SPAC13C5.02	*dre4*	mRNA metabolic process
SPBC354.01	*gtp1*	Cytoplasmic translation
SPAC23H3.04	Conserved fungal multispanning membrane protein	Unknown
SPCC1906.04	*wtf20*	Meiotic drive
SPBC2D10.12	*rhp23*	Protein catabolic process; DNA repair
SPCC13B11.02c	Unknown	Unknown
SPCC794.02	*wtf5*	Meiotic drive
SPBC409.06	*uch2*	Protein catabolic process; Protein modification (deubiquination)
SPBC428.04	*apq12*	Membrane organisation; Lipid metabolic process
SPCP31B10.04	*psg2*	Vesicle-mediated transport
SPAC19G12.16c	*adg2* (*mug46*)	Unknown
SPBC21C3.01c	*vps1301*	Membrane organisation; Protein targeting; Vesicle-mediated transport; Mitochondrion organisation
SPBC27B12.14	*cbp4*	Mitochondrion organisation; Protein-containing complex assembly
SPAC17C9.02c	*lys7*	Cellular amino acid metabolic process
SPBC19C2.14	*smd3*	mRNA metabolic process; Protein-containing complex assembly

SPAC27E2.01	alpha-amylase homologue (predicted)	Cell wall organisation
SPBC365.06	*pmt3*	Chromatin organisation; Protein modification; Telomere organisation; DNA replication
SPAC2F3.12c	*plp1*	Protein folding
SPAC513.06c	*dhd1*	Carbohydrate metabolic process
SPAC2F3.18c	Small endoribonuclease with 2 transmembrane domains (predicted)	Unknown
SPBC2A9.13	Unknown	Unknown
SPBC3D6.09	*dpb4*	Chromatin organisation; Protein-containing complex assembly; Transcription, DNA-templated; DNA replication
SPAC8E11.04c	Palmitoyl-(protein) hydrolase (predicted)	Protein catabolic process
SPBC4B4.07c	*usp102*	mRNA metabolic process; Protein-containing complex assembly
SPAC4G9.19	DNAJ domain protein DNAJB family (predicted)	Protein catabolic process
SPAC1420.03	*rpn501*	Mitotic cell cycle phase transition; Protein catabolic process
SPAC1952.02	*tma23*	Ribosome biogenesis
SPBC947.14c	*cbp6*	Protein-containing complex assembly; Mitochondrion organisation
SPAC683.03	Unknown	Unknown
SPAPB24D3.09c	*pdr1*	Transmembrane transport
SPAC589.11	*pth4*	Mitochondrial gene expression
SPAC6B12.06c	*rrg9*	Mitochondrion organisation
SPBC16A3.07c	*nrm1*	Mitotic cell cycle phase transition; Transcription, DNA-templated
SPBCPT2R1.08c	*tlh2*	DNA recombination; Telomere organisation
SPAC630.15	*mug177*	Unknown
SPBC26H8.12	*cyc3*	Protein-containing complex assembly; Mitochondrion organisation
SPBC2D10.06	*rep1*	Transcription, DNA-templated
SPAC20H4.02	*dsc3*	Protein glycosylation; Protein maturation; Signalling
SPBC365.01	*csr103*	Membrane organisation
SPBC36.10	*ups2*	Membrane organisation; Mitochondrion organisation
SPCC1682.08c	*mpf2*	mRNA metabolic process
SPCC24B10.09	*rps1702*	Ribosome biogenesis; Cytoplasmic translation
SPAC13C5.07	*mre11 (rad32)*	Mitotic cell cycle phase transition; DNA recombination; Meiotic nuclear division; Telomere organisation; DNA repair; Signalling
SPAC27D7.02c	*grp1*	Vesicle-mediated transport
SPAC18B11.07c	*rhp6 (rad6)*	Chromatin organisation; Protein modification (ubiquitination); Protein catabolic process; DNA repair; Signalling
SPAC6F12.12	*par2*	Signalling

SPAC3G9.04	*ssu72*	Chromatin organisation; mRNA metabolic process; Telomere organisation; Transcription, DNA-templated; Signalling
SPBC106.10	*pka1*	Carbohydrate metabolic process; Conjugation with cellular fusion; Nucleocytoplasmic transport; Microtubule cytoskeleton organisation; Transcription, DNA-templated; Signalling
SPBC1105.11c	*hht3*	Chromatin organisation
SPBC31F10.16	*bch1*	Vesicle-mediated transport
SPCC970.07c	*raf2*	Chromatin organisation; Telomere organisation; Protein-containing complex assembly; Transcription, DNA-templated
SPBC146.09c	*lsd1*	Chromatin organisation; DNA replication
SPBC21C3.13	*rps1901*	Ribosome biogenesis; Protein-containing complex assembly; Cytoplasmic translation
SPBC3H7.13	*far10*	Signalling
SPBC776.17	*rrp7*	Ribosome biogenesis; Protein-containing complex assembly
SPCC74.06	*mak3*	Signalling
SPBC1709.14	*ngl1*	Protein catabolic process
SPAC7D4.12c	Plasma membrane ThrE amino acid transmembrane transporter family protein (predicted)	Transmembrane transport
SPCC1902.01	*gaf1*	Conjugation with cellular fusion; Transcription, DNA-templated
SPAC1006.09	*win1*	Signalling
SPAC26F1.01	*sec74*	Vesicle-mediated transport; Signalling
SPAPYUG7.03c	*mid2*	Unknown
SPBC609.03	*iqw1*	Protein modification
SPBP35G2.14	*puf2*	mRNA metabolic process
SPCC11E10.04	*ppr6*	Mitochondrial gene expression
SPCC1322.03	*trp1322*	Transmembrane transport; Metal ion homeostasis
SPAC9G1.06c	*cyk3*	Mitotic cytokinesis; Actin cytoskeleton organisation
SPBC25H2.16c	*gga22*	Protein catabolic process; Vesicle-mediated transport
SPBC1652.02	APC amino acid transmembrane transporter (predicted)	Transmembrane transport
SPAC30D11.10	*rad52 (rad22)*	DNA recombination; Telomere organisation; DNA repair; Protein-containing complex assembly; DNA replication
SPBC1734.11	*mas5*	Chromatin organisation; Protein folding; Protein catabolic process; Transcription, DNA-templated
SPCP1E11.05c	*are2*	Lipid metabolic process
SPAC32A11.02c	DUF4449 family conserved fungal protein, involved in cell-cell communication in *N. crassa*	Unknown
SPAC29B12.10c	*pgt1*	Transmembrane transport

SPAC30D11.11	*izh3*	Metal ion homeostasis
SPBC365.07c	*tmf1*	Unknown
SPBC530.08	DNA-binding transcription factor, membrane-tethered (predicted)	Transcription, DNA-templated
SPBC3D6.02	*but2*	Unknown
SPCC1442.16c	*zta1*	Detoxification
SPCC18B5.03	*wee1*	Mitotic cell cycle phase transition; Signalling
SPBP4H10.11c	*lcf2*	Sulphur compound metabolic process; Lipid metabolic process; Nucleobase-containing small molecule metabolic process
SPBC2G2.01c	*liz1*	Transmembrane transport
SPAC1639.01c	*elo1*	Lipid metabolic process
SPAC1071.05	*hpm1*	Ribosome biogenesis; Protein-containing complex assembly
SPBC725.07	*pex5*	Transmembrane transport; Peroxisome organisation; Protein targeting
SPBC18E5.01	Unknown with similarity to bacterial carboxy-cis,cis-muconate cyclase	Unknown
SPCC31H12.05c	*sds21*	Establishment of cell polarity
SPBC31F10.10c	*mub1*	Protein catabolic process; Establishment of cell polarity
SPAC1D4.03c	*aut12*	Autophagy; Vesicle-mediated transport; Protein targeting
SPBC13G1.04c	*abh1*	tRNA metabolic process
SPAC144.11	*rps1102*	Ribosome biogenesis; Cytoplasmic translation
SPBPB10D8.05c	Transmembrane transporter (predicted)	Transmembrane transport
SPBP4H10.19c	Calreticulin/calnexin homologue (predicted)	Protein folding; Protein catabolic process
SPCC1795.06	*map2*	Conjugation with cellular fusion; Signalling
SPAC4G9.12	*idn1*	Generation of precursor metabolites and energy; Carbohydrate metabolic process; Nucleobase-containing small molecule metabolic process
SPCC338.04	*mix23*	Transmembrane transport; Protein targeting; Mitochondrion organisation
SPBC13A2.04c	*ptr2*	Transmembrane transport
SPCC645.07	*rgf1*	Carbohydrate metabolic process; Cell wall organisation; Signalling
SPBP4H10.17c	Protein repair carboxyl methyl esterase (predicted)	Detoxification
SPBC776.14	*plh1*	Lipid metabolic process
SPCC14G10.04	Unknown	Unknown
SPAC27D7.08c	*mtl16*	snRNA metabolic process; Ribosome biogenesis
SPAPB8E5.10	Conserved fungal protein, with meiosis specific splicing	Unknown
SPCC1020.09	*gnr1*	Signalling
SPAC1002.01	*mrx11*	Mitochondrial gene expression

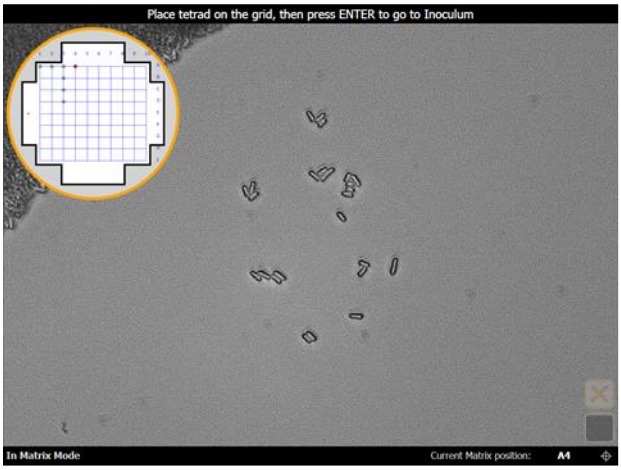
SPBC1921.01c	*rpl35b*	Ribosome biogenesis; Cytoplasmic translation
SPBC18H10.16	*can1*	Transmembrane transport; Metal ion homeostasis
SPAPB1A11.03	Cytochrome b2 (L-lactate cytochrome-c oxidoreductase) (predicted)	Detoxification
SPAC3G9.01	*nsk1*	Mitotic sister chromatid segregation
SPAC6G9.16c	*xrc4*	DNA repair
SPAC23H3.06	*apl6*	Vesicle-mediated transport
SPAC8E11.06	Unknown	Unknown
SPBC106.04	*ada1*	Nucleobase-containing small molecule metabolic process
SPAC22F3.09c	*res2*	Mitotic cell cycle phase transition; Transcription, DNA-templated
SPBC409.08	Spermine family transmembrane transporter (predicted)	Transmembrane transport; Detoxification
SPBC17D11.08	*dca7*	DNA replication
SPAC140.03	*arb1*	Chromatin organisation; Transcription, DNA-templated
SPBP23A10.02	*pkr1*	Protein-containing complex assembly
SPAC2G11.06	*vps4*	Protein catabolic process; Vesicle-mediated transport; Membrane organisation
SPCC18.10	Pyridoxine-pyridoxal-pyridoxamine kinase (predicted)	Vitamin metabolic process
SPAC589.12	*cwh43*	Cell wall organisation; Lipid metabolic process
SPBC19C2.14	*smd3*	mRNA metabolic process; Protein-containing complex assembly
SPBC1778.01c	*zuo1*	Protein folding; Cytoplasmic translation
SPAC16C9.04c	*mot2*	mRNA metabolic process; Protein modification (ubiquitination)
SPAC959.07	*rps403*	Cytoplasmic translation
SPBC119.06	*sco1*	Protein maturation; Protein-containing complex assembly; Mitochondrion organisation
SPBC16H5.13	*wdr7*	Unknown
SPBC1734.08	*hse1*	Ascospore formation; Protein catabolic process; Vesicle-mediated transport
SPCC736.14	*dis1*	Meiotic nuclear division; Mitotic sister chromatid segregation; Microtubule cytoskeleton organisation
SPBC19G7.01c	*msh2*	DNA recombination; DNA repair
SPAC17G8.06c	Dihydroxy-acid dehydratase (predicted)	Cellular amino acid metabolic process
SPBC2D10.18	*abc1*	Ubiquinone biosynthetic process
SPCC1919.10c	*myo52*	Establishment of cell polarity; Mitotic cytokinesis; Actin cytoskeleton organisation
SPAC1399.03	*fur4*	Transmembrane transport
SPBC11B10.07c	*ivn1*	Membrane organisation
SPAC24C9.15c	*spn5*	Membrane organisation; Ascospore formation
SPAPB8E5.03	*mae1*	Transmembrane transport

SPBC1703.13c	Mitochondrial carrier, inorganic phosphate/copper (predicted)	Transmembrane transport
SPBC530.09c	*mrl1*	Vesicle-mediated transport
SPBC577.05c	*rec27*	DNA recombination; Meiotic nuclear division
SPAC1250.02	*mug95*	Unknown
SPBP35G2.02	*txc1*	Unknown
SPAC3A12.10	*rpl2001*	Cytoplasmic translation
SPBC16D10.03	*kae1*	tRNA metabolic process
SPAC26F1.07	NADPH-dependent aldo-keto reductase (predicted)	Detoxification; Carbohydrate metabolic process
SPBC13G1.12	*did2*	Protein targeting; Protein catabolic process; Vesicle-mediated transport
SPAC1952.16	*rga9*	Signalling
SPAC630.06c	DUF2011 family conserved fungal protein	Unknown
SPBC776.02c	*dis2*	Transcription, DNA-templated; Signalling; Establishment of cell polarity; Mitotic sister chromatid segregation; Mitotic cell cycle phase transition
SPBC725.02	*mpr1*	Signalling; Mitotic cell cycle phase transition
SPBC530.01	*gyp1*	Vesicle-mediated transport
SPAC1071.05	*hpm1*	Protein-containing complex assembly; Ribosome biogenesis
SPAC1D4.06c	*csk1*	Transcription, DNA-templated; Signalling
SPBC1861.06c	*mug131*	Unknown
SPCC330.03c	NADPH-hemoprotein reductase (predicted)	Tetrapyrrole metabolic process
SPBC1E8.03c	ER membrane protein, conserved in fungi plants and protozoa (predicted)	Unknown
SPAC2E1P5.03	*erj5*	Protein folding

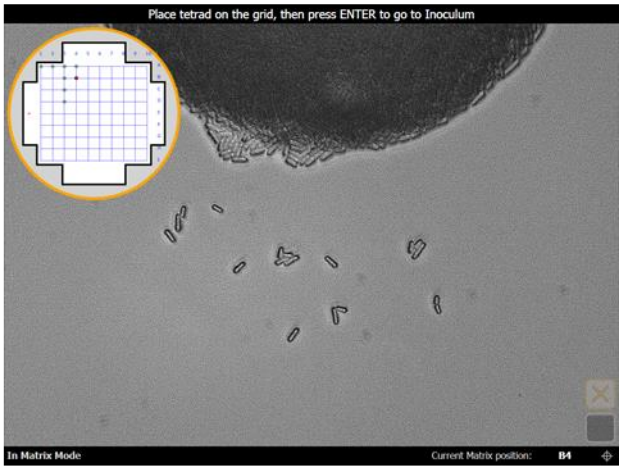
List of "synthetic lethal" hits yielded from the Bioneer screen. **KEY:** No highlighted background (white) – genes are from the V2 Bioneer Library; Yellow-coloured background – genes are from the Replacement and Updated Bioneer libraries; Pink-highlighted – genes that meet the selection criteria (specific GO term/s) outlined in **Chapter 5**. Green-highlighted – genetic interactions assessed via tetrad dissection; Blue background – Known SSL interactions.

Appendix IV:

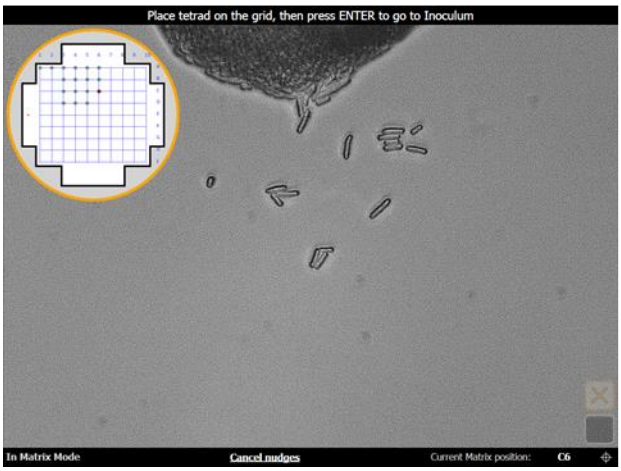
pol3L458P



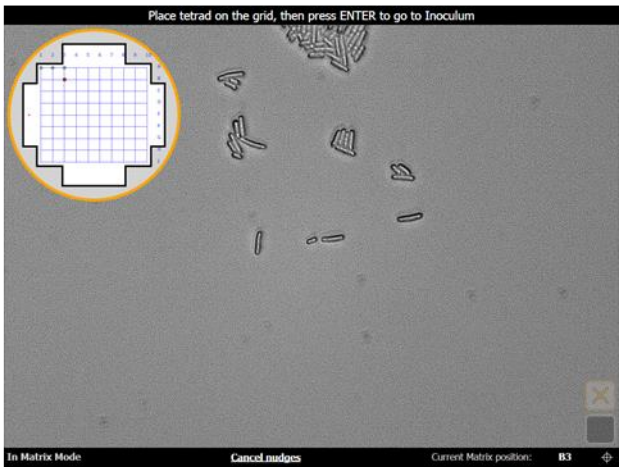
WT



mre11Δ



pol3L458Pmre11Δ



A sporulating cross between *pol3L458P* and *mre11*Δ was tetrad dissected. Photographs were taken, using the dissection microscope (Singer Instruments), of spores germinating post-dissection 1-2 days in 30ºC incubation for the following genotypes: WT, *pol3L458P*, *mre11*Δ and *pol3L458P mre11*Δ. WT and *pol3L458P* do not have elongated cells. *Mre11*Δ and the double mutant have an elongated cell phenotype.

Appendix V: Accepted for publication

Editorial acceptance of PGENETICS-D-21-00425R1 - [EMID:41085621489d0d48]

From: <em.pgenetics.0.73e92e.c6be13af@editorialmanager.com> on behalf of PLOS Genetics <em@editorialmanager.com>
Reply-To: PLOS Genetics <plosgenetics@plos.org>
Date: Friday, 11 June 2021 at 20:04
To: Stephen Kearsey <stephen.kearsey@zoo.ox.ac.uk>
Subject: Editorial acceptance of PGENETICS-D-21-00425R1 - [EMID:41085621489d0d48]

CC: "Ignacio Soriano" ignacio.soriano@igmm.ed.ac.uk, "Enrique Vazquez" quique_vzquez@usal.es;evazquez@cnic.es;quiquevzquez@gmail.com, "Nagore de Leon" nagore.deleonmarcos@igmm.ed.ac.uk;nagoret16@gmail.com, "Sibyl Bertrand" sibyl.bertrand@hotmail.fr, "Ellen Heitzer" ellen.heitzer@medunigraz.at, "Sophia Toumazou" sophia.toumazou@gmail.com, "Zhihan Bo" zhihanbouk@hotmail.com;zhihan.bo@bioch.ox.ac.uk, "Claire Palles" c.palles@bham.ac.uk, "Chen-Chun Pai" chen-chun.pai@oncology.ox.ac.uk, "Timothy C. Humphrey" humphreytc@gmail.com;timothy.humphrey@oncology.ox.ac.uk, "Ian Tomlinson" iant@well.ox.ac.uk, "Sue Cotterill" s.cotterill@sgul.ac.uk

Dear Dr Kearsey,

We are pleased to inform you that your manuscript entitled "Expression of the cancer-associated DNA polymerase ε P286R in fission yeast leads to translesion synthesis polymerase dependent hypermutation and defective DNA replication" has been editorially accepted for publication in PLOS Genetics. Congratulations!

Before your submission can be formally accepted and sent to production you will need to complete our formatting changes, which you will receive in a follow up email. Please be aware that it may take several days for you to receive this email; during this time no action is required by you. Please note: the accept date on your published article will reflect the date of this provisional acceptance, but your manuscript will not be scheduled for publication until the required changes have been made.

Once your paper is formally accepted, an uncorrected proof of your manuscript will be published online ahead of the final version, unless you've already opted out via the online submission form. If, for any reason, you do not want an earlier version of your manuscript published online or are unsure if you have already indicated as such, please let the journal staff know immediately at plosgenetics@plos.org.